POLYTECHNIC SCHOOL OF THE UNIVERSITY OF SÃO PAULO

Department of Structural and Geotechnical Engineering

MARCOS PIRES KASSAB

Advances on a kinematically exact rod model for thin-walled open section members: consistent warping function and nonlinear constitutive equation

São Paulo

2023

POLYTECHNIC SCHOOL OF THE UNIVERSITY OF SÃO PAULO

Department of Structural and Geotechnical Engineering

MARCOS PIRES KASSAB

Advances on a kinematically exact rod model for thin-walled open section members: consistent warping function and nonlinear constitutive equation

Corrected Version

Dissertation submitted to the Polytechnic School of the University of São Paulo for obtention of the degree of Master of Science, in the Post-Graduate Program in Civil Engineering, area of Structural Engineering.

Concentration area:
Structural Engineering

Advisor:
Eduardo de Morais Barreto Campello

São Paulo

2023

Este exemplar foi revisado e corrigido em relação à versão original, sobresponsabilidade única do autor e com a anuência de seu orientador.

São Paulo, 13 de janeiro de 2023

Assinatura do autor:

Assinatura do orientador:

Nome: KASSAB, Marcos Pires

Título: Advances on a kinematically exact rod model for thin-walled open section members: consistent warping function and nonlinear constitutive equation

Dissertação apresentada à Escola Politécnica da Universidade de São Paulo para obtenção de título de Mestre em Ciências, no Programa de Pós-Graduação em Engenharia Civil, área de Engenharia de Estruturas.

Aprovado em 06/12/2022

Banca Examinadora

Prof. Dr.   Eduardo de Morais Barreto Campello

Instituição: PEF - Escola Politécnica - USP

Julgamento: _____

Prof. Dr.   Rodrigo de Moura Gonçalves

Instituição: Universidade NOVA de Lisboa

Julgamento: _____

Prof. Dr.   Humberto Breves Coda

Instituição: Escola de Engenharia de São Carlos - USP

Julgamento: _____

Dedicatória

À minha família, em especial aos meus pais, Luciana e Marcos e à minha irmã Vivian, pelo amor, carinho e suporte incondicionais; a todos meus colegas e amigos, pelo companheirismo nas trincheiras da vida,

dedico este trabalho.

Acknowledgements

ABSTRACT

Structural models accounting for exact kinematics are well-suited for the description of critical loads and post-critical behaviour. For thin-walled open-section members, the associated rod formulations must take cross-sectional non-uniform warping into account, since it becomes a relevant load-carrying mechanism due to the very small torsion stiffness of such members. For this work, advances on kinematically exact rod models for thin-walled open section members, taking into account both primary and secondary cross-sectional warpings and advanced constitutive equations, are proposed. For thin-walled open-section members with linear elastic constitutive equation, the warping effects are fully characterized by the well-known torsion inertia from the Saint-Venant's uniform torsion theory and the warping constant from the Vlasov's theory. The former has a well-known analytic expression, whilst the latter is obtained only considering the so-called primary warping, which is the warping in the direction of the cross-section´s walls lengths. The walls´ thickness warping, or secondary warping, is typically neglected. However, for more advanced constitutive equations, such as the ones of interest here, explicit knowledge of the warping and its directional derivatives are of utmost importance for the stress resultants integrations, justifying the need of a warping function that accounts for both primary and secondary cross-sectional components. This work incorporates two exact constitutive equations (i.e. retaining all the strain terms), in order to enable full bending, compression and torsional strain couplings in the finite strain regime: one based on the Saint-Venant's material, which is generally unsuited to truly finite strains, and another based on the polyconvex neo-Hookean Simo-Ciarlet's material. The model was implemented in PEFSYS, which is an in-house nonlinear finite element program. Validation is performed using existing results from the literature as well as solutions obtained with shell models in ANSYS commercial software.

Keywords: *Kinematically exact rod model, thin-walled open-section members, secondary warping, elastic stability, finite element method.*

RESUMO

Modelos estruturais cinematicamente exatos são adequados para a descrição de cargas críticas e comportamento pós-crítico. Para barras de seção aberta de paredes delgadas, a formulação de barras associada deve levar em consideração o empenamento não uniforme da seção transversal, que se torna um importante mecanismo de transferência de esforços, devido à baixa inércia à torção desses perfis. Neste trabalho, foram propostos avanços em modelos cinematicamente exatos para perfis de seção aberta e paredes delgadas, levando em consideração tanto empenamento primário quanto secundário, e equações constitutivas exatas. Para barras de seção aberta e paredes delgadas com equação constitutiva elástica linear, os efeitos do empenamento são completamente caracterizados pelas propriedades usuais de inércia à torção uniforme de Saint-Venant e pela constante de empenamento, proveniente da teoria de Vlasov. A primeira dessas propriedades é obtida através de expressões analíticas triviais, enquanto a outra é obtida considerando apenas o empenamento primário, que é o empenamento na direção do comprimento das paredes. O empenamento secundário, na direção da espessura das paredes, é desprezado nessa análise. Entretanto, para equações constitutivas mais avançadas, como as que são aqui usadas, informação explícita da função empenamento e suas derivadas são de extrema importância para a integração das resultantes de tensão, justificando a necessidade de uma função empenamento que considere tanto empenamento primário quanto secundário. Este trabalho incorpora duas equações constitutivas exatas (i.e., que retêm todos os termos de deformação), de modo a permitir acoplamento total entre deformações de flexão, compressão e torção em regime de deformações finitas: uma baseada no material de Saint-Venant (inadequado para deformações finitas), e outra baseada no material policonvexo neo-Hookeano de Simo-Ciarlet. O modelo foi implementado no PEFSYS, um programa para análise não linear de estruturas baseado no método dos elementos finitos desenvolvido na instituição deste trabalho. A validação é feita através de resultados da literatura e de simulações feitas com modelos de casca do programa comercial ANSYS.

Palavras-chave: *teoria de barra cinematicamente exata, barra de seção aberta e paredes delgada, empenamento secundário, estabilidade elástica, método dos elementos finitos.*

SUMMARY

LIST OF FIGURES

LIST OF TABLES

LIST OF SYMBOLS

A	Cross-sectional area
S_α	Cross-sectional statical moment
S_ψ, S_ω	Cross-sectional sectorial statical moment, using ψ and ω, respectively
$I_{\alpha\alpha}$	Cross-sectional moment of inertia
$I_{\alpha\beta}$	Cross-sectional product of inertia
I_T	Cross-sectional torsional moment of inertia
I_ψ, I_ω	Cross-sectional warping constant/sectorial moment of inertia
g_α	Cross-sectional centroid
s_α	Cross-sectional shear-centre
$\boldsymbol{Q}$	Rotation tensor
h_i	Auxiliar functions for the rotation tensor and its derivatives
$\boldsymbol{\theta}$	Euler-Rodrigues rotation vector
$\boldsymbol{\omega}$ and $\boldsymbol{\Omega}$	Spin vector and tensor
$\boldsymbol{\kappa}$ and $\boldsymbol{K}$	Specific rotation vector and tensor
$\boldsymbol{\Gamma}$	Auxiliar tensor that arises from the derivatives of $\boldsymbol{Q}$
S_u, S_t	Boundary with applied displacements and loadings, respectively
$\boldsymbol{L}$	Linear momentum
$\boldsymbol{J}$	Angular moment
$\boldsymbol{T}$	Cauchy stress tensor
$\boldsymbol{P}, \boldsymbol{P}^r$	First Piola-Kirchoff stress tensor, usual and back-rotated, respectively
$\boldsymbol{\tau}_i, \boldsymbol{\tau}_i^r$	Columns of $\boldsymbol{P}$ and $\boldsymbol{P}^r$, respectively
$\boldsymbol{S}$	Second Piola-Kirchoff stress tensor
$\boldsymbol{\rho}, \boldsymbol{\rho}^r$	Real and nominal stress vector, respectively
$\boldsymbol{n}, \boldsymbol{n}^r$	Unit vector of external normal direction or normal force, with respect to current or reference configuration, respectively
$\boldsymbol{b}, \boldsymbol{b}^r$	Body forces w.r.t current and initial configurations, respectively
$\boldsymbol{t}, \boldsymbol{t}^r$	Surface forces w.r.t current and initial configurations, respectively
$\boldsymbol{u}$	Displacements vector
$\boldsymbol{F}, \boldsymbol{F}^r$	Deformation gradient, usual and back-rotated, respectively
J	Deformation gradient jacobian
$\boldsymbol{E}$	Green-Lagrange strain tensor
$\boldsymbol{C}$	Cauchy-Green strain tensor
ρ, ρ^r	Specific mass w.r.t current and initial configurations, respectively
P_{int}, P_{ext}	Power of internal and external forces, respectively
P, P_v, P_s	Power associated to point, volume and surface forces, respectively
W_{int}, W_{ext}	Work of internal and external forces, respectively
T	Kinetic energy
$\delta W_{ext}, \delta W_{int}$	Virtual external and internal work, respectively
δT	Virtual kinetic energy

e_i, e_i^r	Reference system, current and reference configuration, respectively
x, ξ	Position of a point, current and reference configuration, respectively
z, ζ	Position of the rod's axis, current and reference configuration, respectively
a, a^r	Cross-sectional coordinates, current and reference configuration, respectively
v, w	Vector of total in- and out-of plane cross-sectional distortion
δ	Total displacement of a generic point
n_v, n_w	Amount of in- and out- of plane distortion functions
ϕ_α, ψ	Vector of in- and out-of plane cross-sectional distortion shape functions
r, p	Vector of in- and out-of plane cross-sectional distortion intensity
ψ, p	Warping shape function and intensity for the specific case of $n_v = 0$ and $n_w = 1$
ψ^R	Saint-Venant torsion warping function for a rectangular cross-section
ψ^L	Correction of the warping function for a pole shift
$\omega^{A,B}$	Vlasov's sectorial area function w.r.t a pole A and origin B
η, η^r	Generalized axial strain vector, usual and back-rotated, respectively
κ, κ^r	Generalized curvature strain vector, usual and back-rotated, respectively
γ, γ^r	Vector with the third column of F and F^r
d_θ	Generalized displacement vector
ε^r	Generalized strain vector
Ψ, Δ	Auxiliary tensors
δd_θ	Virtual generalized displacement vector
$\delta \varepsilon^r$	Virtual generalized strain vector
σ^r	Generalized stress resultants vector
n^r, m^r	Forces and moment resultants vector
Q, B	Bi-shear and bi-moment
D, G_θ, L_θ	Material, geometric and external loading contributions to the tangent operator
$G_{u'\theta}, G_{\theta\theta}, G_{\theta'\theta'}$	Sub-matrices of G_θ
$V(\theta, m)$	Auxiliar expression for obtention of G_θ
$D_{\eta\eta}, D_{\eta\kappa}, D_{\eta p}, D_{\eta p'},$ $D_{\kappa\kappa}, D_{\kappa p}, D_{\kappa p'},$ $D_{pp}, D_{pp'}, D_{p'p'}$	Sub-matrices of D
C_{33}	Auxiliary tensor for obtention of D
c, d	Auxiliary vector for obtention of D
b_α, d_α	Auxiliary scalar for obtention of D
I_i	Invariants of the Cauchy-Green strain tensor
ψ_h	Potential function of an hyperelastic material law
μ, λ	Lamé constants
E, G	Elastic and shear moduli
ν	Poisson's coefficient

$\boldsymbol{N}$	Tensor with FEM polynomial interpolation functions
$\boldsymbol{P}_e$	Elemental residual force vector
$\boldsymbol{k}_e$	Tangent stiffness matrix for one element
$\boldsymbol{R}$	Global residual force vector
$\boldsymbol{K}_T$	Global tangent stiffness matrix
b, b_i, b_f	Flange lengths
t, t_i, t_f, t_v, t_h	Flange thicknesses
h	Web lenght

Marcos Pires Kassab

23

Advances on a kinematically exact rod model for thin-walled open section members: consistent warping function and nonlinear constitutive equation

1. INTRODUCTION

Unidimensional rod models were the first attempt in science and engineering to mathematically represent real life structures. Hierarchically, linear Bernoulli-Euler's beam theory is the simplest approach, followed by less kinematically restrictive beam models, such as the Timoshenko's and Vlasov´s models, and then by geometrically exact formulations. Moving up in the hierarchy, there are bidimensional models (plane stress, plane strain, axisymmetric, shells, etc) and fully three-dimensional models, which require considerably more effort and invariably more advanced computational resources to calculate desired outputs – the number of degrees of freedom sharply increases when compared to equivalent rod models.

Simpler rod theories, although useful and very convenient, tend to incorrectly estimate the structure´s stiffness, due to the several constrains imposed on the rod´s deformation. In addition, if linear, they are intrinsically unsuited for structures undergoing large displacements and rotations, as well as for those that are prone to instabilities. In those cases, geometrical effects become relevant and can no longer be neglected. Thus, non-linear theories are required – and even more so if one is interested in evaluating highly flexible structures or post-critical behaviour.

A wide array of successful non-linear rod models has been developed in the literature in the last four decades or so. Still, when it comes to thin-walled open-section members, they often struggle to simultaneously predict critical loads *and* post critical behaviour, to which torsion and warping become relevant to the load-carrying mechanism and related buckling modes. Most of these models typically introduce the simplifying small strains assumption, implying that only low order strain terms are retained at the constitutive equation. As consequence, the cross-sectional stress resultants may be computed through analytical integration, ending up dependent solely on trivial geometrical properties, which are usually well-known. For the torsion and torsion-bending-related stress resultants, for example, the torsion inertia (I_T) and warping constant (I_ψ) suffice. Those can be achieved by classical expressions for open thin-walled sections, $I_T = \frac{\sum bt^3}{3}$ (t is the thickness and b is the length of each wall segment) and $I_\psi = \int_A \psi^2 dA$ (ψ is the warping function), the latter of which being calculated typically through the Vlasov's sectorial area. This latter, however, is only an approximation to the warping function, representing only the so-called primary warping (or warping in the direction of the walls´ lengths), neglecting the secondary warping, or warping in the direction of the walls´ thickness.

Despite their applicability on various scenarios, it has been verified by some authors (see e.g. Campello [1], Campello and Lago [2], and Pimenta and Campello [3], motivated by the discoveries from Pimenta [4]) that there are simple, although pathological, situations in which the critical loads and the full bifurcation path far away from the trivial solution cannot be adequately predicted by such models. The use of linearized (or at most partially quadratic) constitutive equations, which do not enable full axial, bending and torsion strain coupling and besides are unsuited for finite strains,

combined with the lack of consistent considerations for the secondary warping, may explain the difficulties of these models in the pursuit of certain critical and post-critical solutions.

In order to incorporate more advanced (nonlinear, large-strain) constitutive equations, with higher order strain terms retained for proper strain coupling, the complete warping function (i.e., including both primary and secondary warpings) is required. In this case, computation of the stress resultants is better performed through numerical rather than analytical integration, since the latter, when possible, becomes very cumbersome, leading to numerous higher order cross-sectional geometrical properties that are far from trivial to be computed. The warping function, thus, must be explicitly (and a priori) defined at every point of the cross-section, as to enable the integration.

This research aims to propose contributions to an existent kinematically exact 7-DOF rod model for thin-walled open-section members, by proposing a consistent warping function with both primary and secondary warpings, and by developing an advanced elastic (neo-Hookean, polyconvex) constitutive equation for finite strains with all higher order strain terms for full strain coupling. Its effectiveness and reliability to predict critical loads and post-critical behaviour for rod structures consisted of such members shall be benchmarked. The study is being conducted using PEFSYS, an in-house nonlinear finite element method (FEM) program for structural analysis.

The structure of this document is as follows:

- Chapter 2: a compilation of useful concepts and a brief discussion on the evolution of rod models, evidencing the kinematical assumptions that characterizes each one of them; a generic way to present the kinematical assumptions for rod models is introduced;
- Chapter 3: the formulation of the 7-DOF kinematically exact rod model used in this work is described, and the weak form of the equilibrium (and its linearization) is stated. There, the proposed advances on the considerations of the warping function are presented;
- Chapter 4: the exact hyperelastic constitutive equations for Saint-Venant's and Simo-Ciarlet's materials are developed. The concept of *polyconvexity* is introduced;
- Chapter 5: a brief explanation of Finite Element Method for rods;
- Chapter 6: illustrative examples and benchmark of the proposed advances on the rod model;
- Chapter 7: conclusion;
- Appendix: several basic concepts and demonstrations are shown there.

Marcos Pires Kassab   25

Advances on a kinematically exact rod model for thin-walled open section members: consistent warping function and nonlinear constitutive equation

2. THEORETICAL BACKGROUND AND BIBLIOGRAPHICAL REVIEW

2.1. Notation

In order to be consistent with some of the established literature in the field, the following notation is adopted here:

- Lowercase Latin or Greek letters $(a, b, \dots, \alpha, \beta, \dots)$ denote scalar quantities;
- Bold lowercase Latin or Greek letters $(\boldsymbol{a}, \boldsymbol{b}, \dots, \boldsymbol{\alpha}, \boldsymbol{\beta}, \dots)$ denote vectors;
- Bold capital Latin or Greek letters $(\boldsymbol{A}, \boldsymbol{B}, \dots)$ denote second-order tensors;

Implicit summation convention is used throughout. When indices are Greek letters, they range from 1 to 2 and when they are Latin letters, from 1 to 3. Scalar, cross and dyadic products are represented by "·", "×" and "⊗", respectively. Symbol $\delta(\circ)$ denotes a virtual quantity (or, equivalently, a variation), whereas $(\circ)^r$ denotes either a quantity in the reference configuration, or a back-rotated quantity.

2.2. Solids mechanics concepts

Many concepts that are shown here have its origins on the classical continuum mechanics. In the current context, some of them might be particularized to *solids mechanics*, under *static elasticity*. It is suggested that the reader refers to Appendix A and Appendix B, for the most basic definitions, as some of them are used throughout the text.

2.2.1. Expressing finite rotations

Here, the noun *finite* means "arbitrarily large", and is the antonym of *infinitesimal*, which is the first order approximation (linearization).

In order to develop exact rod models, it is pivotal to exactly describe finite rotations, as it is an important source of non-linear behaviour. Formulations proposed by Argyris [5], [6] were crucial to understand this phenomenon, and allowed the first rod models to be consistently formulated.

In this chapter, an overview of the expressions that are of interest in section 3 are presented.

If a given tensor $\boldsymbol{Q}$ respects

$$det\boldsymbol{Q} = 1 \; and \; \boldsymbol{Q}^T\boldsymbol{Q} = \boldsymbol{I}, \tag{2.1}$$

then the transformation given by

$$\boldsymbol{v} = \boldsymbol{Q}\boldsymbol{v}^r, \tag{2.2}$$

expresses a rotation from the original vector $\boldsymbol{v}^r$ to $\boldsymbol{v}$. Note that, despite its vectorial-like expression, rotations do not obey commutativity. Thus, one cannot compose successive rotations by simple addition. Consider two successive pure rotational rigid body displacements, given by $\boldsymbol{Q}_1$ and $\boldsymbol{Q}_2$. The final position of a vector $\boldsymbol{v}$ is

$$\boldsymbol{v} = (\boldsymbol{Q}_1 \circ \boldsymbol{Q}_2)\boldsymbol{v}^r = \boldsymbol{Q}_2\boldsymbol{Q}_1\boldsymbol{v}^r, \tag{2.3}$$

where the symbol "∘" denotes the composition of two transformations.

As shown in [7], any rotation tensor can be parametrized as

$$Q = I + h_1(\theta)\boldsymbol{\Theta} + h_2(\theta)\boldsymbol{\Theta}^2 \tag{2.4}$$

In the current work, the option was to calculate the rotation tensor through the Euler-Rodrigues formula, expressed in terms of Euler rotation vector $\boldsymbol{\theta}$ ($\theta = ||\boldsymbol{\theta}||$ is the rotation angle magnitude, and $\boldsymbol{\theta}/\theta$ is the axis of rotation), where

$$h_1(\theta) = \frac{\sin\theta}{\theta} \ and \ h_2(\theta) = \frac{1}{2}\left(\frac{\sin\theta/2}{\theta/2}\right)^2 = \frac{1 - \cos\theta}{\theta^2}, \tag{2.5}$$

and $\boldsymbol{\Theta} = Skew(\boldsymbol{\theta})$ is a skew-symmetric tensor whose axial vector is $\boldsymbol{\theta}.$

Using Taylor's expansion, h_1 and h_2 can be expressed as

$$h_1(\theta) = \frac{sen\theta}{\theta} = 1 - \frac{1}{6}\theta^2 + \frac{1}{120}\theta^4 - O(\theta^6);$$
$$h_2(\theta) = \frac{1}{2}\left(\frac{\sin\theta/2}{\theta/2}\right)^2 = \frac{1}{2} - \frac{1}{24}\theta^2 + \frac{1}{720}\theta^4 - O(\theta^6). \tag{2.6}$$

Note that equation (2.4) and (2.5) present singularities in $n2\pi$, where n is an integer. It is shown ([1], [7]) that the singularity in 0 is removable (see equation (2.6)), although the ones in $n2\pi \neq 0$ are not.

Therefore, rotation magnitude in a total description must be limited to

$$0 \leq |\theta| < 2\pi. \tag{2.7}$$

Were more intense rotations to be computed, appropriate description could only be reached through incremental description, or by characterizing rotations with more than 3 parameters. This will not be explored in the current work.

In the context of finite rotations, several results concerning its derivatives are of interest. First, consider the derivative of Q with respect of any scalar.

Taking the scalar *time*, for example, there is a second order tensor skew-symmetric tensor $\boldsymbol{\Omega}$ that satisfies

$$\boldsymbol{\Omega} = \dot{Q}Q^T, axial(\boldsymbol{\Omega}) = \boldsymbol{\omega}. \tag{2.8}$$

The vector $\boldsymbol{\omega}$ is the *spin*, and the explicit expression for $\boldsymbol{\Omega}$ and $\boldsymbol{\omega}$ is

$$\boldsymbol{\Omega} = h_1(\theta)\,\dot{\boldsymbol{\Theta}} + h_2(\theta)\left(\boldsymbol{\Theta}\dot{\boldsymbol{\Theta}} - \dot{\boldsymbol{\Theta}}\boldsymbol{\Theta}\right) + h_3(\theta)\boldsymbol{\Theta}, \tag{2.9}$$

$$\boldsymbol{\omega} = \boldsymbol{\Gamma}\dot{\boldsymbol{\theta}}, \tag{2.10}$$

with

$$\boldsymbol{\Gamma} = I + h_2(\theta)\boldsymbol{\Theta} + h_3(\theta)\boldsymbol{\Theta}^2, \tag{2.11}$$

with

$$h_3(\theta) = \frac{1 - h_1(\theta)}{\theta^2} \tag{2.12}$$

The derivative of $\boldsymbol{\Gamma}$ with respect to scalars are also of interest. Again, taking time as this scalar

$$\dot{\boldsymbol{\Gamma}} = h_2(\theta)\dot{\boldsymbol{\Theta}} + h_3(\theta)(\boldsymbol{\theta}\cdot\dot{\boldsymbol{\theta}})(\boldsymbol{\Theta}\dot{\boldsymbol{\Theta}} + \dot{\boldsymbol{\Theta}}\boldsymbol{\Theta}) + h_4(\theta)(\boldsymbol{\theta}\cdot\dot{\boldsymbol{\theta}})\boldsymbol{\Theta}$$
$$+ h_5(\theta)\left(\boldsymbol{\theta}\cdot\dot{\boldsymbol{\theta}}\right)\boldsymbol{\Theta}^2 \tag{2.13}$$

Marcos Pires Kassab

27

Advances on a kinematically exact rod model for thin-walled open section members: consistent warping function and nonlinear constitutive equation

with

$$h_4(\theta) = \frac{h_1(\theta) - 2h_2(\theta)}{\theta^2}, \tag{2.14}$$

$$h_5(\theta) = \frac{h_2(\theta) - 3h_3(\theta)}{\theta^2}. \tag{2.15}$$

Similarly, for the scalar ζ that represents a cross-section position along the rod axis

$$\boldsymbol{K} = \boldsymbol{Q}'\boldsymbol{Q}^T, \; axial(\boldsymbol{K}) = \boldsymbol{\kappa}. \tag{2.16}$$

Note that, in equation (2.16), $(\circ)' = \frac{\partial}{\partial \zeta}(\circ)$. Thus,

$$\boldsymbol{K} = h_1(\theta)\boldsymbol{\Theta}' + h_2(\theta)(\boldsymbol{\Theta}\boldsymbol{\Theta}' - \boldsymbol{\Theta}'\boldsymbol{\Theta}) + h_3(\theta)\boldsymbol{\Theta}, \tag{2.17}$$

$$\boldsymbol{\kappa} = \boldsymbol{\Gamma}\boldsymbol{\theta}' \tag{2.18}$$

$$\boldsymbol{\Gamma}' = h_2(\theta)\boldsymbol{\Theta}' + h_3(\theta)(\boldsymbol{\Theta}\boldsymbol{\Theta}' + \boldsymbol{\Theta}'\boldsymbol{\Theta}) + h_4(\theta)(\boldsymbol{\theta} \cdot \boldsymbol{\theta}')\boldsymbol{\Theta} + h_5(\theta)(\boldsymbol{\theta} \cdot \boldsymbol{\theta}')\boldsymbol{\Theta}^2. \tag{2.19}$$

Other definitions that are useful for the current work are, for a given constant vector $\boldsymbol{t}$,

$$\boldsymbol{V}(\boldsymbol{\theta}, \boldsymbol{t}) = h_2(\theta)\boldsymbol{T} + h_3(\theta)(\boldsymbol{T}\boldsymbol{\Theta} - 2\boldsymbol{\Theta}\boldsymbol{T}) - h_4(\theta)(\boldsymbol{\Theta}\boldsymbol{t} \otimes \boldsymbol{\theta})$$
$$+ h_5(\theta)(\boldsymbol{\Theta}^2\boldsymbol{t} \otimes \boldsymbol{\theta}) \tag{2.20}$$

in which $\boldsymbol{T} = \boldsymbol{skew}(\boldsymbol{t})$ and

$$\boldsymbol{V}'(\boldsymbol{\theta}, \boldsymbol{t}) = h_4(\theta)(\boldsymbol{\theta} \cdot \boldsymbol{\theta}')\boldsymbol{T} + h_3(\theta)(\boldsymbol{T}\boldsymbol{\Theta}' - 2\boldsymbol{\Theta}'\boldsymbol{T})$$
$$+ h_5(\theta)(\boldsymbol{\theta} \cdot \boldsymbol{\theta}')(\boldsymbol{T}\boldsymbol{\Theta} - 2\boldsymbol{\Theta}\boldsymbol{T})$$
$$- h_4(\theta)(\boldsymbol{\Theta}'\boldsymbol{t} \otimes \boldsymbol{\theta} + \boldsymbol{\Theta}\boldsymbol{t} \otimes \boldsymbol{\theta}') - h_6(\theta)(\boldsymbol{\theta} \cdot \boldsymbol{\theta}')(\boldsymbol{\Theta}\boldsymbol{t} \otimes \boldsymbol{\theta}) \tag{2.21}$$
$$+ h_5(\theta)((\boldsymbol{\Theta}'\boldsymbol{\Theta} + \boldsymbol{\Theta}\boldsymbol{\Theta}')\boldsymbol{t} \otimes \boldsymbol{\theta} + \boldsymbol{\Theta}^2\boldsymbol{t} \otimes \boldsymbol{\theta}')$$
$$+ h_7(\theta)(\boldsymbol{\theta} \cdot \boldsymbol{\theta}')(\boldsymbol{\Theta}^2\boldsymbol{t} \otimes \boldsymbol{\theta})$$

with

$$h_6(\theta) = \frac{1}{\theta^2}[h_3(\theta) - h_2(\theta) - 4h_4(\theta)], \tag{2.22}$$

$$h_7(\theta) = \frac{1}{\theta^2}[h_4(\theta) - 5h_5(\theta)]. \tag{2.23}$$

The deductions of the equations (2.8) to (2.23) can be found in Appendix F. The tensors $\boldsymbol{V}$ and $\boldsymbol{V}'$ does not have any physical meaning – they are auxiliary expressions for the calculation of the geometric stiffness matrix (see section 3.3).

2.2.2. *Equations of motion*

It is recommended that readers that are not used to this topic consults Appendix A and Appendix B for the basic definitions of non-linear elasticity, especially for acknowledging the relations among the Cauchy, first and second Piola-Kirchoff stress tensors and the Nanson's rule.

In continuum mechanics, it is of interest to characterize the so-called *movement equations*. By applying the concepts of Linear and Angular momentum, it is possible to express the differential equations that relate forces to accelerations, and then, by integration, the velocities and displacements

of the continuum. In order to exist a unique solution, it is necessary that boundary conditions are applied. Let V be the whole system volume, with boundary S, in an arbitrary configuration. Then, this boundary can be divided in two partitions S_u and S_t. The region S_u is where kinematic boundary conditions are applied (prescribed displacements) and S_t is where the static boundary conditions are applied (prescribed surface loading). It must be noted that $S_u \cup S_t = S$ and $S_u \cap S_t = \emptyset$. Of course, it is implied that that there are no mixed boundary conditions (i.e. kinematical and statical boundary conditions at the same point). See Figure 1 for details.
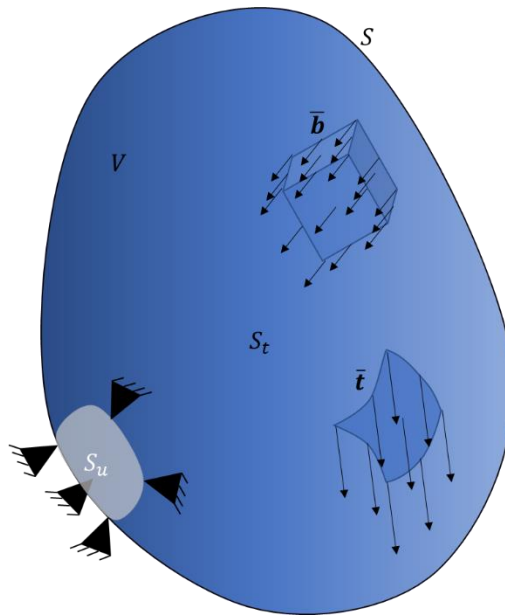
Figure 1 – Description of a body domain and boundary conditions

Having introduced the regions of the continuum, it is now possible to enunciate the motion equations. One can see the following deductions in more details in the book [8], from Wriggers.

2.2.2.1. Linear Momentum

Linear Momentum is defined as

$$\boldsymbol{L} = \int_{V^r} \rho^r \dot{\boldsymbol{u}} dV^r = \int_V \rho \dot{\boldsymbol{u}} dV. \tag{2.24}$$

where ρ^r, ρ is the density of the dominium in the initial and current configurations, respectively.

The principle of linear momentum is

$$\dot{\boldsymbol{L}} = \int_{S^r} \boldsymbol{t}^r dS^r + \int_{V^r} \boldsymbol{b}^r dV^r = \int_S \boldsymbol{t} dS + \int_V \boldsymbol{b} dV. \tag{2.25}$$

Using the divergence theorem in (2.25), one obtains

$$div\boldsymbol{T} + \boldsymbol{b} = \rho \ddot{\boldsymbol{u}}, \tag{2.26}$$

in which $\boldsymbol{T}$ is the Cauchy stress tensor. Using the reference configuration, equation (2.26) becomes

$$div\boldsymbol{P} + \boldsymbol{b}^r = \rho^r \ddot{\boldsymbol{u}}. \tag{2.27}$$

in which, $\boldsymbol{P}$ is the first Piola-Kirchoff stress tensor.

Marcos Pires Kassab   29

Advances on a kinematically exact rod model for thin-walled open section members: consistent warping function and nonlinear constitutive equation

The expressions (2.26) and (2.27) are the differential equations of motion.

2.2.2.2. Angular momentum

Angular momentum is defined as

$$J = \int_V x \times \rho \dot{u} dV = \int_{V^r} x \times \rho^r \dot{u} dV. \tag{2.28}$$

The principle of angular momentum states that

$$\dot{J} = \int_V x \times \bar{b} \, dV + \int_S x \times \bar{t} dS. \tag{2.29}$$

Thus,

$$\int_V x \times \bar{b} \, dV + \int_S x \times \bar{t} dS = \int_V x \times \rho \ddot{u} dV. \tag{2.30}$$

By using the Gauss theorem in the surface integral from equation (2.30), one gets that

$$\int_S x \times \bar{t} dS = \int_S x \times Tn dS = \int_S x \times (t_i \otimes e_i^r) n dS$$

$$= \int_S (x \times t_i) \otimes e_i^r n dS = \int_V div\big((x \times t_i) \otimes e_i^r\big) dV \tag{2.31}$$

$$= \int_V x_{,i} \times t_i + x \times t_{i,i} dV = \int_V 2 dual(T) + x \times div T dV,$$

with $dual(T) = axial(skew(T))$.

Using (2.26) in (2.31), the conclusion is that $dual(T) = o$, thus the Cauchy stress tensor must be symmetric

$$T = T^T. \tag{2.32}$$

2.2.3.   Work and Power of internal and external forces

The power associated to a force applied to a point is the scalar defined as

$$P = f \cdot \dot{u}. \tag{2.33}$$

The power associated to volume and surface forces are given by

$$P_v = \int_{V^r} b^r \cdot \dot{u} dV^r \; ; \; P_s = \int_{S^r} t^r \cdot \dot{u} dS^r, \tag{2.34}$$

where b^r and t^r are body and surface forces, respectively.

External forces power is defined as

$$P_{ext} = P_v + P_s. \tag{2.35}$$

The first Piola-Kirchoff P was already introduced in section 2.2.2. Let us now present the second Piola-Kirchoff S. Its definition and physical meaning can be found in Appendix B. They will be useful in the next definition.

Internal forces power is defined as

$$P_{int} = \int_{V^r} P : \dot{F} dV^r = \int_{V^r} S : \dot{E} dV^r. \tag{2.36}$$

30   Marcos Pires Kassab

Advances on a kinematically exact rod model for thin-walled open section members: consistent warping function and nonlinear constitutive equation

Due to this definition, the pairs $(\boldsymbol{E}, \boldsymbol{S})$ and $(\boldsymbol{F}, \boldsymbol{P})$ are called *energetically conjugated*. The tensors $\boldsymbol{F}$ and $\boldsymbol{E}$ are, respectively the deformation gradient and the Green-Lagrange strain tensors, as defined in Appendix A.

Work is simply the time integration of the power during an interval $[t_0, t]$.

$$W_{ext} = \int_{t_0}^{t} P_{ext}\, dt \; ;$$

$$W_{int} = \int_{t_0}^{t} P_{int}\, dt \; . \tag{2.37}$$

In dynamics, kinetic energy (using the reference configuration for integration) is

$$T = \tfrac{1}{2} \int_{V^r} \rho^r\, \dot{\boldsymbol{u}} \cdot \dot{\boldsymbol{u}}\, dV^r, \tag{2.38}$$

and its time derivative is

$$\dot{T} = \int_{V^r} \rho^r\, \dot{\boldsymbol{u}} \cdot \ddot{\boldsymbol{u}}\, dV^r. \tag{2.39}$$

From (2.34), using (B.5) and the divergence theorem

$$P_s = \int_{S^r} (\boldsymbol{P}\boldsymbol{n}^r) \cdot \dot{\boldsymbol{u}}\, dS^r = \int_{V^r} (div\boldsymbol{P} \cdot \dot{\boldsymbol{u}} + \boldsymbol{P} : div\dot{\boldsymbol{u}})dV^r =$$

$$\int_{V^r} (div\boldsymbol{P} \cdot \dot{\boldsymbol{u}})\boldsymbol{dV^r} + P_{int} \; . \tag{2.40}$$

Using equation (2.27)

$$P_s = \dot{T} - P_V + P_{int} \Rightarrow P_{ext} = P_{int} + \dot{T} \tag{2.41}$$

This is the *Power Theorem.* Integrating (2.41) w.r.t time,

$$W_{ext} = W_{int} + \Delta T, \tag{2.42}$$

where $\Delta T = T_t - T_{t_0}$.

Considering a quasi-static process, $\dot{T}$ and ΔT can be neglected. Then

$$P_{ext} = P_{int} \; ; W_{ext} = W_{int}. \tag{2.43}$$

2.2.4. *Equilibrium weak form: Virtual Work*

Let $\delta\boldsymbol{u} \in \mathcal{H}_1^{0\,1}(V^r)$ be an arbitrary vectorial field, called *virtual displacement*. Let us define the scalars *virtual external work (δW_{ext}), virtual internal work (δW_{int})* and *virtual kinetic energy (δT)*

$$\delta W_{ext} = \int_{V^r} \boldsymbol{b}^r \cdot \delta\boldsymbol{u}\, dV^r + \int_{S^r} \boldsymbol{t}^r \cdot \delta\boldsymbol{u}\, dS^r, \tag{2.44}$$

$$\delta W_{int} = \int_{V^r} \boldsymbol{P} : \delta\boldsymbol{F}\, dV^r, \tag{2.45}$$

$$\delta T = \int_{V^r} \rho^r \ddot{\boldsymbol{u}} \cdot \delta\boldsymbol{u}\, dV^r. \tag{2.46}$$

Note that equations (2.44) to (2.46) are merely definitions, based on the expressions of P_{ext}, P_{int} and $\dot{T}$. Sometimes, authors affirm that the Virtual Works Theorem reflects the minimization of a potential energy functional. This claim is partially correct: for conservative static problems, there is a potential energy functional U, and the Virtual Work theorem is indeed the condition for extremal

---

[1] $\delta\boldsymbol{u} \in \mathcal{H}_1^0 = \delta\boldsymbol{u} \in \boldsymbol{\mathcal{H}}_1 | \delta\boldsymbol{u} = \boldsymbol{0} \; in \; S_u.$

Marcos Pires Kassab   31

Advances on a kinematically exact rod model for thin-walled open section members: consistent warping function and nonlinear constitutive equation

points for functionals $\delta U = 0$. This is, however, a particular case of the weak form, which is valid for general continuum dynamics. In fact, for dynamics, δT (eq. (2.46)) is not even a variation of T (eq. (2.38)), but a convenient definition that arises from the demonstration of the Virtual Works Theorem. Consequently, the most appropriate manner to approach the virtual quantities $\delta \boldsymbol{u}$ is to interpret it only as the trial function of the weak form, instead of a variation.

Since $\delta \boldsymbol{u} = \boldsymbol{0}$ in S_u^r, and already imposing the natural boundary condition $\boldsymbol{t}^r = \bar{\boldsymbol{t}}^r$ in S_t^r, equation (2.44) becomes

$$\delta W_{ext} = \int_{V^r} \boldsymbol{b}^r \cdot \delta \boldsymbol{u} dV^r + \int_{S_t^r} \bar{\boldsymbol{t}}^r \cdot \delta \boldsymbol{u} dS^r. \tag{2.47}$$

Using a similar approach as done in (2.40),

$$\int_{S^r} (\boldsymbol{P}\boldsymbol{n}^r) \cdot \delta \boldsymbol{u} dS^r = \int_{V^r} (div\boldsymbol{P} \cdot \delta \boldsymbol{u} + \boldsymbol{P} \cdot div\delta \boldsymbol{u}) dV^r = \int_{V^r} (div\boldsymbol{P} \cdot \delta \boldsymbol{u}) dV^r + \\ \delta W_{int}. \tag{2.48}$$

Using the definitions (2.45), (2.46), (2.47)

$$\delta W_{ext} = \delta W_{int} + \delta T + \int_{V^r} (div\boldsymbol{P} + \boldsymbol{b}^r - \rho^r \ddot{\boldsymbol{u}}) \cdot \delta \boldsymbol{u} dV^r + \int_{S_t^r} (\bar{\boldsymbol{t}}^r - \boldsymbol{P}\boldsymbol{n}^r) \cdot \delta \boldsymbol{u} dS^r. \tag{2.49}$$

Thus, using the fundamental variational calculus lemma, one gets the Principle of Virtual Works

$$\delta W_{ext} = \delta W_{int} + \delta T, \forall \delta \boldsymbol{u} \in \mathcal{H}_1^0(V^r) \Leftrightarrow \begin{cases} div\boldsymbol{P} + \boldsymbol{b}^r - \rho^r \ddot{\boldsymbol{u}} = \boldsymbol{0} \ in \ V^r \\ \bar{\boldsymbol{t}}^r = \boldsymbol{P}\boldsymbol{n}^r \ in \ S^r \end{cases}. \tag{2.50}$$

For quasi-static processes, $\delta T = 0$, thus

$$\delta W_{ext} = \delta W_{int}, \forall \delta \boldsymbol{u} \in \mathcal{H}_1^0(V^r) \Leftrightarrow \begin{cases} div\boldsymbol{P} + \boldsymbol{b}^r - \rho^r \ddot{\boldsymbol{u}} = \boldsymbol{0} \ in \ V^r \\ \bar{\boldsymbol{t}}^r = \boldsymbol{P}\boldsymbol{n}^r \ in \ S^r \end{cases}, \tag{2.51}$$

hence,

$$\delta W_{ext} = \delta W_{int}, \forall \delta \boldsymbol{u} \in \mathcal{H}_1^0(V^r) \tag{2.52}$$

is a necessary and sufficient condition to achieve equilibrium. Notice that, besides the differential equilibrium expression, natural boundary conditions are also obtained. Essential conditions can be directly imposed through solution

$$\boldsymbol{u} = \bar{\boldsymbol{u}} \ in \ S_u. \tag{2.53}$$

and reactive forces in S_u are usually found after the solution of $\boldsymbol{u}$.

2.3. Rod models: a historical approach

2.3.1.   *Kinematically linear models*

Initial approaches of beam theories required analytical solutions to be manually found. Therefore, simplifying assumptions were invariably necessary. Typically, displacements, rotations and strains were treated as first order approximations, ultimately leading to linear equilibrium differential equations. This is equivalent to assuming small (infinitesimal) displacements, rotations and strains, so that the beam´s equilibrium can be evaluated at the undeformed configuration. Being linear, solutions could also be superimposed, and the behaviour of complex structures could be addressed as a simple summation of elementary solutions. The most relevant linear rod models kinematical hypotheses will

32   Marcos Pires Kassab

Advances on a kinematically exact rod model for thin-walled open section members: consistent warping function and nonlinear constitutive equation

be briefly discussed next. Some of the classical examples can be found in Timoshenko's books [9], [10], or in [11], from Bucalem and Bathe.

Bernoulli-Euler is the most elementary rod model. The kinematical assumption is that cross-sections remain plane and orthogonal to the beam´s axis. Timoshenko's rod model is less restrictive, as the orthogonality condition is removed, allowing for first order shear deformation. As both of them consider cross-sections as rigid planes, torsion is not adequately represented, since the warping deformation is missed.

Only when warping is enabled is that torsional response can be effectively evaluated. This motivated the Saint-Venant's uniform torsion theory, in which a cross-sectional shape function (usually represented by the Greek letter ψ), given from the solution to a certain boundary value problem, is incorporated. After obtaining the section´s warping shape, the section torsional inertia can be calculated. Such solution can be superimposed to other linear models, in order to more accurately predict torsion behaviour. The main drawback of this theory is that its solution is only exact if the torsion is uniform (i.e., constant along the rod´s axis) and both rod´s ends are free to warp. If these requirements are not fulfilled, the solution is only an approximation. Even in the absence of external torsion moments, coupling effects among bending, axial and torsion strains can severely affect the equilibrium and stability behaviour of thin-walled open-section rods if non-uniform torsion is not considered.

Despite its wide application for rods with open thin-walled cross-sections, the torsion phenomena are not satisfactorily explained by Saint-Venant's theory. Given the low torsional inertia of such sections, secondary twisting (or non-uniform torsion, or bi-shear) and warping moment (or bi-moment) play a major role as important load-carrying mechanisms on the rod´s equilibrium, and consequently, on the design of those elements. As an alternative, in the mid 1900´s Vlasov's theory [12] arises. An equivalent model was also proposed later by Timoshenko [9]), and soon became the theoretical foundation of many technical standards around the world for the design of rod structures consisted of thin-walled open-section members, such as steel structures in civil engineering (for example, but definitely not only, the Brazilian NBR8800:2008 [13]). Vlasov´s theory relies on the combination of a uniform torsion with a non-uniform torsion solution. The first one resorts to the Saint-Venant's torsion theory, whereas the latter is based on a quantity named *sectorial area* (usually represented by $\omega(s)$, in which s stands for the walls´ length coordinate), which arises from the assumption that the warping may be non-uniform. It can be calculated along the walls length from the line integral of twice the area comprehended in a particularly built triangular sector, which has as vertices the so-called sectorial pole, the point at which ω is being computed, and an infinitesimal base ds, tangent to the wall at that point. The integration begins at an arbitrary point, which is called sectorial origin. For a proper origin and using the same pole, it can be shown that the Vlasov's sectorial area corresponds to the Saint-Venant's warping function along the thin-walls midline.

Marcos Pires Kassab   33

Advances on a kinematically exact rod model for thin-walled open section members: consistent warping function and nonlinear constitutive equation

2.3.2.   *Kinematically exact models*

As structural design became more audacious, in both civil and mechanical engineering, theories that consider large displacements and rotations urged to be developed. The small displacements and infinitesimal rotations assumptions had to be dropped, introducing considerable non-linearities to the model´s differential equations. It was not until the 1980's that the first consistent exact theories were developed and successfully employed. Hardware improvements in processing capabilities and memory storage, as well as the emergence of advanced numerical methods were pivotal to such progress, as analytical solutions to non-linear systems are usually not available.

Unidimensional exact theories for plane (2D) frames have a peculiarity that allowed a hastier theoretical development: in plane motions (2D frames/plates), rotations can be treated as a part of a vectorial space, wherein the basic property of commutativity is properly satisfied. Reissner [14] is credited as the pioneer of 2D kinematically exact beam theories. A direct major drawback of 2D theories lies on the fact that it is restricted to plane problems, as it becomes impossible to capture out-of-plane deformations such as those arising from coupling effects between bending, tension/compression and torsion strains.

The first three-dimensional kinematically exact rod model was presented by Simo [15], [16], where a Timoshenko-like assumption (for the cross-sectional shearing w.r.t. the rod axis) was developed. The rotational degrees-of-freedom were exactly treated through the Euler-Rodrigues formula, and this was a major breakthrough at the time. Simo and Vu-Quoc [17] and Gruttmann et al. [18] also advanced towards considering a warping function, especially useful for torsion-dominated problems. Later on, several other authors derived their own formulations, many of them having as theoretical basis Simo's pioneering models. A brief list of unique formulations is described next.

Crisfield [19] and Chen and Blandford [20] derived their own kinematically exact models, with co-rotational description, the former being a 6 DOF model, and the latter being based on Vlasov's theory for thin-walled frames, with an additional warping DOF. Still in the co-rotational framework, Genoese *et al.* [21] derived a 7 DOF (with Saint-Venant´s warping) model.

Research group from the Polytechnic School of the University of São Paulo (lead by P. Pimenta and followed by E. M. B. Campello, with the collaboration of other authors such as Yojo, Dasambiago, Fernandes, Lago and da Costa e Silva [1]–[3], [22]–[27]) proposed a wide array of rod models, beginning with a Timoshenko-like 6 DOF model and then progressing towards more complex assumptions, ranging from 7-DOFs thin-walled open cross-section models (warping enabled) to more generic formulations, with an arbitrary amount of DOFs and general in-plane and out-of-plane cross-sectional distortions.

Coda [28], in collaboration with Paccola [29] and Maciel [30] progressed from 2D to 3D static and dynamic models, using a distinct solid-like formulation, wherein the rotational degrees-of-freedom

34   Marcos Pires Kassab

Advances on a kinematically exact rod model for thin-walled open section members: consistent warping function and nonlinear constitutive equation

were avoided by directly mapping cross-sectional position vectors instead, leading to the so-called "unconstrained vectors" formulation. This approach allows to naturally incorporate in- and out-of-plane distortions, having as trade-off an increase on the number of degrees of freedom. Comparatively, in this author's works, each node had 12 DOFs, whereas in [1], [2] and [18], 7 nodal DOFs were used for modelling 3D rods with finite rotations and warping.

Kumar and Mukherjee [31] proposed a rod model with in-plane distortions for cylindrical rods, pursuing to hierarchically link cylindrical shell and rod models. The authors affirm that the model has applications in biotechnology (e.g., can be used "for capturing cross-sectional deformation in DNA, nanotubes, collagen, arteries, etc").

Simo [15] was also the pioneer to consistently deduce the dynamic problem for 3D rods, presenting both material and spatial description for Timoshenko-like rods. Later on, Campello, Pimenta and Wriggers [32] faced the problem of non-conservativeness of usual time-integration schemes, proposing an algorithm that guaranteed exact conservation for dynamic rod problems. Liu *et al.* [33] used a mixed Eulerian-Lagrangian description to implement a dynamic Timoshenko-like rod model, that is able to represent a beam running through a tube, including the contact forces, during this operation.

Le Corvec´s [34] model had a different approach, by abandoning warping shape functions and discretizing the cross-section. Solution was then obtained by placing additional DOFs throughout the cross-section, interpolating values with Lagrangian polynomials and numerically integrating the forces, moments, bi-shear and bi-moment.

Gonçalves [35] and Li and Ma [36] also proposed 7 DOF thin-walled rod models, in which shell-like assumptions are used to characterize the secondary warping, whilst the primary warping is given by the Vlasov's sectorial area.

It is also worth mentioning works developed under the concept of the so-called Generalized Beam Theory (GBT), which, despite usually not following kinematically exact approaches, provide interesting insights into determining cross-sectional warping and in-plane distortion shape functions. This approach was inaugurated by the seminal works of Schardt [37]–[39], from which several others followed, with special mention to the contributions from D. Camotim's research group, such as [40]–[43]). The GBT approach might be an important source to enrich the vectorial space of admissible displacements of the cross-section, potentially permitting to study local (i.e., cross-sectional) buckling behaviour also in the non-linear context. In this framework, Gonçalves et al. [42], and Li and Ma [44] proposed thin-walled rod models in which, by using GBTs techniques, in- and out-of-plane distortion modes were obtained, and then linearly combined, in order to determine displacement modes for the walls midlines. As in the models of the last paragraph, for points along the thickness, Kirchhoff's plate assumption is enforced, thus determining their displacement.

Marcos Pires Kassab

35

Advances on a kinematically exact rod model for thin-walled open section members: consistent warping function and nonlinear constitutive equation

2.3.3. *A flexible description for intricate kinematic assumptions*
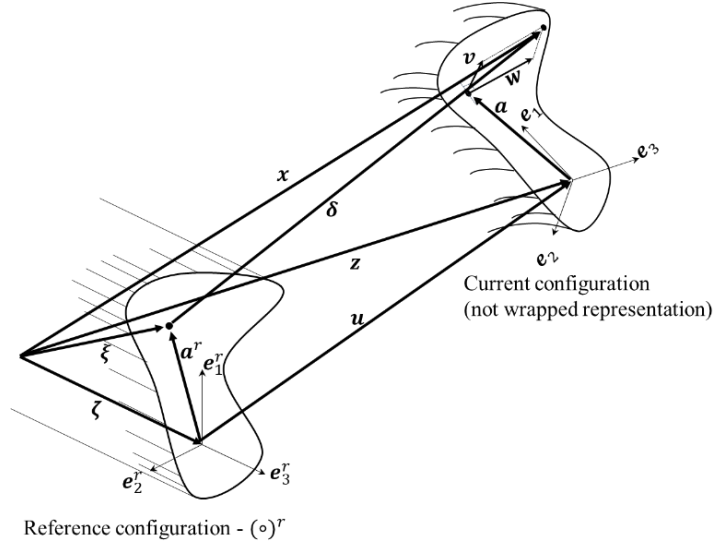
Figure 2 – Schematic representation and basic kinematical quantities used to describe the rod deformation.

Using a purely Lagrangian description, it is possible to map the cross-section allowed motion as a composition of a rigid body motion and a generic in-plane and out-of-plane deformation. Pimenta and Campello, in [23], presented a very robust way to describe such motion, with regards to the kinematical assumptions. This approach, which is the theoretical basis of the model that is incremented in this research, is briefly described in what follows.

Assuming a straight rod reference configuration, with a local orthonormal system $\{e_1^r, e_2^r, e_3^r\}$, with e_3^r coinciding with the rod´s axis (see Fig. 1), the position of every material point in the reference configuration can be described by

$$\xi = \zeta + a^r, \tag{2.54}$$

where

$$\zeta = \zeta e_3^r, \ \zeta \in \Omega = [0, L]. \tag{2.55}$$

The cross-sectional director of a point in the reference configuration is defined by

$$a^r = \xi_\alpha e_\alpha^r, \tag{2.56}$$

where ξ_α (in-plane components of ξ) describes cross-sectional plane of the initial configuration.

Defining now $\{e_1, e_2, e_3\}$ as a local orthonormal system on the current configuration, with e_α being vectors that define the cross-section´s plane before warping, this rotated base is given by a rotation tensor $Q = \widehat{Q}(\zeta)$, such that $e_i = Qe_i^r$. Notice that there is no constraint that imposes agreement between e_3 and the rod axis in the current configuration. Thus, first-order shear deformations are implicitly considered. In the current configuration, the position of every material point is given by the vector field

$$x = z + y, \tag{2.57}$$

where $z = \hat{z}(\zeta)$ represents the position of axis points in the current configuration, and y represents the position of points of the cross-section relatively to the rod´s translated axis (see Figure 2).

The translation of the axis can be represented by

$$u = z - \zeta, \tag{2.58}$$

and for a generic point, the displacement is

$$\delta = x - \xi. \tag{2.59}$$

Vector y may be decomposed into three components:

$$y = a + v + w. \tag{2.60}$$

The components (a, v, w) represent the position of cross-sectional points (w.r.t. the rod´s axis) due to rigid body rotation (a), and their displacements due to in-plane distortion (v) and out-of-plane warping (w). By definition,

$$a = Qa^r, \tag{2.61}$$

wherein Q is the rotation tensor, calculated as in section 2.2.1, expression (2.4). Cross-sectional in-plane displacements and out-of-plane warping are respectively given by

$$v = v_\beta e_\beta; \quad w = w e_3. \tag{2.62}$$

Kinematical assumptions regarding v and w must then be introduced. A great array of assumptions can be made in order to capture cross-sectional behaviour.

In [23], it is assumed that both warping and in-plane displacements may be given as a linear relation between cross-sectional shape functions and the vectors that collect the respective magnitudes. The structure of those shape functions will be discussed later. Accordingly, v and w can be written as

$$v = (e_\beta \otimes \Phi_\beta) r = v_\beta e_\beta; \quad w = (e_3 \otimes \psi) p = w e_3, \tag{2.63}$$

with the directional components

$$v_\beta = \Phi_\beta \cdot r; \quad w = \psi \cdot p . \tag{2.64}$$

In those equations, $\Phi_\beta = \widehat{\Phi}_\beta(\xi_1, \xi_2)$ and $\psi = \widehat{\psi}(\xi_1, \xi_2)$ represent the cross-sectional shape functions for in-plane displacements and out-of-plane warping, respectively, while $r = \hat{r}(\zeta)$ and $p = \hat{p}(\zeta)$ are vectors that collect the corresponding degrees of freedom, with n_v DOFs for in-plane displacements and n_w DOF's for out-of-plane warping. Consequently, along with u and θ (rigid body motions), a model is represented by $6 + n_v + n_w$ DOFs. This approach provides great flexibility to the model description, allowing different kinematics to be enforced and generic shape functions to be adopted. Note that, despite the linear relation, these functions are completely generic so far.

In the next subsections, particular kinematical assumptions will be introduced, recovering some well-established models from the literature as particular cases of [23]. This will help to highlight difficulties and advances that have been performed over the last few decades in the area. As seen in all cited works, despite [2], it is usual that, although finite displacements and rotations are allowed, constitutive equations are truncated as they do not retain (some or all) higher order strain terms. This

Marcos Pires Kassab

37

Advances on a kinematically exact rod model for thin-walled open section members: consistent warping function and nonlinear constitutive equation

simplification allows for the obtention of stress resultants as function of trivial geometrical properties, although limits the application to small strain cases. Were all strain terms to be obtained, two approaches are possible a) numerical integration of stress resultant and tangent matrixes; b) for the particular cases that have analytical solution (usually polynomial on the strain measure stress components) appropriate analytical integration is possible, by determining generalized (non-conventional) geometric properties, which are pre-integrated and used as constant values upon solution.

2.3.3.1. Model with fully rigid cross-section (6 DOFs)

The basic assumption here is that each cross-section moves solely as a rigid body, and thereby remains plane and undistorted after the deformation, without any warping nor in-plane deformations. This implies $v = w = 0$, and is precisely what Simo proposed in [15] and [16] (the latter with the collaboration of Vu-Quoc), and Pimenta and Yojo in [22]. It is important to mention that Simo's formulation presented a non-symmetric geometric stiffness matrix, whereas, in the works from Pimenta, it is symmetric. Fernandes [26] identified that this is due to the fact that the weak form from Simo used a non-conjugated (energetically speaking) virtual quantity in the moment contribution, leading to a Petrov-Galerkin interpolation in the Finite Element Method. Other authors with relevant contributions to these first 3D, 6-DOF beam models can be cited, e.g. Argyris [5], [6], [45] and Ibrahimbegovic [46], [47]. Those works provided valuable knowledge on finite rotations (and their derivatives), one of the greatest challenges for exact beam formulations at the time.

The model ends up with 6 DOFs and is a generalization of Timoshenko's beam theory for finite displacements and rotations. As a consequence, if further assumptions are not taken, the polar moment of inertia (I_0) should characterize the torsional stiffness. As to avoid an artificially stiff cross section, one typically replaces I_0 by expressions containing the Saint-Venant´s torsion inertia (I_T) at the constitutive equation. It should be noted, however, that this apparently *ad-hoc* modification can be formally justified by adequately constraining the kinematically exact 7-DOF model, as done in Gruttmann et al. [48] (see also Appendix J).

2.3.3.2. Model with in-plane rigid and out-of-plane deformable cross-section (7 DOFs)

Simo and Vu-Quoc, in [17], proposed the use of the Saint-Venant´s warping function, in order to more accurately represent torsion phenomena for compact (massive) sections. Later, Pimenta and Campello revisited this topic in in [1], [3], in the context of open thin-walled sections. There, the geometrical properties of torsion inertia (I_T) and warping constant (I_ψ) can be analytically calculated, through the Saint-Venant expression for thin-walled sections ($I_T = \frac{\sum bt^3}{3}$) and Vlasov´s sectorial area (ω), respectively.

38   Marcos Pires Kassab

Advances on a kinematically exact rod model for thin-walled open section members: consistent warping function and nonlinear constitutive equation

Besides the 6 DOFs required to represent the rigid body displacements, 1 new DOF (p) was used for the warping magnitude. Therein, such distortion was represented by the product of a cross-sectional shape function (ψ) and its (unknown) magnitude (p). In-plane distortions were not considered. By introducing an independent DOF for warping, such models allow for out-of-plane non-uniform warping, especially important to more accurately represent the deformation of thin-walled members. Therefore, in this model equation (2.62) simplifies to

$$w = \psi p e_3; \quad v = 0. \tag{2.65}$$

Constitutive equations with the linear elastic, the classical Saint-Venant´s hyperelastic, as well as an advanced neo-Hookean material, therein called Simo-Ciarlet´s material[2], were available upon implementation. For the sake of simplicity, however, in [1], only second-order strain terms related to the specific rotations and displacements were retained in the constitutive equations, along with only first-order terms on the warping strains. In 2001, Pimenta and Campello presented in ECCM [3] an evolution of this model, incorporating second-order warping strains. Even with those new features, post-critical behaviour was still unsatisfactorily represented in a few pathological cases, as reported then.

2.3.3.3. *Model with in-plane rigid and out-of-plane deformable cross-section with secondary warping for open thin-walled members (7 DOFs)*

Lago and Campello [2] presented a kinematically exact rod model that incorporates some kind of secondary warping with "exact" (i.e., with all higher order strain terms retained) hyperelastic (St.-Venant´s) constitutive equation. The warping shape function ψ was admitted to be a composition of Vlasov´s (for primary) and a local Saint-Venant´s (which includes secondary) warping functions for thin-walled sections. For the Saint-Venant's contribution, the cross-section was treated as a composition of thin rectangular segments (see Figure 3). Accordingly, the warping function read

$$\psi(\xi_1, \xi_2) = \omega(s) + \psi_R(\bar{x}, \bar{y}). \tag{2.66}$$

In this context, $\omega(s)$ represents the sectorial area, derived from Vlasov's theory, and $\psi_R(\bar{x}, \bar{y})$ is an approximated solution for uniform torsion on rectangular cross-sections, obtained by Silva [49], with respect to local (wall´s) coordinates $\bar{x}$ and $\bar{y}$, with the form

$$\psi_R(\bar{x}, \bar{y}) = -\frac{(a^6 + 19a^4b^2 - 19a^2b^4 - b^6)\overline{xy}}{a^6 + 14a^4b^2 + 14a^2b^4 + b^6} - \frac{\frac{35}{12}a^2b^2(-4\bar{x}^3\bar{y} + 4\bar{x}\bar{y}^3)}{a^6 + 14a^4b^2 + 14a^2b^4 + b^6}. \tag{2.67}$$

---

[2] Or simply *Simo's material*.

Marcos Pires Kassab   39

Advances on a kinematically exact rod model for thin-walled open section members: consistent warping function and nonlinear constitutive equation
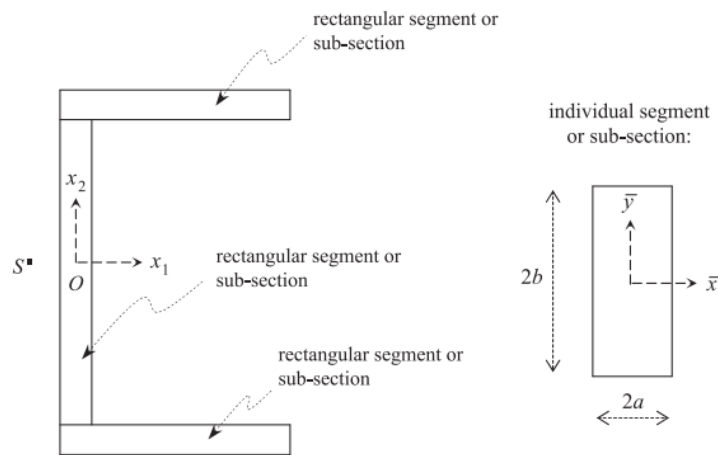
Figure 3 – Cross section composition. Source: Campello and Lago [2]

As a result, the kinematical assumptions became, as in section 2.3.3.2,

$$\boldsymbol{w} = \psi p \boldsymbol{e_3}; \quad \boldsymbol{v} = \boldsymbol{0}, \tag{2.68}$$

but with a different warping function, as presented above.

Lago and Campello [2] also evaluated the importance of having all higher order strain terms on the constitutive equation, by employing the so-called "exact" Saint-Venant´s material instead of linear elastic or incomplete quadratic ones. These new aspects required a slightly different approach to calculate cross-sectional force and moment (as well as bi-shear and bi-moment) stress resultants. Whereas in all other previous models the cross-sectional resultants were computed analytically by adding products of cross-sections geometrical properties (calculated *a priori*) and generalized strains, this work resorted to numerical integration for both stress resultants and material stiffness. Yet, despite the promising results, it was developed only for rectangular, I-shaped (bi-symmetric) and cruciform sections. See section 3.4.2 for a broader discussion about this warping function. Moreover, the effect of the proposed secondary warping was not assessed, as the authors were mainly concerned with the constitutive equation then.

Some authors (see for example Gonçalves [35] or Li and Ma [36]) have proposed a local plate approach, in which the primary warping was given by the Vlasov's sectorial area, and then a secondary warping is obtained by imposing Kirchhoff´s plate assumptions, considering that the related strains are small. Using this same argument, high order strain terms are discarded, rendering linear or, at most, incomplete quadratic constitutive relation. It should be noted that, in those works, the primary warping is exclusively a function of the warping degree of freedom, whereas the beforementioned plate assumptions render a secondary warping that is a function of both warping intensity and local curvature strains. Thus, such approach cannot be directly represented as in equation (2.62), as it allows only for linear combinations of independent warping intensity parameters and warping modes.

40   Marcos Pires Kassab

Advances on a kinematically exact rod model for thin-walled open section members: consistent warping function and nonlinear constitutive equation

2.3.3.4. Model with in-plane and out-of-plane deformable cross-section

This model theory was first presented by Pimenta and Campello in 2003 [23] and can be interpreted as a generalization of the previous approaches allowing for generic $\boldsymbol{v}$ and $\boldsymbol{w}$. Implementation presented by Dasambiago, Pimenta and Campello in [24], [25] (therein called "Multi-Parameter Beam Element" - MPBE) considered both in- and out-of-plane deformations, employing the shape functions approach described above (equation (2.62)). Therein, the authors chose to represent in-plane distortions through quadratic functions that required 3 additional DOFs (grouped into vector $\boldsymbol{r}$). However, the formulation is generic and can be adapted to any shape functions with any amounts of DOFs. Despite the consideration of in-plane distortions, the authors restricted the implementation to rods with rectangular cross-sections only, where the warping deformation could be satisfactorily represented by a linearized Saint-Venant's warping function. The kinematical assumptions for this model are

$$w = \psi p; \qquad v_\beta = \boldsymbol{\phi_\beta} \cdot \boldsymbol{r}; \tag{2.69}$$

$$\psi = \xi_1 \xi_2; \quad \boldsymbol{\phi_1} = \begin{bmatrix} \xi_1 \\ 1/_2\,\xi_1^2 \\ \xi_1\xi_2 \end{bmatrix}, \quad \boldsymbol{\phi_1} = \begin{bmatrix} \xi_2 \\ \xi_1\xi_2 \\ 1/_2\,\xi_2^2 \end{bmatrix} \quad \text{and} \quad \boldsymbol{r} = \begin{bmatrix} r_1 \\ r_2 \\ r_3 \end{bmatrix}. \tag{2.70}$$

More recently, the already mentioned authors (Gonçalves et al. [42] and Li and Ma [44]) worked towards the implementation of rod models with in-plane distortional modes for thin-walled rods. Both of them employ GBT techniques to determine distortional modes for the walls mid-lines, which are linearly combined. Afterwards, a secondary warping is calculated so that Kirchhoff´s assumption for plates holds, assuming small strains. There are differences between how those two models generate those modes: the first one treats in- and out-of-plane modes altogether, whereas the second one generates in-plane distortion mode from GBT and then the warping function is obtained either from Vlasov's sectorial area or from an independent Hermitian interpolation. Both these works induce plate behaviour for each wall, which might present incompatibilities between the local behaviour and global effects, which are treated in an *ad-hoc* fashion, separating membrane and bending deformations, and assuming different constitutive equations for each one of those contributions. Indeed, as mentioned by Gonçalves: "A plane stress state is assumed in all beam walls (…), thus generating a mild inconsistency with the plane strain of (36) and (37)." [42], and by Li and Ma: "Considering that the extension deformation in mid-line direction has not been included in the cross-section deformation modes, unreasonable transverse normal stress is probably introduced if the traditional constitutive relation is used. Therefore, different constitutive relations are employed for membrane deformation and bending deformation, respectively." [44].

In the context of rods, the models mentioned in the current section seem to be the most advanced in the literature, at least for thin-walled sections, despite the use of simple constitutive equation, with excellent results in benchmarks.

Marcos Pires Kassab 41

Advances on a kinematically exact rod model for thin-walled open section members: consistent warping function and nonlinear constitutive equation

3.   ADOPTED MODEL AND PROPOSED WARPING FUNCTION

The model to be advanced in this work is the 7-DOF, Vlasov-like kinematically exact rod model of section 2.2.3.3 (and 2.2.3.2). It is Vlasov-like in the sense that non-uniform warping is considered, allowing for normal stresses that arise from this warping, which generate the so-called bi-moments and bi-shears. A total Lagrangian description is adopted, and rotations are parametrized trough the Euler-Rodrigues rotation vector (this is the reason why the sub-index $(\circ)_\theta$ is sometimes used, as in [1]). As seen in the previous chapter, the formulation is a particularization for 7 DOFs of the generic model for any amount of DOFs, from Campello and Pimenta [23]. A wide array of works from the same research group also uses this approach (see, for example [2], [24]).

This master´s degree research aims to take the next logical step towards a more robust thin-walled rod model of such type: to develop a consistent warping function with both primary and secondary warping contributions for arbitrary thin-walled open sections, and derive an "exact", large-strain (neo-Hookean, Simo-Ciarlet's polyconvex) constitutive equation (this latter will be the object of Chapter 4). The "exact" Saint-Venant's constitutive equation must also be implemented, for the sake of comparison.

The model´s kinematics, weak form and corresponding tangent bilinear form will be detailed next. Then, the warping function will be introduced. A crucial point in this research is to explicitly report the kinematical assumptions and material laws that were explored. Here, they are:

Kinematical assumptions: the allowed motions are cross-sectional rigid body rotations and translations, along with a warping function that accounts for both primary and secondary warping modes. Arbitrary shapes for thin-walled open cross-sections are admitted. Two warping functions are considered and compared: the one from Lago and Campello [2] (equation (2.66)) and an improvement of this equation, shown in section 3.4. As will be illustrated in the next topic, the latter has proven to be more broadly applicable than the former.

Constitutive equation: the final product of this work will consider the neo-Hookean (polyconvex) material law of Simo-Ciarlet. Its corresponding "exact" constitutive equation for rods (i.e., including all strain terms) will be derived and implemented. This will require numerical integration over the cross-section for computation of the cross-sectional stress resultants. The exact form of the non-polyconvex Saint-Venant's material was implemented (as in Campello and Lago [2]), as its detailed expressions were already available and it will be needed in the future for comparison.

A brief description of the model is presented below. For more information, an extensive literature is at disposal. It is suggested, for example, the reading of Simo's and Vu-Quoc's [17] and Campello and Pimenta [3] for more details about 7 DOFs rod models.

3.1. Kinematic description

As already mentioned, this model has 6 rigid-body-related DOFs and an additional one that represents the warping intensity (see Figure 2). Formally, the displacements field is represented by equation (2.60), constrained to $v = 0$ and $w = p\psi e_3$. Therefore,

$$x = \zeta + u + Qa^r + p\psi e_3. \tag{3.1}$$

As already mentioned, the rotations are parametrized by the Euler-Rodrigues formula (equation(2.4)). It is important to remark that $u = \hat{u}(\zeta)$, $Q = \widehat{Q}(\widehat{\theta}(\zeta))$ and $p = \hat{p}(\zeta)$.

As in Pimenta and Campello [3], the deformation gradient must be calculated, rendering

$$F = \frac{\partial x}{\partial \xi} = x_{,\alpha} \otimes e_\alpha^r + x' \otimes e_3^r$$
$$= \left(Qe_\alpha^r + p\psi_{,\alpha}e_3\right) \otimes e_\alpha^r \tag{3.2}$$
$$+ (e_3^r + u' + Q'a^r + p'\psi e_3 + p\psi e_3') \otimes e_3^r$$

Introducing the definitions $\eta = u' + e_3^r - e_3$, one gets

$$F = Q\left(e_\alpha^r + p\psi_{,\alpha}e_3^r\right) \otimes e_\alpha^r + \tag{3.3}$$
$$+(\eta + Qe_3^r + Q'Q^Ta + p'\psi Qe_3^r + p\psi Q'Q^Te_3) \otimes e_3^r.$$

As shown in Pimenta and Yojo [22], the derivatives of Q can be found with the aid of the auxiliar tensor Γ. From equations (2.16)-(2.18), and using the above relation, one gets,

$$F = Q + p\psi_{,\alpha}Qe_3^r \otimes e_\alpha^r + (\eta + K(a + p\psi e_3) + p'\psi e_3) \otimes e_3^r = \tag{3.4}$$
$$= Q[I + p\psi_{,\alpha}e_3^r \otimes e_\alpha^r + Q^T(\eta + \kappa \times (a + p\psi e_3) + p'\psi e_3) \otimes e_3^r].$$

Defining the back-rotated vectors

$$\gamma^r = Q^T\gamma = \eta^r + \kappa^r \times (a^r + p\psi e_3^r) + p'\psi e_3^r, \tag{3.5}$$
$$\eta^r = Q^T\eta = Q^Tz' - e_3^r, \tag{3.6}$$
$$\kappa^r = Q^T\kappa = \Gamma^T\theta', \tag{3.7}$$

the final form of the deformation gradient arises as

$$F = \frac{\partial x}{\partial \xi} = QF^r = Q\left(I + p\psi_{,\alpha}e_3^r \otimes e_\alpha^r + \gamma^r \otimes e_3^r\right), \tag{3.8}$$

It is useful to define the generalized displacement (d_θ) and the generalized strain (ε^r) vectors,

$$d_\theta = \begin{bmatrix} u \\ \theta \\ p \end{bmatrix}_{(7x1)} \quad and \quad \varepsilon^r = \begin{bmatrix} \eta^r \\ \kappa^r \\ p \\ p' \end{bmatrix}_{(8x1)}. \tag{3.9}$$

Note that d_θ groups the degrees of freedom that are calculated at the nodes of the FEM analysis.

Now, it is necessary to find the derivative of F with respect to a scalar variable, for example time, in order to compute the Fréchet derivative, that will be needed in the next section. Thus

$$\dot{F} = \dot{Q}F^r + Q\dot{F}^r. \tag{3.10}$$

Defining the skew-symmetric $\Omega = \dot{Q}Q^T$, and $\omega = axial(\Omega) = \Gamma\dot{\theta}$, one gets

Marcos Pires Kassab

43

Advances on a kinematically exact rod model for thin-walled open section members: consistent warping function and nonlinear constitutive equation

$$\dot{F} = \Omega F + Q(\dot{p}\psi_{,\alpha}e_3^r \otimes e_\alpha^r + \dot{\gamma}^r \otimes e_3^r), \tag{3.11}$$

and it is necessary to find $\dot{\gamma}^r$, and, consequently, $\dot{\eta}^r$ and $\dot{\kappa}^r$.

First, let us deduce $\dot{\eta}^r$. Directly from its definition,

$$\begin{aligned}
\dot{\eta}^r &= \frac{d}{dt}(Q^T z' - e_3^r) = \dot{Q}^T z' + Q^T \dot{z}' = -Q^T \Omega z' + Q^T \dot{u}' \\
&= Q^T(\dot{u}' - \Omega z') = Q^T(\dot{u}' - \omega \times z') = Q^T(\dot{u}' - \Gamma\dot{\theta} \times z') \\
&= Q^T(\dot{u}' - Z'\Gamma\dot{\theta}),
\end{aligned} \tag{3.12}$$

where $Z' = skew(z')$.

Then, let us deduce $\dot{\kappa}^r$. Using the definitions above, using the properties of skew-symmetry of Q and Ω, one gets,

$$\dot{\kappa}^r = \dot{Q}^T \kappa + Q^T \dot{\kappa} = -Q^T \Omega \kappa + Q^T \dot{\kappa} = Q^T(\dot{\kappa} - \omega \times \kappa). \tag{3.13}$$

Some auxiliary algebra is needed. First, let us make

$$\begin{cases} \dot{Q} = \Omega Q \\ Q' = KQ \end{cases} \Rightarrow \begin{cases} \dot{Q}' = \Omega' Q + \Omega Q' & (a) \\ \dot{Q}' = \dot{K}Q + K\dot{Q} & (b) \end{cases}, \tag{3.14}$$

and imposing $(a) = (b)$, and multiplying by Q^T, one gets

$$\Omega' = \dot{K} + K\Omega - \Omega K. \tag{3.15}$$

With the aid of the intermediate result that, for vectors $a|axial(a) = A$ and $b|axial(b) = B$, $skew(a \times b) = AB - BA$, it is possible to find

$$\omega' = \dot{\kappa} + \kappa \times \omega \Rightarrow \omega' = \dot{\kappa} - \omega \times \kappa. \tag{3.16}$$

Therefore,

$$\dot{\kappa}^r = Q^T \omega' = Q^T(\Gamma'\theta + \Gamma\theta'). \tag{3.17}$$

Now, $\dot{\gamma}^r$ is easily calculated as

$$\dot{\gamma}^r = \dot{\eta}^r + \dot{\kappa}^r \times (a^r + p\psi e_3^r) + \kappa^r \times (\dot{p}\psi e_3^r) + \dot{p}'\psi e_3^r, \tag{3.18}$$

and

$$\dot{F} = \Omega F + Q(\dot{p}\psi_{,\alpha}e_3^r \otimes e_\alpha^r + \dot{\gamma}^r \otimes e_3^r), \tag{3.19}$$

The tensor Ω is the angular velocity, that arises from the derivation of Q with respect to time, and is documented in Pimenta and Yojo [22].

The time derivative of d_θ and ε^r can be compactly related in the following matrix notation,

$$\dot{\varepsilon}^r = \Psi \Delta \dot{d}_\theta = \begin{bmatrix} Q^T \dot{u}' + Q^T Z'\Gamma\dot{\theta} \\ Q^T \Gamma'\dot{\theta} + Q^T \Gamma\dot{\theta}' \\ \dot{p} \\ \dot{p}' \end{bmatrix}, \tag{3.20}$$

with the auxiliary operators

$$\Psi = \begin{bmatrix} Q^T & 0 & o & o \\ 0 & Q^T & o & o \\ o^T & o^T & 1 & 0 \\ o^T & o^T & 0 & 1 \end{bmatrix} \begin{bmatrix} I & Z'\Gamma & 0 & o & o \\ 0 & \Gamma' & \Gamma & o & o \\ o^T & o^T & o^T & 1 & 0 \\ o^T & o^T & o^T & 0 & 1 \end{bmatrix} \text{ and} \tag{3.21}$$

44   Marcos Pires Kassab

Advances on a kinematically exact rod model for thin-walled open section members: consistent warping function and nonlinear constitutive equation

$$\Delta = \begin{bmatrix} I\frac{\partial}{\partial\zeta} & \mathbf{0} & \mathbf{o} \\ \mathbf{0} & I & \mathbf{o} \\ \mathbf{0} & I\frac{\partial}{\partial\zeta} & \mathbf{o} \\ \mathbf{o}^T & \mathbf{o}^T & 1 \\ \mathbf{o}^T & \mathbf{o}^T & \frac{\partial}{\partial\zeta} \end{bmatrix}$$

3.2. Statics: Equilibrium weak form

Consider a rod element. Its volume in the reference configuration is V^r, with a cross-sectional area A^r and the axial coordinate $\zeta \in \Omega = [0, L]$, in which L represents the length of such element.

The equilibrium can be imposed by the weak form. Let $\delta \boldsymbol{d}_\theta = [\delta \boldsymbol{u} \quad \delta \boldsymbol{\theta} \quad \delta p]^T$ be the virtual displacements field. The notation $\mathcal{H}_1$ denotes a Sobolev space. Thus, the condition $\delta \boldsymbol{d}_\theta(\zeta) \in \mathcal{H}_1^0(V^r)$ means that **a)** $\delta \boldsymbol{d}_\theta$ is locally integrable and **b)** the appropriate components from $\delta \boldsymbol{d}_\theta$ are taken as 0 for the prescribed generalized displacements at the extremities with applied kinematic boundary conditions. For rods, one gets

$$\delta W = \delta W_{int} - \delta W_{ext} = 0 \, , \quad \forall \delta \boldsymbol{d}_\theta(\zeta) \in \mathcal{H}_1^0(V^r). \tag{3.22}$$

Using the energetically conjugated pair $(\boldsymbol{F}, \boldsymbol{P})$, wherein $\boldsymbol{P}$ is the first Piola-Kirchhoff stress tensor, and having in mind that the scalar derivatives (equation (3.19)) are useful for calculating the virtual quantities, for the internal power, one gets

$$P_{int} = \int_{V^r} \boldsymbol{P} : \dot{\boldsymbol{F}} dV^r = \int_0^L \int_{A^r} \boldsymbol{P} : \dot{\boldsymbol{F}} dA^r d\zeta. \tag{3.23}$$

Let us focus on the internal product $\boldsymbol{P} : \dot{\boldsymbol{F}}$. Using equation (3.11), this product is

$$\boldsymbol{P} : \dot{\boldsymbol{F}} = \boldsymbol{P} : \boldsymbol{\Omega} \boldsymbol{F} + \boldsymbol{P} : \boldsymbol{Q} \{ \psi_{,\alpha} \dot{p} \boldsymbol{e}_3^r \otimes \boldsymbol{e}_\alpha^r + \dot{\boldsymbol{\gamma}}^r \otimes \boldsymbol{e}_3^r \}. \tag{3.24}$$

Knowing that the internal product of a skew-symmetric and a symmetric tensor is zero, and remembering that, by consequence of (B.4) and (2.32), $\boldsymbol{P}\boldsymbol{F}^T$ is symmetric, it can be concluded that the first term is null. Defining the back-rotated first Piola-Kirchoff tensor as $\boldsymbol{P}^r = \boldsymbol{Q}^T \boldsymbol{P} = \boldsymbol{\tau}_i^r \otimes \boldsymbol{e}_i^r$ (thus, $\boldsymbol{\tau}_i^r$ are the column-vectors $\boldsymbol{P}^r$)**,** it is possible to rearrange the last equation, leading to

$$\boldsymbol{P} : \dot{\boldsymbol{F}} = \boldsymbol{\tau}_i^r \otimes \boldsymbol{e}_i^r : \{ \psi_{,\alpha} \dot{p} \boldsymbol{e}_3^r \otimes \boldsymbol{e}_\alpha^r + \dot{\boldsymbol{\gamma}}^r \otimes \boldsymbol{e}_3^r \}. \tag{3.25}$$

Note that the real stress $\boldsymbol{\tau}_i$, represented on the current base $\boldsymbol{e}_i$ (components $(\boldsymbol{\tau}_i \cdot \boldsymbol{e}_i)$) are component-wise equivalent to the back-rotated stress $\boldsymbol{\tau}_i^r$, represented on the reference base $\boldsymbol{e}_i^r$ (components $(\boldsymbol{\tau}_i^r \cdot \boldsymbol{e}_i^r)$). This can be easily shown by writing $(\boldsymbol{\tau}_i \cdot \boldsymbol{e}_i)\boldsymbol{e}_i$ and $\boldsymbol{\tau}_i^r = (\boldsymbol{\tau}_i^r \cdot \boldsymbol{e}_i^r)\boldsymbol{e}_i^r \to \boldsymbol{\tau}_i^r = \boldsymbol{Q}^T \boldsymbol{\tau}_i \Rightarrow (\boldsymbol{\tau}_i^r \cdot \boldsymbol{e}_i^r)\boldsymbol{e}_i^r = (\boldsymbol{\tau}_i \cdot \boldsymbol{e}_i)\boldsymbol{Q}^T \boldsymbol{e}_i \Rightarrow (\boldsymbol{\tau}_i^r \cdot \boldsymbol{e}_i^r) = (\boldsymbol{\tau}_i \cdot \boldsymbol{e}_i)$. Therefore, it is important to remark that the vector $\boldsymbol{\tau}_3^r = \tau_{3\alpha}^r \boldsymbol{e}_\alpha^r + \tau_{33}^r \boldsymbol{e}_3^r$ does not represent the real stress, despite being numerically equivalent.

In terms of $\boldsymbol{\eta}^r$ and $\boldsymbol{\kappa}^r$, this product is

Marcos Pires Kassab 45

Advances on a kinematically exact rod model for thin-walled open section members: consistent warping function and nonlinear constitutive equation

$$\boldsymbol{P}\!:\!\dot{\boldsymbol{F}} = \boldsymbol{\tau}_\alpha^r \cdot \psi_{,\alpha} \dot{p} \boldsymbol{e}_3^r + \boldsymbol{\tau}_3^r \cdot \left[\dot{\boldsymbol{\eta}}^r + \dot{\boldsymbol{\kappa}}^r \times (\boldsymbol{a}^r + p\psi \boldsymbol{e}_3^r) + \boldsymbol{\kappa}^r \times (\dot{p}\psi \boldsymbol{e}_3^r) + \dot{p}'\psi \boldsymbol{e}_3^r \right]$$

$$= \begin{bmatrix} \boldsymbol{\tau}_3^r \\ (\boldsymbol{a}^r + p\psi \boldsymbol{e}_3^r) \times \boldsymbol{\tau}_3^r \\ \psi_{,\alpha} \boldsymbol{\tau}_\alpha^r \cdot \boldsymbol{e}_3^r + \psi \boldsymbol{\tau}_3^r \cdot (\boldsymbol{\kappa}^r \times \boldsymbol{e}_3^r) \\ \psi \boldsymbol{\tau}_3^r \cdot \boldsymbol{e}_3^r \end{bmatrix} \cdot \begin{bmatrix} \dot{\boldsymbol{\eta}}^r \\ \dot{\boldsymbol{\kappa}}^r \\ \dot{p} \\ \dot{p}' \end{bmatrix}. \tag{3.26}$$

Substituting (3.26) in (3.23), and performing the area integration, the internal power for rods is obtained

$$P_{int} = \int_0^L \boldsymbol{\sigma}^r \cdot \dot{\boldsymbol{\varepsilon}}^r d\zeta = \int_0^L \boldsymbol{\sigma}^r \cdot \boldsymbol{\Psi} \boldsymbol{\Delta} \dot{\boldsymbol{d}}_\theta d\zeta, \tag{3.27}$$

where

$$\boldsymbol{\sigma}^r = \int_{A^r} \begin{bmatrix} \boldsymbol{\tau}_3^r \\ (\boldsymbol{a}^r + p\psi \boldsymbol{e}_3^r) \times \boldsymbol{\tau}_3^r \\ \psi_{,\alpha} \boldsymbol{\tau}_\alpha^r \cdot \boldsymbol{e}_3^r + \psi \boldsymbol{\tau}_3^r \cdot (\boldsymbol{\kappa}^r \times \boldsymbol{e}_3^r) \\ \psi \boldsymbol{\tau}_3^r \cdot \boldsymbol{e}_3^r \end{bmatrix} dA^r = \begin{bmatrix} \boldsymbol{n}^r \\ \boldsymbol{m}^r \\ Q \\ B \end{bmatrix} \tag{3.28}$$

is the generalized stress resultants vector. As in the case of the nominal stresses, in equation (3.28), $\boldsymbol{n}^r$ and $\boldsymbol{m}^r$ are NOT the true force resultants (normal and shear forces) and moment resultants (bending moments and torsion moment), but are again component-wise equivalent to those resultants $\boldsymbol{n} = \boldsymbol{Q}\boldsymbol{n}^r$ and $\boldsymbol{m} = \boldsymbol{Q}\boldsymbol{m}^r$, if $\boldsymbol{n}, \boldsymbol{m}$ are in the base $\boldsymbol{e}_i$ and $\boldsymbol{n}^r, \boldsymbol{m}^r$ are in the base $\boldsymbol{e}_i^r$. The bi-shear (Q) and is the bi-moment (B), are scalars, thus, do not depend on any base.

The virtual internal work can be directly derived from the internal power. Thus, it is

$$\delta W_{int} = \int_{V^r} \boldsymbol{P}\!:\!\delta \boldsymbol{F} dV^r = \int_0^L \boldsymbol{\sigma}^r \cdot \delta \boldsymbol{\varepsilon}^r d\zeta =$$

$$\int_0^L \boldsymbol{\sigma}^r \cdot \boldsymbol{\Psi} \boldsymbol{\Delta} \delta \boldsymbol{d}_\theta d\zeta \,, \forall \delta \boldsymbol{d}_\theta(\zeta) \in \mathcal{H}_1^0(\Omega), \tag{3.29}$$

where $\boldsymbol{\delta \varepsilon}^r = [\delta \boldsymbol{\eta}^r \quad \delta \boldsymbol{\kappa}^r \quad \delta p \quad \delta p']^T$ is the generalized virtual strain vector, with

$$\delta \boldsymbol{\eta}^r = \boldsymbol{Q}^T \delta \boldsymbol{u}' + \boldsymbol{Q}^T \boldsymbol{Z}' \boldsymbol{\Gamma} \delta \boldsymbol{\theta} \quad \text{and} \quad \delta \boldsymbol{\kappa}^r = \boldsymbol{Q}^T (\boldsymbol{\Gamma}' \delta \boldsymbol{\theta} + \boldsymbol{\Gamma} \delta \boldsymbol{\theta}'). \tag{3.30}$$

The external power is

$$P_{ext} = \int_0^L \left[\int_{C^r} \bar{\boldsymbol{t}} \cdot \boldsymbol{\delta} dC^r + \int_{A^r} \bar{\boldsymbol{b}} \cdot \boldsymbol{\delta} dA^r \right] d\zeta, \tag{3.31}$$

where $\bar{\boldsymbol{t}}$ represents the surface forces per reference area unit and $\overline{\boldsymbol{b}}$ represents the volume forces per *reference* area or volume unit, both acting in the *current* configuration. C^r and A^r are the contour and the area of the cross-section in the reference configuration. The speed $\boldsymbol{\delta}$ is

$$\dot{\boldsymbol{\delta}} = \dot{\boldsymbol{x}} = \dot{\boldsymbol{z}} + \dot{\boldsymbol{a}} + \dot{\boldsymbol{w}} = \dot{\boldsymbol{u}} + \dot{\boldsymbol{Q}} \boldsymbol{a}^r + \psi p \dot{\boldsymbol{Q}} \boldsymbol{e}_3 + \psi \dot{p} \boldsymbol{e}_3$$

$$= \dot{\boldsymbol{u}} + \boldsymbol{\Omega} \boldsymbol{Q} (\boldsymbol{a}^r + \psi p \boldsymbol{e}_3^r) + \psi \dot{p} \boldsymbol{e}_3 = \tag{3.32}$$

$$= \dot{\boldsymbol{u}} + \boldsymbol{\omega} \times (\boldsymbol{a} + \psi p \boldsymbol{e}_3) + \psi \dot{p} \boldsymbol{e}_3.$$

Substituting (3.32) in (3.31), and remembering that $\dot{\boldsymbol{u}}, \boldsymbol{\omega} = \boldsymbol{\Gamma} \dot{\boldsymbol{\theta}}, p$ and $\dot{p}$ are functions only in ζ, one gets

$$P_{ext} = \int_0^L \left\{ \dot{\boldsymbol{u}} \cdot \left[\int_{C^r} \bar{\boldsymbol{t}} dC^r + \int_A \bar{\boldsymbol{b}} dA^r \right] + \boldsymbol{\Gamma} \dot{\boldsymbol{\theta}} \right.$$

$$\cdot \left[\int_{C^r} (\boldsymbol{a} + \psi p \boldsymbol{e_3}) \times \bar{\boldsymbol{t}} dC^r + \int_{A^r} (\boldsymbol{a} + \psi p \boldsymbol{e_3}) \times \bar{\boldsymbol{b}} dA^r \right] \qquad (3.33)$$

$$\left. + \dot{p} \left[\int_{C^r} \psi \bar{\boldsymbol{t}} \cdot \boldsymbol{e_3} dC^r + \int_{A^r} \psi \bar{\boldsymbol{b}} \cdot \boldsymbol{e_3} dA^r \right] \right\} d\zeta.$$

Introducing the generalized external resultant forces vector $\bar{\boldsymbol{q}} = [\bar{\boldsymbol{n}} \quad \bar{\boldsymbol{\mu}} \quad \bar{B}]^T$,

$$P_{ext} = \int_0^L \bar{\boldsymbol{q}} \cdot \boldsymbol{d_\theta} d\zeta, \qquad (3.34)$$

where

$$\bar{\boldsymbol{q}} = \begin{bmatrix} \bar{\boldsymbol{n}} \\ \bar{\boldsymbol{\mu}} \\ \bar{B} \end{bmatrix} = \begin{bmatrix} \left[\int_{C^r} \bar{\boldsymbol{t}} dC^r + \int_{A^r} \bar{\boldsymbol{b}} dA^r \right] \\ \boldsymbol{\Gamma}^{\mathrm{T}} \left(\int_{C^r} (\boldsymbol{a} + \psi p \boldsymbol{e_3}) \times \bar{\boldsymbol{t}} dC^r + \int_{A^r} (\boldsymbol{a} + \psi p \boldsymbol{e_3}) \times \bar{\boldsymbol{b}} dA^r \right) \\ \int_{C^r} \psi \bar{\boldsymbol{t}} \cdot \boldsymbol{e_3} dC^r + \int_{A^r} \psi \bar{\boldsymbol{b}} \cdot \boldsymbol{e_3} dA^r \end{bmatrix}. \qquad (3.35)$$

In equation (3.35), $\bar{\boldsymbol{n}}$ represents the external forces, $\bar{\boldsymbol{\mu}} = \boldsymbol{\Gamma}^{\mathrm{T}} \bar{\boldsymbol{m}}$ is defined as the external pseudo-moment and $\bar{B}$ is the external bi-moment. Note that, in this formulation, the pseudo-moment is the energetically conjugated of the rotations, not the moment itself. Discussions about this fact have been broadly carried in many references, such as in Pimenta and Yojo [22], Campello [1], and Fernandes [26].

With the aid of the external power expressions, the virtual external work is directly obtained, and is given by

$$\delta W_{ext} = \int_0^L \bar{\boldsymbol{q}} \cdot \delta \boldsymbol{d_\theta} d\zeta, \quad \forall \delta \boldsymbol{d_\theta}(\zeta) \in \mathcal{H}_1^0(\Omega) \qquad (3.36)$$

Were concentrated loadings to be included, a certain formalism must be introduced. Let δ_{ζ^*} represent the Dirac delta function[3], ζ^* are the points with applied concentrated loads and $\boldsymbol{q}^*$ the concentrated loads[4]. Thus, rewriting equation (3.36), one gets

$$\delta W_{ext} = \int_0^L (\bar{\boldsymbol{q}} + \delta_{\zeta^*} \boldsymbol{q}^*) \cdot \delta \boldsymbol{d_\theta} d\zeta, \quad \forall \delta \boldsymbol{d_\theta}(\zeta) \in \mathcal{H}_1^0(\Omega). \qquad (3.37)$$

Thus

---

[3] This is not a function in the usual sense, but has as properties $\delta_a = \begin{cases} +\infty, \zeta = a \in \mathbb{R} \\ 0, \text{otherwise} \end{cases}$ and $\int_{-\infty}^{+\infty} f(\zeta) \delta_a d\zeta = f(\zeta)$. Therefore, it is useful to the integration of pulses in the trial functions.

[4] If the solution is obtained from the differential equation, it must include the loads from the connection with adjacent rods, since, element-wise, they are external. When the weak form is used, this is not needed, since the integral is performed throughout the whole domain, and this kind of interaction is accounted for in the global virtual internal work.

Marcos Pires Kassab

47

Advances on a kinematically exact rod model for thin-walled open section members: consistent warping function and nonlinear constitutive equation

$$\delta W_{ext} = \int_0^L \overline{\boldsymbol{q}} \cdot \delta \boldsymbol{d}_\theta \, d\zeta + \boldsymbol{q}^* \cdot \delta \boldsymbol{d}_\theta|^{\zeta^*}. \tag{3.38}$$

Inserting (3.37) in (3.22), the weak form of equilibrium for this model is achieved

$$\delta W = \int_0^L (\boldsymbol{\sigma}^r \cdot \delta \boldsymbol{\varepsilon}^r - \overline{\boldsymbol{q}} \cdot \delta \boldsymbol{d}_\theta) d\zeta - \boldsymbol{q}^* \cdot \delta \boldsymbol{d}_\theta|^{\zeta^*} = 0, \qquad \delta \boldsymbol{d}_\theta(\zeta) \in \mathcal{H}_1^0(\Omega) \tag{3.39}$$

By the structure of equation (3.39), it is evident that the virtual work must be integrable, but with the first derivatives piece-wise continuous (i.e, discontinuous at a finite number of points). Therefore, the solution belongs to the Sobolev space ($\mathcal{H}_1^0$), from where the trial functions are also taken.

Integrating by parts, and using the definitions of the virtual quantities, one gets

$$\delta W = \int_0^L -(\boldsymbol{n}' + \overline{\boldsymbol{n}}) \cdot \delta \boldsymbol{u} - (\boldsymbol{m}' + \boldsymbol{z}' \times \boldsymbol{n} + \overline{\boldsymbol{m}}) \cdot (\boldsymbol{\Gamma} \delta \boldsymbol{\theta}) - (B' - Q + \overline{B}) d\zeta$$
$$+ (\boldsymbol{n} - \boldsymbol{n}^*) \cdot \delta \boldsymbol{u}|^{\zeta^*} + (\boldsymbol{\Gamma}^T \boldsymbol{m} - \boldsymbol{\Gamma}^T \boldsymbol{m}^*) \cdot \delta \boldsymbol{\theta}|^{\zeta^*} + (B - B^*) \cdot \delta p|^{\zeta^*} = 0. \tag{3.40}$$

By performing integration by parts in equation (3.39), the strong form of the equilibrium is achieved. It is strong in the sense that now, $\boldsymbol{d}_\theta \in \mathcal{C}^2(0, L)$, besides the boundary conditions. By the fundamental lemma of variational calculus, equation (3.59) is only satisfied for $\forall \delta \boldsymbol{d}_\theta(\zeta) \in \mathcal{H}_1^0(\Omega)$ if

$$\text{Local equilibrium} \begin{cases} \boldsymbol{n}' + \overline{\boldsymbol{n}} = \boldsymbol{o} \\ \boldsymbol{m}' + \boldsymbol{z}' \times \boldsymbol{n} + \overline{\boldsymbol{m}} = \boldsymbol{o}; \\ B' - Q + \overline{B} = 0 \end{cases}$$

$$\text{Natural boundary conditions} \begin{cases} \boldsymbol{n} = \boldsymbol{n}^* \\ \boldsymbol{\Gamma}^T \boldsymbol{m} = \boldsymbol{\Gamma}^T \boldsymbol{m}^* \text{ in } \zeta^r. \\ B = B^* \end{cases} \tag{3.41}$$

Equation (3.41) is the differential form of equilibrium, and the natural boundary conditions were consistently derived from the Virtual Work Theorem, with a fairly intuitive result: it is expected that the stress resultants at the edges are equal to the prescribed ones. Essential boundary conditions are directly imposed upon solution, by prescribing the displacements $\boldsymbol{d}_\theta = \boldsymbol{d}_\theta^*$ in ζ^u.

There are some observations concerning the bi-shear:

a) although the bi-shear has a major role on the differential equation, it does not possess an associated natural boundary condition;

b) depending on how the formulation is built, the bi-shear and the bi-moment might end up with swapped signals. Here, the bi-shear has a negative (-) sign in the differential equation ($B' - Q = 0$, in the absence of $\overline{B}$), which is NOT consistent with the definition from Vlasov's classical theory, for which $Q = -\phi''' EI_\omega = -B'$, where ϕ is the torsion rotation. Thus, for comparison with the classical theory, the bi-shear obtained from PEFSYS must be multiplied by -1. It should be noted, though, that as long as the differential equation that relates B and Q is consistently deduced, there should be no problems;

c) the bi-shear and bi-moment require an additional equation, since there is no kinematical constraint between torsional rotation and warping, differently from what is seen in the linear Saint-Venant's or Vlasov's rod theory.

3.3. Tangent bilinear form

In order to solve the weak form through numerical methods, in the current case, the Finite Element Method (FEM), a tangent operator is needed. After discretizing the weak form, such operator leads to the stiffness matrix for each step, and, in the non-linear case, it is never constant. In the context of structural theories, such as rods and shells, the exact consideration of finite rotations is one of the main sources of non-linearity, and as will be shown in this section, many derivatives of $\boldsymbol{\theta}$ are present. This tangent operator is obtained through the consistent linearization of the weak form (equation (3.39)). Using again a derivative with respect to a scalar, the Fréchet derivative is obtained.

$$\delta^2 W = \int_0^L [(\boldsymbol{D\Psi\Delta\delta d_\theta}) \cdot (\boldsymbol{\Psi\Delta\delta d_\theta}) + (\boldsymbol{G_\theta\Delta\delta d_\theta}) \cdot (\boldsymbol{\Delta\delta d_\theta}) - (\boldsymbol{L_\theta\delta d_\theta}) \cdot \delta\boldsymbol{d_\theta}]d\zeta, \qquad (3.42)$$

where $\boldsymbol{D}$, $\boldsymbol{G_\theta}$ and $\boldsymbol{L_\theta}$ are, respectively, the material, geometric and external loading contributions to the tangent operator. For the specific case of this 7-DOF rod model, those contributions are (see Appendix G)

$$\boldsymbol{D} = \frac{\partial \boldsymbol{\sigma^r}}{\partial \boldsymbol{\varepsilon^r}} = \begin{bmatrix} \dfrac{\partial \boldsymbol{n^r}}{\partial \boldsymbol{\eta^r}} & \dfrac{\partial \boldsymbol{n^r}}{\partial \boldsymbol{\kappa^r}} & \dfrac{\partial \boldsymbol{n^r}}{\partial p} & \dfrac{\partial \boldsymbol{n^r}}{\partial p'} \\ \dfrac{\partial \boldsymbol{m^r}}{\partial \boldsymbol{\eta^r}} & \dfrac{\partial \boldsymbol{m^r}}{\partial \boldsymbol{\kappa^r}} & \dfrac{\partial \boldsymbol{m^r}}{\partial p} & \dfrac{\partial \boldsymbol{m^r}}{\partial p'} \\ \dfrac{\partial Q}{\partial \boldsymbol{\eta^r}} & \dfrac{\partial Q}{\partial \boldsymbol{\kappa^r}} & \dfrac{\partial Q}{\partial p} & \dfrac{\partial Q}{\partial p'} \\ \dfrac{\partial B}{\partial \boldsymbol{\eta^r}} & \dfrac{\partial B}{\partial \boldsymbol{\kappa^r}} & \dfrac{\partial B}{\partial p} & \dfrac{\partial B}{\partial p'} \end{bmatrix}, \qquad (3.43)$$

$$\boldsymbol{G_\theta} = \begin{bmatrix} \boldsymbol{O} & \boldsymbol{G_{u'\theta}} & \boldsymbol{O} & \boldsymbol{o} & \boldsymbol{o} \\ \boldsymbol{G_{u'\theta}^T} & \boldsymbol{G_{\theta\theta}} & \boldsymbol{G_{\theta'\theta'}} & \boldsymbol{o} & \boldsymbol{o} \\ \boldsymbol{O} & \boldsymbol{G_{\theta'\theta'}^T} & \boldsymbol{O} & \boldsymbol{o} & \boldsymbol{o} \\ \boldsymbol{o^T} & \boldsymbol{o^T} & \boldsymbol{o^T} & 0 & 0 \\ \boldsymbol{o^T} & \boldsymbol{o^T} & \boldsymbol{o^T} & 0 & 0 \end{bmatrix}, \qquad (3.44)$$

$$\boldsymbol{L_\theta} = \begin{bmatrix} \boldsymbol{L_{uu}} & \boldsymbol{L_{u\theta}} & \boldsymbol{L_{up}} \\ \boldsymbol{L_{\theta u}} & \boldsymbol{L_{\theta\theta}} & \boldsymbol{L_{p\theta}} \\ \boldsymbol{L_{pu}} & \boldsymbol{L_{p\theta}} & \boldsymbol{L_{pp}} \end{bmatrix} = \begin{bmatrix} \dfrac{\partial \boldsymbol{\bar{n}}}{\partial \boldsymbol{u}} & \dfrac{\partial \boldsymbol{\bar{n}}}{\partial \boldsymbol{\theta}} & \dfrac{\partial \boldsymbol{\bar{n}}}{\partial p} \\ \dfrac{\partial (\boldsymbol{\Gamma^T\bar{m}})}{\partial \boldsymbol{u}} & \dfrac{\partial (\boldsymbol{\Gamma^T\bar{m}})}{\partial \boldsymbol{\theta}} & \dfrac{\partial (\boldsymbol{\Gamma^T\bar{m}})}{\partial p} \\ \dfrac{\partial \bar{B}}{\partial \boldsymbol{u}} & \dfrac{\partial \bar{B}}{\partial \boldsymbol{\theta}} & \dfrac{\partial \bar{B}}{\partial p} \end{bmatrix}. \qquad (3.45)$$

The first deduction of the tangent operator $\delta^2 W$ is often credited to Simo [15], despite the important contribution from Pimenta and Yojo [22], who consistently wrote the weak form using the conjugated pair $(\delta\boldsymbol{\theta}, \boldsymbol{\mu})$ for the first time, rendering a symmetric expression for $\boldsymbol{G_\theta}$. Simo, instead, used $(\delta\boldsymbol{\theta}, \boldsymbol{m})$, which is not an energetically conjugated pair, obtaining a non-symmetric $\boldsymbol{G_\theta}$. Formally, Simo's approach is not incorrect, but unintentionally lead to a Petrov-Galerkin type of projection, in which the trial function comes from a different space than the field being approximated, which naturally renders the mentioned asymmetry.

Marcos Pires Kassab 49

Advances on a kinematically exact rod model for thin-walled open section members: consistent warping function and nonlinear constitutive equation

The sub-matrices from (3.44) are highly non-linear terms, that use the definitions from previous works, such as Simo and Vu-Quoc [15] and Pimenta and Yojo [22], and the skew-symmetric tensors $\boldsymbol{N}, \boldsymbol{M}$ and $\boldsymbol{Z}'$ (from $\boldsymbol{n}, \boldsymbol{m}$ and $\boldsymbol{z}'$, respectively). They are

$$\boldsymbol{G}_{u'\theta} = -\boldsymbol{N}\boldsymbol{\Gamma} \text{ and } \boldsymbol{G}_{u'\theta}^T = \boldsymbol{\Gamma}^T\boldsymbol{N}$$

$$\boldsymbol{G}_{\theta\theta} = \boldsymbol{\Gamma}^T\boldsymbol{Z}'\boldsymbol{N}\boldsymbol{\Gamma} - \boldsymbol{V}(\boldsymbol{\theta}, \boldsymbol{z}' \times \boldsymbol{n}) + \boldsymbol{V}'(\boldsymbol{\theta}, \boldsymbol{m}) - \boldsymbol{\Gamma}'\boldsymbol{M}\boldsymbol{\Gamma} \tag{3.46}$$

$$\boldsymbol{G}_{\theta'\theta'} = \boldsymbol{V}(\boldsymbol{\theta}, \boldsymbol{m}) \text{ and } \boldsymbol{G}_{\theta'\theta'}^T = \boldsymbol{V}^T(\boldsymbol{\theta}, \boldsymbol{m}),$$

where, for a certain vector $\boldsymbol{t}$, there is an operator $\boldsymbol{V}(\boldsymbol{\theta}, \boldsymbol{t})$ that arises from the derivations present on the geometric contribution of the tangent operator, and is described in [1], for example.

As shown in the aforementioned works from Simo, Pimenta and Campello, the geometric contribution is also symmetric.

For the material contribution to the tangent operator, one has the following symmetric matrix

$$\boldsymbol{D} = \frac{\partial \boldsymbol{\sigma}^r}{\partial \boldsymbol{\varepsilon}^r} = \begin{bmatrix} \boldsymbol{D}_{\eta\eta} & \boldsymbol{D}_{\eta\kappa} & \boldsymbol{D}_{\eta p} & \boldsymbol{D}_{\eta p'} \\ & \boldsymbol{D}_{\kappa\kappa} & \boldsymbol{D}_{\kappa p} & \boldsymbol{D}_{\kappa p'} \\ & & \boldsymbol{D}_{pp} & \boldsymbol{D}_{p'p'} \\ Sym. & & & \boldsymbol{D}_{p'p'} \end{bmatrix}. \tag{3.47}$$

Using the chain rule, the stress resultants definitions, and some auxiliary expressions (presented in [3]), the submatrices of $\boldsymbol{D}$ can be calculated:

$$\boldsymbol{D}_{\eta\eta} = \frac{\partial \boldsymbol{n}^r}{\partial \boldsymbol{\eta}^r} = \int_A \frac{\partial \boldsymbol{\tau}_3^r}{\partial \boldsymbol{\gamma}^r}\frac{\partial \boldsymbol{\gamma}^r}{\partial \boldsymbol{\eta}^r} dA = \int_A \boldsymbol{C}_{33} dA$$

$$\boldsymbol{D}_{\eta\kappa} = \frac{\partial \boldsymbol{n}^r}{\partial \boldsymbol{\kappa}^r} = \int_A \frac{\partial \boldsymbol{\tau}_3^r}{\partial \boldsymbol{\gamma}^r}\frac{\partial \boldsymbol{\gamma}^r}{\partial \boldsymbol{\kappa}^r} dA = \int_A -\boldsymbol{C}_{33}(\boldsymbol{A}^r + p\psi \boldsymbol{E}_3^r) dA$$

$$\boldsymbol{D}_{\eta p} = \frac{\partial \boldsymbol{n}^r}{\partial p} = \int_A \frac{\partial \boldsymbol{\tau}_3^r}{\partial p} dA = \int_A \boldsymbol{c} dA$$

$$\boldsymbol{D}_{\eta p'} = \frac{\partial \boldsymbol{n}^r}{\partial p'} = \int_A \frac{\partial \boldsymbol{\tau}_3^r}{\partial p'} dA = \int_A \boldsymbol{d} dA$$

$$\boldsymbol{D}_{\kappa\kappa} = \frac{\partial \boldsymbol{m}^r}{\partial \boldsymbol{\kappa}^r} = \int_A \frac{\partial}{\partial \boldsymbol{\kappa}^r}\left[(\boldsymbol{A}^r + p\psi \boldsymbol{E}_3^r)\boldsymbol{\tau}_3^r\right] dA \tag{3.48}$$

$$= \int_A -(\boldsymbol{A}^r + p\psi \boldsymbol{E}_3^r)\boldsymbol{C}_{33}(\boldsymbol{A}^r + p\psi \boldsymbol{E}_3^r) dA$$

$$\boldsymbol{D}_{\kappa p} = \frac{\partial \boldsymbol{m}^r}{\partial p} = \int_A \frac{\partial}{\partial p}\left[(\boldsymbol{A}^r + p\psi \boldsymbol{E}_3^r)\boldsymbol{\tau}_3^r\right] dA$$

$$= \int_A \left[\psi \boldsymbol{E}_3^r\boldsymbol{\tau}_3^r + (\boldsymbol{A}^r + p\psi \boldsymbol{E}_3^r)\boldsymbol{c}\right] dA$$

$$\boldsymbol{D}_{\kappa p'} = \frac{\partial \boldsymbol{m}^r}{\partial p'} = \int_A \frac{\partial}{\partial p'}\left[(\boldsymbol{A}^r + p\psi \boldsymbol{E}_3^r)\boldsymbol{\tau}_3^r\right] dA = \int_A \left[(\boldsymbol{A}^r + p\psi \boldsymbol{E}_3^r)\boldsymbol{d}\right] dA$$

$$\boldsymbol{D}_{pp} = \frac{\partial Q}{\partial p} = \int_A \frac{\partial}{\partial p} \left[\psi_{,\alpha} \boldsymbol{\tau}_\alpha^r \cdot \boldsymbol{e}_3^r + \psi \boldsymbol{\tau}_3^r \cdot (\boldsymbol{\kappa}^r \times \boldsymbol{e}_3^r) \right] dA$$

$$= \int_A \left[\boldsymbol{b}_\alpha \psi_{,\alpha} + \psi(\boldsymbol{\kappa}^r \times \boldsymbol{e}_3^r) \cdot \boldsymbol{c} \right] dA$$

$$\boldsymbol{D}_{pp'} = \frac{\partial Q}{\partial p'} = \int_A \frac{\partial}{\partial p'} \left[\psi_{,\alpha} \boldsymbol{\tau}_\alpha^r \cdot \boldsymbol{e}_3^r + \psi \boldsymbol{\tau}_3^r \cdot (\boldsymbol{\kappa}^r \times \boldsymbol{e}_3^r) \right] dA$$

$$= \int_A \left[\boldsymbol{d}_\alpha \psi_{,\alpha} + (\boldsymbol{\kappa}^r \times \boldsymbol{e}_3^r) \psi \cdot \boldsymbol{d} \right] dA$$

$$\boldsymbol{D}_{p'p'} = \frac{\partial B}{\partial p'} = \int_A \frac{\partial}{\partial p'} \left[(\boldsymbol{\tau}_3^r \cdot \boldsymbol{e}_3^r) \psi \right] dA = \int_A \left[\psi(\boldsymbol{e}_3^r \cdot \boldsymbol{d}) \right] dA,$$

with $\boldsymbol{A}^r = skew(\boldsymbol{a}^r)$ and $\boldsymbol{E}_3^r = skew(\boldsymbol{e}_3^r)$. For different elastic models, equations (3.47) and (3.48) hold, although not the expressions related to the auxiliary quantities $C_{33} = \frac{\partial \tau_3^r}{\partial \gamma^r}$, $\boldsymbol{c} = \frac{\partial \tau_3^r}{\partial p}$, $\boldsymbol{d} = \frac{\partial \tau_3^r}{\partial p'}$, $\boldsymbol{b}_\alpha = \frac{\partial (\tau_\alpha^r \cdot \boldsymbol{e}_3^r)}{\partial p}$ and $\boldsymbol{d}_\alpha = \frac{\partial (\tau_\alpha^r \cdot \boldsymbol{e}_3^r)}{\partial p'}$. Note that the chain rule for $\frac{\partial \tau_3^r}{\partial \eta^r} = \frac{\partial \tau_3^r}{\partial \gamma^r} \frac{\partial \gamma^r}{\partial \eta^r}$ and $\frac{\partial \tau_3^r}{\partial \kappa^r} = \frac{\partial \tau_3^r}{\partial \gamma^r} \frac{\partial \gamma^r}{\partial \kappa^r}$ are only valid if η^r and κ^r are arguments exclusively of γ^r. In section 4.3, their expressions will be derived for Saint-Venant's and Simo-Ciarlet's material.

As $\boldsymbol{G}_\theta$ and $\boldsymbol{D}$ are symmetric, the symmetry of $\boldsymbol{L}_\theta$ is the only remaining condition to make $\delta^2 W$ to also have this property. In general, the contribution from the external loads $\boldsymbol{L}_\theta$ is not null, except for some specific cases (e.g., constant external force). Many works contain a broader discussion about this subject (see [1] ,[22], [26], for instance). For now, it is only said that conservative loadings (which are the type of loadings to be considered in this work) render symmetric, but not null, $\boldsymbol{L}_\theta$.

3.4. The warping shape function

This section is, the most important of the whole work: here, the pertinent modifications on the warping function from Campello and Lago's [2] are shown, with the respective justification

The Saint-Venant's warping function is a popular choice for most kinematically exact rod models, but, when simplified material laws are used, only well-known geometric moments of inertia of different orders are needed (for example, Saint-Venant's torsion inertia (I_T), sectorial moment of inertia (I_ω), etc), which, for thin-walled members, do not require the full expression of the warping function for computation. However, when explicit integration for the stress resultants (and tangent stiffness matrix) is needed, the warping function ψ must be exactly determined *a priori* in the whole cross-section. This has motivated Campello and Lago [2] to propose a method to generate a warping function that contemplates primary and secondary warping modes, but without the need of neither solving any kind of boundary value problem, nor any eigenproblem. In their article, they have shown that this approach provides excellent results for I-shaped, cruciform and rectangular sections. However, it was not clear whether it could be used for more arbitrary geometries, and, during the development of the current work, the author verified that certain modifications were indeed necessary.

Marcos Pires Kassab

51

Advances on a kinematically exact rod model for thin-walled open section members: consistent warping function and nonlinear constitutive equation

Both Campello and Lago's [2] and the current approach make use of local walls solutions. It is assumed that the cross-section is open and consisted of thin rectangular sub-sections, as depicted in Fig. 3. It is important to define the section global (ξ_1, ξ_2) and walls local $(\bar{x}_i, \bar{y}_i)$ systems (sub-index i is used to refer to wall i), attached to the global (O) and local (O_i) references. The local system´s component $\bar{y}_i$ is always aligned with the respective wall length. It is also useful to define non-rotated local systems, given by (ξ_1^i, ξ_2^i).
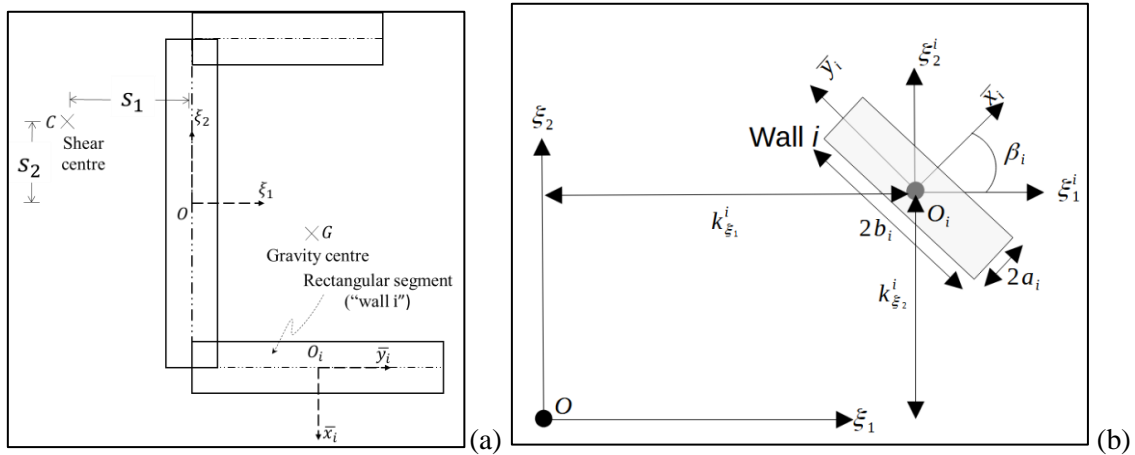
Figure 4 – a) Global, local and auxiliary systems b) detail of a generic wall i.

First, let us have a closer look on the classical Vlasov's sectorial area, which represent the warping function along the walls midline. Then let us analyse Campello and Lago's [2] warping function. Lastly, the proposed function will be introduced.

3.4.1. Vlasov's warping function – sectorial area

The primary warping definition is found in Vlasov's book [12]. The sectorial area function (ω) consists on a line integral of twice the area comprehended among a fixed point (sectorial pole, point A), a fixed starting point (sectorial origin, point B) and the current evaluation point (M) (henceforth, the notation $\omega^{A,B}(s_M)$ is employed).

In the original description, the area increment was positive if spinning clockwise, relatively to A. See Figure 5 for details.
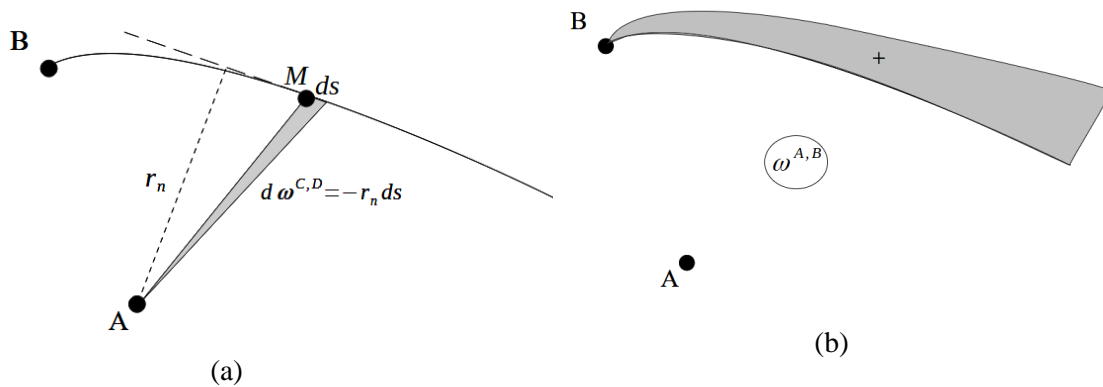
Figure 5 – Defining sectorial area for a generic cross-section. a) Increment; b) Function $\omega^{A,B}$.

From Figure 5, it is conspicuous that the sectorial area increment is given by

$$d\omega = -r_n ds, \tag{3.49}$$

and, consequently, in a given point M,

$$\omega^{A,B}(s_M) = \oint_B^M -r_n ds. \tag{3.50}$$

Some examples of the sectorial area for usual geometries (I-section, C-section, top hat, Z-section, V-section) can be found in section 3.4.5.

Fruchtengarten, in [50], shows that the Saint-Venant's solution along the wall midline for open thin-walled cross-section is exactly the result of equation (3.50). Therefore, the Vlasov's theory itself can be interpreted as an extension of the pure torsion warping function: the constrain $p = \theta_3'$ (warping intensity equal to the specific torsion rotation) remains, but p is not constant anymore. As consequence, axial normal stresses arise, together with additional self-balanced shear stresses, which originate the bi-moment and bi-shear. The torsion becomes non-uniform (varies along the rod´s axis) and both the bi-shear and bi-moment depends on the warping intensity and torsional specific rotation.

Therefore, with the aid of equation (3.50), one can interpret that the sectorial area represents an average warping value on each wall. In fact, by imposing this assumption, Vlasov has obtained the normal stresses that are constant along the wall thickness and equal to the value at the midline. Thus, with the thin-walled assumption, together with the respective tangential stress assumption needed to respect local equilibrium, the bi-shear and bi-moment contributions to the resisting mechanism are obtained.

Whenever torsion is of interest, the concept of shear centre (synonyms: torsion centre – when Poisson's effects are neglected – and principal pole) is important in order to uncouple first order torsion, bending and axial effects. To find the shear centre coordinates (s_1, s_2) and the principal origin, it is usual to impose three orthogonality conditions:

$$S_\omega^{C,D} = I_{\omega x_1}^{C,D} = I_{\omega x_2}^{C,D} = 0, \tag{3.51}$$

with

Marcos Pires Kassab   53

Advances on a kinematically exact rod model for thin-walled open section members: consistent warping function and nonlinear constitutive equation

$$S_\omega = \int_A \omega \, dA; \quad I_{\omega x_1} = \int_A \xi_1 \omega \, dA; \quad I_{\omega x_2} = \int_A \xi_2 \omega \, dA, \tag{3.52}$$

where (ξ_1, ξ_2) is the cross-section coordinates with respect to the given arbitrary orthonormal basis (e_1, e_2), S_ω is the sectorial static moment and $I_{\omega x_1}, I_{\omega x_2}$ are the sectorial products of inertia with respect to the reference axis. The superscripts C, D mean that those quantities are referred to the shear centre and principal origin.

The static moment condition is the easiest to be met: after calculating a generic $\omega^{A,B}$, a simple constant translation, given by

$$\omega^{A,B^*} = \omega^{A,B} - \frac{S_\omega^{A,B}}{A}, \tag{3.53}$$

generates a new function with zero sectorial static moment, having as sectorial origin the point B^*, indirectly determined by finding where $\omega^{A,B^*} = 0$[5] . In fact, this is implicitly done by Timoshenko in [9], when defining the relation between normal stress and warping function. In Vlasov's and Timoshenko's works (and many of their successors'), the quantity $\frac{S_\omega^{A,B}}{A}$ is referred to as the *average sectorial area* $(\overline{\omega}^{A,B})$, and is equal to the sectorial area calculated between the old and the new sectorial origins $(\omega^{A,B}(s_{B^*}))$

In [50], it is shown that the sectorial area function is affected by the change of sectorial pole by the relation

$$\omega^{A^*,B^*} = \omega^{A,B^*} + \left(\xi_2^A - \xi_2^{A^*}\right)\left(\xi_1 - \xi_1^{B^*}\right) + \left(\xi_1^A - \xi_1^{A^*}\right)\left(\xi_2 - \xi_2^{B^*}\right), \tag{3.54}$$

where ξ_α^A and $\xi_\alpha^{A^*}$ are the coordinates of the poles A and A^*.

Using definitions from (3.52) and (3.54), one gets

$$\begin{aligned}
I_{\omega x_1}^{A^*,B^*} &= \int_A \omega^{C,B^*} \xi_1 \, dA \\
&= \int_A \left(\omega^{A,B^*} + \left(\xi_2^A - \xi_2^{A^*}\right)\left(\xi_1 - \xi_1^{B^*}\right) \right. \\
&\quad \left. + \left(\xi_1^A - \xi_1^{A^*}\right)\left(\xi_2 - \xi_2^{B^*}\right)\right) \xi_1 \, dA; \\
I_{\omega x_2}^{A^*,B^*} &= \int_A \omega^{A^*,B^*} \xi_2 \, dA = \int_A \left(\omega^{A,B^*} + \left(\xi_2^A - \xi_2^{A^*}\right)\left(\xi_1 - \xi_1^{B^*}\right) + \right. \\
&\quad \left. \left(\xi_1^A - \xi_1^{A^*}\right)\left(\xi_2 - \xi_2^{B^*}\right)\right) \xi_2 \, dA.
\end{aligned} \tag{3.55}$$

By performing the multiplications, and using the moment definitions, it can be directly found that

---

[5] Note that it is not possible yet to assert that the point B^* obtained from equation (3.53) is the principal origin D, since only when the three orthogonality conditions from equation (3.51) are simultaneously met that C and D are determined. The same is valid for A^* in equation (3.54).

$$\begin{aligned}
I_{\omega x_1}^{A^*,B^*} &= I_{\omega x_1}^{A,B^*} + \left(\xi_2^A - \xi_2^{A^*}\right)I_2 + \left(\xi_2^A - \xi_2^{A^*}\right)\xi_1^{B^*}S_2 + \left(\xi_1^A - \xi_1^{A^*}\right)I_{12} \\
&\quad - \left(\xi_1^A - \xi_1^{A^*}\right)\xi_2^{B^*}S_2; \\
I_{\omega x_2}^{A^*,B^*} &= I_{\omega x_2}^{A,B^*} - \left(\xi_2^A - \xi_2^{A^*}\right)I_{12} + \left(\xi_2^A - \xi_2^{A^*}\right)\xi_1^{B^*}S_1 - \left(\xi_1^A - \xi_1^{A^*}\right)I_1 \\
&\quad + \left(\xi_1^A - \xi_1^{A^*}\right)\xi_2^{B^*}S_1,
\end{aligned} \tag{3.56}$$

with the definitions of the elementary static moments and moments of inertia

$$S_1 = \int_A \xi_2\, dA; \quad S_2 = -\int_A \xi_1\, dA;$$

$$I_1 = \int_a \xi_2^2\, dA; \quad I_2 = \int_A \xi_1^2\, dA; \quad I_{12} = -\int_A \xi_1 \xi_2\, dA. \tag{3.57}$$

After calculating $\omega^{A,B}$ for an arbitrary pole (A) and origin (B), the pair (C, D) that meets (3.51) can be obtained.

The most direct way to determine C, D is by imposing an auxiliary coordinate system on the gravity centre, and then going through the following the steps:

Step 1: With a first trial $\omega^{A,B}$, apply equations (3.56), imposing $I_{\omega x_1}^{A^*,B} = I_{\omega x_2}^{A^*,B} = 0$. This will result in the system

$$\begin{bmatrix} \xi_2^B S_2 - I_{12} & \xi_1^B S_2 - I_2 \\ -\xi_2^B S_1 + I_1 & \xi_1^B S_1 + I_{12} \end{bmatrix} \begin{bmatrix} \xi_1^{A^*} - \xi_1^A \\ \xi_2^{A^*} - \xi_2^A \end{bmatrix} = \begin{bmatrix} I_{\omega x_1}^{A,B} \\ I_{\omega x_2}^{A,B} \end{bmatrix}, \tag{3.58}$$

that allows to find the coordinate of a new sectorial pole, as the auxiliary system was placed on the gravity centre, such that $S_1 = S_2 = 0$. Solving for $\Delta\boldsymbol{\xi}_S = \begin{bmatrix} \xi_1^{A^*} - \xi_1^A \\ \xi_2^{A^*} - \xi_2^A \end{bmatrix}$ yields

$$\Delta\boldsymbol{\xi}_S = \frac{1}{I_1 I_2 - I_{12}^2}\begin{bmatrix} -I_{12}I_{\omega x_1}^{A,B} + I_2 I_{\omega x_2}^{A,B} \\ -I_1 I_{\omega x_1}^{A,B} - I_{12}I_{\omega x_2}^{A,B} \end{bmatrix}. \tag{3.59}$$

With $\Delta\boldsymbol{\xi}_S$, the new pole (A^*) coordinates are directly found.

Step 2: Calculate the new sectorial area function $(\omega^{A^*,B})$;

Step 3: Apply equation (3.53), generating a sectorial area function that satisfies $S_\omega^{A^*,B^*} = 0$. A new sectorial origin B^* is indirectly obtained, as mentioned above;

Step 4: Verify if the imposition of a new sectorial origin interferes with the sectorial products of inertia with respect of the axis.

$$\omega^{A^*,B^*} = \omega^{A^*,B} + \omega^{A^*,B^*}(s_B). \tag{3.60}$$

Substituting on the sectorial moments of inertia definitions, one gets

$$I_{\omega x_1}^{A^*,B^*} = \int_A \left(\omega^{A^*,B} + \omega^{A^*,B^*}(s_B)\right)\xi_1\, dA = I_{\omega x_1}^{A^*,B} - \omega^{A^*,B^*}(s_B)S_2;$$

$$I_{\omega x_2}^{A^*,B^*} = \int_A \left(\omega^{A^*,B} + \omega^{A^*,B^*}(s_B)\right)\xi_2\, dA = I_{\omega x_2}^{A^*,B} + \omega^{A^*,B^*}(s_B)S_1. \tag{3.61}$$

Marcos Pires Kassab

55

Advances on a kinematically exact rod model for thin-walled open section members: consistent warping function and nonlinear constitutive equation

Since the adopted axis are on the gravity centre, $I_{\omega x_1}^{A^*,B^*} = I_{\omega x_1}^{A^*,B} = 0$ and $I_{\omega x_2}^{A^*,B^*} = I_{\omega x_2}^{A^*,B} = 0$. In fact, equation (3.61) shows that, if the axes pass through the gravity centre, the sectorial products of inertia with respect to the axes do not depend on the sectorial origin.

Therefore,

$$S_\omega^{A^*,B^*} = I_{\omega x_1}^{A^*,B^*} = I_{\omega x_2}^{A^*,B^*} = 0, \tag{3.62}$$

so, the determined points A^*, B^* are indeed the principal pole (C) and the principal origin (D), respectively. Note that this procedure is only direct if the auxiliar system is placed on the gravity centre. For any other system, step 4 renders $I_{\omega x_1}^{A^*,B^*} = I_{\omega x_2}^{A^*,B^*} \neq 0$, due to equation (3.61).

It is important to observe, however, that the translation of the coordinate system does not change the position of neither C nor D. In fact, if a new system $< \boldsymbol{e_1^g}, \boldsymbol{e_2^g} >$ is used, so that

$$\begin{aligned} \xi_1 &= \xi_1^g + k_{\xi_1} \\ \xi_2 &= \xi_2^g + k_{\xi_2}, \end{aligned} \tag{3.63}$$

then

$$I_{\omega x_1}^{C,D} = \int_A \omega^{C,D}\xi_1 dA = \int_A \omega^{C,D}\xi_1^g dA + \int_A \omega^{C,D}k_{\xi_1} dA = I_{\omega x_1^g}^{C,D} + k_{\xi_1}S_\omega^{C,D}. \tag{3.64}$$

Due to the orthogonality conditions, which were already satisfied, $S_\omega^{C,D} = 0$, and then $I_{\omega x_1}^{C,D} = I_{\omega x_1^g}^{C,D} = 0$. The conclusion is analogous for $I_{\omega x_2^g}^{C,D} = 0$. It is worth mentioning that ω is always independent from the system choice, and so is S_ω. Therefore, the sectorial area function can be directly obtained with the described procedure, regardless of any translation of the reference axis.

3.4.2.   *Campello and Lago warping function*

This warping function was presented by Campello and Lago, in [2]. As mentioned throughout the text, it contemplates primary and secondary warping contributions. In this case, the primary warping is given by the Vlasov's sectorial area, whereas the secondary warping is given by adding a local Saint-Venant's torsion solution for rectangular cross-sections for each wall of the section (equation (3.65) and (3.66)). Following the notation introduced in Fig. 3 (note that a_i and b_i are the wall semi-length and semi-thickness, respectively), for each rectangular sub-section the warping function is reproduced bellow:

$$\psi(\xi_1,\xi_2) = \omega(s) + \psi_R(\bar{x}_i,\bar{y}_i), \tag{3.65}$$

$$\psi_R(\bar{x}_i,\bar{y}_i) = -\frac{(a_i^6 + 19a_i^4b_i^2 - 19a_i^2b_i^4 - b_i^6)\overline{x_iy_i}}{a_i^6 + 14a_i^4b_i^2 + 14a_i^2b_i^4 + b^6} - \frac{\frac{35}{12}a_i^2b_i^2(-4\bar{x}_i^3\bar{y}_i + 4\bar{x}_i\bar{y}_i^3)}{a_i^6 + 14a_i^4b_i^2 + 14a_i^2b_i^4 + b_i^6}. \tag{3.66}$$

Note that ψ_R is a polynomial approximation to the Saint-Venant's warping function for rectangular sections and centre on the gravity centre (see Figure 6). It was obtained by Silva [49], using the Galerkin method. It should be noted that this function is an odd function.
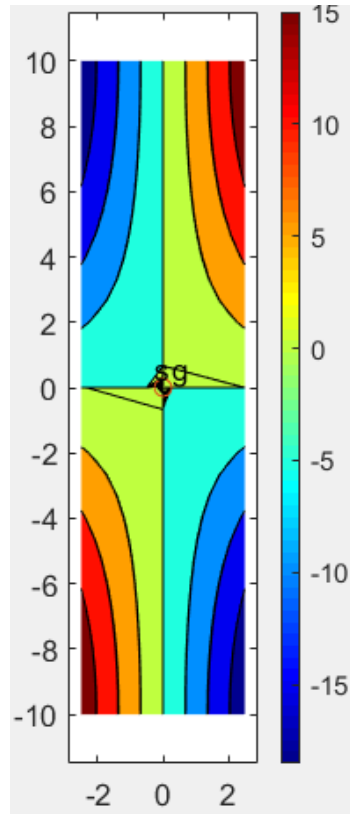
Figure 6 – Function ψ_R ***for a rectangular section with dimensions 5x20 (arbitrary unit).***

The discussion from section 3.4.1 was focusing solely on the function ω. However, the same conclusions and procedures are valid for the Campello's and Lago's warping function (equation (2.66)), for the corresponding quantities S_ψ, $I_{\psi x_1}$ and $I_{\psi x_2}$ (equivalent to the definitions (3.52), but using ψ instead of ω). See the demonstration below.

The sectorial static moment is still zero when the secondary warping is added. By definition, one gets

$$S_\psi = \int_A \psi(\xi_1, \xi_2)\, dA = \int_A \omega(s) + \psi_R(\bar{x}, \bar{y})\, dA = S_\omega + S_{\psi_R} = S_\omega, \qquad (3.67)$$

since $S_{\psi_R} = \sum_{i=1}^{no.\ walls} \int_{A_i} \psi_R dA_i = 0$, for ψ_R being odd on each wall.

For the sectorial products of inertia, auxiliary axes are defined (Figure 4b), and they are related to the original axes through the relation (see Figure 4)

$$\boldsymbol{\xi^i} = \begin{bmatrix} \xi_1^i \\ \xi_2^i \end{bmatrix} = \begin{bmatrix} \xi_1 \\ \xi_2 \end{bmatrix} - \begin{bmatrix} k_{\xi_1}^i \\ k_{\xi_2}^i \end{bmatrix}. \qquad (3.68)$$

The local axes $(\bar{x}_\iota, \bar{y}_\iota)$ from equation (2.67) are related to the new auxiliary axes ($\boldsymbol{\xi^i}$, for each wall i) through the rotation equation

$$\boldsymbol{\xi^*} = \begin{bmatrix} cos\beta_i & -sin\beta_i \\ sin\beta_i & cos\beta_i \end{bmatrix} \begin{bmatrix} \bar{x}_i \\ \bar{y}_i \end{bmatrix}. \qquad (3.69)$$

Using the definition for $I_{\psi x_1}^{C,D}$, one gets

Marcos Pires Kassab   57

Advances on a kinematically exact rod model for thin-walled open section members: consistent warping function and nonlinear constitutive equation

$$I_{\psi x_1}^{C,D} = \int_A \psi \xi_1 dA = \int_A (\omega + \psi_R)\xi_1 dA = \underbrace{I_{\omega x_1}^{C,D}}_{0} + \int_A \psi_R \xi_1 dA. \tag{3.70}$$

Using the auxiliary axes (ξ_1^*, ξ_2^*) and then rotating them, it is obtained

$$I_{\psi x_1}^{C,D} = k_{\xi_1} S_{\psi_R} + \int_A \psi_R \xi_1^i dA = \int_A \psi_R \xi_1^i dA. \tag{3.71}$$

Then, by rotating the axis, the result is given by

$$I_{\psi x_1}^{C,D} = \sum_{i=1}^{no.\ walls} \int_{A_i} \psi_R (cos\beta_i \bar{x} - sin\beta_i \bar{y}) dA_i$$

$$= \sum_{i=1}^{no.\ walls} [cos\beta_i \int_{A_i} \psi_R \bar{x} dA_i - sin\beta_i \int_{A_i} \psi_R \bar{y} dA_i] = 0, \tag{3.72}$$

since the functions $\psi_R \bar{x}$ and $\psi_R \bar{y}$ are antisymmetric w.r.t. one of the axis and symmetric w.r.t to the other one. The same result is obtained for $I_{\psi x_2}^{C,D}$.

Therefore, the position of the pair (C, D) that is determined by the analysis of ω is not affected by the addition of ψ_R.

Two important measures of the section stiffness are the torsional inertia – or Saint-Venant's torsion inertia – (I_T) and the warping constant (or warping inertia) (I_ψ). The torsional inertia is given by

$$I_T = I_0^A - e_{\alpha\beta} \int_A (\xi_\alpha - \xi_\alpha^A)\psi_{,\beta} dA, \tag{3.73}$$

where I_0^A is the polar moment of inertia w.r.t the adopted pole A, $e_{\alpha\beta} = \begin{bmatrix} 0 & 1 \\ -1 & 0 \end{bmatrix}$. The warping constant is

$$I_\psi = \int_A \psi^2 dA. \tag{3.74}$$

The uniform torsion resisting mechanism stiffness is measured by I_T, whilst I_ψ shall be used to evaluate the cross-sectional non-uniform torsion stiffness for a generic warping function. The relation $k = \sqrt{\frac{EI_\psi}{GI_T}}$ (E is the Young's modulus and G is the shear modulus) may be used to measure which one of the mentioned torsion-carrying mechanisms is preponderant.

In the Vlasov's linear theory, equation (3.74) becomes the sectorial moment of inertia

$$I_\omega = \int_A \omega^2 dA. \tag{3.75}$$

After some examination (see the examples from section 3.4.5), it was evident that this approach always generates a warping function with a coherent I_ψ measure. However, this was not true for I_T. Indeed, the only cross-sections for which I_T rendered representative are the ones studied in [2]: bi-symmetric I-shaped, rectangular and cruciform. Thus, some modification or correction is of utmost necessity, in order to obtain a truly robust 7 DOF model. Such improvement is shown below.

58   Marcos Pires Kassab

Advances on a kinematically exact rod model for thin-walled open section members: consistent warping function and nonlinear constitutive equation

3.4.3.   *Proposed warping function*

It was detected during numeric evaluations that the previous approach was not robust enough for arbitrary cross-sections. It seemed to work well only for the geometries that were tested in [2]. This was evidenced here when I_T was evaluated for other cross-sections, such as C-channels and Z-sections. Yet, it was noted that I_ψ rendered always coherent, irrespective of the section´s geometry. As the evaluation of I_ψ for open thin-walled sections is dominated by the primary warping, the author intuited that the pathological point to I_T was on how the secondary warping was built. In order to track down to the root of the issue, let us go back to the elementary boundary value problem from the Saint-Venant's torsion theory. For a given cross-section A, with boundary S and shear centre position (s_1, s_2), the warping function ψ^C w.r.t the shear centre is solution of

$$\psi^C_{,\alpha\alpha} = 0, \quad \text{in } A, \tag{3.76}$$

with the Dirichlet boundary condition

$$\nabla\psi^C \cdot \boldsymbol{v} = \psi^C_{,\alpha}v_\alpha = -e_{\alpha\beta}(\xi_\alpha - s_\alpha)v_\beta \quad \text{in } S, \tag{3.77}$$

where $\boldsymbol{v}$ is the normal to the contour S. The dependency on the shear centre coordinates is only used to build the principal warping function, i.e. to uncouple the warping from bending and axial first order effects. Still, it is not unique up to a constant. In order to eliminate this source of non-uniqueness, it is usual to impose that $\int_A \psi dA = 0$. By doing so, this last imposition, together with the shear centre dependency, the already mentioned orthogonality conditions are fulfilled.

Note that the shear centre position is unknow. A possible technique to determine it is to solve the problem for an auxiliary function ψ^A_0, which satisfies

$$\psi^A_{0,\alpha\alpha} = 0, \quad \text{in } A, \text{ and } \nabla\psi^A_0 \cdot \boldsymbol{v} = \psi^A_{0,\alpha}v_\alpha = -e_{\alpha\beta}\xi_\alpha v_\beta \quad \text{in } S. \tag{3.78}$$

Comparing the boundary condition from equations (3.77) and (3.78), it is possible to conclude that

$$\psi^C = \psi^A_0 - e_{\alpha\beta}s_\beta\xi_\alpha + c, \tag{3.79}$$

where c is a constant. It is important to remark that, if a point different from the shear centre is used as reference to build the warping function, the function value will differ from a plane function, as suggested by equation (3.79).

It is not a coincidence that that the relationship between ψ^C and ψ^A_0 has a similar structure to the one between ω^C and ω^A (see equation (3.54)), since, as can be found in Fruchtengarten [50], the primary warping is exactly correspondent to what is expected for the Saint-Venant's warping along the walls midlines. In fact, the auxiliary solution ψ^A_0 is nothing but the warping function with its pole in (0,0).

Those equations allow for an auxiliary function ψ^A_0 to be used to generate the principal warping function, which satisfies the orthogonality conditions. However, at first glance, nothing is said about building the auxiliary solution itself. It is proposed below a procedure that allows one to generate an

Marcos Pires Kassab   59

Advances on a kinematically exact rod model for thin-walled open section members: consistent warping function and nonlinear constitutive equation

approximation to the Saint-Venant's warping function for thin-walled open sections, for any desired pole or centre, using only the equation (3.79), and local walls solutions.

Consider a generic cross section, composed by n thin walls, as in Figure 4. Let us assume that, at the intersections, the boundary conditions along the thickness might be neglected at the walls intersection points, as the walls are thin. Therefore, if the warping function for rectangular sections (ψ_R) is known, the complete cross-sectional warping can be determined as a composition of local solutions, which must be adjusted using equation (3.79) so that each local solution is built w.r.t the cross-section current pole (here, adopted as the shear centre). Accordingly, for each wall or sub-section one gets

$$\psi(\xi_1, \xi_2) = \psi_L(\xi_1, \xi_2) + \psi_R(\bar{x}_i, \bar{y}_i), \tag{3.80}$$

with

$$\psi_L(\xi_1, \xi_2) = -(s_2 - k_{\xi_2}^i)(\xi_1 - k_{\xi_1}^i) + (s_1 - k_{\xi_1}^i)(\xi_2 - k_{\xi_2}^i) + c_i. \tag{3.81}$$

The coefficients $(s_2 - k_{\xi_2}^i)$ and $(s_1 - k_{\xi_1}^i)$ in (3.81) are different for each wall (justifying the index i), and given as function of the distance between C and O_i. The constant term c_i, in turn, is settled so that there is continuity of ψ along the intersecting walls midlines (for the first wall 1, one can impose initially $c_1 = 0$, in order to obtain ψ^A. Later, this is adjusted to comply with the orthogonality conditions).

Function ψ_L is a linear function that can be interpreted as the result of the pole shift from the local system of where the local Saint-Venant's warping function (ψ_R) is conceived to the shear centre. By applying equations (3.80) and (3.81) to every wall, the proposed warping function is obtained, and is exactly the warping function that is obtained when the thin-wall approximation is introduced in the classical Saint-Venant's theory. As in the warping function from Campello and Lago [2], function ψ_R is taken here as the one from [49], which is a polynomial approximation to the exact solution of the Saint-Venant's warping function for rectangular cross-sections.

Remarkably, it can be proven that values of ψ_L calculated on the wall midline are precisely the same as those given by $\omega(s)$. Moreover, the only difference between equations (3.65) and (3.80) is a linear term in the secondary warping of each wall, i.e., along each wall thickness. Such term can be made explicit by expressing (3.81) in the walls local system. Note that the linear variation of the out-of-plane displacements along the thickness is a common assumption for shell models, and has even been used for similar rod models (see Gonçalves [35], where only the linear terms are present in the warping function, even though the secondary warping is defined as to enforce Kirchhoff's plate assumption).

Using the same algorithm as in the last section, the shear centre (principal pole) is obtained. Note, however, that it cannot be guaranteed that the warping functions generated with (3.65) and (3.80) share the exact same coordinates for C, although they were nearly identical at the performed evaluations.

3.4.4.   Implementation

Based on what was shown in the last sections, an algorithm was developed for arbitrary open thin-walled cross sections, constituted of rectangular walls or sub-sections. It was considered that inputs always respect those attributes, and no checking is made as to verify whether there are any loops (leading to a closed section) in the section description. Sections with loose segments should not be treated with this algorithm (for example, disconnected double C-channels). The rod axis is always at (0,0).

Step 1: Determine the sequence for building the warping function (generates a list Ord, in which the first element is ALWAYS the first wall of the list), and determine which wall is the predecessor of a given segment (generates a list $Pred$). The following arbitrary cross section will be taken as an illustrative example:
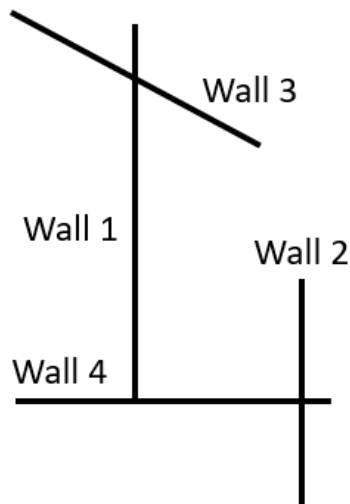
Figure 7 – Example of cross-section for sorting algorithm.

With the pseudo-code below, one gets the sequence of integration $Ord = [1,3,4,2]$ and the list of predecessors is $Pred = [0,4,1,1]$ (for example, wall 2 is the last one to be calculated, and uses as reference the results from wall 1).

<u>*Pseudo-code for Step 1:*</u>

! For a given list of straight segments that define the thin walls, return a list with the sequence for building the warping function and the respective precedents of each wall. Wall 1 is always the initial wall.

Start subroutine

Marcos Pires Kassab   61

Advances on a kinematically exact rod model for thin-walled open section members: consistent warping function and nonlinear constitutive equation

Initiate a vector (here, called **Ord**), with the number of the walls in crescent order $Ord = [1,2,3,...]$

Initiate a zero vector (here, called **Pred**), with the number of the precedented wall (wall from which the construction of the warping function will resume) $Pred = [0,0,0,...]$

$pos = 2$

For i=1 to "number of walls"

    For j=i+1 to "number of walls"

        if (Wall j intersects Wall i then)

            swap values in $Ord(pos)$ and $Ord(j)$

            $Pred(j) = Ord(i)$

            $pos = pos+1$

        end if

    end for

  end for

end subroutine

Step 2: Using the sequence from **Pred**, calculate $\psi^{A,B}$ (according to either section 3.4.2 or 3.4.3, depending on the assumption that is under evaluation). *A* is initially on $(0,0)$ and *B* is on the initial point of Wall 1. Note that this choice is arbitrary.

Step 3: Using the procedure from section 3.4.2, update the sectorial pole and origin, so that they become the principal pole and principal origin.

Step 4: Naturally, when the pole is updated, step 2 must be recalculated, in order to obtain $\psi^{C,D}$.

This procedure was implemented in PEFSYS, as a pre-processing interface that generates the desired warping function and its directional derivatives. To validate the approach and its implementation, the torsion-related geometrical properties (i.e., shear centre, sectorial moments, sectorial products of inertia, torsion inertia and warping constant) of some common sections were computed through numerical integration, via the composed Simpson's method (see figure Figure 8), and the results compared to analytical ones from the literature. This same integration scheme is employed to evaluate other cross-sectional integrals of the rod model, such as the stress resultants and tangent stiffness matrix from equation (3.28) and (3.43),
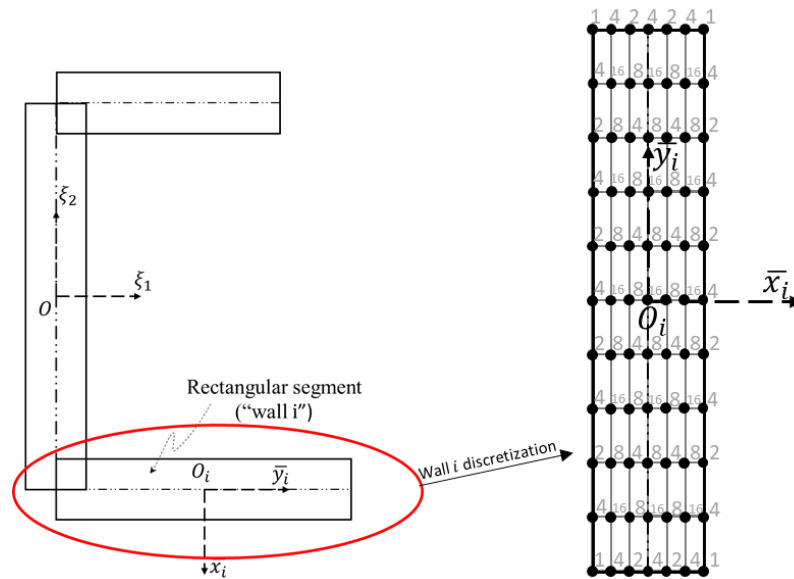
Figure 8 – Wall "i" discretization for Simpson´s method integration. The weights are represented at the nodes, where the integrands are calculated

3.4.5.   *Validation*

The proposed algorithm was tested for some usual cross-sections, presented below. Note that the analytical result for the warping constant I_ψ is typically calculated only with the primary (Vlasov's) warping.

3.4.5.1. *I-section (mono-symmetric)*
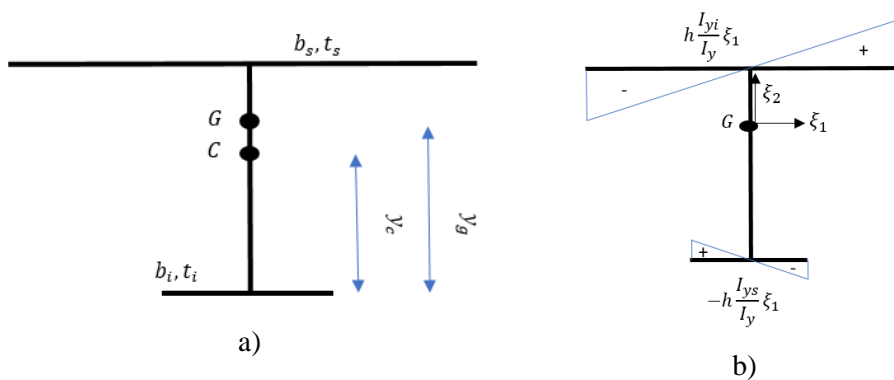
Figure 9 – a) Cross-section geometry. b) Sectorial area for principal pole and origin ($\omega^{C,D}$).

The analytical geometrical properties´ expressions were deduced in [50], and the results are

$$y_g = \frac{h\left(b_s t_s + \frac{h t_w}{2}\right)}{A} \tag{3.82}$$

$$A = h t_w + b_i t_i + b_s t_s \tag{3.83}$$

$$I_{yi} = \frac{t_i b_i^3}{12} ; I_{ys} = \frac{t_s b_s^3}{12} \tag{3.84}$$

$$I_y = I_{yi} + I_{ys} = \frac{t_i b_i^3}{12} + \frac{t_s b_s^3}{12} \tag{3.85}$$

$$I_\omega = \frac{h^2 I_{yi} I_{ys}}{I_y} \tag{3.86}$$

$$y_C = h \frac{I_{ys}}{I_y} = \frac{h t_s b_s^3}{12} \tag{3.87}$$

A benchmark was made for some bi-symmetric commercial profiles (CVS, VS ,W ,HP), and for a fictitious mono-symmetric profile (Table 1).

Marcos Pires Kassab

Advances on a kinematically exact rod model for thin-walled open section members: consistent warping function and nonlinear constitutive equation

Table 1 – Geometric characterization – I-section test

ID		Geometry						
	(unit)	bi	h	bs	ti	tw	ts
CVS 150x22	cm	12	13.4	12	0.8	0.63	0.8
CVS 1000x486	cm	70	93.7	70	3.15	1.9	3.15
VS 400x34	cm	16	38.4	16	0.8	0.475	0.8
W 150x13	cm	10	13.82	10	0.49	0.43	0.49
HP 310 x 125	cm	31.2	27.72	31.2	1.74	1.74	1.74
I-mono-sym.	cm	4	10	5.3	0.6	0.6	0.6

Table 2 – Warping function generator algorithm – I-section test

ID	Analytic			Campello and Lago						Proposed function					
				Numeric			Relative error			Numeric			Relative error		
	I_T	y_c	I_ω	I_T	y_c	I_ψ	I_T	y_c	I_ψ	I_T	y_c	I_ψ	I_T	y_c	I_ψ
	(cm^4)	(cm)	(cm^6)	(cm^4)	(cm)	(cm^6)		(%)		(cm^4)	(cm)	(cm^6)		(%)	
CVS 150x22	5.21	6.70	1.03E+04	5.16	6.70	1.03E+04	-1.3	0.0	0.2	5.16	6.70	1.04E+04	-1.3	0.0	0.2
CVS 1000x486	1.67E+03	46.9	3.95E+08	1.67E+03	46.85	3.95E+08	-0.6	0.0	0.1	1.67E+03	46.85	3.95E+08	-0.6	0.0	0.1
VS 400x34	6.83	19.2	2.01E+05	6.80	19.2	2.01E+05	-0.5	0.0	0.0	6.80	19.2	2.013E+05	-0.5	0.0	0.0
W 150x13	1.15	6.91	3.90E+03	1.15	6.91	3.90E+03	-0.5	0.0	0.1	1.15	6.91	3.90E+03	-0.5	0.0	0.1
HP 310 x 125	158	13.9	1.69E+06	156.8	13.86	1.69E+06	-0.9	0.0	0.2	156.82	13.86	1.69E+06	-0.9	0.0	0.2
I-mono-sym	1.35	6.57	197	21.1	6.57	200	1468	0.0	1.1	1.31	6.54	199	-3.0	-0.45	1.1

Marcos Pires Kassab   65

Advances on a kinematically exact rod model for thin-walled open section members: consistent warping function and nonlinear constitutive equation

3.4.5.2. Top hat ($b_i > 0$) and C-section (with ($b_i < 0$) or without ($b_i = 0$) stiffener)

(a)

(b)
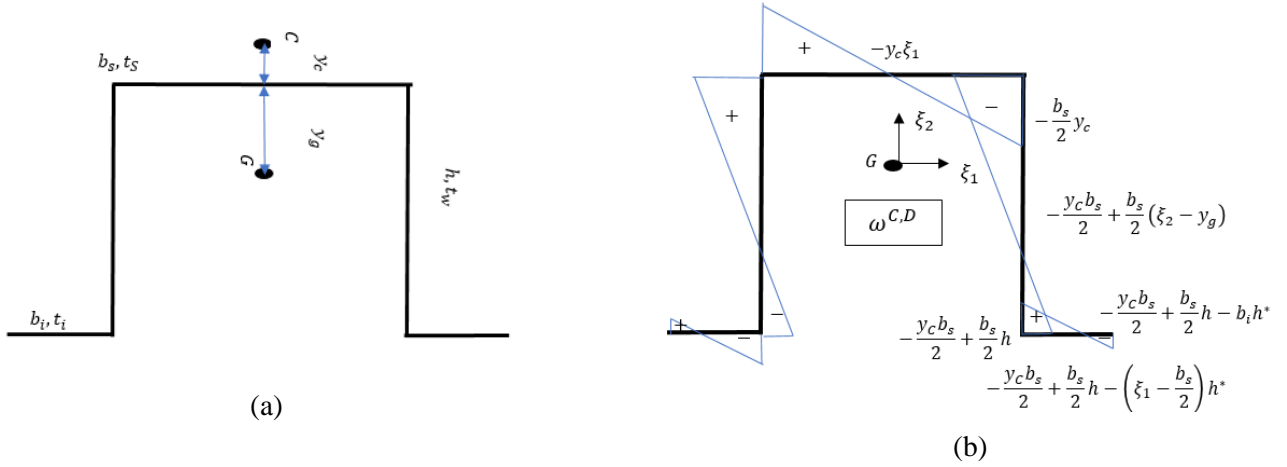
Figure 10 – a) Cross-section geometry. b) Sectorial area for principal pole and origin ($\omega^{C,D}$).

The analytical geometrical properties expressions were deduced, and can be found in the Appendix A.

$$|y_g| = \frac{(h^2 t_w + 2ht_i|b_i|)}{A} \tag{3.88}$$

$$A = 2ht_w + 2|b_i|t_i + b_s t_s \tag{3.89}$$

$$y_C = \frac{\dfrac{b_s^2 h^2 t_w}{4} + \dfrac{b_s^2 h|b_i|t_i}{2} - \dfrac{2|b_i^3|ht_i}{3}}{I_y} \tag{3.90}$$

$$I_\omega = \frac{b_s^3 t_s \Delta\xi_2^2}{12} + \frac{b_s^2}{6} t_w(h^3 - 3h^2 y_c + 3hy_c^2)$$

$$+ \frac{2|b_i|}{3}(3k^2 - 3kb_i h^* + b_i^2 h^{*2})t_i \tag{3.91}$$

with $k = \frac{b_s}{2}(h - y_c)$ and $h^* = h + y_c$.

Advances on a kinematically exact rod model for thin-walled open section members: consistent warping function and nonlinear constitutive equation

Table 3 – Geometric characterization – C section and top hat test

| ID | Geometry | | | | | | |
	(unit)	bi	h	b	ti	tw	tf
Top hat 50x2,81	cm	2.5	5	5	0.19	0.19	0.19
Top hat 110x10,37	cm	2.5	11	10	0.38	0.38	0.38
C 76x6,11	cm	0	7.62	3.58	0	0.43	0.69
C 305x30,7	cm	0	29.21	7.115	0	0.71	1.27
C (stff)110x10,38	cm	-2.5	11	10	0.38	0.38	0.38

Table 4 – Warping function generator algorithm – C section test

ID	Analytic			Campello and Lago						Proposed function					
				Numeric			Relative error			Numeric			Relative error		
	I_T	y_c	I_ω	I_t	y_c	I_ψ	I_T	y_c	I_ψ	I_T	y_c	I_ψ	I_T	y_c	I_ψ
	(cm^4)	(cm)	(cm^6)	(cm^4)	(cm)	(cm^6)	(%)			(cm^4)	(cm)	(cm^6)	(%)		
Top hat 50x2.81	0.0457	1.79	60.1	48.3	1.77	60.1	105527	0.0	0.0	0.0454	1.79	60.2	-0.8	-0.1	0.3
Top hat 110x10.37	0.658	4.69	3.30E+03	800	4.69	3.30E+03	121403	0.0	0.0	0.650	4.68	3.31E+03	-1	-0.1	0.3
C 76x6.11	0.986	1.47	118	53.3	1.47	118	5304	0.0	0.0	0.911	1.46	121	-7	-0.5	2.0
C 305x30.7	13.2	2.57	2.98E+04	692	2.57	2.98E+04	5139	0.0	0.0	12.4	2.57	2.99E+04	-6	-0.1	0.5
C (stff) 110x10.38	0.658	5.52	7.19E+03	870	5.48	7.19	132004	-1.0	0.0	0.650	5.49	7.20E+03	-1	-0.7	0.2

Marcos Pires Kassab 67

Advances on a kinematically exact rod model for thin-walled open section members: consistent warping function and nonlinear constitutive equation

3.4.5.3. Z-section

(a)   (b)
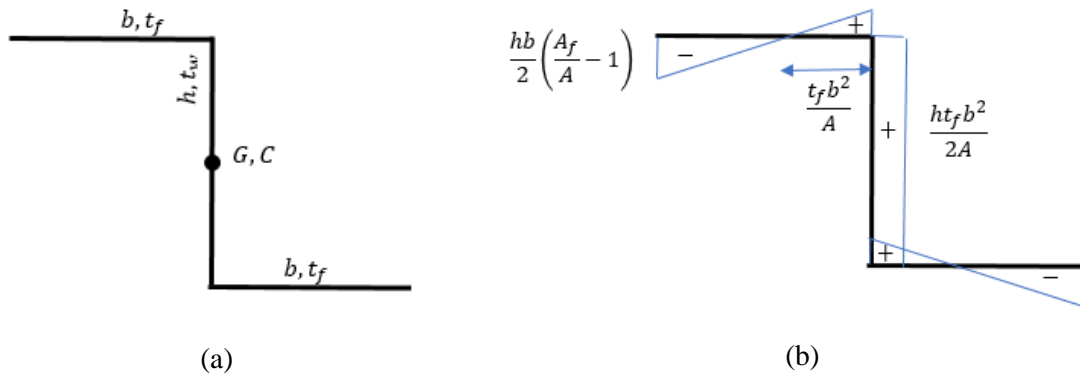
Figure 11 – a) Cross-section geometry. b) Sectorial area for principal pole and origin ($\omega^{C,D}$).

The analytic geometric properties expressions were deduced in [50]. They are

$$x_g = x_c = 0; \tag{3.92}$$

$$I_\omega = \frac{h^2 t_f b^3}{12A}(t_f b + 2ht_w); \tag{3.93}$$

A benchmark was made for two commercial profiles (Table 5).

Marcos Pires Kassab

Advances on a kinematically exact rod model for thin-walled open section members: consistent warping function and nonlinear constitutive equation

Table 5 – Geometric characterization – Z section test

ID		Geometry			
	(unit)	b	h	tf	tw
Z 50x2,10	cm	2.5	5	0.152	0.152
Z 150x3,62	cm	5	15	0.461	0.461

Table 6 – Warping function generator algorithm – Z section test

ID	Analytic			Campello and Lago						Proposed function					
				Numeric			Relative error			Numeric			Relative error		
	I_T	x_c	I_ω	I_T	x_c	I_ψ	I_T	x_c	I_ψ	I_T	x_c	I_ψ	I_T	x_c	I_ψ
	(cm^4)	(cm)	(cm^6)	(cm^4)	(cm)	(cm^6)		(%)		(cm^4)	(cm)	(cm^6)		(%)	
Z 50x2,10	0.0117	0	6.18	1192	0	6.19	10143	0.00	0.06	0.0116	0	6.19	-0.80	0	0.1
Z 150x3,62	0.816	0	1513	29.6	0	1515	3527	0.00	0.16	0.81	0	1515	-1.30	0	0.2

Marcos Pires Kassab   69

Advances on a kinematically exact rod model for thin-walled open section members: consistent warping function and nonlinear constitutive equation

3.4.5.4. V-section (with or without stiffener)
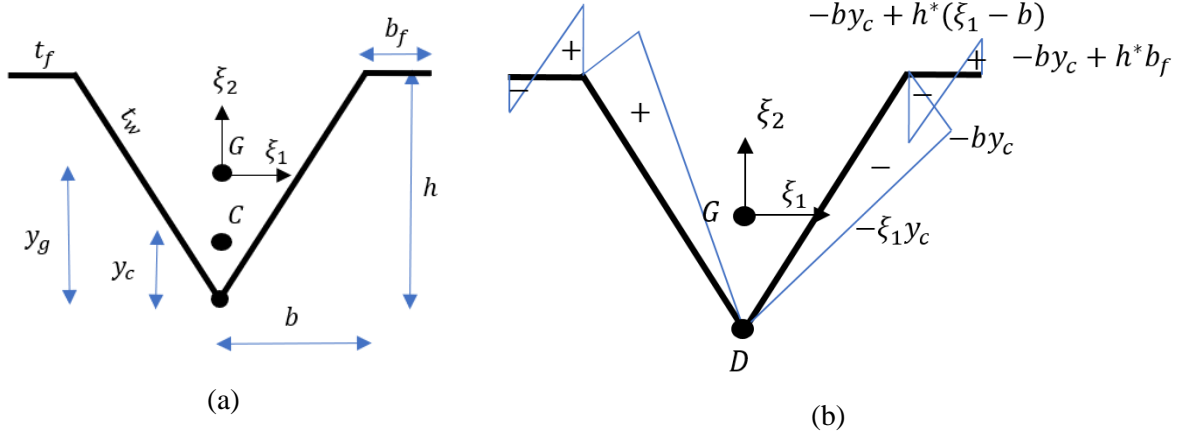
Figure 12 – a) Cross-section geometry. b) Sectorial area for principal pole and origin ($\omega^{C,D}$).

The analytic geometric properties expressions were deduced, and can be found in Appendix D. They are

$$y_g = \frac{ht_w l + 2t_f b_f h}{A};$$ (3.94)

$$A = 2lt_w + 2b_f t_f;$$ (3.95)

$$I_y = \frac{2}{3}b^2 l t_w + 2\left[\frac{b_f^3 t_f}{12} + \left(b + \frac{b_f}{2}\right)^2 b_f t_f\right];$$ (3.96)

$$y_c = \frac{2ht_f\left(\frac{b_f^3}{3} + \frac{b_f^2 b}{2}\right)}{I_y};$$ (3.97)

$$I_\omega = \frac{2}{3}lb^2 y_c^2 t_w + \frac{2}{3}b_f\left(3b^2 y_c^2 - 3by_c h^* b_f + \left(h^* b_f\right)^2\right)t_f,$$ (3.98)

with $l = \sqrt{b^2 + h^2}$ and $h^* = h - y_c$. A few examples are presented below (Table 7).

Advances on a kinematically exact rod model for thin-walled open section members: consistent warping function and nonlinear constitutive equation

Table 7 – Geometric characterization – V section test

ID	(unit)	Geometry				
		b	bf	h	tf	tw
NO_STFF_1	cm	5	0	10	0	1
NO_STFF_2	cm	3	0	10	0	0.38
STFF_1	cm	5	2	10	1	1
STFF_2	cm	3	3	10	0.1	0.38

Table 8 – Warping function generator algorithm – V section test

ID	Analytic			Campello and Lago						Proposed function					
				Numeric			Relative error			Numeric			Relative error		
	I_T	y_c	I_ω	I_T	y_c	I_ψ	I_T	y_c	I_w	I_T	y_c	I_ψ	I_T	y_c	I_ψ
	(cm^4)	(cm)	(cm^6)	(cm^4)	(cm)	(cm^6)	(%)			(cm^4)	(cm)	(cm^6)	(%)		
NO_STFF_1	7.45	0.00	0.00	706	0.00	18	9372	0.0	100	7.26	0.0496	76.6	-2.5	100	100
NO_STFF_2	0.382	0.00	0.00	217	0.00	0.863	56613	0.0	100	0.380	0.0200	3.46	-0.4	100	100
STFF_1	8.78	0.764	340	691	0.764	359	7760	0.0	6.0	8.19	0.788	415	-6.8	3.2	22
STFF_2	0.38	1.24	124	142	1.24	125	36833	0.0	1.0	0.382	1.25	127	-0.4	0.8	2.0

Note that, for the non-stiffened V sections, a non-zero warping inertia was obtained numerically due to the secondary warping, rendering the 100% relative error. The same happens for the shear centre position when the proposed warping function is used.

Marcos Pires Kassab 71

Advances on a kinematically exact rod model for thin-walled open section members: consistent warping function and nonlinear constitutive equation

3.4.6.   Validation conclusion – choosing the warping function

As stated on the beginning of this section, the proposed function is more general than the one proposed by Campello and Lago [2] for arbitrary thin-walled open sections. For a few specific cases, both methods generate exactly the same functions, and, for this reason, in the mentioned reference, the simulations were coherent. Having said that, to achieve more robustness, this work advances with the proposed warping function. With the proposed equation (3.80), for all the tested geometries, the numerical results are practically identical to the analytical ones, supporting that the proposed equation, the algorithm for generating the warping function and its implementation are correct. Possible sources of slight differences are the numerical integration and the neglect of the secondary warping in the analytical expressions. Here, it was assumed that the orthogonality conditions are adopted, without further explanation. In Appendix E, the reader finds a detailed (and important) discussion about this decision. The reading of such extract is strongly recommended.

Marcos Pires Kassab   73

Advances on a kinematically exact rod model for thin-walled open section members: consistent warping function and nonlinear constitutive equation

4. CONSTITUTIVE EQUATION AND PROPOSED CONTRIBUTION

In continuum mechanics, a constitutive equation characterizes a material behaviour, mapping the stress tensors as functions of kinematic fields (strains, velocity, etc). In this work, only isotropic hyperelastic materials are of interest.

A material is *elastic* if the stress field is formally a function of only its strain field, and therefore, for a given strain tensor $\boldsymbol{E}$, there is only one corresponding stress state $\boldsymbol{S}$.

A material is classified as *hyperelastic* if a specific strain energy function ($\psi_h(\boldsymbol{E})$) exists such that

$$\boldsymbol{S} = \frac{\partial \psi_h}{\partial \boldsymbol{E}}. \tag{4.1}$$

Thus, hyperelastic materials are, necessarily, elastic.

A material is isotropic if its properties (particularly, mechanical ones) are strictly the same in every direction. For isotropic materials, its potential function can be written as function of the three invariants of the right Cauchy-Green strain tensor ($\boldsymbol{C}$)

$$I_1 = \boldsymbol{I}{:}\boldsymbol{C}, \quad I_2 = \frac{1}{2}\boldsymbol{I}{:}\boldsymbol{C^2}, \quad \text{and } I_3 = det\boldsymbol{F}. \tag{4.2}$$

It should be noted that $det\boldsymbol{C} = det\boldsymbol{F}^2$, justifying the usage of $\boldsymbol{F}$ in I_3.

For this work, the stress tensor $\boldsymbol{P}^r$ is needed, rather than $\boldsymbol{S}$. Using the identities $\boldsymbol{P}^r = \boldsymbol{Q}^T\boldsymbol{P}$, (B.7), (3.8) and (4.2), one gets

$$\boldsymbol{P}^r = \boldsymbol{F}^r \frac{\partial \psi_h}{\partial \boldsymbol{E}}, \tag{4.3}$$

With equations (A.7), (4.3) and applying the chain rule

$$\boldsymbol{P}^r = \boldsymbol{F}^r \frac{\partial \psi_h}{\partial \boldsymbol{C}} \frac{\partial \boldsymbol{C}}{\partial \boldsymbol{E}}. \tag{4.4}$$

It is easy to show that $\frac{\partial \boldsymbol{C}}{\partial \boldsymbol{E}} = 2\boldsymbol{I}$, thus (4.5) becomes

$$\boldsymbol{P}^r = 2\boldsymbol{F}^r \frac{\partial \psi_h}{\partial \boldsymbol{C}}. \tag{4.5}$$

Let us calculate the derivative of the right-hand side of the above equation. First, let us rewrite

$$\frac{\partial \psi_h}{\partial \boldsymbol{C}} = \frac{\partial \psi_h}{\partial I_i} \frac{\partial I_i}{\partial \boldsymbol{C}}. \tag{4.6}$$

The terms $\frac{\partial \psi_h}{\partial I_i}$ will only depend on the specific adopted material, whilst the terms $\frac{\partial I_i}{\partial \boldsymbol{C}}$ can be readily obtained. The derivatives of I_1, I_2 and I_3 are

$$\frac{\partial I_1}{\partial \boldsymbol{C}} = \boldsymbol{I}, \tag{4.7}$$

$$\frac{\partial I_2}{\partial \boldsymbol{C}} = \boldsymbol{C}. \tag{4.8}$$

In order to find the derivatives of I_3, some auxiliar results are needed (see Appendix H). The result is

$$\frac{\partial I_3}{\partial \boldsymbol{C}} = \frac{J}{2}\left(\boldsymbol{F}^{r-1}\boldsymbol{F}^{r-T}\right). \tag{4.9}$$

With (4.8) and (4.9), it is possible to rewrite (4.6) as

$$\boldsymbol{P}^r = \frac{\partial \psi_h}{\partial J} J \boldsymbol{F}^{r-T} + 2\frac{\partial \psi_h}{\partial I_1}\boldsymbol{F}^r + 2\frac{\partial \psi_h}{\partial I_2}\boldsymbol{F}^r \boldsymbol{C}. \tag{4.10}$$

Note that, using the fact that $(\boldsymbol{a} \otimes \boldsymbol{b})(\boldsymbol{c} \otimes \boldsymbol{d}) = (\boldsymbol{b} \cdot \boldsymbol{c})(\boldsymbol{a} \otimes \boldsymbol{d})$, $\boldsymbol{C}$ and $\boldsymbol{F}^r\boldsymbol{C}$ can be expressed by the column-vectors of $\boldsymbol{F}^r$

$$\boldsymbol{C} = \boldsymbol{F}^{rT}\boldsymbol{F}^r = (\boldsymbol{e}_i^r \otimes \boldsymbol{f}_i^r)(\boldsymbol{f}_j^r \otimes \boldsymbol{e}_j^r) = (\boldsymbol{f}_i^r \cdot \boldsymbol{f}_j^r)(\boldsymbol{e}_i^r \otimes \boldsymbol{e}_j^r) \tag{4.11}$$

$$\boldsymbol{F}^r\boldsymbol{C} = (\boldsymbol{f}_i^r \cdot \boldsymbol{f}_j^r)(\boldsymbol{e}_k^r \otimes \boldsymbol{f}_k^r)(\boldsymbol{e}_i^r \otimes \boldsymbol{e}_j^r) = (\boldsymbol{f}_i^r \cdot \boldsymbol{f}_j^r)(\boldsymbol{e}_i^r \cdot \boldsymbol{e}_k^r)(\boldsymbol{f}_k^r \otimes \boldsymbol{e}_j^r)$$
$$= (\boldsymbol{f}_i^r \cdot \boldsymbol{f}_j^r)(\boldsymbol{f}_i^r \otimes \boldsymbol{e}_j^r) \tag{4.12}$$

Also, knowing that $det\boldsymbol{F}^r = det\boldsymbol{F} = J$, and using that the inverse matrix can be calculated as

$$\boldsymbol{F}^{r-1} = \frac{1}{J}adj(\boldsymbol{F}^r) = \frac{1}{J}cof(\boldsymbol{F}^r)^T, \tag{4.13}$$

where the operator $adj(\cdot)$ represents the adjoint matrix, and $cof(\cdot)$ represents the cofactors matrix, one gets that

$$J\boldsymbol{F}^{r-T} = cof(\boldsymbol{F}^r). \tag{4.14}$$

Defining

$$cof(\boldsymbol{F}^r) = \boldsymbol{g}_i^r \otimes \boldsymbol{e}_i^r, \tag{4.15}$$

with, for 3x3 matrixes,

$$\boldsymbol{g}_1^r = \boldsymbol{f}_2^r \times \boldsymbol{f}_3^r, \boldsymbol{g}_2^r = \boldsymbol{f}_3^r \times \boldsymbol{f}_1^r, \boldsymbol{g}_3^r = \boldsymbol{f}_1^r \times \boldsymbol{f}_2^r, \tag{4.16}$$

or, more concisely,

$$\boldsymbol{g}_i^r = \frac{1}{2}\epsilon_{ijk}\boldsymbol{f}_j^r \times \boldsymbol{f}_k^r, \tag{4.17}$$

in which ϵ_{ijk} represents the permutation symbol for three dimensions, it is now possible to substitute (4.11), (4.12) and (4.15) in (4.10), rendering

$$\boldsymbol{P}^r = \boldsymbol{\tau}_i^r \otimes \boldsymbol{e}_i^r = \frac{\partial \psi_h}{\partial J}\boldsymbol{g}_i \otimes \boldsymbol{e}_i^r + 2\frac{\partial \psi_h}{\partial I_1}\boldsymbol{f}_i^r \otimes \boldsymbol{e}_i^r$$
$$+ 2\frac{\partial \psi_h}{\partial I_2}(\boldsymbol{f}_i^r \cdot \boldsymbol{f}_j^r)(\boldsymbol{f}_i^r \otimes \boldsymbol{e}_j^r). \tag{4.18}$$

Thus, using the fact that $(\boldsymbol{f}_i^r \cdot \boldsymbol{f}_j^r)(\boldsymbol{f}_i^r) = (\boldsymbol{f}_j^r \otimes \boldsymbol{f}_j^r)\boldsymbol{f}_i^r$, the column-vectors $\boldsymbol{\tau}_i^r$ are

$$\boldsymbol{\tau}_i^r = \frac{\partial \psi_h}{\partial J}\boldsymbol{g}_i^r + 2\frac{\partial \psi_h}{\partial I_1}\boldsymbol{f}_i^r + 2\frac{\partial \psi_h}{\partial I_2}(\boldsymbol{f}_j^r \otimes \boldsymbol{f}_j^r)\boldsymbol{f}_i^r. \tag{4.19}$$

Note that (4.19) is valid for any isotropic hyperelastic material. This presentation of $\boldsymbol{P}^r$, in terms of the columns of $\boldsymbol{F}^r$ was taken from Dasambiagio [25].

It is also possible to define the fourth order tensor of the tangent elastic modulus, $\mathbb{D} = \frac{\partial \boldsymbol{S}}{\partial \boldsymbol{E}}$, but since it will not be employed directly in the rod model, no further discussion about it will be done here.

Some variables that will be used in the constitutive equations must now be defined. Let λ, μ be the (generalized) Lamé elastic moduli. From elasticity theory, the following expressions are valid

Marcos Pires Kassab 75

Advances on a kinematically exact rod model for thin-walled open section members: consistent warping function and nonlinear constitutive equation

$$\mu = G \quad \text{and} \quad \lambda + 2\mu = \frac{E(1-\nu)}{(1+\nu)(1-2\nu)}, \tag{4.20}$$

wherein E is the longitudinal elastic modulus, G is the transverse elastic modulus and ν is the Poisson's coeficient. Were Poisson effects to be neglected, equation $(4.20)_2$ could be modified to emulate the implied uniaxial state. This renders $\lambda + 2\mu \approx E$, and should help to avoid volumetric locking.

Three isotropic hyperelastic material laws are commonly of interest in the context of kinematically exact rod models: the linear elastic, the *Saint-Venant´s*[6] and the *Simo-Ciarlet´s* material. The last two are 2-parameter hyperelastic constitutive equations that apply to 3D deformations and relate more general (objective) stress and strain tensors.

Here, the exact form of the constitutive equations are employed (i.e., retaining all higher order strains in the stress resultants expressions), differently from what was done in [1], [3] (and in almost every other work, except [2]), where only some of the higher order terms were retained. As a downside, in the current approach, stress resultants and the tangent stiffness matrix must be numerically integrated, increasing the total time for building the correspondent vectors and matrices. Even though some operations might even be possible to analytically integrate beforehand, the structure of the constitutive equations requires a lot of algebraic effort that would still be dependent on a large amount of high-order geometrical properties, which are not trivial. That said, the option was to evaluate the stress resultants and their derivatives through numerical integration of their analytical expressions, for both Saint-Venant's and Simo-Ciarlet's materials (see Appendix I for another approach).

4.1. Particularizing elastic constitutive equations for rods

In rod models, the concept of cross-sectional stress resultants, which implies integration of stresses over the cross-sectional area, allows one to write the constitutive equation in the following general form

$$\boldsymbol{\sigma}^r = \widehat{\boldsymbol{\sigma}^r}(\boldsymbol{\varepsilon}^r), \quad \boldsymbol{D} = \frac{\partial \boldsymbol{\sigma}^r}{\partial \boldsymbol{\varepsilon}^r}, \tag{4.21}$$

where $\boldsymbol{\sigma}^r$ is a vector that collects the cross-sectional resultants (forces, moments and, occasionally, bi-shear and bi-moment), $\boldsymbol{\varepsilon}^r$ is a vector that contains generalized strain measures and $\boldsymbol{D} = \widehat{\boldsymbol{D}}(\boldsymbol{\varepsilon})$ is a tangent elastic matrix that relates those quantities (being a function of the material parameters and the cross-sectional geometrical properties, such as area, moments of inertia, etc). As shown in [23], [24], when stresses are analytically integrated over the cross-section, as to allow for the cross-sectional force and moment resultants, an explicit expression for $\boldsymbol{D}$ is obtained**,** which depends on the cross-section´s geometry and the adopted material law for the model at hand. This is also shown in detail in section 3.2 and 3.3.

---

[6] Sometimes, this material is also referred to as the *Kirchhoff-Saint-Venant*'s material.

Using the formulation for isotropic hyperelastic materials, it is possible to integrate $\boldsymbol{\sigma}^r$ and $\boldsymbol{D}$. Whilst $\boldsymbol{\sigma}^r$ is obtained directly from the integration of $\boldsymbol{\tau}_i^r$ (see equation (3.28)), for the calculation of $\boldsymbol{D}$ (equation (3.43)), the auxiliar expressions $\boldsymbol{C}_{33}$, $\boldsymbol{c}$, $\boldsymbol{d}$, $\boldsymbol{d}_\alpha$, $\boldsymbol{b}_\alpha$ are needed. Constraining the formulation for the 7 DOF rod model, one gets from equation (3.8), the particular cases

$$\boldsymbol{f}_\alpha^r = \boldsymbol{e}_\alpha^r + p\psi_{,\alpha}\boldsymbol{e}_3^r, \ \ \boldsymbol{f}_3^r = \boldsymbol{e}_3^r + \boldsymbol{\gamma}^r, \tag{4.22}$$

and, for $\alpha \neq \beta$

$$\boldsymbol{g}_\alpha^r = \boldsymbol{e}_\alpha^r - (\boldsymbol{\gamma}^r \cdot \boldsymbol{e}_\alpha^r)\boldsymbol{e}_3^r + (\boldsymbol{\gamma}^r \cdot \boldsymbol{e}_3^r)\boldsymbol{e}_\alpha^r + \psi_{,\beta}p\big[(\boldsymbol{\gamma}^r \cdot \boldsymbol{e}_\alpha^r)\boldsymbol{e}_\beta^r - (\boldsymbol{\gamma}^r \cdot \boldsymbol{e}_\beta^r)\boldsymbol{e}_\alpha^r\big],$$
$$\boldsymbol{g}_3^r = \boldsymbol{e}_3^r - p\psi_{,\alpha}\boldsymbol{e}_\alpha^r, \tag{4.23}$$

The following auxiliary results will be necessary (where needed, $\boldsymbol{v}$ is a constant vector)

$$\frac{\partial \boldsymbol{f}_\alpha^r}{\partial \boldsymbol{\gamma}^r} = \boldsymbol{0}, \ \frac{\partial \boldsymbol{f}_3^r}{\partial \boldsymbol{\gamma}^r} = \boldsymbol{I}, \tag{4.24}$$

$$\frac{\partial \boldsymbol{f}_\alpha^r}{\partial p} = \psi_\alpha \boldsymbol{e}_3^r, \ \frac{\partial \boldsymbol{f}_3^r}{\partial p} = \frac{\partial \boldsymbol{\gamma}^r}{\partial p} = \boldsymbol{\kappa}^r \times \psi \boldsymbol{e}_3^r, \tag{4.25}$$

$$\frac{\partial \boldsymbol{f}_\alpha^r}{\partial p'} = \boldsymbol{o}, \ \frac{\partial \boldsymbol{f}_3^r}{\partial p'} = \psi \boldsymbol{e}_3^r, \tag{4.26}$$

$$\frac{\partial J}{\partial \boldsymbol{\gamma}^r} = \frac{\partial \boldsymbol{g}_3^r \cdot \boldsymbol{f}_3^r}{\partial \boldsymbol{\gamma}^r} = \frac{\partial \boldsymbol{g}_3^{rT} \boldsymbol{f}_3^r}{\partial \boldsymbol{\gamma}^r} = \boldsymbol{g}_3^{rT} \frac{\partial \boldsymbol{f}_3^r}{\partial \boldsymbol{\gamma}^r} = \boldsymbol{g}_3^{rT} \boldsymbol{I} = \boldsymbol{g}_3^{rT}, \tag{4.27}$$

$$\frac{\partial J}{\partial p} = \left(\frac{\partial \boldsymbol{g}_3^r}{\partial p} \cdot \boldsymbol{f}_3^r + \boldsymbol{g}_3^r \cdot \frac{\partial \boldsymbol{f}_3^r}{\partial p}\right) = \left(\left(\frac{\partial \boldsymbol{f}_1^r}{\partial p} \times \boldsymbol{f}_2^r + \boldsymbol{f}_1^r \times \frac{\partial \boldsymbol{f}_2^r}{\partial p}\right) \cdot \boldsymbol{f}_3^r + \boldsymbol{g}_3^r \cdot \frac{\partial \boldsymbol{f}_3^r}{\partial p}\right) =$$
$$\left(\boldsymbol{g}_i^r \cdot \frac{\partial \boldsymbol{f}_i^r}{\partial p}\right) = \boldsymbol{g}_\alpha^r \cdot \psi_{,\alpha} \boldsymbol{e}_3^r + \boldsymbol{g}_3^r \cdot \boldsymbol{\kappa}^r \times \psi \boldsymbol{e}_3^r = -\big[(\boldsymbol{\gamma}^r \cdot \boldsymbol{e}_\alpha^r)\psi_{,\alpha} + $$
$$p\psi\psi_{,\alpha}(\boldsymbol{\kappa}^r \times \boldsymbol{e}_3^r) \cdot \boldsymbol{e}_\alpha^r\big], \tag{4.28}$$

$$\frac{\partial J}{\partial p'} = \frac{\partial \boldsymbol{g}_3^r \cdot \boldsymbol{f}_3^r}{\partial p'} = \boldsymbol{g}_3^{rT} \frac{\partial \boldsymbol{f}_3^r}{\partial p'} = \boldsymbol{g}_3^r \cdot \psi \boldsymbol{e}_3^r = \psi, \tag{4.29}$$

$$\frac{\partial \boldsymbol{g}_\alpha^r}{\partial p} \cdot \boldsymbol{e}_3^r = -\left(\frac{\partial \boldsymbol{\gamma}^r}{\partial p} \cdot \boldsymbol{e}_\alpha^r\right) = (-\boldsymbol{\kappa}^r \times \psi \boldsymbol{e}_3^r \cdot \boldsymbol{e}_\alpha^r) = -\epsilon_{\alpha\beta}\psi(\boldsymbol{e}_\beta^r \cdot \boldsymbol{\kappa}^r), \tag{4.30}$$

$$\frac{\partial \boldsymbol{g}_3^r}{\partial \boldsymbol{\gamma}^r} = \boldsymbol{f}_1^r \times \boldsymbol{f}_2^r = \boldsymbol{0}, \tag{4.31}$$

$$\frac{\partial \boldsymbol{g}_3^r}{\partial p} = \frac{\partial \boldsymbol{f}_1^r}{\partial p} \times \boldsymbol{f}_2^r + \boldsymbol{f}_1^r \times \frac{\partial \boldsymbol{f}_2^r}{\partial p} = \epsilon_{\alpha\beta}\psi_{,\alpha}\boldsymbol{e}_3^r \times (\boldsymbol{e}_\beta^r + \psi_{,\beta}p\boldsymbol{e}_3^r) = -\psi_{,\alpha}\boldsymbol{e}_\alpha^r, \tag{4.32}$$

$$\frac{\partial \boldsymbol{g}_\alpha^r}{\partial p'} = \epsilon_{\alpha\beta3}\frac{\partial \boldsymbol{f}_\beta^r \times \boldsymbol{f}_3^r}{\partial p'} = \epsilon_{\alpha\beta3}\boldsymbol{f}_\beta^r \times \frac{\partial \boldsymbol{f}_3^r}{\partial p'} = \epsilon_{\alpha\beta3}\boldsymbol{e}_\beta^r \times \psi \boldsymbol{e}_3^r = \psi \boldsymbol{e}_\alpha^r, \tag{4.33}$$

$$\frac{\partial \boldsymbol{g}_3^r}{\partial p'} = \boldsymbol{0}, \tag{4.34}$$

$$tr\boldsymbol{C} = tr(\boldsymbol{F}^{rT}\boldsymbol{F}^r) = tr\left((\boldsymbol{e}_i^r \otimes \boldsymbol{f}_i^r)(\boldsymbol{f}_j^r \otimes \boldsymbol{e}_i^r)\right) = tr\left((\boldsymbol{f}_i^r \cdot \boldsymbol{f}_j^r)(\boldsymbol{e}_i^r \otimes \boldsymbol{e}_j^r)\right)$$
$$= \boldsymbol{f}_j^r \cdot \boldsymbol{f}_j^r \tag{4.35}$$

$$\frac{\partial (tr\boldsymbol{C})\boldsymbol{v}}{\partial \boldsymbol{\gamma}^r} = \boldsymbol{v}\frac{\partial \boldsymbol{f}_j^r \cdot \boldsymbol{f}_j^r}{\partial \boldsymbol{\gamma}^r} = \boldsymbol{v}\frac{\partial \boldsymbol{f}_3^r \cdot \boldsymbol{f}_3^r}{\partial \boldsymbol{\gamma}^r} = \boldsymbol{v}\frac{\partial \boldsymbol{f}_3^r \cdot \boldsymbol{f}_3^r}{\partial \boldsymbol{f}_3^r}\frac{\partial \boldsymbol{f}_3^r}{\partial \boldsymbol{\gamma}^r} = 2\boldsymbol{v}\boldsymbol{I}\boldsymbol{f}_3^{rT}\boldsymbol{I} = 2\boldsymbol{v}\boldsymbol{f}_3^{rT} = 2\boldsymbol{v} \otimes \boldsymbol{f}_3^r \tag{4.36}$$

Marcos Pires Kassab 77

Advances on a kinematically exact rod model for thin-walled open section members: consistent warping function and nonlinear constitutive equation

$$\frac{\partial tr\boldsymbol{C}}{\partial p} = \frac{\partial \boldsymbol{f}_j^r \cdot \boldsymbol{f}_j^r}{\partial p} = \frac{\partial \boldsymbol{f}_j^{r^T} \boldsymbol{f}_j^r}{\partial p} = \frac{\partial \boldsymbol{f}_j^{r^T}}{\partial p} \boldsymbol{f}_j^r + \boldsymbol{f}_j^{r^T} \frac{\partial \boldsymbol{f}_j^r}{\partial p} = 2\frac{\partial \boldsymbol{f}_j^r}{\partial p} \cdot \boldsymbol{f}_j^r$$

$$= 2\big[(\psi_{,\alpha} \boldsymbol{e}_3^r) \cdot (\boldsymbol{e}_\alpha^r + p\psi_{,\alpha} \boldsymbol{e}_3^r) + (\boldsymbol{\kappa}^r \times \psi \boldsymbol{e}_3^r) \cdot (\boldsymbol{e}_3^r + \boldsymbol{\gamma}^r)\big] \tag{4.37}$$

$$= 2\big[p\psi_{,\alpha}\psi_{,\alpha} + (\boldsymbol{\kappa}^r \times \psi \boldsymbol{e}_3^r) \cdot (\boldsymbol{\gamma}^r)\big]$$

,
$$\frac{\partial tr\boldsymbol{C}}{\partial p'} = 2\frac{\partial \boldsymbol{f}_j^r}{\partial p'} \cdot \boldsymbol{f}_j^r = 2\psi(1 + \boldsymbol{\gamma}^r \cdot \boldsymbol{e}_3^r) \tag{4.38}$$

$$\frac{\partial \boldsymbol{f}_j^r \otimes \boldsymbol{f}_j^r}{\partial \boldsymbol{\gamma}^r} \boldsymbol{v} = \frac{\partial (\boldsymbol{f}_j^r \cdot \boldsymbol{v}) \boldsymbol{f}_j^r}{\partial \boldsymbol{\gamma}^r} = \frac{\partial (\boldsymbol{f}_j^r \cdot \boldsymbol{v})}{\partial \boldsymbol{\gamma}^r} \boldsymbol{f}_j^r + (\boldsymbol{f}_j^r \cdot \boldsymbol{v}) \frac{\partial \boldsymbol{f}_j^r}{\partial \boldsymbol{\gamma}^r}$$

$$= \boldsymbol{f}_j^r \frac{\partial (\boldsymbol{v}^T \boldsymbol{f}_j^r)}{\partial \boldsymbol{\gamma}^r} + (\boldsymbol{f}_j^r \cdot \boldsymbol{v}) \frac{\partial \boldsymbol{f}_j^r}{\partial \boldsymbol{\gamma}^r} \tag{4.39}$$

$$= \boldsymbol{f}_j^r \boldsymbol{v}^T \frac{\partial (\boldsymbol{f}_j^r)}{\partial \boldsymbol{\gamma}^r} + (\boldsymbol{f}_j^r \cdot \boldsymbol{v}) \frac{\partial \boldsymbol{f}_j^r}{\partial \boldsymbol{\gamma}^r} = \boldsymbol{f}_3^r \boldsymbol{v}^T \boldsymbol{I} + (\boldsymbol{f}_3^r \cdot \boldsymbol{v}) \boldsymbol{I}$$

$$= \boldsymbol{f}_3^r \otimes \boldsymbol{v} + (\boldsymbol{f}_3^r \cdot \boldsymbol{v}) \boldsymbol{I}$$

$$\frac{\partial \boldsymbol{f}_j^r \otimes \boldsymbol{f}_j^r}{\partial p} = \frac{\partial \boldsymbol{f}_j^r}{\partial p} \otimes \boldsymbol{f}_j^r + \boldsymbol{f}_j^r \otimes \frac{\partial \boldsymbol{f}_j^r}{\partial p}$$

$$= (\psi_{,\alpha} \boldsymbol{e}_3^r) \otimes (\boldsymbol{f}_\alpha^r) + (\boldsymbol{\kappa}^r \times \psi \boldsymbol{e}_3^r) \otimes (\boldsymbol{f}_3^r) + (\boldsymbol{f}_\alpha^r) \tag{4.40}$$

$$\otimes (\psi_{,\alpha} \boldsymbol{e}_3^r) + (\boldsymbol{f}_3^r) \otimes (\boldsymbol{\kappa}^r \times \psi \boldsymbol{e}_3^r)$$

$$\frac{\partial \boldsymbol{f}_j^r \otimes \boldsymbol{f}_j^r}{\partial p'} = \frac{\partial \boldsymbol{f}_j^r}{\partial p'} \otimes \boldsymbol{f}_j^r + \boldsymbol{f}_j^r \otimes \frac{\partial \boldsymbol{f}_j^r}{\partial p'} = \psi \boldsymbol{e}_3^r \otimes (\boldsymbol{f}_3^r) + (\boldsymbol{f}_3^r) \otimes \psi \boldsymbol{e}_3^r \tag{4.41}$$

4.2. Linear and second order elasticity

The linear elastic constitutive equation is also known as the generalised Hooke's law. For small strains, it relates Cauchy's stress tensor with the infinitesimal strain tensor $\boldsymbol{E}_l$ through the well-known equation

$$\boldsymbol{T} = (\lambda \boldsymbol{I} \otimes \boldsymbol{I} + 2\mu \mathbb{I}_S) \boldsymbol{E}_l. \tag{4.42}$$

In the linear regime (small strains), $\boldsymbol{T} \approx \boldsymbol{S} \approx \boldsymbol{P}$, and the expression (4.42) can be used to integrate the cross-sectional resultants, rendering

$$\boldsymbol{\sigma}^r = \boldsymbol{D}_L \boldsymbol{\varepsilon}^r, \tag{4.43}$$

in which $\boldsymbol{D}_L$ emerges with the classical expression from the strength of materials. Only trivial cross-sectional geometrical properties are required. For 7 DOF models, for example, they totalize 10 quantities: area (A), 5 moments of inertia ($I_1, I_2, I_{12}, I_\psi, I_T$), centroid's coordinates (x_1, x_2) and shear centre coordinates (s_1, s_2). Such matrix was presented in [1], admitting that the warping function was generated w.r.t the shear centre, and is given by

$$
\boldsymbol{D}_L =
\begin{bmatrix}
GA & 0 & 0 & 0 & 0 & -GAg_2 & GA(g_2 - s_2) & 0 \\
 & GA & 0 & 0 & 0 & GAg_1 & -GA(g_1 - s_1) & 0 \\
 & & EA & EAg_2 & -EAg_1 & 0 & 0 & 0 \\
 & & & EI_1 & EI_{12} & 0 & 0 & 0 \\
 & & & & EI_2 & 0 & 0 & 0 \\
 & & & & & GI_0 & G(I_T - I_0 + Ag_\alpha s_\alpha) & 0 \\
 & Sym. & & & & & G(I_0^S - I_T) & 0 \\
 & & & & & & & EI_\psi
\end{bmatrix},
\tag{4.44}
$$

and with $\boldsymbol{\varepsilon}^r = [\boldsymbol{\eta}^r \quad \boldsymbol{\kappa}^r \quad p \quad p']^T$, the stress resultants $\boldsymbol{\sigma}^r$ can be calculated.

Despite clear practical advantages, small strains are implicitly assumed, and this ultimately (although unintentionally) may lead to the loss of important coupling effects, notably the ones related to torsion/warping and axial strains.

Attempting to mitigate this issue, Pimenta and Campello, using more advanced material laws (Saint-Venant's and Simo-Ciarlet's material) gradually incorporated higher order strains terms in the constitutive equation. In [1], second-order axial and curvature strains, as well as first order-warping strains, were considered. Four additional third-order geometrical moments of inertia were necessary for calculation. In [3], second-order terms on all strains were retained, and the number of geometrical properties amounted to 42. Even though, albeit some improvements, a few inconsistent results and convergence issues persisted.

When second-order terms are retained, the stress vector $\boldsymbol{\sigma}^r$ is calculated with the aid of cross-sectional geometrical properties (although several of which are nontrivial), and the result may be conveniently written as[7]

$$
\boldsymbol{\sigma}^r = \left(\boldsymbol{D}_L + \tfrac{1}{2} \boldsymbol{D}_Q \right) \boldsymbol{\varepsilon}^r,
\tag{4.45}
$$

where $\boldsymbol{D}_Q$ has terms up to the first order in $\boldsymbol{\varepsilon}^r$.

It must be highlighted that, when only first-order strain terms are retained, both Saint-Venant´s and Simo-Ciarlet´s materials collapse to the linear elastic form.

Lago and Campello proposed in [2] a different approach: while restricting their analysis to the Saint-Venant's material, but considering both primary and secondary warpings (as described in section 2.3.3.3), the authors used the exact expression (i.e., with all strain terms retained), and then numerically integrated $\boldsymbol{\sigma}^r$ and $\boldsymbol{D}$. Despite the promising results obtained, where some of the pathological cases reported previously were overcome, two major drawbacks can be cited: 1) the adopted material (Saint-Venant's) is not polyconvex, and 2) the developments were carried out for only a few (and simple) types of cross-sections, namely, by-symmetric I-shaped, rectangular, cruciform and T (although for this latter there was an apparent inconsistent result).

Therefore, in order to address those issues, it is proposed here the deduction and implementation of both the Saint-Venant's and Simo-Ciarlet's material, so that comparison becomes possible.

---

[7] With $\boldsymbol{D}_L$ as the same as in (4.5). See the mentioned references for details on $\boldsymbol{D}_Q$.

4.3. Exact constitutive equation for Saint-Venant's material

The exact form of the constitutive equation that follows from this material for application in rod models was first presented in [2]. It was re-implemented in this work for comparison purposes, but now considering the improved warping function developed in Chapter 3. Here, it is represented using the approach from equation (4.19). In Appendix H, the same material law is represented, but the expressions are represented as in [2] (despite some rectifications). It should be noted that difference between the expressions that are in this section and in said appendix is merely the notation.

The potential function for this material is

$$\psi_h(\boldsymbol{E}) = \frac{1}{2}\lambda(tr\boldsymbol{E})^2 + \mu tr(\boldsymbol{E}^2) \tag{4.46}$$

In order to rewrite (4.46) as function of $\boldsymbol{C}$, let us remember that

$$\boldsymbol{E} = \frac{1}{2}(\boldsymbol{C} - \boldsymbol{I}), \tag{4.47}$$

thus

$$tr\boldsymbol{E} = \frac{1}{2}tr(\boldsymbol{C} - \boldsymbol{I}) = \frac{1}{2}tr\boldsymbol{C} - \frac{3}{2} = \frac{1}{2}I_1 - \frac{3}{2}, \tag{4.48}$$

$$tr\boldsymbol{E}^2 = tr\left(\frac{1}{4}(\boldsymbol{C} - \boldsymbol{I})^2\right) = \frac{1}{4}(tr\boldsymbol{C}^2 - 2tr\boldsymbol{C} + 3) = \frac{I_2}{2} - \frac{I_1}{2} + \frac{3}{4}. \tag{4.49}$$

Substituting (4.48) and (4.49) in (4.46), one gets

$$\psi_h(\boldsymbol{C}) = \frac{\lambda}{8}I_1^2 - \frac{1}{4}(3\lambda + 2\mu)I_1 + \frac{\mu}{2}I_2 + \frac{15}{8}. \tag{4.50}$$

Calculating $\frac{\partial\psi_h}{\partial I_i}$, one gets

$$\frac{\partial\psi_h}{\partial I_1} = \frac{\lambda}{4}I_1 - \frac{1}{4}(3\lambda + 2\mu), \qquad \frac{\partial\psi_h}{\partial I_2} = \frac{\mu}{2} \text{ and } \qquad \frac{\partial\psi_h}{\partial I_3} = 0. \tag{4.51}$$

Using (4.51) in (4.19), the $\boldsymbol{P}^r$ stress column-vectors are obtained,

$$\boldsymbol{\tau}_i^r = \left[\frac{\lambda}{2}I_1\boldsymbol{I} + \mu(\boldsymbol{f}_j^r \otimes \boldsymbol{f}_j^r) - \frac{1}{2}(3\lambda + 2\mu)\boldsymbol{I}\right]\boldsymbol{f}_i^r. \tag{4.52}$$

The operators $\boldsymbol{C}_{33}, \boldsymbol{c}, \boldsymbol{d}, b_\alpha$ and d_α for the Saint-Venant's material are defined as (using the auxiliary results (4.23)-(4.41))

$$\boldsymbol{C}_{33} = \frac{\partial\boldsymbol{\tau}_3^r}{\partial\boldsymbol{\gamma}^r} = \frac{\partial\left[\frac{\lambda}{2}I_1\boldsymbol{I} + \mu\left(\boldsymbol{f}_j^r \otimes \boldsymbol{f}_j^r\right) - \frac{1}{2}(3\lambda + 2\mu)\boldsymbol{I}\right]}{\partial\boldsymbol{\gamma}^r}\boldsymbol{f}_3^r + \left[\frac{\lambda}{2}I_1\boldsymbol{I} + \mu\left(\boldsymbol{f}_j^r \otimes \boldsymbol{f}_j^r\right) - \right.$$

$$\frac{1}{2}(3\lambda + 2\mu)\boldsymbol{I}\Big]\frac{\partial\boldsymbol{f}_3^r}{\partial\boldsymbol{\gamma}^r} = \lambda\boldsymbol{f}_3^r \otimes \boldsymbol{f}_3^r + \mu(\boldsymbol{f}_3^r \otimes \boldsymbol{f}_3^r + \boldsymbol{f}_3^r \cdot \boldsymbol{f}_3^r\boldsymbol{I}) + \left[\frac{\lambda}{2}I_1\boldsymbol{I} + \right. \tag{4.53}$$

$$\mu\left(\boldsymbol{f}_j^r \otimes \boldsymbol{f}_j^r\right) - \frac{1}{2}(3\lambda + 2\mu)\boldsymbol{I}\Big],$$

$$\boldsymbol{c} = \frac{\partial\boldsymbol{\tau}_3^r}{\partial p} = \frac{\partial\left[\frac{\lambda}{2}I_1\boldsymbol{I} + \mu\left(\boldsymbol{f}_j^r \otimes \boldsymbol{f}_j^r\right) - \frac{1}{2}(3\lambda + 2\mu)\boldsymbol{I}\right]}{\partial p}\boldsymbol{f}_3^r + \left[\frac{\lambda}{2}I_1\boldsymbol{I} + \mu\left(\boldsymbol{f}_j^r \otimes \boldsymbol{f}_j^r\right) - \right.$$

$$\frac{1}{2}(3\lambda + 2\mu)\boldsymbol{I}\Big]\frac{\partial\boldsymbol{f}_3^r}{\partial p} = \{\lambda[p\psi_{,\alpha}\psi_{,\alpha} + (\boldsymbol{\kappa}^r \times \psi\boldsymbol{e}_3^r) \cdot \boldsymbol{\gamma}^r] + \mu[(\psi_{,\alpha}\boldsymbol{e}_3^r) \otimes$$

$$(\boldsymbol{f}_\alpha^r) + (\boldsymbol{\kappa}^r \times \psi\boldsymbol{e}_3^r) \otimes (\boldsymbol{f}_3^r) + (\boldsymbol{f}_\alpha^r) \otimes (\psi_{,\alpha}\boldsymbol{e}_3^r) + (\boldsymbol{f}_3^r) \otimes (\boldsymbol{\kappa}^r \times \tag{4.54}$$

$$\psi\boldsymbol{e}_3^r)]\}\boldsymbol{f}_3^r + \left[\frac{\lambda}{2}I_1\boldsymbol{I} + \mu\left(\boldsymbol{f}_j^r \otimes \boldsymbol{f}_j^r\right) - \frac{1}{2}(3\lambda + 2\mu)\boldsymbol{I}\right](\boldsymbol{\kappa}^r \times \psi\boldsymbol{e}_3^r),$$

$$\boldsymbol{d} = \frac{\partial \tau_3^r}{\partial p'} = \frac{\partial \left[\frac{\lambda}{2} I_1 \boldsymbol{I} + \mu \left(\boldsymbol{f}_j^r \otimes \boldsymbol{f}_j^r\right) - \frac{1}{2}(3\lambda + 2\mu)\boldsymbol{I}\right]}{\partial p'} \boldsymbol{f}_3^r + \left[\frac{\lambda}{2} I_1 \boldsymbol{I} + \mu \left(\boldsymbol{f}_j^r \otimes \boldsymbol{f}_j^r\right) - \right.$$

$$\frac{1}{2}(3\lambda + 2\mu)\boldsymbol{I}\left]\frac{\partial \boldsymbol{f}_3^r}{\partial p'} = \left[\lambda \psi (1 + \boldsymbol{\gamma}^r \cdot \boldsymbol{e}_3^r)\boldsymbol{I} + \mu (\psi \boldsymbol{e}_3^r \otimes \boldsymbol{f}_3^r + \boldsymbol{f}_3^r \otimes \psi \boldsymbol{e}_3^r)\right]\boldsymbol{f}_3^r + \quad (4.55)$$

$$+ \left[\frac{\lambda}{2} I_1 \boldsymbol{I} + \mu \left(\boldsymbol{f}_j^r \otimes \boldsymbol{f}_j^r\right) - \frac{1}{2}(3\lambda + 2\mu)\boldsymbol{I}\right]\psi \boldsymbol{e}_3^r,$$

$$b_\alpha = \frac{\partial (\tau_\alpha^r \cdot \boldsymbol{e}_3^r)}{\partial p} = \left(\frac{\partial \left[\frac{\lambda}{2} I_1 \boldsymbol{I} + \mu \left(\boldsymbol{f}_j^r \otimes \boldsymbol{f}_j^r\right) - \frac{1}{2}(3\lambda + 2\mu)\boldsymbol{I}\right]}{\partial p} \boldsymbol{f}_\alpha^r\right) \cdot \boldsymbol{e}_3^r + \left[\frac{\lambda}{2} I_1 \boldsymbol{I} + \right.$$

$$\mu \left(\boldsymbol{f}_j^r \otimes \boldsymbol{f}_j^r\right) - \frac{1}{2}(3\lambda + 2\mu)\boldsymbol{I}\left]\frac{\partial \boldsymbol{f}_\alpha^r}{\partial p} \cdot \boldsymbol{e}_3^r = \lambda (\psi_{,\beta} \psi_{,\beta} p + (\boldsymbol{\kappa}^r \times \psi \boldsymbol{e}_3^r) \cdot \right.$$

$$\boldsymbol{\gamma}^r)\psi_{,\alpha} p + \mu \left(\frac{\partial \boldsymbol{f}_j^r \otimes \boldsymbol{f}_j^r}{\partial p} \boldsymbol{f}_\alpha^r\right) \cdot \boldsymbol{e}_3^r + \left[\frac{\lambda}{2} I_1 \boldsymbol{I} + \mu \left(\boldsymbol{f}_j^r \otimes \boldsymbol{f}_j^r\right) - \frac{1}{2}(3\lambda + \quad (4.56)\right.$$

$$2\mu)\boldsymbol{I}\left] (\psi_{,\alpha} \boldsymbol{e}_3^r) \cdot \boldsymbol{e}_3^r,\right.$$

$$d_\alpha = \left(\frac{\partial \left[\frac{\lambda}{2} I_1 \boldsymbol{I} + \mu \left(\boldsymbol{f}_j^r \otimes \boldsymbol{f}_j^r\right) - \frac{1}{2}(3\lambda + 2\mu)\boldsymbol{I}\right]}{\partial p'} \boldsymbol{f}_\alpha^r\right) \cdot \boldsymbol{e}_3^r + \left[\frac{\lambda}{2} I_1 \boldsymbol{I} + \mu \left(\boldsymbol{f}_j^r \otimes \boldsymbol{f}_j^r\right) - \right.$$

$$\frac{1}{2}(3\lambda + 2\mu)\boldsymbol{I}\left]\frac{\partial \boldsymbol{f}_\alpha^r}{\partial p'} \cdot \boldsymbol{e}_3^r = \lambda \psi (1 + \boldsymbol{\gamma}^r \cdot \boldsymbol{e}_3^r)\psi_{,\alpha} p + \mu \left(\frac{\partial \boldsymbol{f}_j^r \otimes \boldsymbol{f}_j^r}{\partial p'} \boldsymbol{f}_\alpha^r\right) \cdot \boldsymbol{e}_3^r, \quad (4.57)\right.$$

4.4. Exact constitutive equation for Simo-Ciarlet's material

In the work from Dasambiagio [25], there is a deduction for the Simo-Ciarlet's material for rods that leaves the results as functions of the columns of $\boldsymbol{F}^r$, but no further detailing is done, nor numerical implementation is performed, as he allows for very generic displacement fields. A similar deduction was developed in the current work, but the terms were particularized for the current 7-DOF rod model and expanded, allowing for best visualization of the coupling interactions. The goal is the same as in Campello and Lago's [2]: to express all the terms from $\boldsymbol{\sigma}^r$ and $\boldsymbol{D}$ without neglecting any strain terms.

The Simo-Ciarlet's material is characterized by the potential function

$$\psi_h(J, I_1) = \frac{\lambda}{2}\left[\frac{1}{2}(J^2 - 1) - lnJ\right] + \frac{\mu}{2}(I_1 - 3 - 2lnJ). \quad (4.58)$$

Calculating $\frac{\partial \psi_h}{\partial I_i}$, one gets

$$\frac{\partial \psi_h}{\partial I_1} = \frac{\mu}{2}, \qquad \frac{\partial \psi_h}{\partial I_2} = 0 \text{ and } \qquad \frac{\partial \psi_h}{\partial I_3} = \frac{\lambda}{2}\left[J - \frac{1}{J}\right] - \mu\frac{1}{J}. \quad (4.59)$$

Thus

$$\boldsymbol{\tau}_i^r = \left[\frac{\lambda}{2}\left(J - \frac{1}{J}\right) - \mu\frac{1}{J}\right]\boldsymbol{g}_i^r + \mu\boldsymbol{f}_i^r. \quad (4.60)$$

The operators $\boldsymbol{C}_{33}$, $\boldsymbol{c}$, $\boldsymbol{d}$, b_α and d_α for the Simo-Ciarlet's material are defined as (using the auxiliary results (4.23)-(4.41))

Marcos Pires Kassab 81

Advances on a kinematically exact rod model for thin-walled open section members: consistent warping function and nonlinear constitutive equation

$$C_{33} = \frac{\partial \boldsymbol{\tau}_3^r}{\partial \boldsymbol{\gamma}^r} = \left[\frac{\lambda}{2}\left(1 + \frac{1}{J^2}\right) + \mu \frac{1}{J^2}\right] \boldsymbol{g}_3^r \frac{\partial J}{\partial \boldsymbol{\gamma}^r} + \left[\frac{\lambda}{2}\left(J - \frac{1}{J}\right) - \mu \frac{1}{J}\right] \frac{\partial \boldsymbol{g}_3^r}{\partial \boldsymbol{\gamma}^r} + \mu \frac{\partial \boldsymbol{f}_3^r}{\partial \boldsymbol{\gamma}^r}$$

$$= \left[\frac{\lambda}{2}\left(1 + \frac{1}{J^2}\right) + \mu \frac{1}{J^2}\right] \boldsymbol{g}_3^r (\boldsymbol{f}_1^r \times \boldsymbol{f}_2^r)^T \boldsymbol{I} + \mu \boldsymbol{I}$$

$$= \left[\frac{\lambda}{2}\left(1 + \frac{1}{J^2}\right) + \mu \frac{1}{J^2}\right] \boldsymbol{g}_3^r \boldsymbol{g}_3^{r\,T} + \mu \boldsymbol{I}$$

$$= \left[\frac{\lambda}{2}\left(1 + \frac{1}{J^2}\right) + \mu \frac{1}{J^2}\right] \boldsymbol{g}_3^r \otimes \boldsymbol{g}_3^r + \mu \boldsymbol{I}$$

(4.61)

$$\boldsymbol{c} = \frac{\partial \boldsymbol{\tau}_3^r}{\partial p} = \left[\frac{\lambda}{2}\left(1 + \frac{1}{J^2}\right) + \mu \frac{1}{J^2}\right] \frac{\partial J}{\partial p} \boldsymbol{g}_3^r + \left[\frac{\lambda}{2}\left(J - \frac{1}{J}\right) - \mu \frac{1}{J}\right] \frac{\partial \boldsymbol{g}_3^r}{\partial p} + \mu \frac{\partial \boldsymbol{f}_3^r}{\partial p} =$$

$$\left[\frac{\lambda}{2}\left(1 + \frac{1}{J^2}\right) + \mu \frac{1}{J^2}\right] \left(\boldsymbol{g}_i^r \cdot \frac{\partial \boldsymbol{f}_i^r}{\partial p}\right) \boldsymbol{g}_3^r + \left[\frac{\lambda}{2}\left(J - \frac{1}{J}\right) - \mu \frac{1}{J}\right] \left(\epsilon_{\alpha\beta} \frac{\partial \boldsymbol{f}_\alpha^r}{\partial p} \times \boldsymbol{f}_\beta^r\right) + \mu \frac{\partial \boldsymbol{f}_3^r}{\partial p} =$$

$$\left[\frac{\lambda}{2}\left(1 + \frac{1}{J^2}\right) + \mu \frac{1}{J^2}\right] \left[-(\boldsymbol{\gamma}^r \cdot \boldsymbol{e}_\alpha^r)\psi_{,\alpha} - p\psi\psi_{,\alpha}(\boldsymbol{\kappa}^r \times \boldsymbol{e}_3^r) \cdot \boldsymbol{e}_\alpha^r\right] \boldsymbol{g}_3^r + \left[\frac{\lambda}{2}\left(J - \frac{1}{J}\right) - \right.$$

$$\left. \mu \frac{1}{J}\right] (-\psi_{,\alpha}) \boldsymbol{e}_\alpha^r + \mu(\boldsymbol{\kappa}^r \times \psi \boldsymbol{e}_3^r),$$

(4.62)

$$\boldsymbol{d} = \frac{\partial \boldsymbol{\tau}_3^r}{\partial p'} = \left[\frac{\lambda}{2}\left(1 + \frac{1}{J^2}\right) + \mu \frac{1}{J^2}\right] \frac{\partial J}{\partial p'} \boldsymbol{g}_3^r + \left[\frac{\lambda}{2}\left(J - \frac{1}{J}\right) - \mu \frac{1}{J}\right] \frac{\partial \boldsymbol{g}_3^r}{\partial p'} + \mu \frac{\partial \boldsymbol{f}_3^r}{\partial p'} =$$

$$\left[\frac{\lambda}{2}\left(1 + \frac{1}{J^2}\right) + \mu \frac{1}{J^2}\right] \left(\boldsymbol{g}_3^r \cdot \frac{\partial \boldsymbol{f}_3^r}{\partial p'}\right) \boldsymbol{g}_3^r + \mu \frac{\partial \boldsymbol{f}_3^r}{\partial p'} = \left[\frac{\lambda}{2}\left(1 + \frac{1}{J^2}\right) + \mu \frac{1}{J^2}\right] (\boldsymbol{g}_3^r \otimes \boldsymbol{g}_3^r) \frac{\partial \boldsymbol{f}_3^r}{\partial p'} +$$

$$\mu \boldsymbol{I} \frac{\partial \boldsymbol{f}_3^r}{\partial p'} = \boldsymbol{C}_{33} \frac{\partial \boldsymbol{f}_3^r}{\partial p'} = \psi \boldsymbol{C}_{33} \boldsymbol{e}_3^r,$$

(4.63)

$$b_\alpha = \frac{\partial (\boldsymbol{\tau}_\alpha^r \cdot \boldsymbol{e}_3^r)}{\partial p} = \left[\frac{\lambda}{2}\left(1 + \frac{1}{J^2}\right) + \mu \frac{1}{J^2}\right] \frac{\partial J}{\partial p} \boldsymbol{g}_\alpha^r \cdot \boldsymbol{e}_3^r + \left[\frac{\lambda}{2}\left(J - \frac{1}{J}\right) - \mu \frac{1}{J}\right] \frac{\partial \boldsymbol{g}_\alpha^r}{\partial p} \cdot \boldsymbol{e}_3^r +$$

$$\mu \frac{\partial \boldsymbol{f}_\alpha^r}{\partial p} \cdot \boldsymbol{e}_3^r = \left[\frac{\lambda}{2}\left(1 + \frac{1}{J^2}\right) + \mu \frac{1}{J^2}\right] \left(\boldsymbol{g}_i^r \cdot \frac{\partial \boldsymbol{f}_i^r}{\partial p}\right) (\boldsymbol{g}_\alpha^r \cdot \boldsymbol{e}_3^r) + \left[\frac{\lambda}{2}\left(J - \frac{1}{J}\right) - \mu \frac{1}{J}\right] \frac{\partial \boldsymbol{g}_\alpha^r}{\partial p} \cdot$$

$$\boldsymbol{e}_3^r + \mu \frac{\partial \boldsymbol{f}_\alpha^r}{\partial p} \cdot \boldsymbol{e}_3^r = \left[\frac{\lambda}{2}\left(1 + \frac{1}{J^2}\right) + \mu \frac{1}{J^2}\right] (\boldsymbol{g}_\beta^r \cdot \psi_{,\beta} \boldsymbol{e}_3^r + \boldsymbol{g}_3^r \cdot \boldsymbol{\kappa}^r \times \psi \boldsymbol{e}_3^r)(-\boldsymbol{\gamma}^r \cdot$$

$$\boldsymbol{e}_\alpha^r) + \left[\frac{\lambda}{2}\left(J - \frac{1}{J}\right) - \mu \frac{1}{J}\right] \epsilon_{\alpha\beta} \psi (\boldsymbol{e}_\beta^r \cdot \boldsymbol{\kappa}^r) + \mu \psi_{,\alpha} = \left[\frac{\lambda}{2}\left(1 + \frac{1}{J^2}\right) + \mu \frac{1}{J^2}\right] \left[-(\boldsymbol{\gamma}^r \cdot\right.$$

$$\left. \boldsymbol{e}_\beta^r)\psi_{,\beta} - p\psi\psi_{,\beta}(\boldsymbol{\kappa}^r \times \boldsymbol{e}_3^r) \cdot \boldsymbol{e}_\beta^r\right](-\boldsymbol{\gamma}^r \cdot \boldsymbol{e}_\alpha^r) + \left[\frac{\lambda}{2}\left(J - \frac{1}{J}\right) - \mu \frac{1}{J}\right] \epsilon_{\alpha\beta} \psi (\boldsymbol{e}_\beta^r \cdot \boldsymbol{\kappa}^r) +$$

$$\mu \psi_{,\alpha},$$

(4.64)

$$d_\alpha = \frac{\partial (\boldsymbol{\tau}_\alpha^r \cdot \boldsymbol{e}_3^r)}{\partial p'} = \left[\frac{\lambda}{2}\left(1 + \frac{1}{J^2}\right) + \mu \frac{1}{J^2}\right] \frac{\partial J}{\partial p'} \boldsymbol{g}_\alpha^r \cdot \boldsymbol{e}_3^r + \left[\frac{\lambda}{2}\left(J - \frac{1}{J}\right) - \mu \frac{1}{J}\right] \frac{\partial \boldsymbol{g}_\alpha^r}{\partial p'} \cdot \boldsymbol{e}_3^r =$$

$$\left[\frac{\lambda}{2}\left(1 + \frac{1}{J^2}\right) + \mu \frac{1}{J^2}\right] \psi (-\boldsymbol{\gamma}^r \cdot \boldsymbol{e}_\alpha^r).$$

(4.65)

82   Marcos Pires Kassab

Advances on a kinematically exact rod model for thin-walled open section members: consistent warping function and nonlinear constitutive equation

4.5. Notions on polyconvexity

The Saint-Venant's material law is a kind of constitutive model that can lead to a loss of ellipticity in the equilibrium equations at moderate to large strains, and making the problem numerically ill-conditioned. One way to avoid this issue is by adopting a polyconvex constitutive model. Polyconvexity is a special condition on the strain energy function that defines the material, as first noted by Ball [51].

In this section, the author intends to proportionate to the reader a contextualization about what is the first and one of the only theorems that guarantees the existence of the solution for solids with hyperelastic materials. The explanation has, by any means, the intention to exhaust the discussion about this subject. In fact, Ball [51] has a book dedicated to such topic, and Ciarlet [52], in his book about mathematical elasticity, supported by the aforementioned work, provides a robust framework of theorems about the existence of solution for elasticity problems.

In this section, the discussion is centred around theorems that are sufficient for the existence of minimizers for the bodies total energy; therefore, they are only valid for conservative problems. Therefore, as by definition, hyperelastic materials have an associated potential function, it must be assumed that the loading is conservative in order to the polyconvexity condition be sufficient for the existence of solution.

4.5.1.   Convexity

As defined in Ciarlet [52], a given subset U of a normed vector space V is said convex whenever, for every two pair of points u, v from such subset, the closed segment linking those points $[u, v]$ is contained in U.

The convexity of functions can be defined over convex or non-convex sets (in the latter case, a convex extension of the original set must be performed). Let U be a convex subset of a vector space V Consider a function $W : U \to \mathbb{R}$. Then, the function W is considered convex if

$$W(\lambda u + (1 - \lambda)v) \leq \lambda W(u) + (1 - \lambda)W(v), \forall u, v \in U, \lambda \in [0,1] \qquad (4.66)$$

Note that the definition above remains correct if the domain is extended so that $\{+\infty\}$ is included. This is an important case, which in the context of elasticity, will represent the stored potential energy in extreme strain situations.

4.5.2.   Polyconvexity

First, based on the physical experience for solids, an important property for the internal strain potential energy W_s is of interest: for the extreme defomation cases, with $det\boldsymbol{F} \to 0$ or $detF \to \infty$, then $W_s \to \infty$. It can be proven that the aforementioned statement is incompatible with the convexity condition (the demonstration can be seen in Ciarlet [52], for example).

Marcos Pires Kassab 83

Advances on a kinematically exact rod model for thin-walled open section members: consistent warping function and nonlinear constitutive equation

However, a weaker statement, proposed and proven by Ball [51] is of utmost importance: polyconvexity is a sufficient condition for quasiconvexity, which, in turn, at least for the class of problems of interest, implies the Legendre-Hadamard ellipticity condition, which is pivotal for material stability. Also, as pointed by Ciarlet [52], "polyconvexity does not conflict with any physical requirement and indeed, it is satisfied by realistic models". Therefore, having a polyconvex constitutive equation is crucial to avoid undesirable material instability upon solution.

Let us define polyconvexity for the three-dimensional case: consider a scalar function $W = \widehat{W}(\boldsymbol{A}, \boldsymbol{H}, \delta)$, with the arguments $\boldsymbol{A}, \boldsymbol{H} \in M^{3x3}$ (M^{3x3} denotes 3x3 matrices) and $\delta \in \mathbb{R}^+$. If W is convex, then the potential energy function $W_s = W(\boldsymbol{F}, cof\boldsymbol{F}, det\boldsymbol{F})$ is polyconvex ($cof\boldsymbol{F}$ is the matrix of the cofactors of $\boldsymbol{F}$). In summary, if one can write the potential energy as a convex function having as explicit arguments the minors of $\boldsymbol{F}$ ($\boldsymbol{F}$ itself, $cof\boldsymbol{F}$ and $det\boldsymbol{F}$), then such function is polyconvex.

This is the case of the Simo-Ciarlet's hyperelastic material (for λ and $\mu > 0$), since by analysing its associated potential energy, it is clear that it is constituted by a sum of convex functions in $\boldsymbol{F}$ and in $det\boldsymbol{F}$. The Saint-Venant's material, however, is not polyconvex (see demonstration by Raoult [53] which proves by a counter-example that the function $W(A, H, \delta)$ of the St. Venant's material is not convex).

References such Ciarlet [52], Lahuerta [54] et al. ,and Campello and Lago [2], are also worth reading for discussions about this subject.

Note that the polyconvexity condition, although desirable, is not mandatory for the existence of solution for particular cases: it is known, for example, that the Saint-Venant's material is broadly appliable in a wide array of practical situations, mainly in low-strain configurations. For this reason. it is often regarded as a finitedeformation/low and moderate-strain material.

Advances on a kinematically exact rod model for thin-walled open section members: consistent warping function and nonlinear constitutive equation

Marcos Pires Kassab

85

Advances on a kinematically exact rod model for thin-walled open section members: consistent warping function and nonlinear constitutive equation

5. ROD MODEL SOLUTION THROUGH THE FINITE ELEMENT METHOD (FEM)

The FEM method is a robust numerical procedure for solving partial differential equations, allowing for generic geometries, materials, boundary conditions and solution refinement, in the structural mechanical context. In fact, one of the first application of this method was to solve a mechanical problem intimately related to the current research: the Saint-Venant warping function for pure torsion (see [55], in which an incipient form of the FEM was introduced). Later, the method was formalized, and as research advanced, it was discovered that it could be used to solve a wide array of problems governed by differential equations, originated from different contexts. We refer to Appendix K for an introduction of the method and how integration is performed in the framework of isoparametric elements.

The model that is currently being studied was implemented in PEFSYS, which is an already existent in-house FEM program for nonlinear static and dynamic analysis of structures. The main contribution of this work for the said software were the implementation of an interface for inputting open-section thin-walled geometries (which automatically generates the warping function from equation (3.80)), the implementation of constitutive equations derived from the Saint-Venant's and Simo-Ciarlet's material laws, and a brand-new subroutine for outputting results for ParaView©.

Therefore, the model´s FEM solution that is described in this chapter is not particularly new, but is presented for completeness.

5.1. Element FEM formulation

First, let us take the weak form of the equilibrium (equation (3.39)) as the desired projection problem (see Appendix K), and apply on both the displacements and virtual displacements the same interpolation function

$$d_\theta = Np, \quad \delta d_\theta = N\delta p, \tag{5.1}$$

where p is a vector that contains sub-vectors p_i (δp is its virtual counterpart). Each of those sub-vectors contains the degrees of freedom (7 in this case) of a node i,

$$p = \begin{bmatrix} p_1 \\ p_2 \\ \vdots \\ p_n \end{bmatrix} \text{ and } p_i = \begin{bmatrix} u \\ \theta \\ p \end{bmatrix}_i, \tag{5.2}$$

$N = N(\mathrm{Z})$ is an operator that holds the Lagrange interpolation functions l_a^i for n nodes, which can be built with

$$N = [N_1 \quad N_2 \quad ... \quad N_n], \tag{5.3}$$

where

$$N_a = l_a^{n-1} I_p, \tag{5.4}$$

with

$$N_a = l_a^{n-1} = \frac{(\mathrm{Z}-\mathrm{Z}_1)(\mathrm{Z}-\mathrm{Z}_2)...(\mathrm{Z}-\mathrm{Z}_{a-1})(\mathrm{Z}-\mathrm{Z}_{a+1})...(\mathrm{Z}-\mathrm{Z}_n)}{(\mathrm{Z}_a-\mathrm{Z}_1)(\mathrm{Z}_a-\mathrm{Z}_2)...(\mathrm{Z}_a-\mathrm{Z}_{a-1})(\mathrm{Z}_a-\mathrm{Z}_{a+1})...(\mathrm{Z}_a-\mathrm{Z}_n)}, \tag{5.5}$$

and $\boldsymbol{I_p}$ is the identity matrix with dimension consistent with the vector $\boldsymbol{p}$ (7, in this case).

Analysing (5.5), it is easy to perceive that, for a given node a, the Lagrangian interpolation has as main characteristic to be zero for every other node $k \neq a$. In the current work, elements with 2 and 3 nodes are of interest. Thus, the interpolation can be linear or quadratic, respectively (see Table 13 in Appendix K).

For one element with integration domain L_e, this renders,

$$\delta W = \int_{L_e}(\boldsymbol{\sigma}^r \cdot \boldsymbol{\Psi\Delta N}\delta\boldsymbol{p} - \overline{\boldsymbol{q}} \cdot \boldsymbol{N}\delta\boldsymbol{p})d\zeta - \boldsymbol{q}^* \cdot (\boldsymbol{N}\delta\boldsymbol{p})|^{\zeta_t^r} =$$

$$\left(\int_{L_e}((\boldsymbol{\Delta N})^{\mathrm{T}}\boldsymbol{\Psi}^{\mathrm{T}}\boldsymbol{\sigma}^r - \boldsymbol{N}^{\mathrm{T}}\overline{\boldsymbol{q}})d\zeta\right) \cdot \delta\boldsymbol{p} - (\boldsymbol{N}^{\mathrm{T}}\boldsymbol{q}^*)|^{\zeta_t^r} \cdot \delta\boldsymbol{p} = 0, \tag{5.6}$$

where ζ_t^r denotes the nodes with prescribed concentrated loads and with $\boldsymbol{\sigma}^r$ calculated based on the interpolated displacements and strains. Defining the quantity in parenthesis as the elemental residual force vector $\boldsymbol{P}_e$ (this vector is exceptionally represented by a capital letter), one writes, in order to respect the equilibrium

$$\boldsymbol{P}_e \cdot \delta\boldsymbol{p} = (\boldsymbol{N}^{\mathrm{T}}\boldsymbol{q}^*)\big|^{\zeta_t^r} \cdot \delta\boldsymbol{p}, \forall \delta\boldsymbol{p} \Leftrightarrow \boldsymbol{P} = (\boldsymbol{N}^{\mathrm{T}}\boldsymbol{q}^*)\big|^{\zeta_t^r} \tag{5.7}$$

Using the fact that an interpolation function $N_a = 0$ in other interpolated points, and by considering that only the extremities (coordinates 0 and l) have concentrated loads, one gets

$$\boldsymbol{P}_e = \int_0^L (\boldsymbol{\Delta N})^{\mathrm{T}}\boldsymbol{\Psi}^{\mathrm{T}}\boldsymbol{\sigma}^r - \boldsymbol{N}^T\overline{\boldsymbol{q}})d\zeta = (\boldsymbol{N}^{\mathrm{T}}\boldsymbol{q}^*)\big|^{\zeta_t^r} = \boldsymbol{N}_n^T\boldsymbol{q}^*(l) + \boldsymbol{N_1}\boldsymbol{q}^*(0). \tag{5.8}$$

Let us define the tangent stiffness matrix for one element

$$\boldsymbol{k}_e = \frac{\partial \boldsymbol{P}_e}{\partial \boldsymbol{p}}. \tag{5.9}$$

The result of this operation is known, since it is possible to make an analogy with the obtention of the tangent bilinear form of the equilibrium, the only difference lying on the fact that, in equation (5.8), the discretization and interpolation process were already performed. Therefore

$$\boldsymbol{k}_e = \boldsymbol{k}_C + \boldsymbol{k}_G - \boldsymbol{k}_L$$

$$= \int_{L_e}(\boldsymbol{\Delta N})^{\mathrm{T}}\boldsymbol{\Psi}^{\mathrm{T}}\boldsymbol{D}\boldsymbol{\Psi\Delta N}d\zeta + \int_{L_e}(\boldsymbol{\Delta N})^{\mathrm{T}}\boldsymbol{G_\theta}(\boldsymbol{\Delta N})d\zeta$$

$$- \int_{L_e}(\boldsymbol{N}^T\boldsymbol{L_\theta}\mathbf{N})d\zeta. \tag{5.10}$$

Note that the operators $\boldsymbol{D}, \boldsymbol{G_\theta}$ and $\boldsymbol{L_\theta}$ were already defined in section 3.2.

5.2. Global assembly of residual force vector and tangent stiffness matrix

The residual force vector (equation (5.8)) and tangent stiffness matrix (equation (5.10)) are valid for one isolated element. Now, the *global* residual vector and tangent matrix must be assembled. This operation consists of the arrangement of those equations in the correspondent blocks, complying with the numbering of the DOFs. Formally, consider that an element e, with associated nodal DOFs $\boldsymbol{p}_e$. Let

Marcos Pires Kassab   87

Advances on a kinematically exact rod model for thin-walled open section members: consistent warping function and nonlinear constitutive equation

A_e be the *connectivity* matrix, that associates the numbering of the DOFs from p_e to the global numbering of the structure, so that

$$p_e = A_e r, \tag{5.11}$$

where r is the global vector of generalized nodal displacements.

The structure of A_e is simple: it is a matrix with n_{DOF_e} lines and n_{DOF_T} columns, where n_{DOF_e} and n_{DOF_T} are the number of degrees of freedom on an element and on the whole structure, respectively, containing "ones" on the appropriate positions that relate the local to the global numbering and "zeros" elsewhere. Note that the A_e^T performs the opposite role, by taking local contributions and adequately allocating on the global matrix

The global residual force vector R (this vector is exceptionally represented by a capital letter) is then given by

$$R = \sum_{e=1}^{N_e} A_e^T P_e \tag{5.12}$$

Now, global equilibrium is achieved by imposing

$$R = \widehat{R}(r) = 0. \tag{5.13}$$

Equation (5.13) is highly nonlinear, mainly due to the inherent nonlinearities from the exact kinematical description and the constitutive equation. Therefore, for a given set of external loadings, Newton's method must be used to solve these equations. Applying said method for (5.13), with an initial prediction r^i, one gets

$$r^{i+1} = r^i - \left(\frac{\partial R(r^i)}{\partial r}\right)^{-1} R(r^i). \tag{5.14}$$

Note that the inversion does not have to be directly applied. It is possible, for example, to solve the linear system

$$K_T \Delta r^i = -R(r^i), \tag{5.15}$$

with $\Delta r^i = \left(r^{i+1} - r^i\right)$ and $K_T = \left(\frac{\partial R(r^i)}{\partial r}\right)$, and then update r. Calculating K^T, one gets

$$
\begin{aligned}
K_T &= \frac{\partial R(r^i)}{\partial r} = \frac{\partial}{\partial r}\left(\sum_{e=1}^{N_e} A_e^T P_e\right) = A_e^T\left(\sum_{e=1}^{N_e} \frac{\partial P_e}{\partial r}\right) = A_e^T \sum_{e=1}^{N_e} \frac{\partial P_e}{\partial p_e}\frac{\partial p_e}{\partial r} \\
&= \sum_{e=1}^{N_e} A_e^T k_e A_e
\end{aligned}
\tag{5.16}
$$

It should be noted that, A_e is a compact way to formally represent the connectivity, albeit never being used in the programming practice. Usually, a tracker list is used to appropriately allocate the information.

It is also worth mentioning that the solution can be carried out entirely using the global reference system, without any base transformation. Usually, the components of σ^r are outputted w.r.t the local reference system for analysis purposes.

5.3. PEFSYS general aspects

The described model was implemented in PEFSYS, which is written in Fortran. PEFSYS is a finite element program for advanced structural analysis, capable of static and dynamic non-linear analysis of solids and structures, specializing on thin members (rods, shells and membranes). Under development since the late 1990's at the Department of Structural and Geotechnical Engineering of the Polytechnic School of the University of São Paulo, by a FAPESP thematic project coordinated by Prof. Paulo M. Pimenta, it has been serving as a programming platform for students and researchers of this master´s advisor's group, for state-of-the-art research on rods, shells and membranes. It is coded in FORTRAN 90/95/2003, setting up a modern programming environment based on the OOP (Object-Oriented Programming) paradigm, with full usage of encapsulation, polymorphism, inheritance and operator overloading. It contains advanced methods for the solution of large systems of non-linear equations as well as for time integration of the equations of motion, with exact kinematics (finite displacements, rotations and strains) and inelastic behaviour.

In PEFSYS, the solver is direct, solving each step of the Newton's method by Crout's LDU decomposition, taking advantage of the symmetry of the system when applicable. The solver uses the incremental method to achieve the final load states and lacks yet the arc-length method.

The program has a graphical interface for pre- and post-processing built on the auxiliary program GiD©, and a brand-new Paraview© outputting interface version has been developed here. In comparison with GiD, ParaView provides a wide array of native Python routines (personalized ones can also be implemented) that allows for better results manipulation but lacks pre-processing capabilities. It also has a significantly higher graphic quality and optimizes output files memory-wise.

Marcos Pires Kassab

89

Advances on a kinematically exact rod model for thin-walled open section members: consistent warping function and nonlinear constitutive equation

6. NUMERICAL EXAMPLES AND DISCUSSION

In order to benchmark the developments carried out in this work, some already existent models (available in PEFSYS, ANSYS or the literature) were chosen. They can be sorted according to the following hierarchical order:
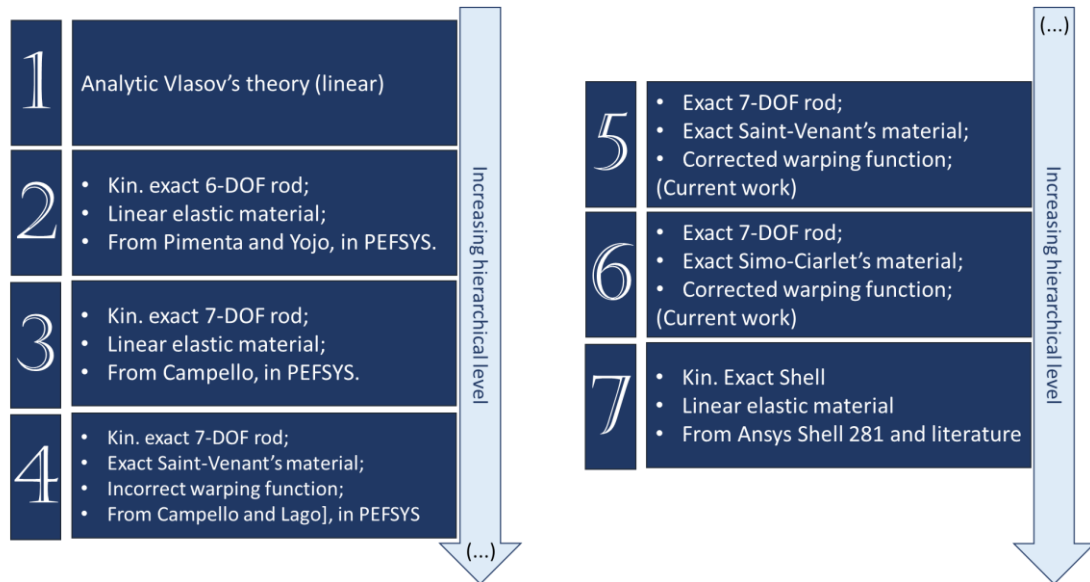
Figure 13– Benchmark framework. Used models from [2], [12], [22] and [3].

In the current work, kinematically exact shell models (*Ansys Shell 281* element – large displacement: *on* – simulated by the author, or other shell models from the literature) are used as the hierarchically highest order reference solution.

For the sake of conciseness, the following standard is used to denote the geometry of the analysed cross sections:

Table 9 – Cross-sectional geometrical description

Type	Geometry
Rectangular	

To be continued

Advances on a kinematically exact rod model for thin-walled open section members: consistent warping function and nonlinear constitutive equation

Continued
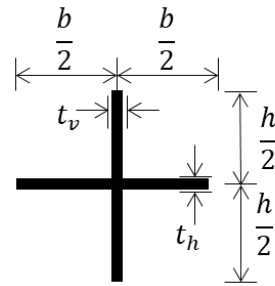
Cruciform section	
T-section	
Bisymmetric I-section	
Symmetric C-channel	
Axisymmetric Z-section	
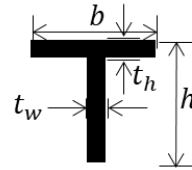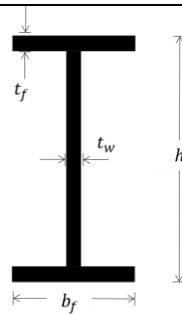
Marcos Pires Kassab   91
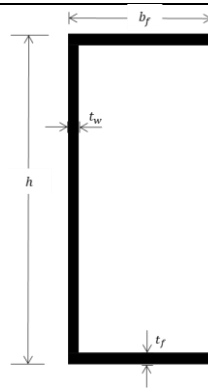
Advances on a kinematically exact rod model for thin-walled open section members: consistent warping function and nonlinear constitutive equation
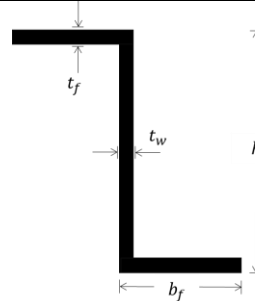
6.1. Validation on examples without buckling

The examples 6.1.1 to 6.1.4 were taken from [50] – the analytical Vlasov's solution is taken from there. For all rod examples, the mesh was made of 10 same-sized elements with linear interpolation (2 nodes), except in example 6.1.3, in which 30 elements were used. For the shell models, also a regular mesh was used. It was refined until a sufficiently fine mesh (>90000 nodes) was obtained, which is almost the limit of the software´s academic version (100000 nodes).

It should be noted that, in some models, the total torsion moment stress resultant (T) includes both the bi-shear (Q) and uniform torsion (M_u) contributions. In these cases, the uniform torsion can be found by doing $M_u = T - Q$, since the models typically output Q and T. Also, as mentioned in section 3.2, the values of Q were multiplied by -1, to be coincident with the linear Vlasov theory.

6.1.1.   I-cantilever with external torsional moment

For this example, two cross-sections are evaluated: I 254x52,1 and CS 250x52 (see Figure 14). The material parameters are $E = 205\ GPa$ and $G = 80\ GPa$. In this example, the clamped end constrains all degrees of freedom: there are no displacements, rotations nor warping.

As already shown in section 3.4, the warping functions obtained from equations (2.66) and (3.80), are rigorously the same for bi-symmetric I-sections, and therefore there is no point in simulating the example with both of them. In Figure 15, the warping functions used for the current model are depicted.
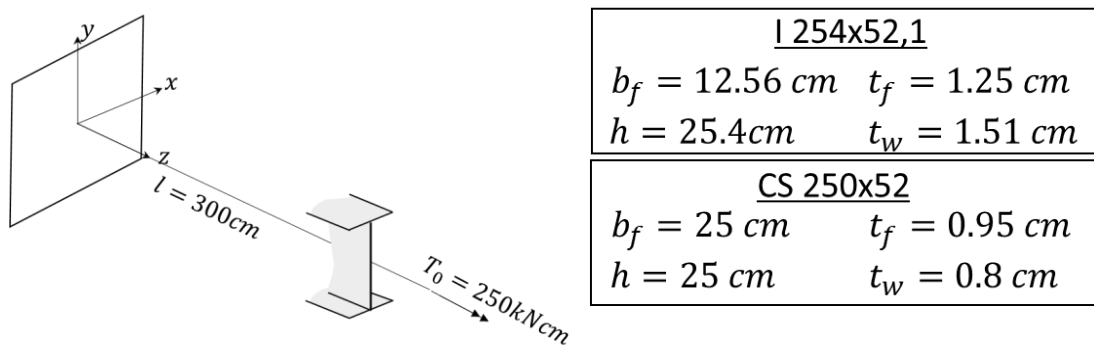
Figure 14–Description of the example 6.1.1.
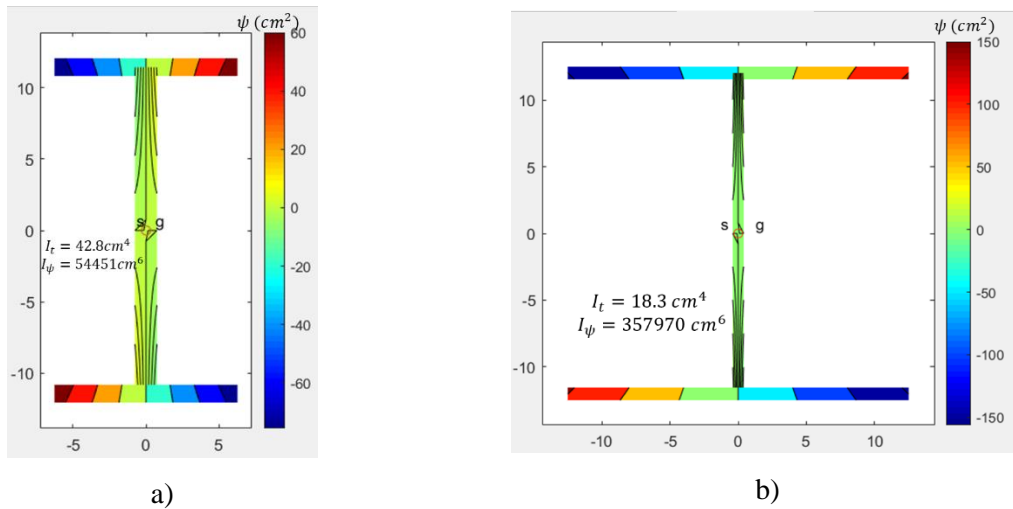
Figure 15 – Warping function for a) I 254x52,1; b) CS 250x52. Dimensions in cm.

By investigating the stiffness properties of each cross-section, it is possible to infer whether it prioritizes the uniform torsion or the non-uniform torsion. Such preference can be quantified through the parameter $k = \sqrt{\frac{GI_T}{EI_\omega}}$. For the I 254x52,1, $k = 0.0175\ cm^{-1}$ and for the CS 250x52, $k = 0.00452\ cm^{-1}$. This implies that, necessarily, for the former, uniform torsion is more intense in the load-carrying mechanism, and therefore the bi-shear is expected to be lower, whereas, in the latter, the opposite is expected. Indeed, this behaviour can be seen in Figure 16a) and Figure 17a). For the same reason, when compared with 6 DOF rod models (in which only the uniform torsion effect is accounted for), the results of the I 254x52,1 is significantly closer than the ones of the CS 250x52. Nevertheless, it is evident that the bi-shear is an important torsion-resisting mechanism, leading to smaller torsion rotations when such effect is considered. Note that, in both cases, every torsion-related quantity is in perfect agreement with the Vlasov's theory[8], and are almost coincident with shell models. The only noticeable difference is a slightly lower warping and bi-shear for the second example for the Simo-Ciarlet material. For the other curves, the St.-Venant's and Simo-Ciarlet's materials are coincident.

---

[8] the warping intensity in the analytic Vlasov's model is the second derivative of the torsion rotation.

Advances on a kinematically exact rod model for thin-walled open section members: consistent warping function and nonlinear constitutive equation
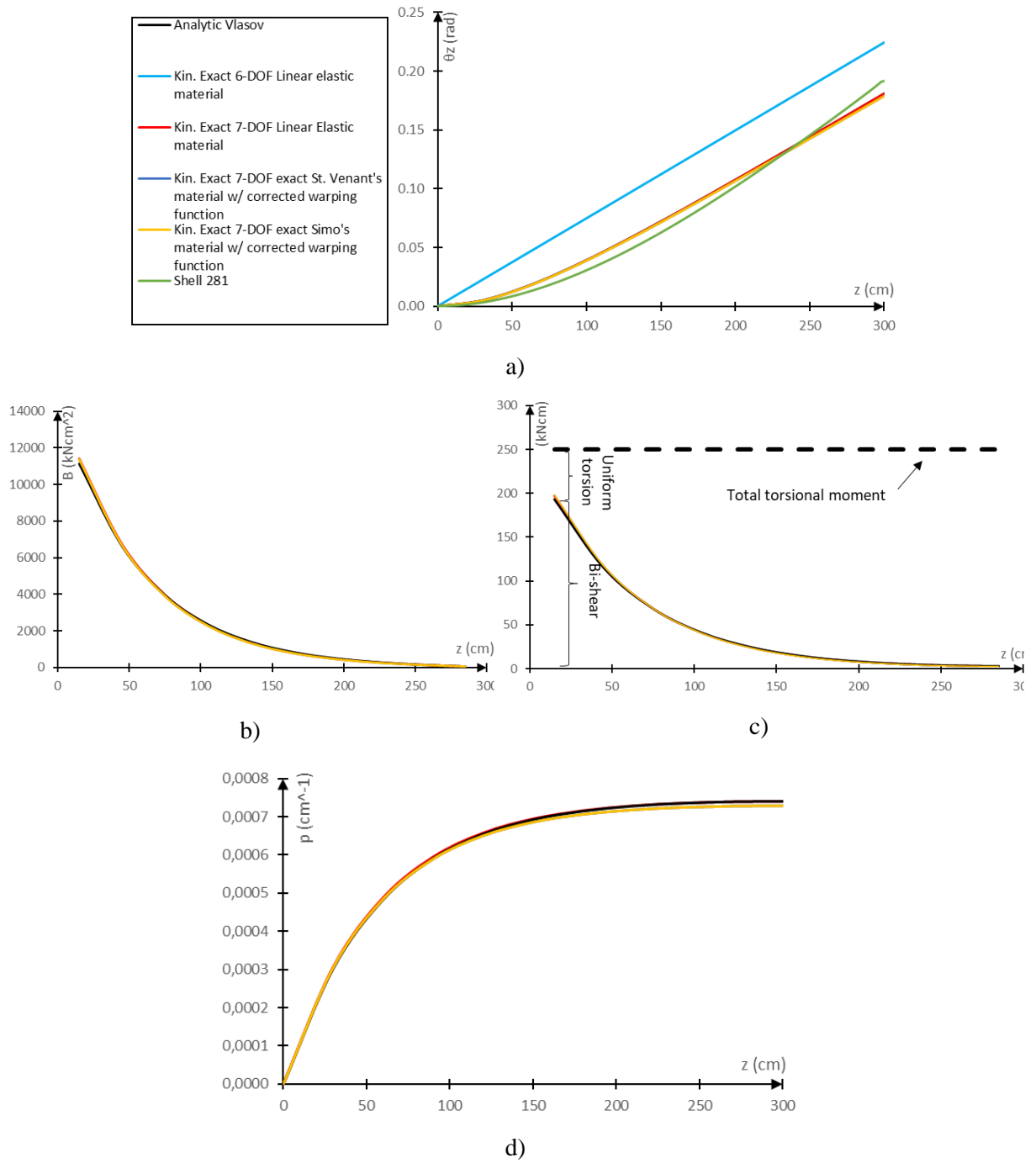
Figure 16 – Beam diagrams for example 6.1.1, I 254x52,1: a) torsional rotation; b) warping intensity; c) torsional moment and bi-shear; d) bi-moment.

Advances on a kinematically exact rod model for thin-walled open section members: consistent warping function and nonlinear constitutive equation

a)

b)

c)

d)
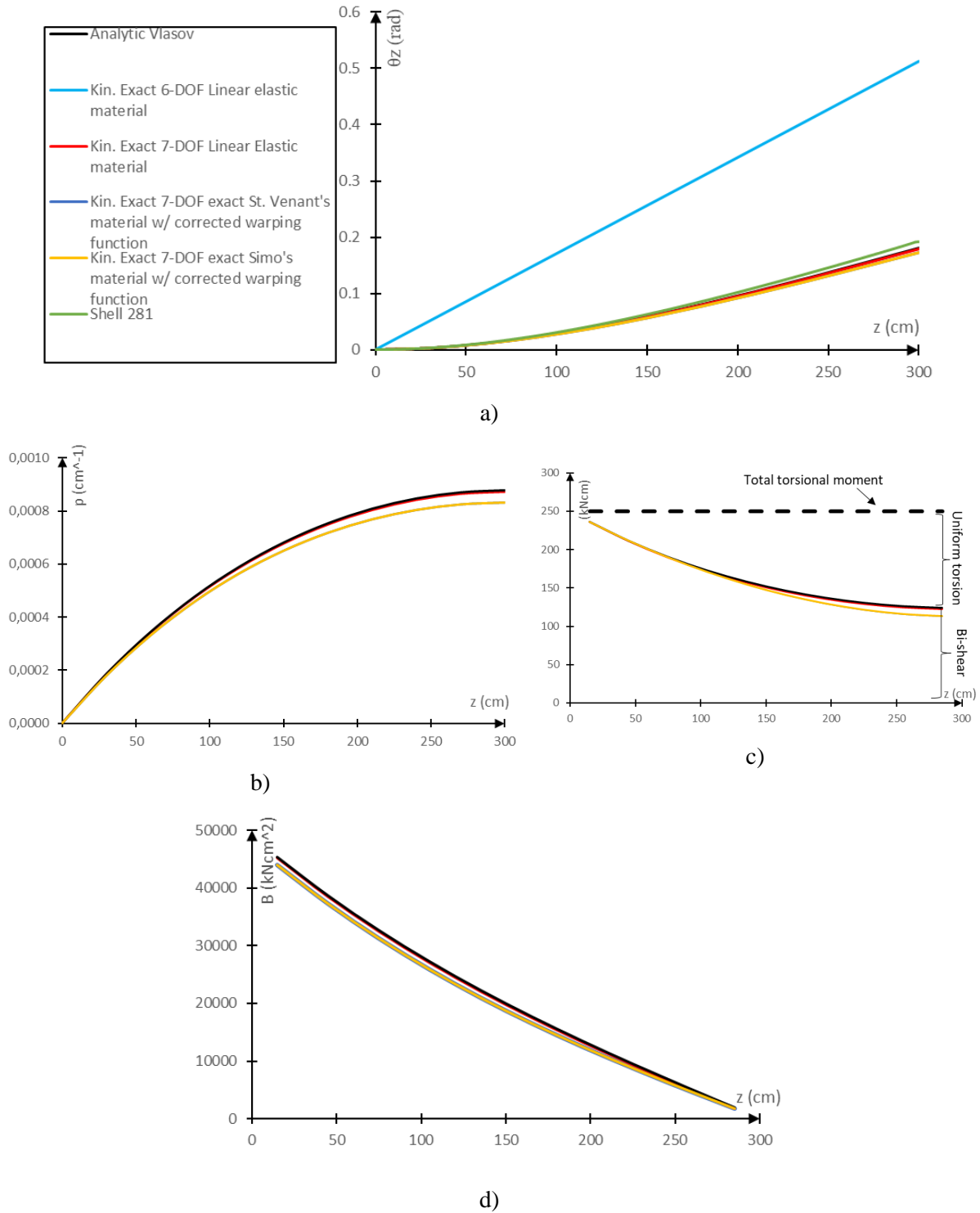
Figure 17 – Beam diagrams for example 6.1.1, CS 250x52: a) torsional rotation; b) warping intensity; c) torsional moment and bi-shear; d) bi-moment.

Marcos Pires Kassab   95

Advances on a kinematically exact rod model for thin-walled open section members: consistent warping function and nonlinear constitutive equation

6.1.2.   *Simply supported beam with distributed load*

In this example, two similar situations are studied: **a)** an I-section beam, loaded with a uniformly distributed vertical load $f_y = 0.215\ kN/cm$ and a uniformly distributed torsional moment $m_z = 0.688\ kNcm/cm$ and length $L = 500\ cm$ is studied. This loading emulates a brick wall with unbalanced mortar coating (see Figure 18); **b)** a C-section beam, loaded with a uniformly distributed vertical load $f_y = 3\ kN/cm$ at the web plane (off the shear centre, thus torsion shall occur) and length $L = 400\ cm$. Those are relatively low torsional moment of a realistic design situation, but still capable of mobilizing relevant non-uniform torsion effects. The profile is a CS 250x52 (see Figure 14). The material parameters are $E = 205\ GPa$ and $G = 80\ GPa$.
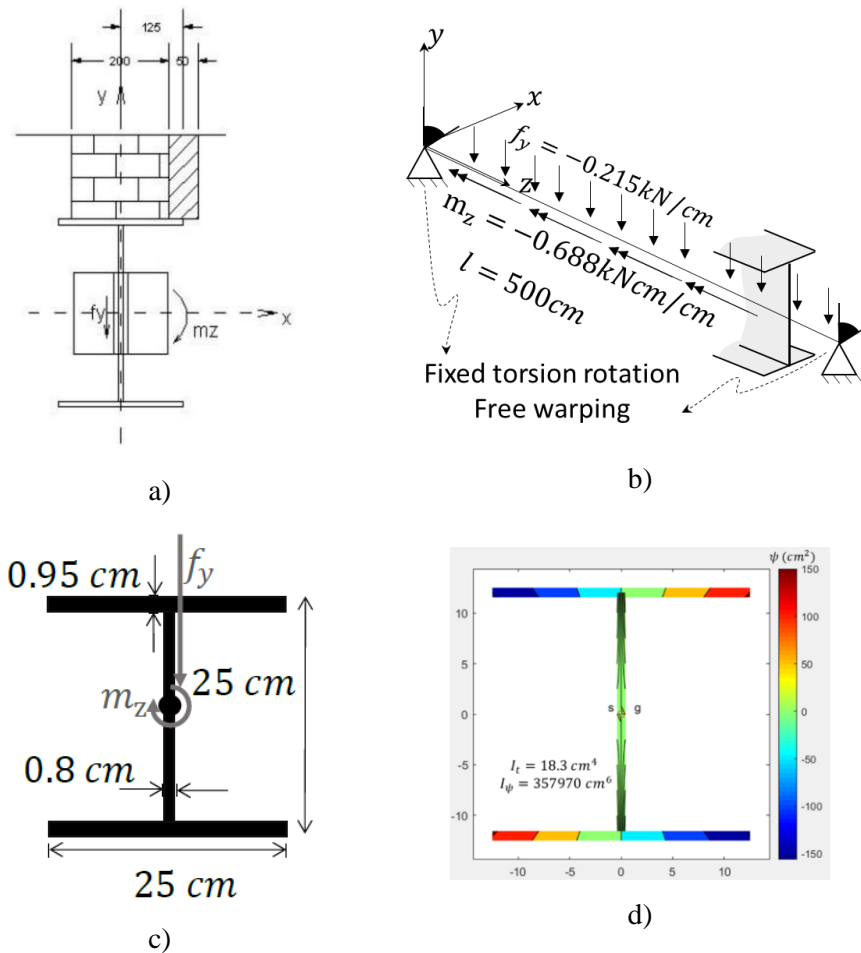
Figure 18– Description of the example 6.1.2a): a) Design situation: wall with mortar coating, from [50]; b) problem schematics; c) cross-section description; d) warping function (units in cm).

a)

b)

c)

d)
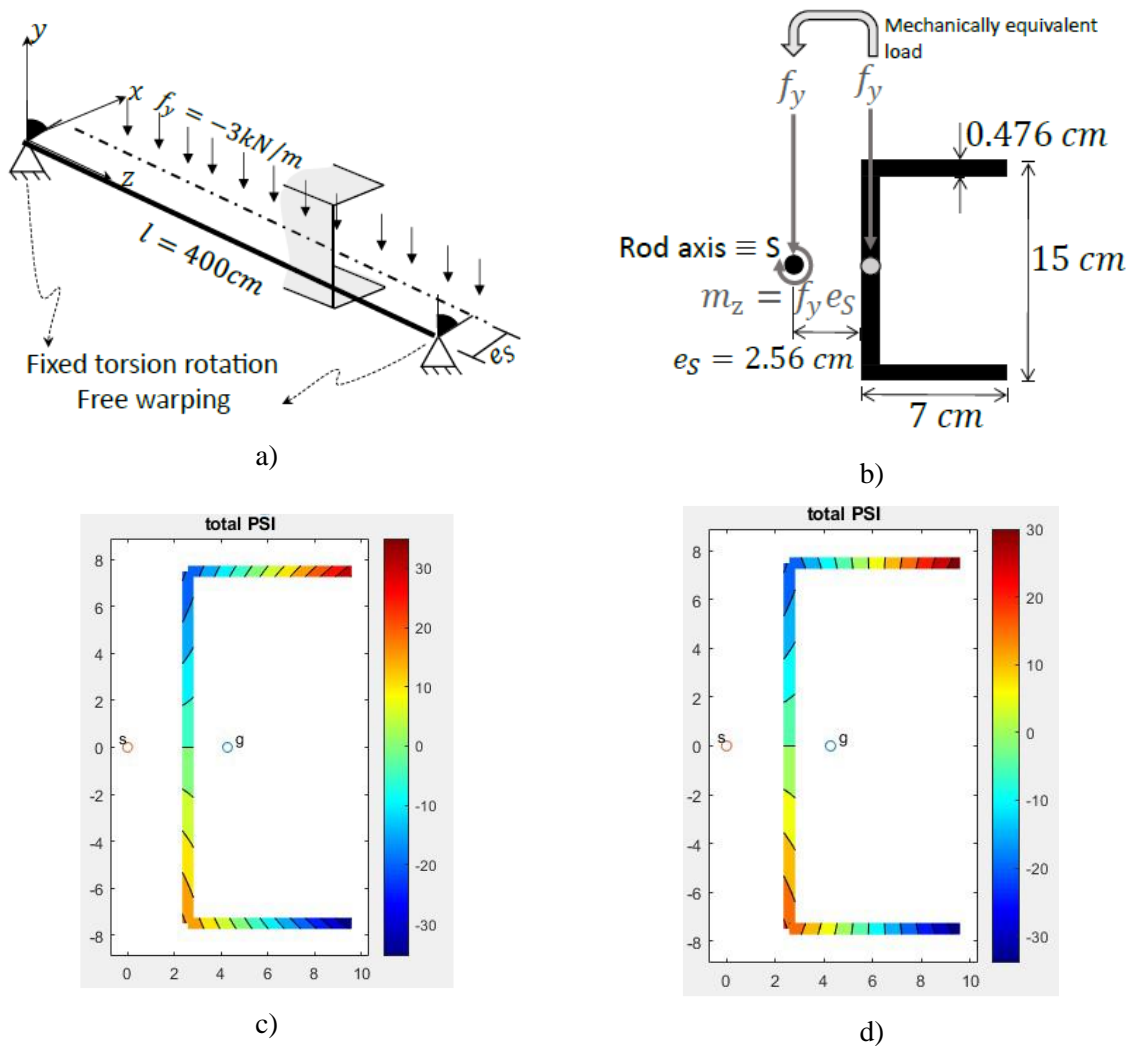
Figure 19– Description of the example 6.1.2b): a) Problem schematics; b) cross-section description; c) present warping function; d) incorrect warping function from [2] (dimensions in cm).

The strains from this example are small. Therefore, for torsion, there should be good adherence among linear Vlasov's model and the kinematically exact 7-DOF rod models. The warping function generated by both equation (3.80) and from [2] for I-sections are the same and can be seen in Figure 15b). Thus, this case is good for assessing the implementation of the Saint-Venant's and Simo-Ciarlet's material laws.

Firstly, it can be seen in Figure 20a) and d) that the consideration of non-uniform torsion is of utmost importance. Without this important load carrying mechanism, as in the 6 DOF rod model, the torsion rotation is severely overestimated in both cases. When the warping degree of freedom is introduced, the obtained torsion rotation is the same as the one provided by both the shell model and the linear theory.

For the I-section, one can see in Figure 20 that all constitutive equations presented nearly the same behaviour for both vertical displacement due to bending (see Figure 20 (b)) and torsion rotation (see Figure 20 (a) and (c)). They are also in good agreement with the shell´s results.

Marcos Pires Kassab   97

Advances on a kinematically exact rod model for thin-walled open section members: consistent warping function and nonlinear constitutive equation

For the C-channel, by examining Figure 21, it becomes evident that the model with the warping function from [2] yields inconsistent results – torsional response is extremely stiff. Apart from this one, the other rod models (i.e, with linear elastic, Saint-Venant's and Simo-Ciarlet's materials) are in accordance with the Vlasov's theory. Vertical displacements are virtually the same for all cases, except for the case with incorrect warping function, in which the torsional contribution is severely underestimated. Results from 7-DOF rod models are also nearly coincident with the ones from the shell model, for both displacements and torsional rotation, which supports the proposed warping function.
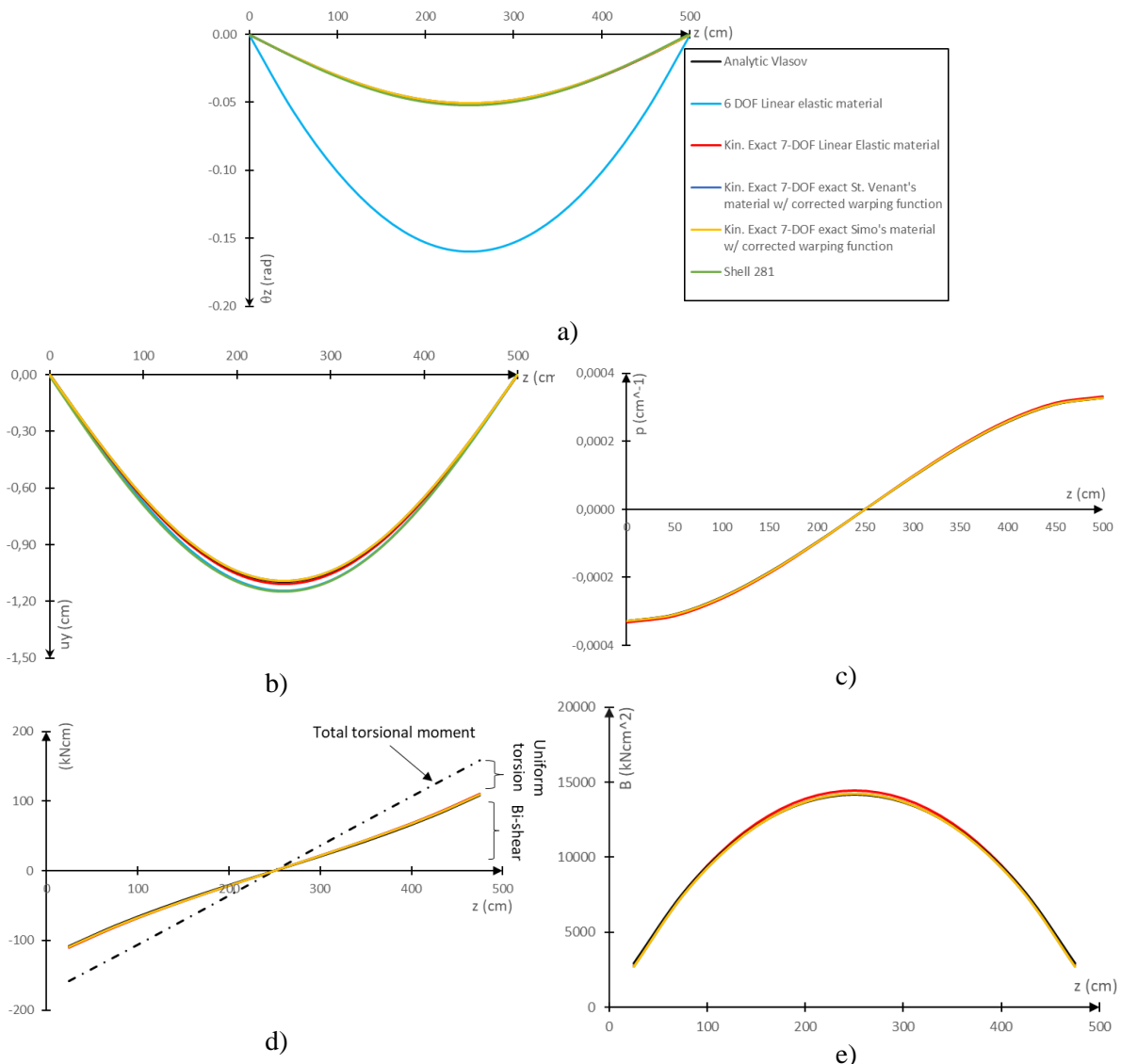
Figure 20 – Beam diagrams for example Simply supported beam with distributed load 6.1.2a): a) torsional rotation; b) vertical displacement; c) warping intensity; d) torsional moment and bi-shear; e) bi-moment.

a)

b)

c)

d)

e)
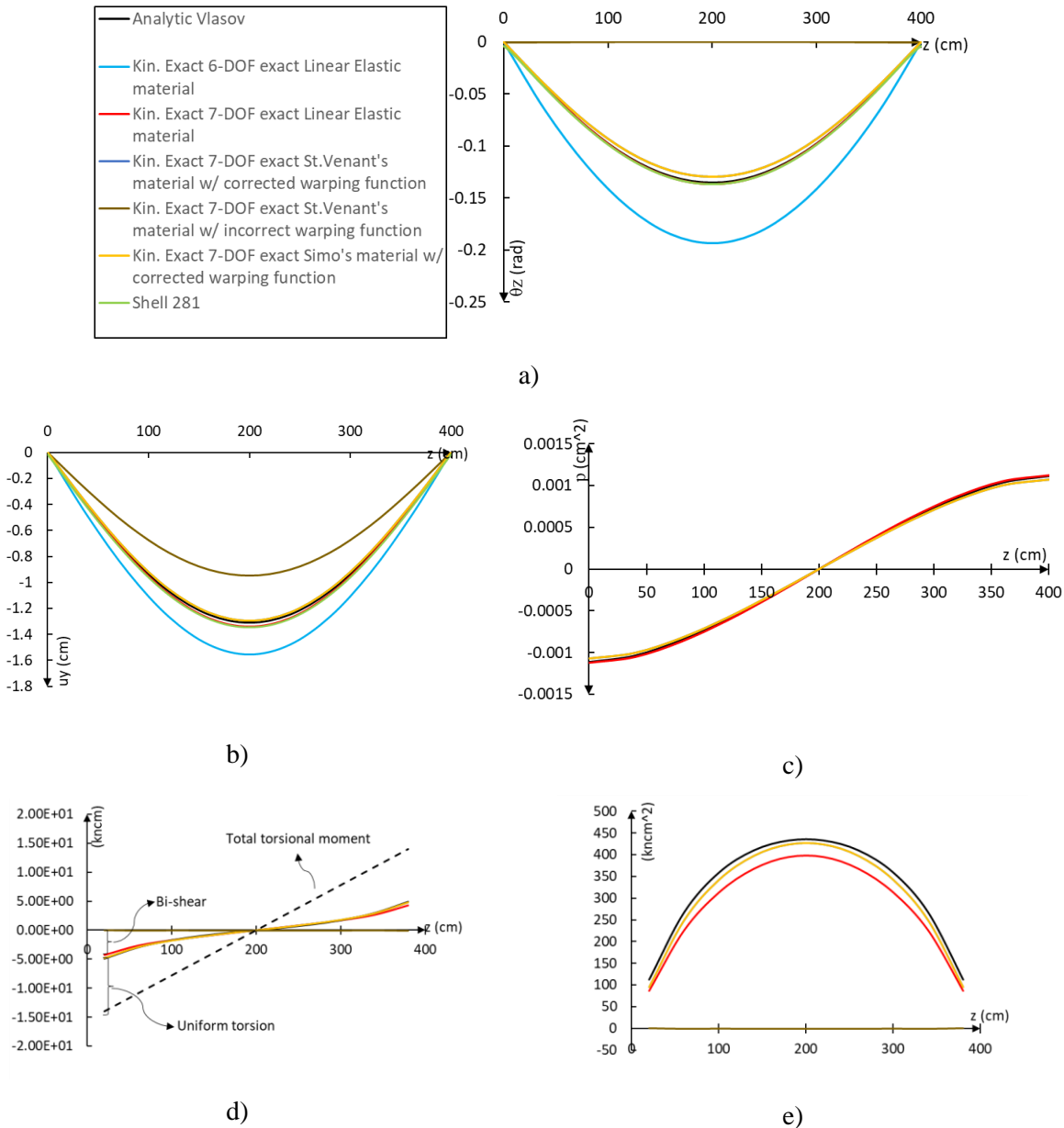
Figure 21 – Beam diagrams for example 6.1.2b): a) torsional rotation; b) vertical displacement; c) warping intensity; d) torsional moment and bi-shear; e) bi-moment.

6.1.3.   *Transversely loaded C-channel cantilever*

In this example, a C-channel cantilever (length $l = 900\ cm$) is loaded with a concentrated load P at the free tip, at the web/top chord intersection. The load is incremented up to $20\ kN$. At the clamped end, the deformation is completely restricted. For the rod models the axis is positioned at the web/top chord intersection, thus the load is exactly at the axis. A graphical description of this example can be seen in Figure 22. As the load is off the shear-centre, torsion is expected to occur. It is assumed $E = 210\ GPa$ and $G = 80\ GPa$. For the rod models, uniform mesh with 30 2-noded elements is used, in order to maintain consistency with the original benchmark from Gruttmann [18], [48]. This simulation can also be found in Gonçalves [35], with their 7-DOF rod.

Marcos Pires Kassab 99

Advances on a kinematically exact rod model for thin-walled open section members: consistent warping function and nonlinear constitutive equation

For this example, a profile (here denominated C 300x100x10x16) is evaluated (see Figure 22). This is not the same cross-section used in reference [50], but the expression for the analytical solution, taken from that reference, is the same.
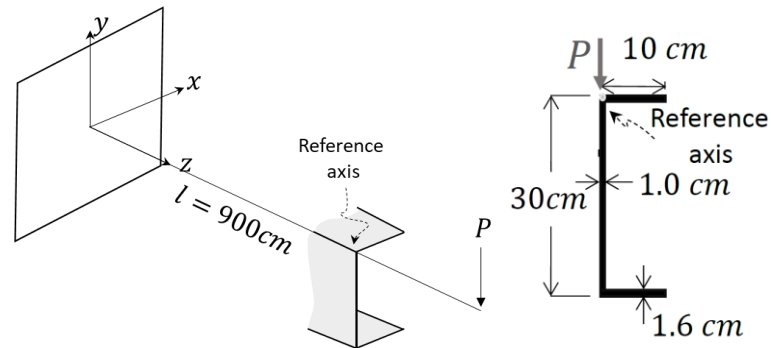
Figure 22 – Description of the example 6.1.3.

For C-sections, it was already discussed how important it is to adopt the corrected warping function (see Figure 23). It will be shown in a complete example the impact of adopting either equation (3.65) or (3.80).
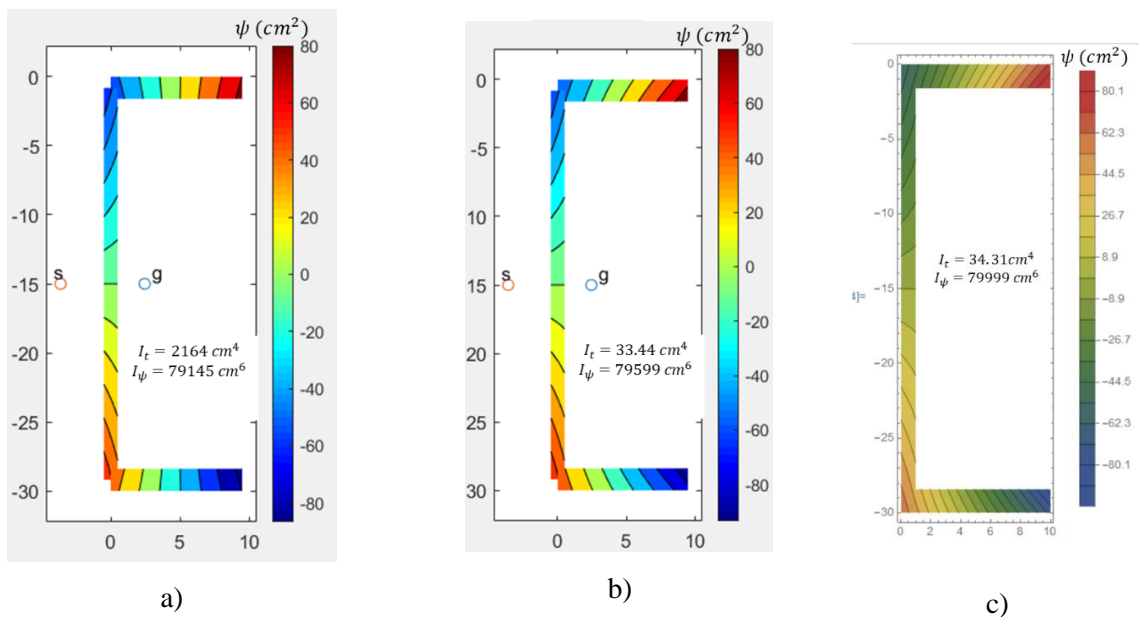
Figure 23 – Warping function of section C 300x100x10x16 using a) old equation (2.66); b) proposed equation (3.80). Dimensions in cm. c) solving Saint-Venant's warping function in Mathematica software, pole in shear centre.

A qualitative perspective of the simulations can be found in Figure 24.
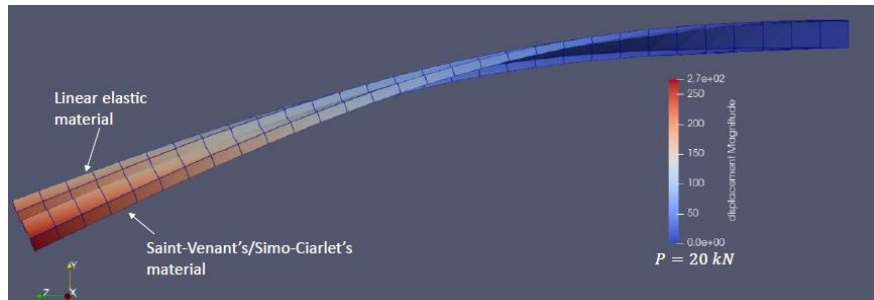
a)
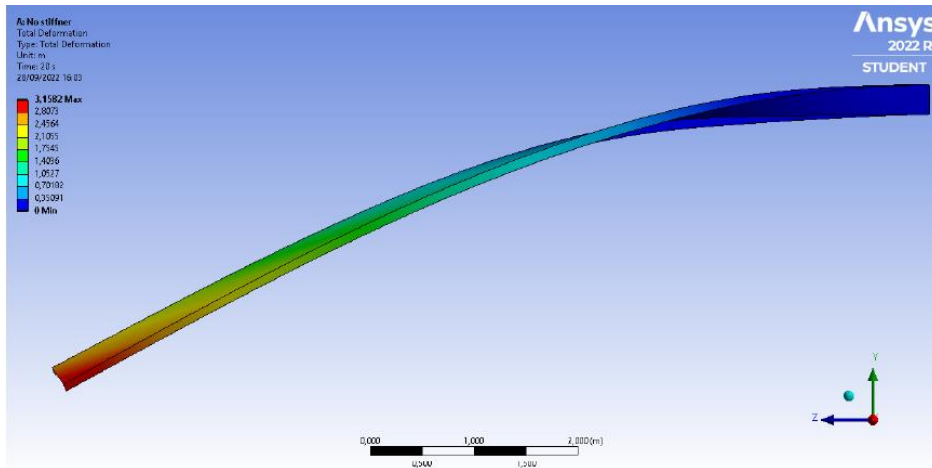
b)

Figure 24 – Simulation result, deformation in original scale ($P = 20kN$) a) PEFSYS rod model with Linear elastic and Saint-Venant's/Simo-Ciarlet's materials (superimposed, units in cm); b) Ansys, shell elements (in m);
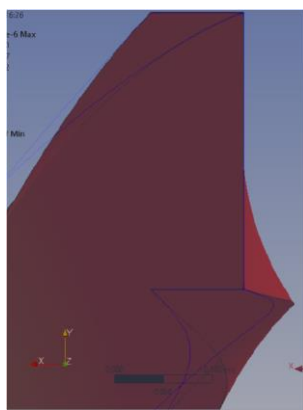
a)
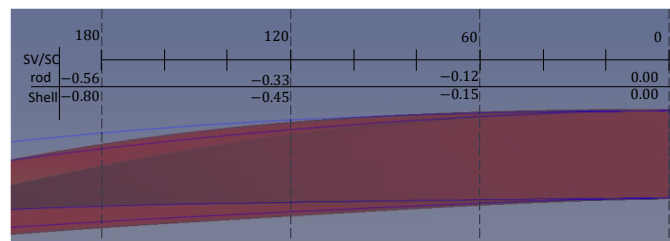
b)

Figure 25 – Superimposed view of rod with Saint-Venant's/Simo-Ciarlet's material (blue line) and Ansys's shell (black line) a) View from the cantilever support; b) detail near the clamped end, with respective torsion rotation (rad).

In Figure 26, the equilibrium path for a point at the loaded extremity, at mid-height of the web, is represented.

Advances on a kinematically exact rod model for thin-walled open section members: consistent warping function and nonlinear constitutive equation
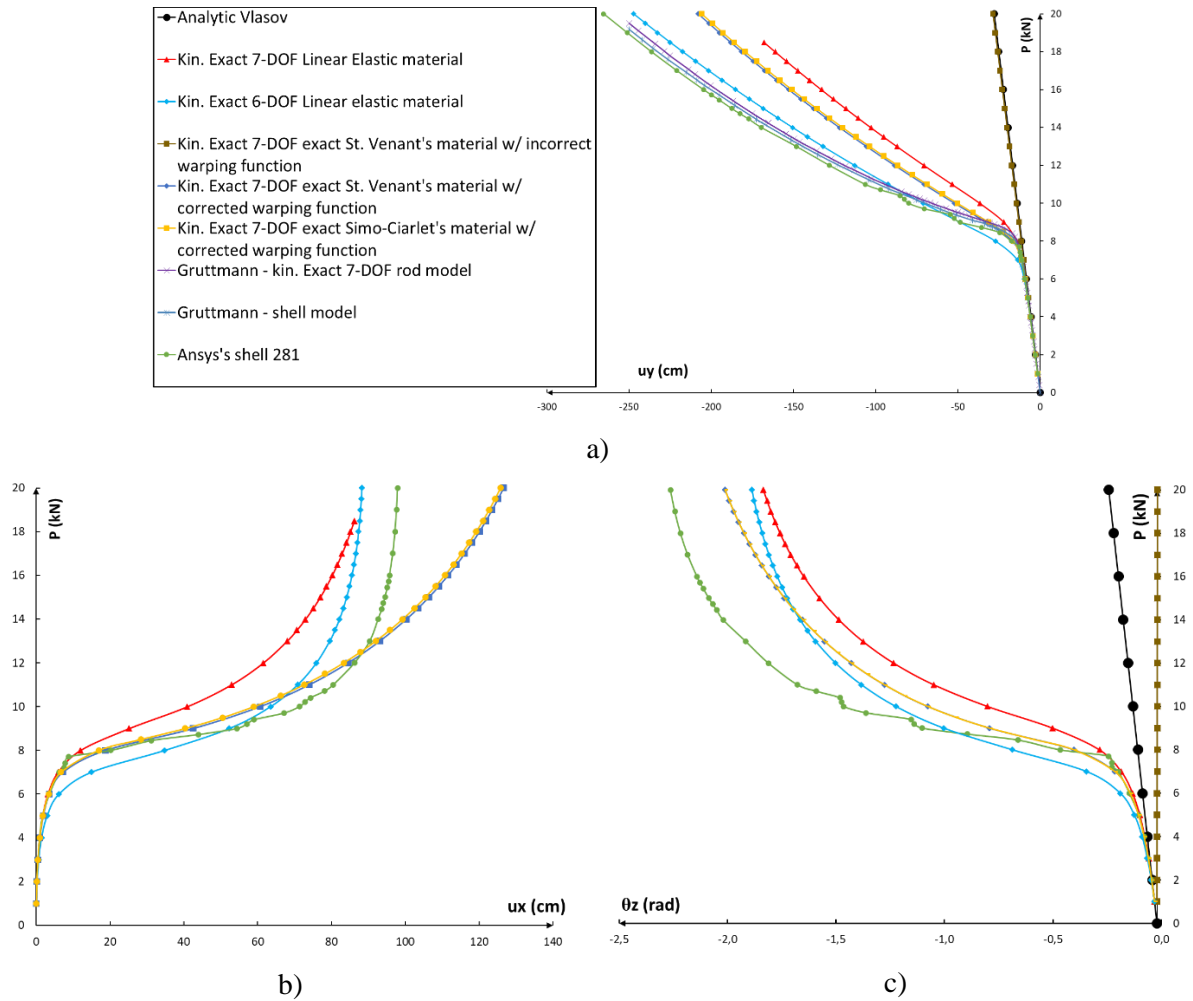
Figure 26 – Results from example 6.1.3. a) Vertical displacement; b) Lateral displacement; c) Torsional rotation. Gruttmann reference is [18].

As it can be seen in Figure 26, up to $P \approx 8\ kN$, all models (even the linear Vlasov's model) are almost in complete agreement. However, after this load level, results from the 7-DOFs models calculated with PEFSYS (linear elastic, exact Saint-Venant's and Simo-Ciarlet's material with corrected warping function) presented a rather stiffer solution than the corresponding ones from Gruttmann [18]. Theoretically, Gruttmann's model should be equivalent to the 7-DOF model with linear elastic material implemented in PEFSYS – documented in [1]. Only two noticeable differences are present:

- Gruttmann interpolates the base vectors $\boldsymbol{e}_i$ instead of the Euler-Rodrigues parameters $\boldsymbol{\theta}$ which generates a non-orthogonal base at the Gauss points (the base is only orthogonal at the nodes). This might have an effect similar to the imposition of a shear correction factor, as some in-plane distortion is allowed due to the loss of the orthogonal base.;
- for Gruttmann, the pole of the warping function is always coincident with the rod axis, instead of the principal pole, as done here. It must be mentioned that tests performed by the authors indicated that taking the axis as the pole leaded to worse results (said outputs were omitted for conciseness). It is worth mentioning that when the principal pole is not

coincident with the centroid, a choice must be made to either **a)** take the pole at the axis, which renders first-order coupling between axial force, bending moments and bi-moment; or **b)** take the pole at the shear centre, which uncouples the normal stress-dependent resultants, but creates an additional shear tension contribution for the shear forces, torsional moment and bi-shear. See Appendix E for a discussion about orthogonality conditions.

In Figure 25, one can see that, despite the differences due to different flexural torsion behaviour, the cross-section near the support undergoes rather intense in-plane distortion, a behaviour that cannot be described by the current 7-DOF models. Were in-plane distortional modes explicitly considered in the kinematical assumptions, such response could have been detected. It must also be highlighted that, comparing linear elastic rod and shell models, the most important torsional discrepancy is near the clamped end (for $z < 400\ cm$), where local web/flange distortions are more intense. The authors intend to address this issue in a future work, by enriching the rod´s kinematics. It should be also remarked that the torsional response is severely impacted by the usage of the advanced constitutive equations, when compared to the linear elastic material Figure 27, suggesting that torsional/bending strain coupling does occur at the level of the constitutive equation, and cannot be neglected for a proper beam´s response.

By analysing Figure 26a), the reader might also be surprised that the vertical displacement calculated with the PEFSYS model with 6 DOFs and linear elastic material (documented in [22]) seems to be in better agreement with Gruttmann´s and shells´ results than the higher level models; this is, however a coincidence. As the bi-shear and bi-moment are not present in this model, the torsional stiffness of the system near to the clamped end is severely underestimated, leading to an exaggerated torsion rotation (see Figure 27b), which penalises the whole system stiffness due to the amplification of the higher order contribution of the lateral sway of the rod, leading to a greater vertical displacement overall (see Figure 27a).

a)

b)
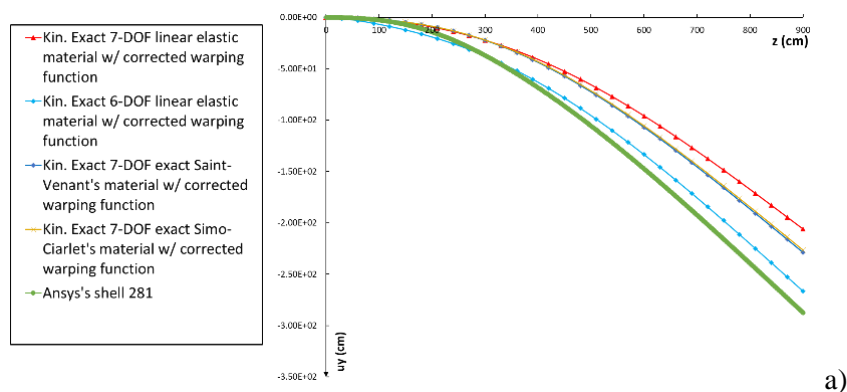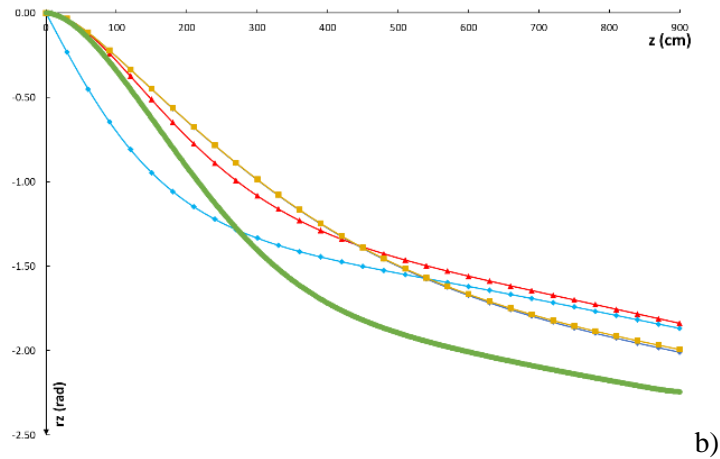
Figure 27- Results from example 6.1.3. a) Vertical displacement and b) torsional rotation for $P = 20kN$.

It should be noted again that the results of the Saint-Venant's and Simo-Ciarlet's material are in perfect agreement.

6.1.4.   *Z-section cable with axial tension*

This example features a Z-section rod (lenght $L = 300\ cm$) that acts as a cable: it is loaded with concentrated axial tensile force N on both ends, inducing a bi-moment $B = N\psi^O$ (O is the point of the concentrated load application). Formally, this is achieved by using the definition of bi-moment and the Dirac delta function. Note that this is, in general, a peculiar boundary condition, since $B = \hat{B}(N)$. Despite that, in this case, the reaction at the support is known beforehand, due to how the problem is constrained. Warping is allowed at both extremities.

Therefore, torsional rotation occurs, even without any external torsional moment In order to prevent rigid body motion, axial displacement (u_z) and torsion rotation (θ_z) is restricted at one of the ends, as well as transverse displacements at both ends (u_x, u_y). A graphical description of this example can be seen in Figure 28. It is assumed $E\ =\ 205\ GPa$ and $G\ =\ 80\ GPa$. For the rod models, uniform mesh with 10 linear elements is used.

For this example, the profile Z 100x50x3,0 is evaluated (see Figure 28). For this section, the function that are generated using equations (2.66) and (3.80) can be seen in Figure 29.
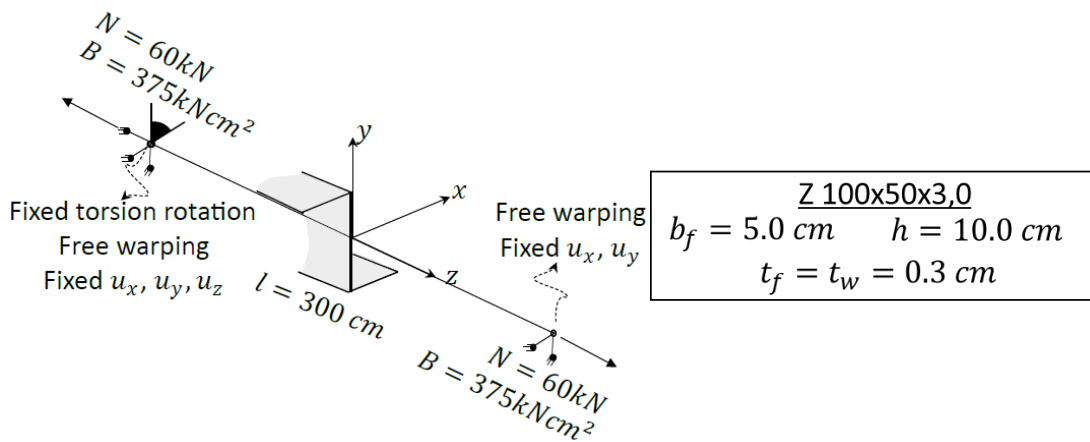
Figure 28 – Description of the example 6.1.4.

The diagrams of the relevant resultants and displacements are shown in Figure 30, while displacements result from the Ansys' shell model is shown in Figure 31.

a)

b)
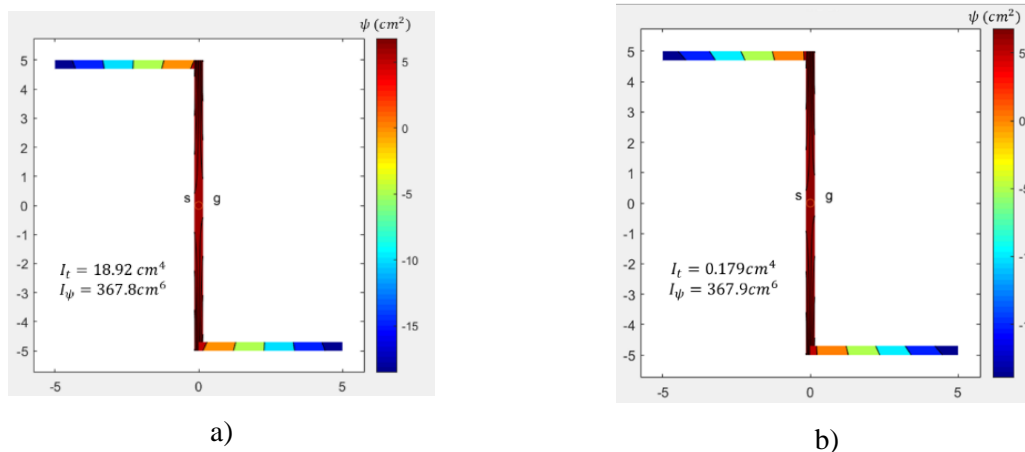
Figure 29 – Warping function of section Z 100x50x3,0 using a) old equation (2.66); b) proposed equation (3.80). Dimensions in cm.

Thus, let us first analyse the torsional behaviour (Figure 30 (a), (c)-(e)): when the 7-DOF model with linear elastic material is used, the analytic Vlasov's solution for torsion is recovered, as expected. However, despite the fact that this is a small strains example when the 7-DOF model considers the exact Saint-Venant's and Simo-Ciarlet's materials and the proposed warping function (i.e., corrected and with secondary warping included) or shell elements are used, there is an apparent torsion/tension coupling effect that somewhat stiffens the torsion rotation. We draw the attention to the fact that the St.-Venant's and Simo-Ciarlet's materials are virtually coincident, and both much closer to the shell´s solution than the linear elastic material. Regarding axial displacement (u_z, Figure 30(b)), all the rod models estimated somewhat lower u_z when compared to the shell model. By analysing Figure 31(b), at both ends of the shell curve, it becomes evident that such output is due to a local deformation at the region where the concentrated load is introduced, which is much captured in the shell model. This can be clearly seen in (see Figure 31c). Despite this difference, analysing sections not so close to the

Marcos Pires Kassab   105

Advances on a kinematically exact rod model for thin-walled open section members: consistent warping function and nonlinear constitutive equation

extremities, the deformation rates are fairly coincident – the curves of $u_z(z)$ are parallel –, suggesting that such discrepancy are primarily due to the aforementioned reason. It is also worth mentioning that, in this example, the warping term $p\psi^O$ has an important contribution to the total axial displacement. For this reason, the model with the incorrect warping function also presents a discrepant axial displacement value. It is again stated that the use of the corrected warping function is mandatory to accurately model torsion phenomena.

Also, as expected, the 6-DOF model is unable to identify any torsion whatsoever, since it does not contemplate bi-moment and bi-shear capabilities. As consequence, there is no warping contribution for the axial displacement.
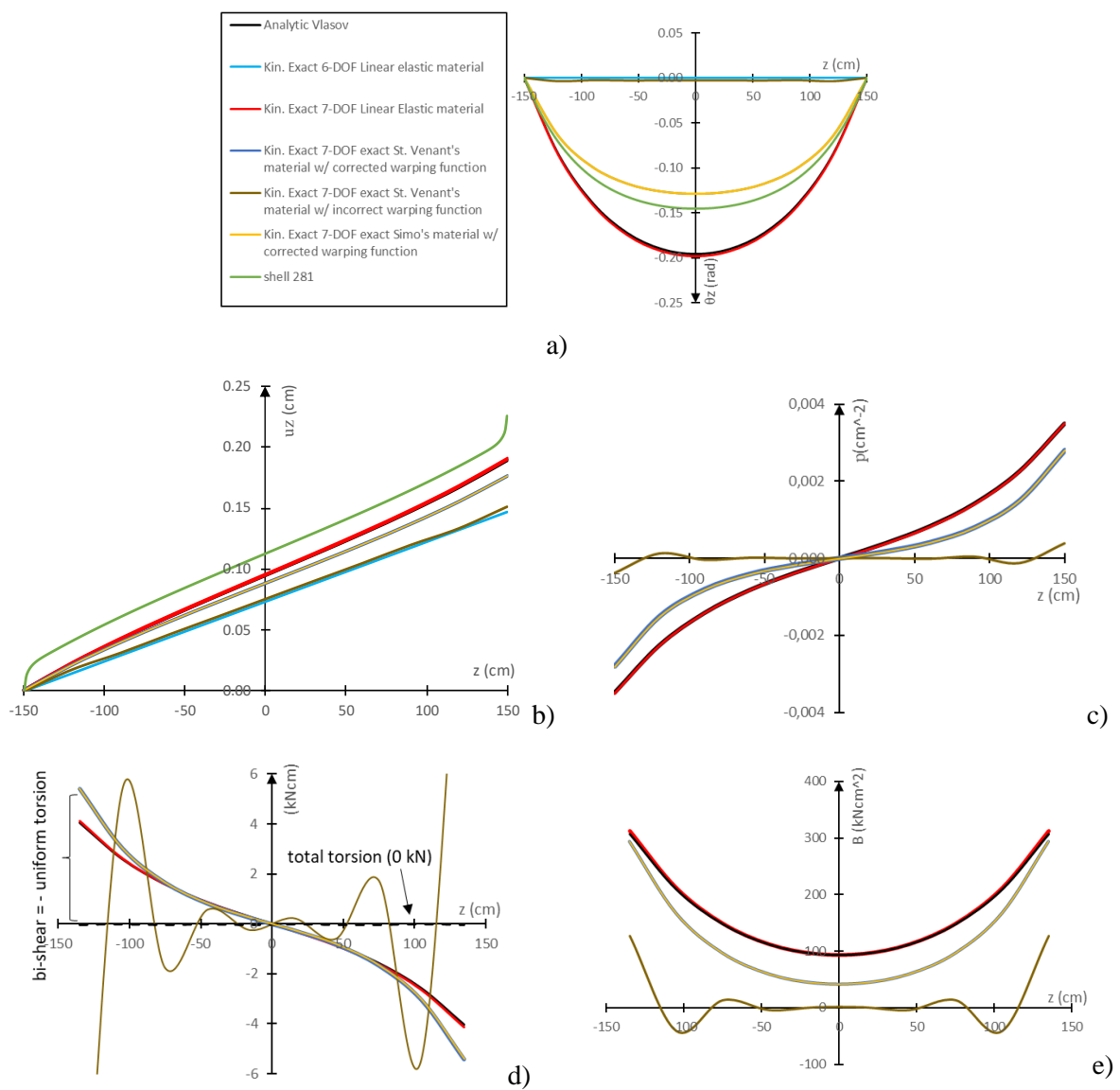
Figure 30 – Beam diagrams for example 6.1.4: a) torsional rotation; b) axial displacement; c) warping intensity; d) torsional moment and bi-shear; e) bi-moment.

a)

b)

c)
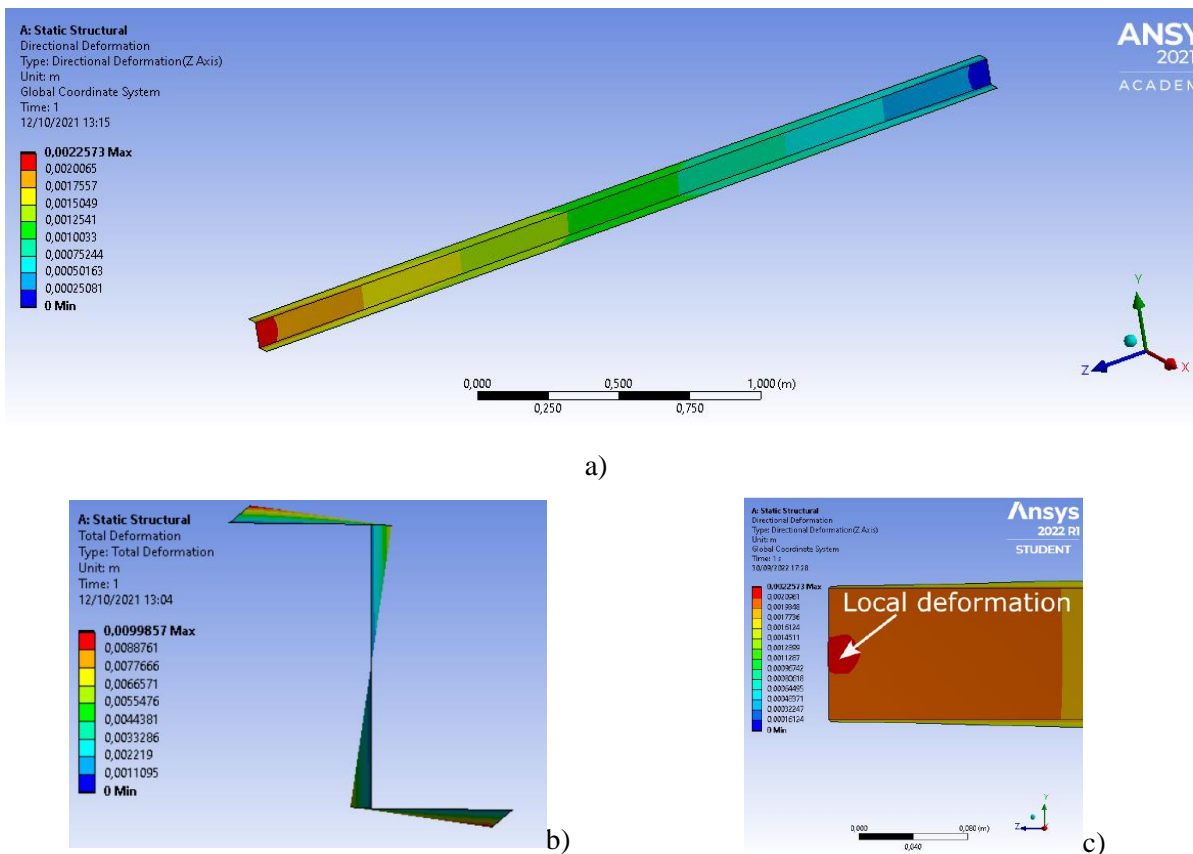
Figure 31 – results from Ansys shell 281 model. a) isometric global view –
axial displacements and b) cross-sectional view, magnitude of total displacements (original
scale); c) detail of an extremity, axial displacements. Units in m

6.2. Validation on examples with buckling

6.2.1.   *Buckling of a compressed I-cantilever*

In this example, a I-section cantilever (lenght $l = 240\ cm$) is studied. At the clamped end, the displacements are fully restricted. The evaluated profile is an I-section, (see Figure 32). The material parameters are $E = 200\ GPa$ and $G = 80\ GPa$. The compressive loading (P) is incrementally increased, until $100\ kN$. A transverse lateral load perturbation (0.1% of the main load) is added in order to transpose the bifurcation at the load application point. The axis coincides with the line of centroids. At the free end, forces are applied at the centroid.

Marcos Pires Kassab 107

Advances on a kinematically exact rod model for thin-walled open section members: consistent warping function and nonlinear constitutive equation
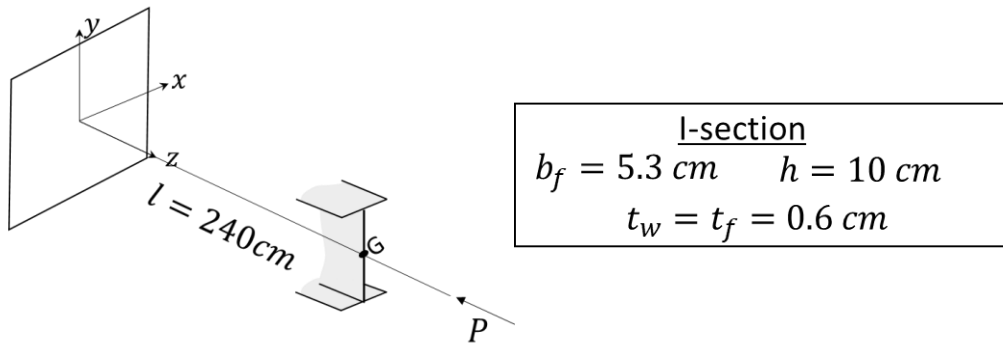
Figure 32 – Description of the example 6.2.1.

The used warping function, as developed in this work, can be seen in Figure 33.
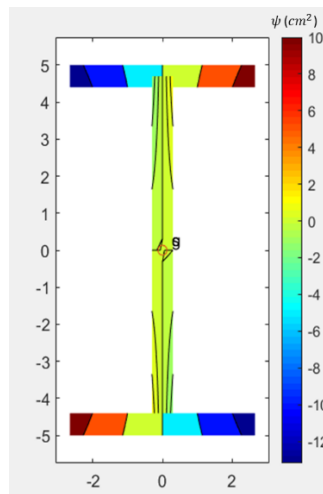
Figure 33 – Warping function for example 6.2.1. Dimensions in cm.

This is a classic case of buckling of a compressed column that, after reaching the critical load, deflects sideways and bends. The theoretical Euler critical load is $P = \frac{\pi^2 EI}{4l^2} = 12.89kN$. For rod models without the Poisson effect, (such as the ones presented in this work), the motion is completely bidimensional, and there is no torsion nor warping, and therefore, the only possible coupling is between compression and bending strains. As can be seen in Figure 34, linear elastic models presented similar results as those from the exact Saint-Venant's and Simo-Ciarlet's material. Thus, it can be deduced that such coupling had little effect on the solution. Also, the 6 DOF rod model was perfectly suitable for this simulation, as there is no torsion. As it can be seen, both the critical load and post-critical equilibrium path from the kinematically exact rod models are in agreement with the Ansys shell model. At about $20\ kN$, the Ansys solver was not able to proceed incrementing the load, which probably indicates the existence of a second critical load associated to local instability, which was naturally not detected by the in-plane rigid rod models. Had rod models incorporated in-plane distortional DOFs, they might had stood a chance to capture such local behaviour, as done in Gonçalves et al. [42].
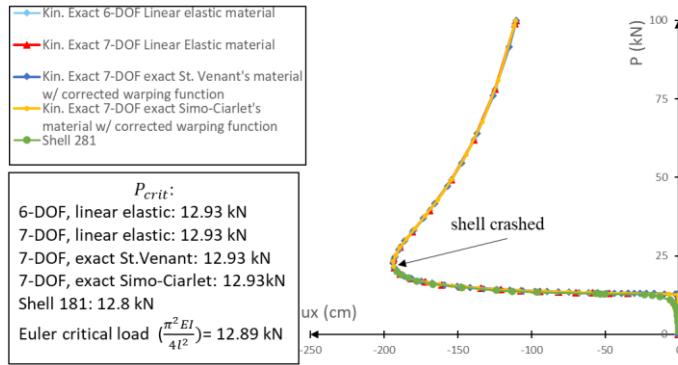
Figure 34–Critical load and equilibrium path for the example 6.2.1, with respect to the lateral displacement.

6.2.2.   *Lateral buckling of a transversely loaded I-cantilever (load on centroid)*

This example shares the same configuration of the previous example, but with transversal loading (Figure 35). The transversal loading (P) is incrementally increased, until $40\ kN$. A transverse perturbation (0.1% of the main load) is added at the load application point in order to transpose the bifurcation. The used warping function is in Figure 33. Again, for I-sections, the warping function generated by the (incorrect) equation (2.66) coincides with the one from equation (3.80), and therefore, there is no point in simulating both cases.
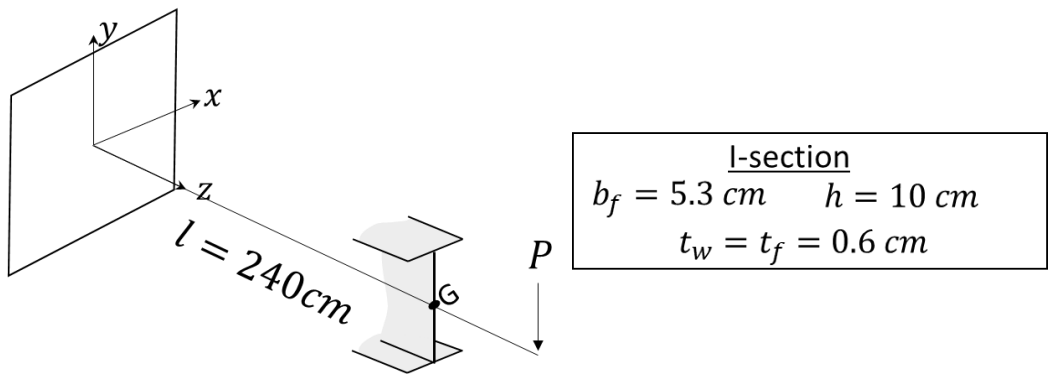
Figure 35 – Description of the example 6.2.2.

The beam presents a lateral torsional buckling (see Figure 37). The critical loads are depicted in Figure 36. Relevant non-uniform torsion occurs, and therefore the behaviour predicted by the 6-DOF rod model is not in agreement with higher level models, as shown in Figure 36. This is expected, since 6-DOF rod models are less suited for thin-walled members with non-uniform torsion. When 7-DOF models are used, the critical load predicted by rod models with all materials are in excellent agreement with the one predicted by the *Ansys Shell 281* model.

However, while the 7-DOF model with linear elastic constitutive equation provides virtually the same result as the shell model with linear elastic constitutive equation, even for well-developed post-critical states, the models with both hyperelastic exact constitutive equations present significant (and

Marcos Pires Kassab 109

Advances on a kinematically exact rod model for thin-walled open section members: consistent warping function and nonlinear constitutive equation

similar between each other) coupling effects. This evidences a relevant coupling at a constitutive level, highlighting the importance of the completeness of the material law. Mainly in Figure 36(a), it is clear that the solution differs rather markedly from the models with linear elastic material (including shell) after approximately $10\ kN$ (corresponds to a $35\ cm$ lateral displacement, see Figure 36a)).

In the shell model, as in the previous example, a local buckling apparently occurs at $\sim 20\ kN$, and, for the same reason as in the previous example, the tested rod models were unable to detect such instability. The deformed configurations for rod and shell models can be seen in Figure 37.
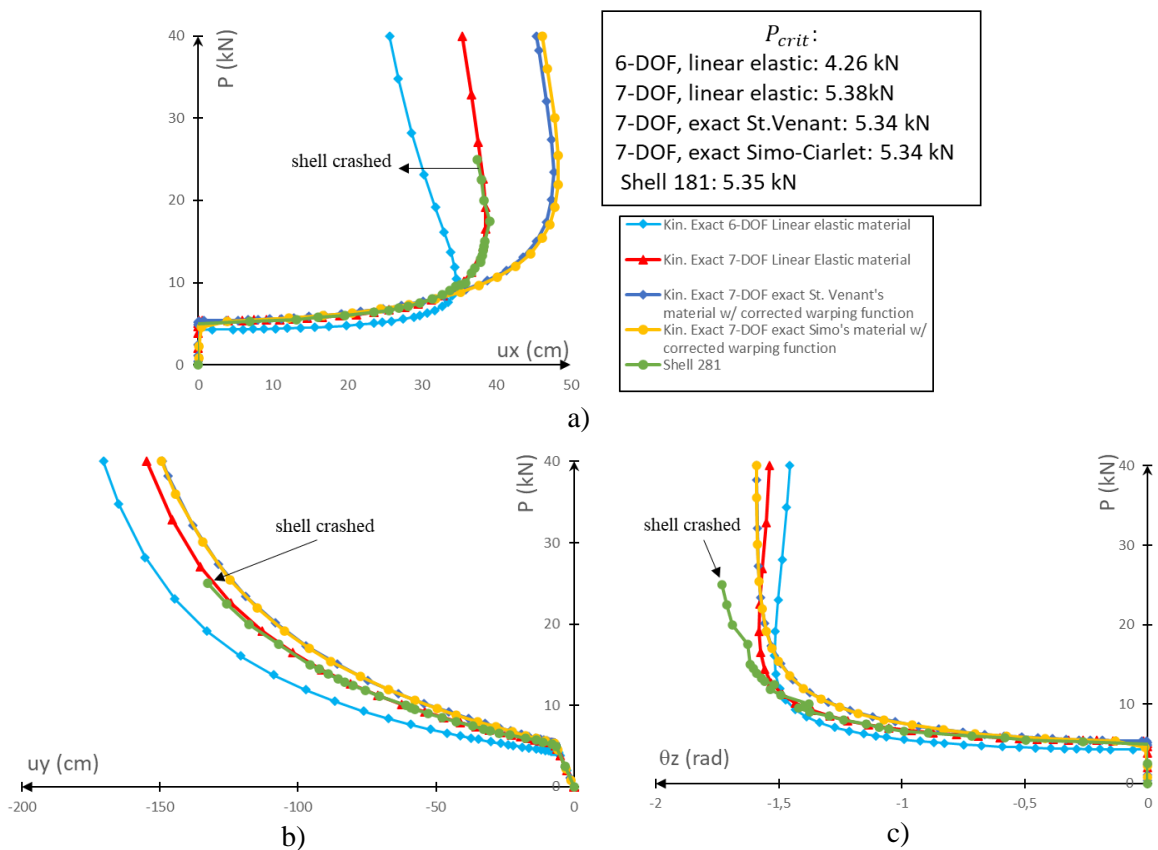
Figure 36 – Critical load and equilibrium path for the example 6.2.2, for the point at the mid-web of the free extremity, with respect to a) the lateral displacement; b) vertical displacement; c) torsional rotations.

Advances on a kinematically exact rod model for thin-walled open section members: consistent warping function and nonlinear constitutive equation

<div align="center">a)</div>

<div align="center">b)</div>
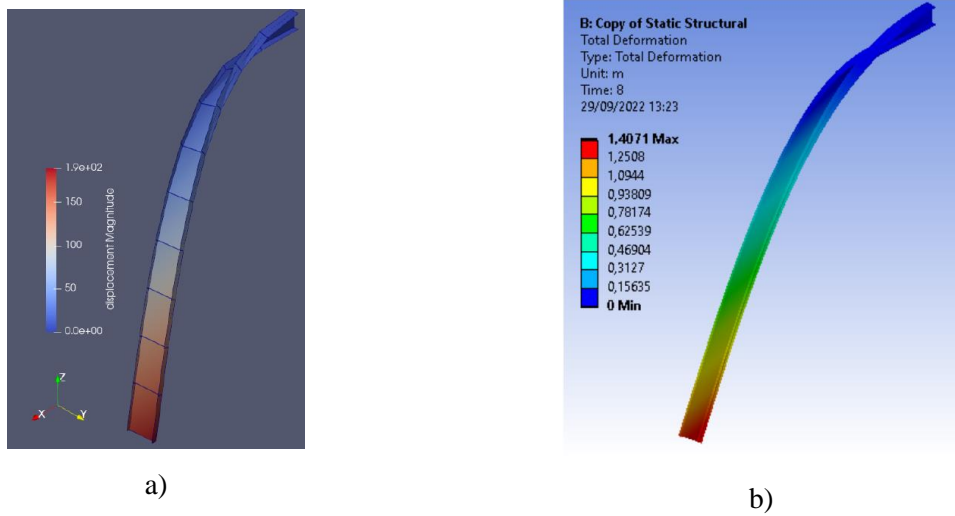
Figure 37 – Simulation result, deformation in original scale ($P = 25\ kN$) a) PEFSYS, exact Saint-Venant's and Simo-Ciarlet's material (superimposed) (in cm); b) Ansys (shell) (in m). Notice the rather stiffer solution from the shell model at the post-critical stage.

6.2.3.   *Buckling of compressed cruciform and T-section cantilever*

This example features two clamped columns. Two cross-sections are evaluated: **a)** cruciform (lenght $l\ =\ 50\ cm$) and **b)** T-shaped sections (lenght $l\ =\ 24\ cm$). In both cases, a compressive load acts at the section centroid at the free end. A graphical description of this example can be seen in Figure 38. In both cases, torsional buckling under compression is expected to occur (the theoretical critical load, according to Vlasov´s theory, is $P_{crit} = GA \frac{I_T}{I_s^0}$) due to the low torsional inertia of the profiles and to the shortness of the columns. It is assumed $E\ =\ 200\ GPa$ and $G\ =\ 80\ GPa$. For the rod models, uniform mesh with 10 linear elements is used. A torsional moment perturbation of $T = 0.01P\ cm$ is used to transpose the bifurcation point. The compressive loading, which is applied at the centroid, is incrementally increased until $1500\ kN$ and $2000\ kN$, for the former and the latter section, respectively.
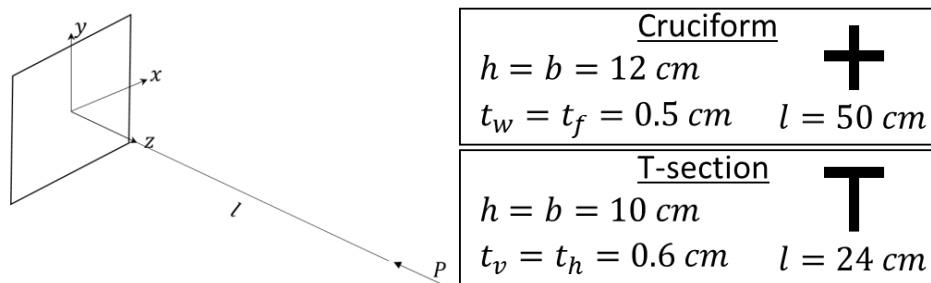
Figure 38 – Description of the example 6.2.3.

Let us compare the warping function that is generated from both equation (3.65) and (3.80): for the cruciform section, they generate the same function; however, this is not the case for the T-section (especially at the web). Those functions can be seen in Figure 39.

Marcos Pires Kassab   111

Advances on a kinematically exact rod model for thin-walled open section members: consistent warping function and nonlinear constitutive equation
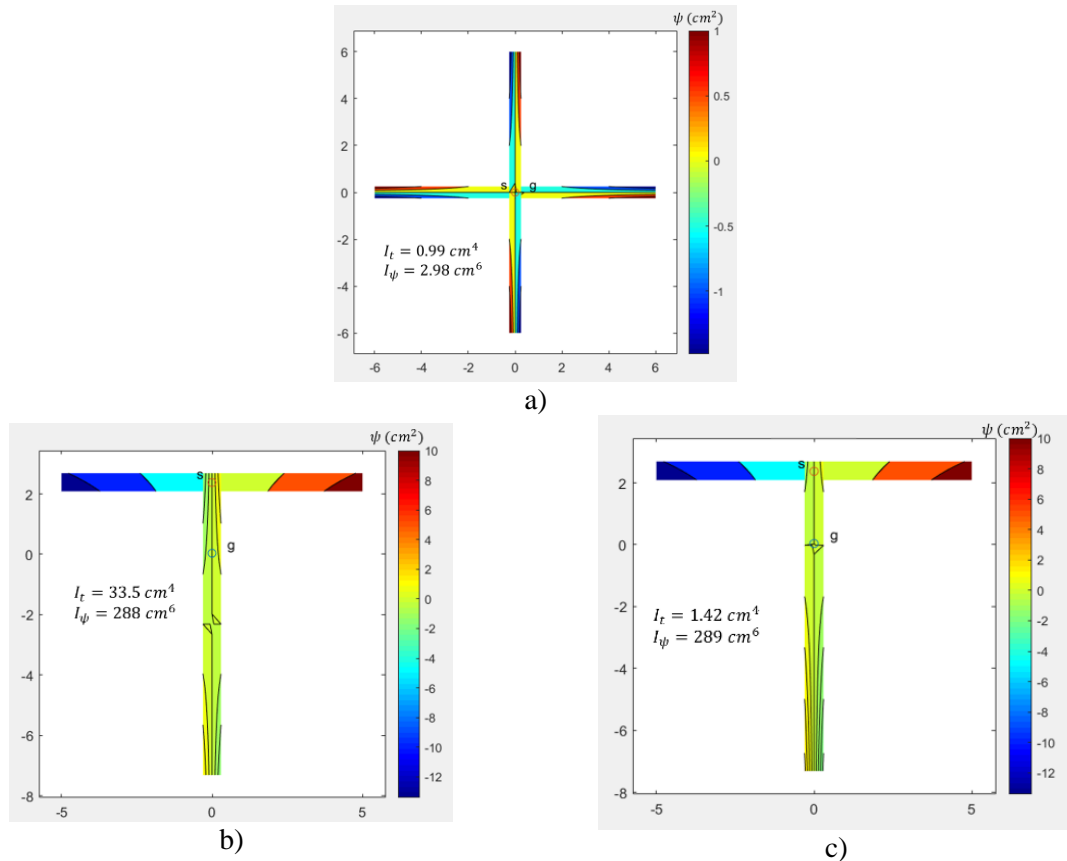
Figure 39 – Warping function for example 6.2.3. a) Cruciform section b) T-section with equation (2.66) c) T-section with equation (3.80). Dimensions in cm.

This set of examples is one of the main motivations of this research: short columns with low torsional inertia, undergoing torsion buckling (see Figure 40). This behaviour is not captured by linear elastic rod models. Only when the Saint-Venant's and Simo-Ciarlet's material with higher order strain terms are used that the coupling between compression and torsion strains allows for the identification of the critical load. It should be noted that, for the T-section, if the incorrect warping expression is employed, the torsion inertia is so overestimated that the first buckling mode is the Euler´s (bending) mode, which has a rather higher critical load when compared to the torsional mode.

As can be seen in Figure 40(b) (T-section), the corrected warping function proved crucial to accurately predict the critical load – the previous function (from [2]) estimates a 25% higher critical load than the shell model. It is also worth mentioning that incomplete versions of Saint-Venant's and Simo-Ciarlet's materials failed completely or partially at the task of finding critical load and post-critical equilibrium paths (as reported in [1]–[3]), but the advances herein proposed solved this issue. Interestingly, Vlasov's analytical expressions somewhat overestimates the critical load for this example.

However, in the post-critical regime, the torsion rotation is severely underestimated by the current rod models as compared to the shell model (see Figure 40). By analysing the deformed configuration from the *Ansys Shell 281* model, it is possible to observe that cross-sectional in-plane distortions take

place, which obviously are not captured by the rod models (see Figure 41 and Figure 42). It should also be noted that this shell model uses linear elastic material. Therefore, it might be possible that rod models with more complex kinematical assumptions, such as in-plane distortion modes, could also predict this sort of deformation, with a better prevision for the large displacement post-buckling regime, possibly even with the simpler linear elastic material.
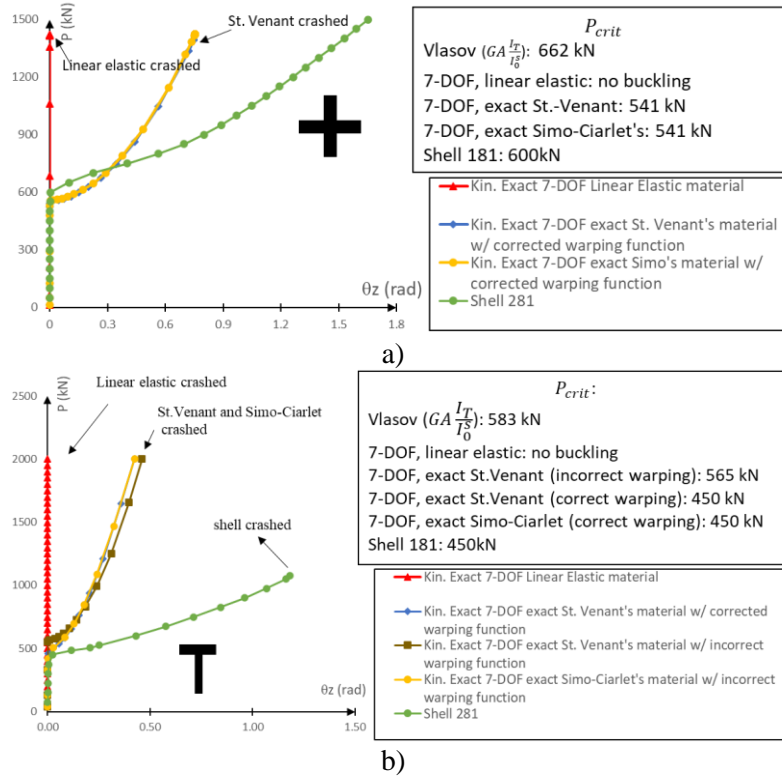
Figure 40 – Critical load and equilibrium path for the example 6.2.3, in the centroid of the free extremity, with respect to the torsional rotation for a) cruciform section; b) T-section.

Marcos Pires Kassab 113

Advances on a kinematically exact rod model for thin-walled open section members: consistent warping function and nonlinear constitutive equation
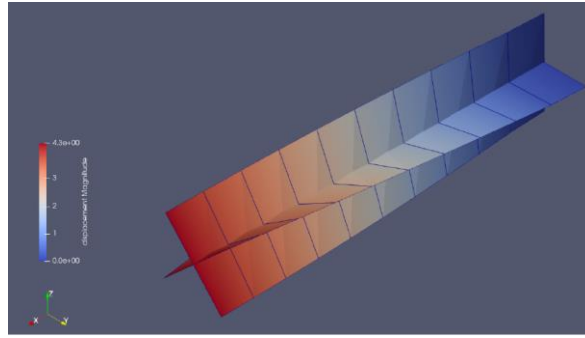
a)
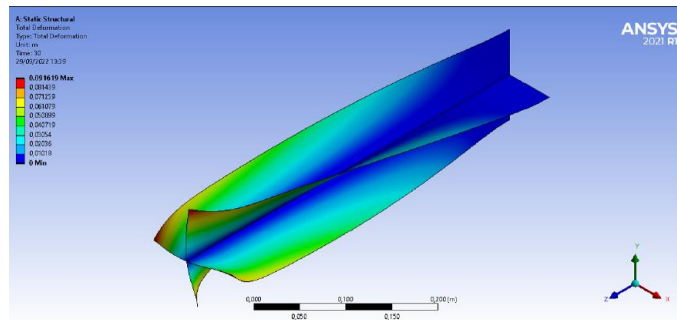
b)

Figure 41 – Simulation result, deformation in original scale (P=1500 kN) a) PEFSYS, Saint-Venant's and Simo-Ciarlet's material (in cm); b) Ansys (in m).
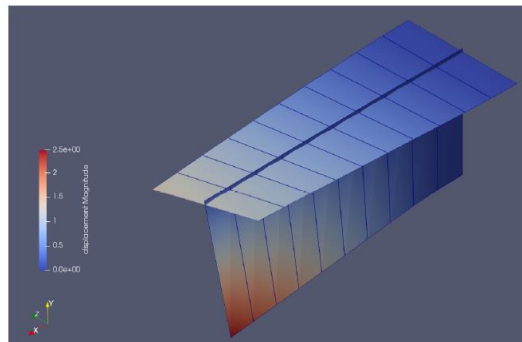
a)
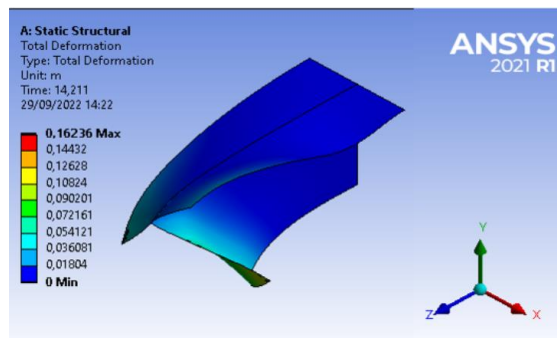
b)

Figure 42 – Simulation result, deformation in original scale (P=1350 kN) a) PEFSYS, Saint-Venant's and Simo-Ciarlet's material (in cm); b) Ansys (in m).

6.2.4.   *Flexural torsional buckling of a simple truss system*

This example features a study of a symmetric truss, which is conceived to have constant normal load at the top chord so that comparation with Vlasov's analytical is possible. All the profiles are U 150x70x2 (see Figure 43b)). Transversal displacements and torsional rotation at both extremities are fixed. Axial displacement is restricted at one end and free at the other. Warping is free at both supports. A vertical load is imposed at the midpoint of the top chord. See Figure 43 for details. Only rod models are studied. The material parameters are $E = 200\ GPa$ and $G = 80\ GPa$.
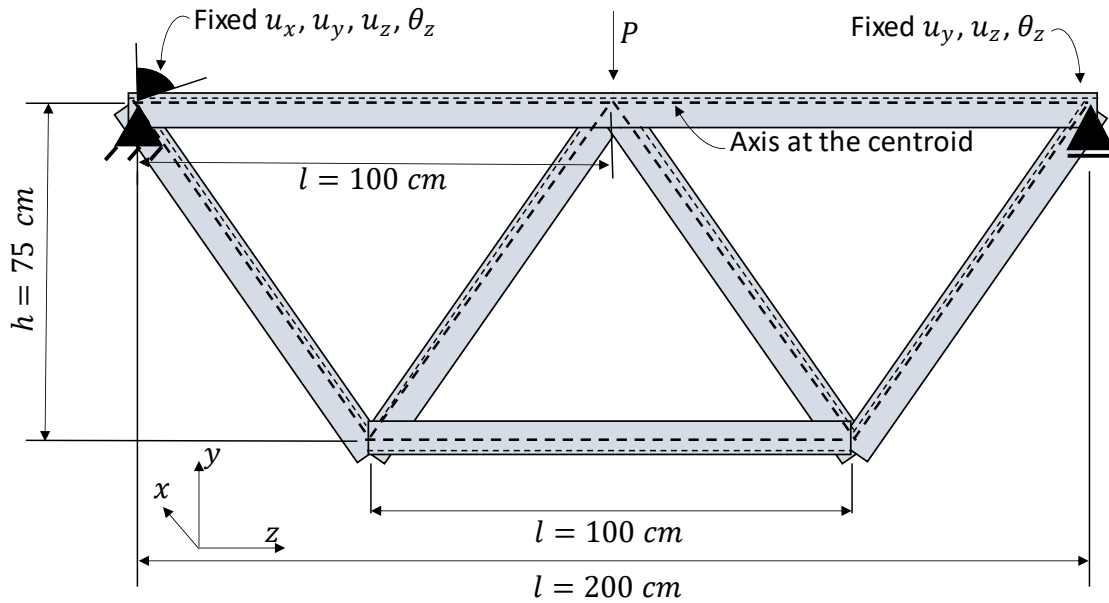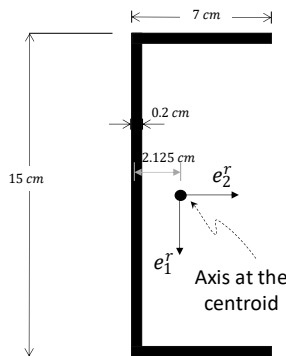
a)

b)

Figure 43– Schematics of studied truss a) General attributes; b) Cross-section and relevant constrain observations

It must be remarked that, by equilibrium, the compressive load at the top chord is $N = \dfrac{P}{3}$ in the linear context.

Marcos Pires Kassab   115

Advances on a kinematically exact rod model for thin-walled open section members: consistent warping function and nonlinear constitutive equation

6.2.4.1. Simplified isolated rod model

First, let us produce a reduced order model: only the top chord is simulated. The vertical displacement at the midpoint is fixed, in order to emulate the vertical constraints imposed by the diagonals. A compressive load is imposed at centroid of extremity in which axial displacement is free. See Figure 44 for a schematic representation of the simplified model.
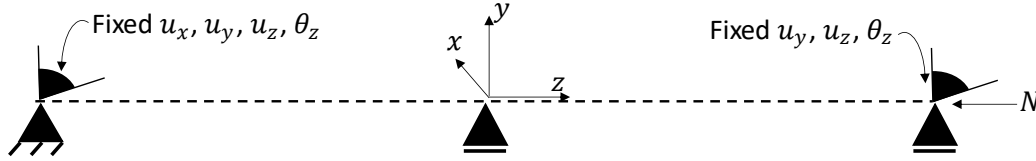
Figure 44 – Schematics of simplified top chord model

Critical load from Vlasov's second order theory for axially loaded mono-symmetric beams is the minimum absolute solution in N of

$$(N - N_{1e})\left[r_o^2(N - N_{2e})(N - N_\psi) - N^2 s_2^2\right] = 0 \tag{6.1}$$

in which

$$N_{1e} = -\frac{\pi^2 EI_{11}}{l_1^2}, \; N_{2e} = -\frac{\pi^2 EI_{22}}{l_2^2}, \; N_\psi = -\frac{\frac{\pi^2}{l_\psi^2}EI_\psi + GI_T}{r_o^2} \tag{6.2}$$

where l_1, l_2, l_ψ are the buckling lengths associated to flexural bending buckling around the local $\boldsymbol{e}_1^r$ and $\boldsymbol{e}_2^r$ axis (coincident to the x and y global axis) and torsional buckling, respectively, $r_0^2 = \frac{I_0^G}{A} + s_1^2 + s_2^2$ and s_1 and s_2 are the coordinates of the shear centre with respect to the centroid (in this case). For this example, $l_1 = 100 \; cm$, $l_2 = 200 \; cm$, $l_\psi = 100 \; cm$, $I_{11} = 214 \; cm^4$, $I_{22} = 29 \; cm^4$, $I_T = 0.077 \; cm^4$, $I_\psi = 1151 \; cm^6$ and $r_0^2 = 60.1 \; cm^2$. Calculating the critical load for this case one gets $N_{1e} = -1055 \; kN, N_{2e} = -576 \; kN, N_{\psi e} = -105 \; kN$ and $N_{crit} = -102 \; kN$. This example is a case of flexural-torsional buckling, from the coupling the modes that arises from $N_{\psi e}$ and N_{2e}. Note that the critical load is much closer to $N_{\psi e}$ than to N_{2e}.

With PEFSYS, this simplified model is simulated with linear elastic, Saint-Venant's and Simo-Ciarlet's materials. Results from those simulations are in Figure 45. A uniform mesh with 20 rod elements with linear interpolation is employed.

As in the example 6.2.3, the linear elastic material was unable to find a torsion/compression coupled-buckling mode and the simulation was not able to proceed even before the Euler critical load ($576 \; kN$, much greater than the actual $101 \; kN$ critical load) was reached.

Only when the advanced material laws were employed that the correct critical load was found, which was consistent with the Vlasov's analytical value. The simulation proceeded up to $412 \; kN$, and then PEFSYS could not find balanced configurations with greater load factor. If the arc-length method was implemented, it might have been possible to find a viable and more developed equilibrium path. It

should be remarked that both Saint-Venant's and Simo-Ciarlet's materials yielded virtually the same results.
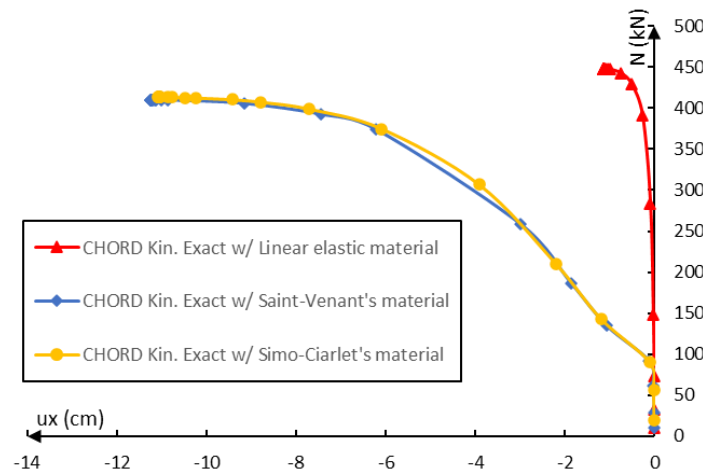
Figure 45 – Equilibrium path for lateral displacement of the top chord midpoint when modelled as an isolated member
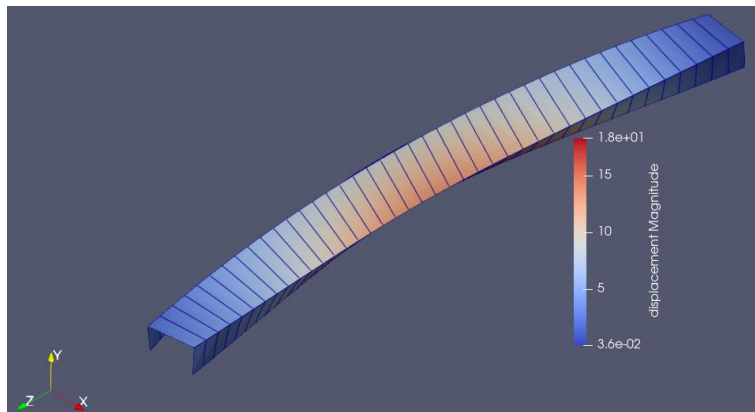
Figure 46 – Flexural-torsional buckling of U-channel subjected to compressive load, when modeled as an isolated member. Configuration at N = 430 kN. Image generated with ParaView.

6.2.4.2. Complete truss model

In order to model the truss, some modelling techniques shall be employed to represent the hinged connections, since PEFSYS does not have explicit kinematical constraints for this situation. It must be highlighted that the imposition of hinges in the context of finite rotations is not trivial and nonlinear since the rotation axis varies as the structures deforms. Thus, transition elements with penalized inertia are employed. Apart from those special elements, each rod is discretized in 10 elements. A sensibility study is performed to evaluate the modelling of the special transition elements, and results are shown in Figure 47.

Marcos Pires Kassab   117

Advances on a kinematically exact rod model for thin-walled open section members: consistent warping function and nonlinear constitutive equation
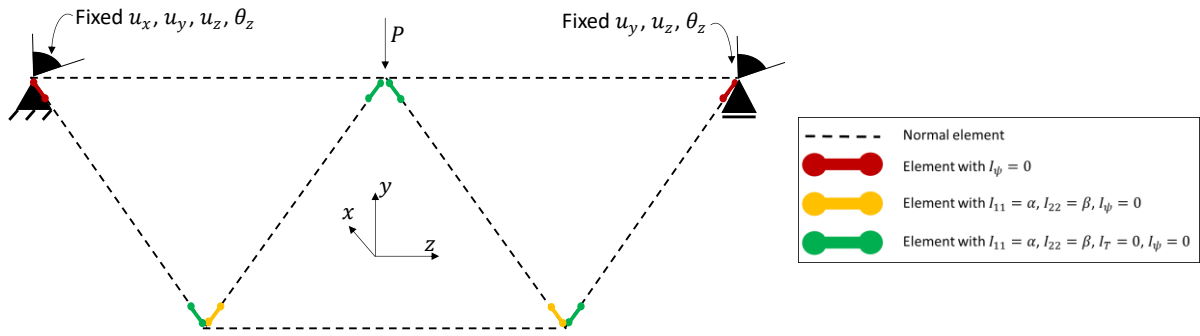
Figure 47 – Rod model with representation of special elements for hinge representation

In that study, Simo-Ciarlet's material is employed in all elements, with exception of the transition ones, in which the linear elastic material is used. The warping constant in all the special elements is null. The torsional inertia is only null at one end of each diagonal, so that the initial configuration is not unstable. The main dilemma, however, is that elements with **a)** zero flexural inertia provides initial unstable configuration although **b)** elements with slightly higher inertia stiffens considerably the system, leading to sensitively higher critical loads. Thus, a set of small (although non-zero) set of inertias must be meticulously chosen. Following the nomenclature from Figure 43b) the moment of inertia relative to the local axis e_1^r is $I_{11} = \alpha$, and the one relative to e_2^r is $I_{22} = \beta$. In Figure 48 it can be seen that the critical load is sensitive the choice of α and β. Supported by the results depicted in Figure 45, the model with $\alpha = 1 \; cm^4$ and $\beta = 0.1 \; cm^4$ was chosen as the representative one, so that the critical load is consistent with the one from the simplified isolated rod model.
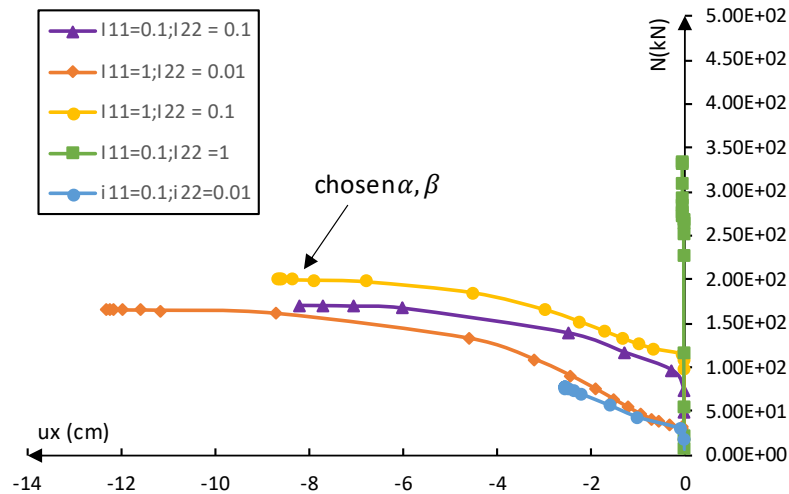
Figure 48 – Equilibrium path for the lateral displacement of the top chord midpoint with respect to the normal force resultant $N = \frac{P}{3}$.

Let us now compare the simplified isolated rod model to the complete truss. Both models share the important characteristics of presenting flexural-torsional buckling mode that is NOT detected by models with linear elastic material, only by the ones with Saint-Venant's or Simo-Ciarlet's material

(see Figure 50). This supports the importance of the inclusion of higher order strain terms in the constitutive equation. Both models also fail to converge at higher loading levels, indicating the need of arc-length method for further calculation. The main difference is that the post-critical behaviour is fairly different, which was indeed expected, as after buckling, the truss itself does not provide a vertical support at the midpoint of the top chord anymore (remember that the simplified model has such vertical support).

a)

b)

c)
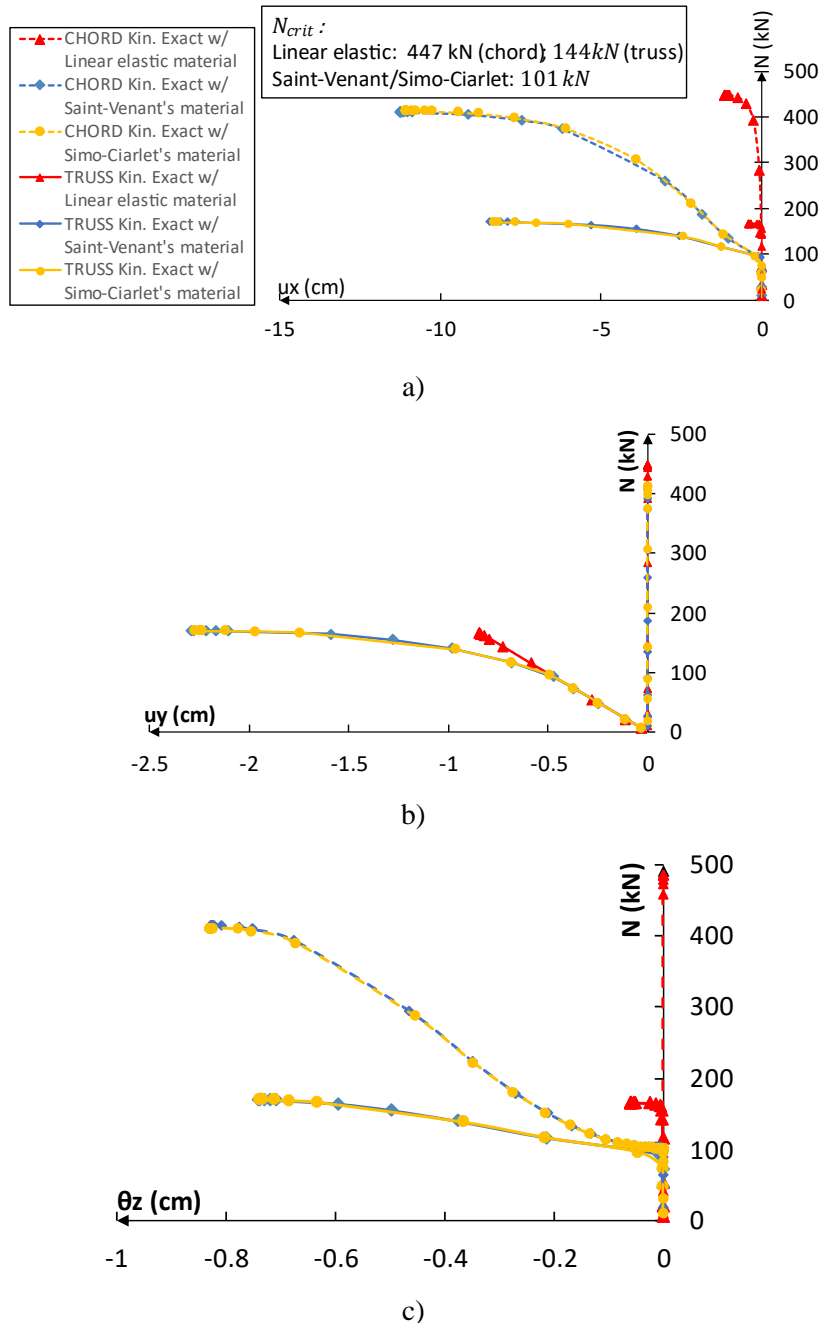
Figure 49 – Equilibrium path for the top chord midpoint (normal force) with respect to the a) lateral and b) vertical displacements and c) torsion rotation in the isolated member model (dashed lines) and complete truss model (full line).

Advances on a kinematically exact rod model for thin-walled open section members: consistent warping function and nonlinear constitutive equation
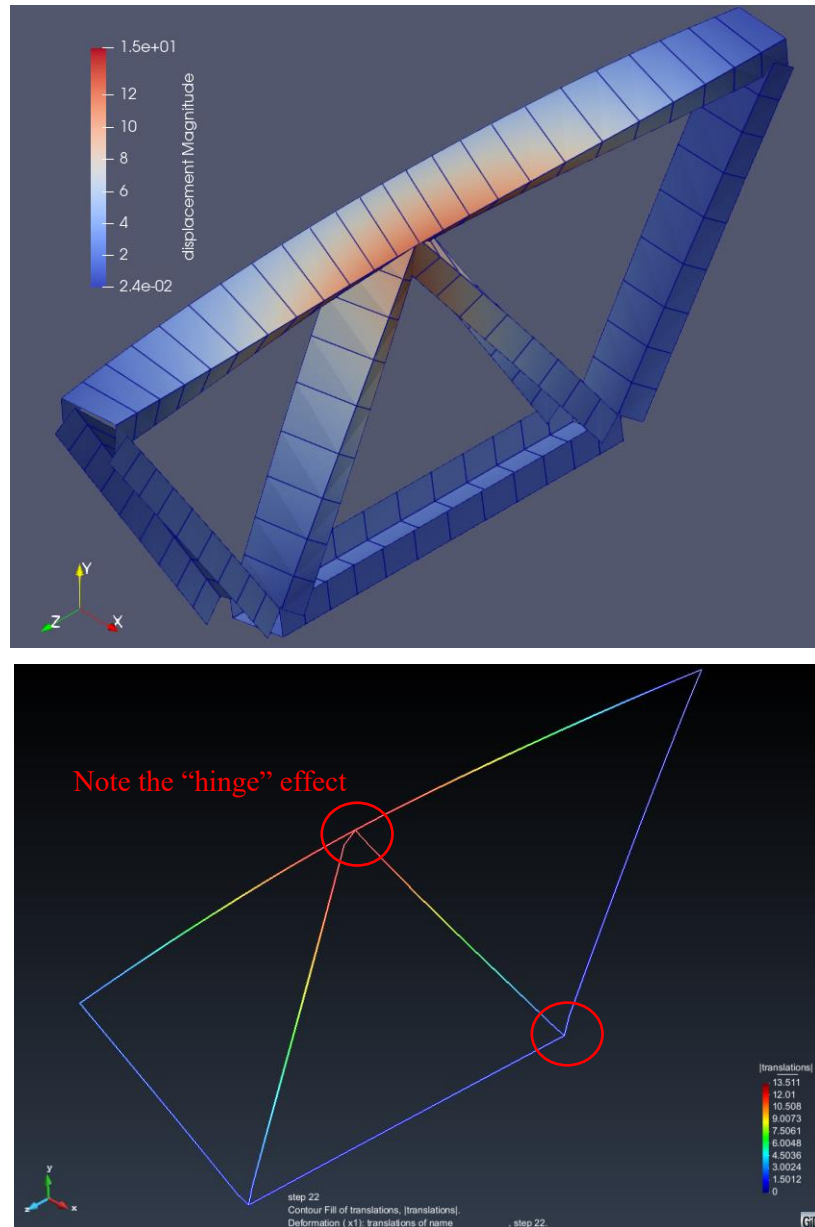
***Figure 50 – Post-critical configuration of the complete truss model with Saint-Venant's/Simo-Ciarlet's material.
Applied vertical load $P = 510$ kN, and normal resultant $N = 170$ kN. The change of curvature of the rod at the special transition elements represents the hinge effect. Image generated with a) ParaView and b)GiD.***

Marcos Pires Kassab
121

Advances on a kinematically exact rod model for thin-walled open section members: consistent warping function and nonlinear constitutive equation

7.   CONCLUSION

The advancement of a 7-DOF, kinematically exact rod model with secondary-warping with the option of either exact (i.e. retaining all strain terms) Saint-Venant's or exact Simo-Ciarlet's constitutive equations was achieved. The model was validated in pre-critical loading situations, buckling load determination and in the post-critical regime – including some cases that were not correctly described by simpler rod models: the coupling effects between torsion strains and other degrees of freedom proved crucial at the constitutive equation for proper torsional bucking representation.

While the Simo-Ciarlet's material has the advantage of being polyconvex, and therefore, theoretically more suitable for finite displacements and large strain, the Saint-Venant's material can be implemented in a more efficient way, dispensing the numerical integration of stress resultants and material tangent matrix along the cross-section (see Appendix I). For practical applications with the discussed rod model, both seemed virtually identical in the proposed examples.

The warping function from Campello and Lago [2] was corrected by incorporation of a missing (linear through-the-thickness) term. As soon as the author began to deal with more complex cross-sections, he realized that a modification was mandatory, originating expression (3.80). Later, it was discovered that the proposed approach renders a very good approximation to the Saint-Venant's warping function for thin-walled open sections, composed by rectangular segments, with no need to solve any differential equation. As a subproduct of this process, a simple, yet general, algorithm for generating thin-walled sections´ warping functions was implemented in PEFSYS. Also, an initial version for an interface with ParaView was implemented, for post-processing.

It should be noted that the expression (3.80) can be used to generate the warping function w.r.t any centre, the author decided to always use the shear centre, in order to uncouple warping and axial/bending effects. There are some works (Gruttmann [18], Gonçalves [35], for example) in which the orthogonality conditions for the warping mode are not enforced, leading to a different expression for the material stiffness contribution. Some examples in Appendix E suggest that the origin must indeed be the shear centre, to allow for a more coherent kinematical assumption.

For the tested cases in which the rod models diverged from the shell to completely describe the displacement field, it was clear that the bottleneck of the current formulation is the lack of richer kinematical assumptions for the displacement field, which can be achieved by incorporating in- and out-of-plane distortional degrees of freedom.

That said, the next logical step toward robust rod formulation is to study techniques to generate such distortional contributions, such as the Generalized Beam Theory (GBT), and posteriorly implement them in PEFSYS.

Marcos Pires Kassab 123

Advances on a kinematically exact rod model for thin-walled open section members: consistent warping function and nonlinear constitutive equation

8. BIBLIOGRAPHY

[1] E. M. B. Campello, 'Análise não-linear de perfis metálicos conformados a frio', *São Paulo*, p. 106, 2000.

[2] E. M. B. Campello and L. B. Lago, 'Effect of higher order constitutive terms on the elastic buckling of thin-walled rods', *Thin-Walled Structures*, vol. 77, pp. 8–16, Apr. 2014, doi: 10.1016/j.tws.2013.11.001.

[3] P. M. Pimenta and E. M. B. Campello, 'Geometrically nonlinear analysis of thin-walled space frames', Proceedings of the II ECCM (European Conference on Computational Mechanics), 2001, p. 20.

[4] P. M. Pimenta, 'Constitutive second order effects on ageometrically exact finite strain rod model', in *Recent developments in solid mechanics*, Rio de Janeiro: LNCC, 1996, pp. 79–85.

[5] J. Argyris, 'An excursion into large rotations', *Computer Methods in Applied Mechanics and Engineering*, vol. 32, no. 1–3, pp. 85–155, Sep. 1982, doi: 10.1016/0045-7825(82)90069-X.

[6] J. H. Argyris, P. C. Dunne, and D. W. Scharpf, 'ON LARGE DISPLACEMENT-SMALL STRAIN ANALYSIS OF STRUCTURES WITH ROTATIONAL DEGREES OF FREEDOM.', p. 51.

[7] M. de L. T. Moreira, 'Parametrização das rotações em teorias de barras e cascas.', Doutorado em Engenharia de Estruturas, Universidade de São Paulo, São Paulo, 2009. doi: 10.11606/T.3.2009.tde-01092009-152009.

[8] P. Wriggers, *Nonlinear finite element methods*. Berlin: Springer, 2008.

[9] S. P. Timoshenko and J. M. Gere, *Theory of Elastic Stability*, 2nd edition. Stanford University: McGRAW-HILL BOOK COMPANY, 1985.

[10] S. Timoshenko, *Theory of elasticity*, 3th edition (2010). India: McGRAW-HILL BOOK COMPANY, 1934.

[11] M. L. Bucalem and K.-J. Bathe, *The mechanics of solids and structures: hierarchical modeling and the finite element solution*. Heidelberg: Springer, 2011.

[12] V. Z. Vlasov, *Thin-walled Elastic Beams*, 2nd ed. Jerusalem: Israel Program for Scientific Translation, 1961.

[13] ASSOCIAÇÃO BRASILEIRA DE NORMAS TÉCNICAS, *ABNT NBR 8800:2008: Projeto de estruturas de aço e de estruturas mistas de aço e concreto de edifícios*. Rio de Janeiro: ABNT, 2008.

[14] E. Reissner, 'On one-dimensional finite-strain beam theory: The plane problem', *Journal of Applied Mathematics and Physics (ZAMP)*, vol. 23, no. 5, pp. 795–804, Sep. 1972, doi: 10.1007/BF01602645.

[15] J. C. Simo, 'A finite strain beam formulation. The three-dimensional dynamic problem. Part I', *Computer Methods in Applied Mechanics and Engineering*, vol. 49, no. 1, pp. 55–70, May 1985, doi: 10.1016/0045-7825(85)90050-7.

[16] J. C. Simo and L. Vu-Quoc, 'A three-dimensional finite-strain rod model. part II: Computational aspects', *Computer Methods in Applied Mechanics and Engineering*, vol. 58, no. 1, pp. 79–116, Oct. 1986, doi: 10.1016/0045-7825(86)90079-4.

[17] J. C. Simo and L. Vu-Quoc, 'A Geometrically-exact rod model incorporating shear and torsion-warping deformation', *International Journal of Solids and Structures*, vol. 27, no. 3, pp. 371–393, 1991, doi: 10.1016/0020-7683(91)90089-X.

[18] F. Gruttmann, R. Sauer, and W. Wagner, 'Theory and numerics of three–dimensional beams with elastoplastic material behaviour', *International Journal for Numerical Methods in Engineering*, p. 33, 2000, doi: 10.1002/1097-0207(20000830)48:123.0.CO;2-6.

[19] M. A. Crisfield, 'A consistent co-rotational formulation for non-linear, three-dimensional, beam-elements', *Computer Methods in Applied Mechanics and Engineering*, vol. 81, no. 2, pp. 131–150, Aug. 1990, doi: 10.1016/0045-7825(90)90106-V.

[20] H. Chen and G. E. Blandford, 'Thin-Walled Space Frames. I: Large-Deformation Analysis Theory', *Journal of Structural Engineering*, vol. 117, no. 8, pp. 2499–2520, Aug. 1991, doi: 10.1061/(ASCE)0733-9445(1991)117:8(2499).

124   Marcos Pires Kassab

Advances on a kinematically exact rod model for thin-walled open section members: consistent warping function and nonlinear constitutive equation

[21] A. Genoese, A. Genoese, A. Bilotta, and G. Garcea, 'A geometrically exact beam model with non-uniform warping coherently derived from the Saint Venant rod', *Engineering Structures*, vol. 68, pp. 33–46, Jun. 2014, doi: 10.1016/j.engstruct.2014.02.024.

[22] P. M. Pimenta and T. Yojo, 'Geometrically Exact Analysis of Spatial Frames', *Applied Mechanics Reviews*, vol. 46, no. 11S, pp. S118–S128, Nov. 1993, doi: 10.1115/1.3122626.

[23] P. M. Pimenta and E. M. B. Campello, 'A fully nonlinear multi-parameter rod model incorporating general cross-sectional in-plane changes and out-of-plane warping', *Latin American Journal of Solids and Structures*, p. 22, 2003.

[24] E. R. Dasambiagio, P. M. Pimenta, and E. M. B. Campello, 'A finite strain rod model that incorporates general cross section deformation and its implementation by the Finite Element Method', in *Mechanics of Solids in Brazil 2009*, 1st ed., vol. 1, H. S. da Costa Mattos and M. Alves, Eds. Rio de Janeiro: Brazilian Society of Mechanical Sciences and Engineering, 2009, pp. 145–168.

[25] E. R. Dasambiagio, 'Um modelo geometricamente exato de barras com grandes deformações, que considera a distorção e o empenamento geral da seção transversal, e sua discretização pelo método dos elementos finitos.', Mestrado em Engenharia de Estruturas, Universidade de São Paulo, São Paulo, 2008. doi: 10.11606/D.3.2008.tde-25092008-122259.

[26] C. M. T. T. Fernandes, 'Meshless methods: Extending the linear formulation and its generalization to geometrically exact structural analysis', Universidade Técnica de Lisboa, Instituto Superior Técnico, Lisboa, 2007.

[27] C. da Costa e Silva, S. F. Maassen, P. M. Pimenta, and J. Schröder, 'A simple finite element for the geometrically exact analysis of Bernoulli–Euler rods', *Comput Mech*, vol. 65, no. 4, pp. 905–923, Apr. 2020, doi: 10.1007/s00466-019-01800-5.

[28] H. B. Coda, 'A solid-like FEM for geometrically non-linear 3D frames', *Computer Methods in Applied Mechanics and Engineering*, vol. 198, no. 47–48, pp. 3712–3722, Oct. 2009, doi: 10.1016/j.cma.2009.08.001.

[29] H. B. Coda and R. R. Paccola, 'A FEM procedure based on positions and unconstrained vectors applied to non-linear dynamic of 3D frames', *Finite Elements in Analysis and Design*, vol. 47, no. 4, pp. 319–333, Apr. 2011, doi: 10.1016/j.finel.2010.11.001.

[30] D. N. Maciel and H. B. Coda, 'POSITIONAL FINITE ELEMENT METHODOLOGY FOR GEOMETRICALLY NONLINEAR ANALYSIS OF 2D FRAMES', *Revista Minerva - Pesquisa & Tecnologia*, vol. 5, p. 12, 2008.

[31] A. Kumar and S. Mukherjee, 'A Geometrically Exact Rod Model Including In-Plane Cross-Sectional Deformation', *Journal of Applied Mechanics*, vol. 78, no. 1, p. 011010, Jan. 2011, doi: 10.1115/1.4001939.

[32] P. M. Pimenta, E. M. B. Campello, and P. Wriggers, 'An exact conserving algorithm for nonlinear dynamics with rotational DOFs and general hyperelasticity. Part 1: Rods', *Comput Mech*, vol. 42, no. 5, pp. 715–732, Oct. 2008, doi: 10.1007/s00466-008-0271-5.

[33] J.-P. Liu, Z.-B. Cheng, and G.-X. Ren, 'An Arbitrary Lagrangian–Eulerian formulation of a geometrically exact Timoshenko beam running through a tube', *Acta Mech*, vol. 229, no. 8, pp. 3161–3188, Aug. 2018, doi: 10.1007/s00707-018-2161-z.

[34] V. Le Corvec, 'Nonlinear 3d frame element with multi-axial coupling under consideration of local effects', Dissertation, University of California, Berkeley, 2012.

[35] R. Gonçalves, 'An assessment of the lateral-torsional buckling and post-buckling behaviour of steel I-section beams using a geometrically exact beam finite element', *Thin-Walled Structures*, vol. 143, p. 106222, Oct. 2019, doi: 10.1016/j.tws.2019.106222.

[36] W. Li and H. Ma, 'A geometrically exact thin-walled beam element with simplified strain definition', *Thin-Walled Structures*, vol. 117, pp. 49–62, Aug. 2017, doi: 10.1016/j.tws.2017.04.003.

[37] R. Schardt, 'Eine Erweiterung der Technischen Biegetheorie zur Berechnung prismatischer Faltwerke', *Der Stahlbau*, no. 35(6), pp. 161–171, 1966.

[38] R. Schardt, *Verallgemeinerte Technische Biegetheorie*. Berlin, Heidelberg: Springer Berlin Heidelberg, 1989. doi: 10.1007/978-3-642-52330-4.

Marcos Pires Kassab   125

Advances on a kinematically exact rod model for thin-walled open section members: consistent warping function and nonlinear constitutive equation

[39] R. Schardt, 'Generalized beam theory—an adequate method for coupled stability problems', *Thin-Walled Structures*, vol. 19, no. 2–4, pp. 161–180, Jan. 1994, doi: 10.1016/0263-8231(94)90027-2.

[40] P. B. Dinis, D. Camotim, and N. Silvestre, 'GBT formulation to analyse the buckling behaviour of thin-walled members with arbitrarily "branched" open cross-sections', *Thin-Walled Structures*, vol. 44, no. 1, pp. 20–38, Jan. 2006, doi: 10.1016/j.tws.2005.09.005.

[41] R. Gonçalves and D. Camotim, 'GBT local and global buckling analysis of aluminium and stainless steel columns', *Computers & Structures*, vol. 82, no. 17–19, pp. 1473–1484, Jul. 2004, doi: 10.1016/j.compstruc.2004.03.043.

[42] R. Gonçalves, M. Ritto-Corrêa, and D. Camotim, 'A large displacement and finite rotation thin-walled beam formulation including cross-section deformation', *Computer Methods in Applied Mechanics and Engineering*, vol. 199, no. 23–24, pp. 1627–1643, Apr. 2010, doi: 10.1016/j.cma.2010.01.006.

[43] R. Gonçalves, M. Ritto-Corrêa, and D. Camotim, 'A new approach to the calculation of cross-section deformation modes in the framework of generalized beam theory', *Comput Mech*, vol. 46, no. 5, pp. 759–781, Oct. 2010, doi: 10.1007/s00466-010-0512-2.

[44] W. Li and H. Ma, 'A nonlinear cross-section deformable thin-walled beam finite element model with high-order interpolation of warping displacement', *Thin-Walled Structures*, vol. 152, p. 106748, Jul. 2020, doi: 10.1016/j.tws.2020.106748.

[45] J. H. Argyris and Sp. Symeonidis, 'Nonlinear finite element analysis of elastic systems under nonconservative loading-natural formulation. part I. Quasistatic problems', *Computer Methods in Applied Mechanics and Engineering*, vol. 26, no. 1, pp. 75–123, Apr. 1981, doi: 10.1016/0045-7825(81)90131-6.

[46] A. Ibrahimbegović, 'On finite element implementation of geometrically nonlinear Reissner's beam theory: three-dimensional curved beam elements', *Computer Methods in Applied Mechanics and Engineering*, vol. 122, no. 1–2, pp. 11–26, Apr. 1995, doi: 10.1016/0045-7825(95)00724-F.

[47] A. Ibrahimbegovic, 'On the choice of finite rotation parameters', *Computer Methods in Applied Mechanics and Engineering*, vol. 149, no. 1–4, pp. 49–71, Oct. 1997, doi: 10.1016/S0045-7825(97)00059-5.

[48] F. Gruttmann, R. Sauer, and W. Wagner, 'A geometrical nonlinear eccentric 3D-beam element with arbitrary cross-sections', *Computer Methods in Applied Mechanics and Engineering*, vol. 160, no. 3–4, pp. 383–400, Jul. 1998, doi: 10.1016/S0045-7825(97)00305-8.

[49] H. F. Silva, 'Formulação do problema da torção uniforme em barras de seção transversal maciça.', Mestrado em Engenharia de Estruturas, Universidade de São Paulo, São Paulo, 2005. doi: 10.11606/D.3.2005.tde-20022006-150915.

[50] J. Fruchtengarten and E. M. B. Campello, *PEF5734 – Fundamentos das estruturas de aço-Notas de aula*. São Paulo, 2003.

[51] J. M. Ball, 'Convexity conditions and existence theorems in nonlinear elasticity', *Arch. Rational Mech. Anal.*, vol. 63, no. 4, pp. 337–403, Dec. 1976, doi: 10.1007/BF00279992.

[52] P. G. Ciarlet, *Mathematical elasticity*, vol. 1, 3 vols. Amsterdam ; New York : New York, N.Y., U.S.A: North-Holland ; Sole distributors for the U.S.A. and Canada, Elsevier Science Pub. Co, 1988.

[53] A. Raoult, 'Non-polyconvexity of the stored energy function of a Saint Venant-Kirchhoff material', *Appl. Math.*, vol. 31, no. 6, pp. 417–419, 1986, doi: 10.21136/AM.1986.104220.

[54] R. D. Lahuerta, E. T. Simões, E. M. B. Campello, P. M. Pimenta, and E. C. N. Silva, 'Towards the stabilization of the low density elements in topology optimization with large deformation', *Comput Mech*, vol. 52, no. 4, pp. 779–797, Oct. 2013, doi: 10.1007/s00466-013-0843-x.

[55] R. Courant, 'Variational methods for the solution of problems of equilibrium and vibrations', *Bulletin of the American Mathematical Society*, vol. 49, pp. 1–23, 1943.

[56] A. Ibrahimbegović, F. Frey, and I. Kožar, 'Computational aspects of vector-like parametrization of three-dimensional finite rotations', *Int. J. Numer. Meth. Engng.*, vol. 38, no. 21, pp. 3653–3673, Nov. 1995, doi: 10.1002/nme.1620382107.

Marcos Pires Kassab 127

Advances on a kinematically exact rod model for thin-walled open section members: consistent warping function and nonlinear constitutive equation

APPENDIX

APPENDIX A. BASIC CONCEPTS: KINEMATIC CHARACTERIZATION

Let the domain of a continuum in the reference configuration, denoted by V^r, with the contour S^r undergo a transformation that results in the current configuration, denoted by V, with the contour S, as in. Figure 51. For the sake of simplicity, it will be assumed that the reference configuration is the same as the initial configuration, although this is not necessary in general.
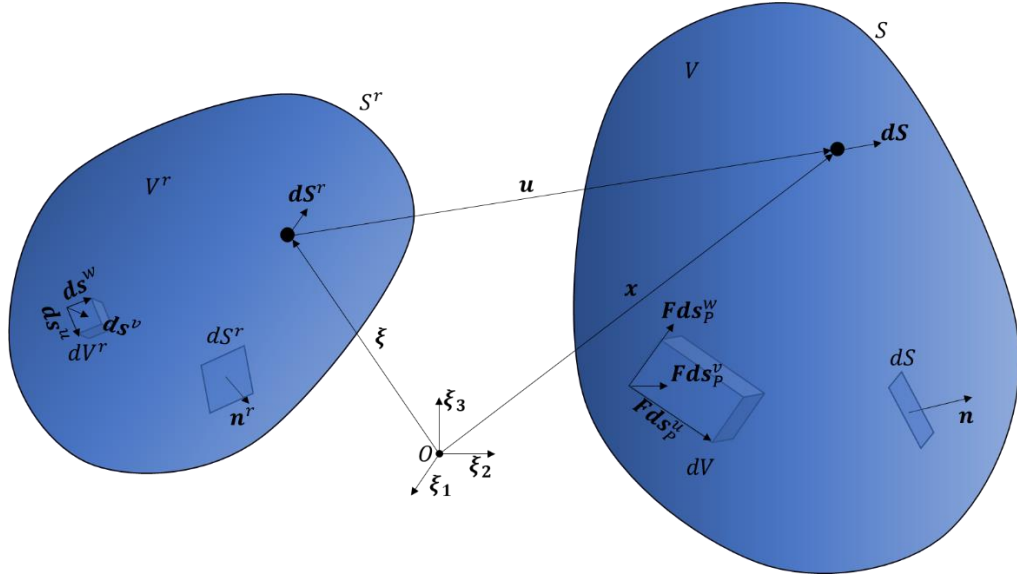
Figure 51 – Transformation of a continuum, from a reference configuration to the current configuration.

Let $\boldsymbol{\xi}$ be the reference position of a given point of a solid and $\boldsymbol{x}$ be its current position, after a generic deformation. The displacement, for each point is given by

$$\boldsymbol{u} = \boldsymbol{x} - \boldsymbol{\xi}. \tag{A.1}$$

Then, the deformation gradient ($\boldsymbol{F}$) is the second order tensor given by

$$\boldsymbol{F} = \frac{\partial \boldsymbol{x}}{\partial \boldsymbol{\xi}} = \nabla \boldsymbol{u} + \boldsymbol{I}. \tag{A.2}$$

The transformation $\boldsymbol{F}$ relates a solid infinitesimal fibre $\boldsymbol{ds}^r$ on the reference configuration to its state on the current configuration ($\boldsymbol{ds}$)

$$\boldsymbol{ds} = \boldsymbol{F}\boldsymbol{ds}^r. \tag{A.3}$$

An important quantity is the Jacobian (J) associated to $\boldsymbol{F}$. It expresses the volume variation of an infinitesimal region of the studied continuum, with the expression

$$\frac{dV}{dV^r} = \frac{< \boldsymbol{F}\boldsymbol{ds}^u, \boldsymbol{F}\boldsymbol{ds}^v, \boldsymbol{F}\boldsymbol{ds}^w >}{< \boldsymbol{ds}^u, \boldsymbol{ds}^v, \boldsymbol{ds}^w >} = det\boldsymbol{F} = J, \tag{A.4}$$

where $< \boldsymbol{a}, \boldsymbol{b}, \boldsymbol{c} >= (\boldsymbol{a} \times \boldsymbol{b}) \cdot \boldsymbol{c}$ is the triple product of a linear independent triplet $\boldsymbol{a}, \boldsymbol{b}, \boldsymbol{c}$.

Similarly, it is possible to study area variations. This can be achieved through Nanson's rule

$$dS\hat{\boldsymbol{n}} = JF^{-T}\widehat{\boldsymbol{n}^r}dS^r \implies dS = J\|F^{-T}\widehat{\boldsymbol{n}^r}\|dS^r. \tag{A.5}$$

The Cauchy-Green ($\boldsymbol{C}$) and Green-Lagrange ($\boldsymbol{E}$) tensors are calculated as

Marcos Pires Kassab

Advances on a kinematically exact rod model for thin-walled open section members: consistent warping function and nonlinear constitutive equation

$$\boldsymbol{C} = \boldsymbol{F}^T \boldsymbol{F}, \tag{A.6}$$

$$\boldsymbol{E} = \frac{1}{2}(\boldsymbol{C} - \boldsymbol{I}). \tag{A.7}$$

Marcos Pires Kassab   129

Advances on a kinematically exact rod model for thin-walled open section members: consistent warping function and nonlinear constitutive equation

APPENDIX B. BASIC CONCEPTS: STRESS CHARACTERIZATION

In the context of solids and fluids dynamics, it is important to introduce Cauchy's principle: it states that, for a hypothetical sectioned continuum, the actions and respective reactions of one part over the another are a) distributed forces over the sections area and b) only present on each section surface. Consequently, the vectorial stress field ($\boldsymbol{\rho}$) must be a function of a) the coordinate of the considered point ($\boldsymbol{x}$) and b) the local normal direction to the adopted section ($\boldsymbol{n}$). Therefore, $\boldsymbol{\rho} = \widehat{\boldsymbol{\rho}}(\boldsymbol{x}, \boldsymbol{n})$
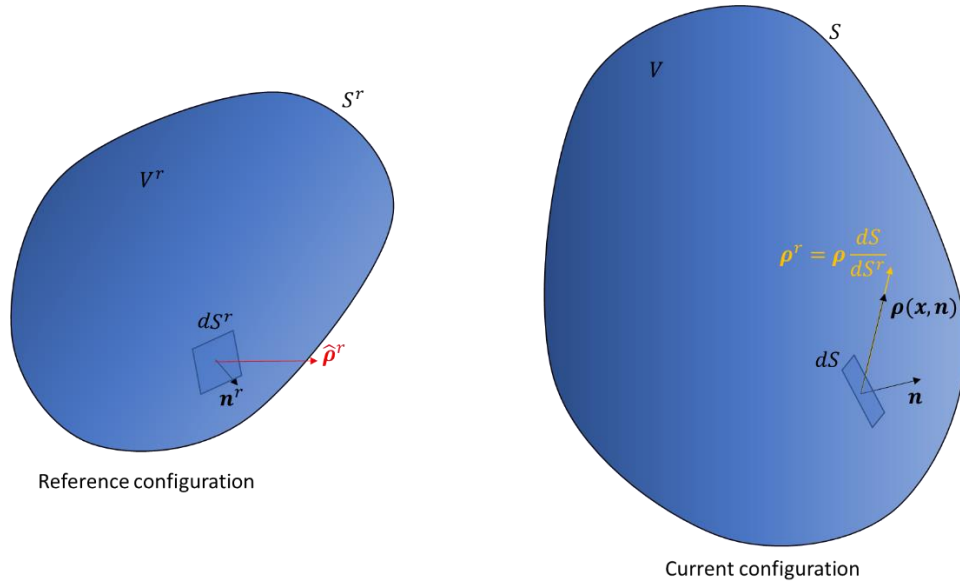
Figure 52 – Relevant stress vector representation for the Cauchy (black arrow), 1st (yellow arrow) and 2nd Piola-Kirchoff (red arrow) tensors.

Cauchy stress tensor ($\boldsymbol{T}$)

This tensor interpretation is direct. Each of its column contain one stress vector with respect to a determined face, normal to one vector of the three-dimensional base.

The real (true) stress $\boldsymbol{\rho}$ in a surface can be determined by $\boldsymbol{T}$, w.r.t the normal unitary vector $\boldsymbol{n}$ (Figure 52)**,**

$$\boldsymbol{\rho} = \boldsymbol{Tn}. \tag{B.1}$$

1st Piola-Kirchoff tensor ($\boldsymbol{P}$)

This tensor represents the nominal stress state of a body. Whereas $\boldsymbol{T}$ had as reference area the current configuration, $\boldsymbol{P}$ uses the reference configuration area (see Figure 52). Thus, if

$$\boldsymbol{\rho}^r dS^r = \boldsymbol{\rho} dS, \tag{B.2}$$

then, admitting that $\boldsymbol{\rho}^r$ can be calculated by a linear transformation of the unitary vector $\boldsymbol{n}^r$,

$$\boldsymbol{Pn}^r dS^r = \boldsymbol{Tn} dS. \tag{B.3}$$

Using (A.5), one obtains

$$P = TJF^{-T}. \tag{B.4}$$

This tensor is not generically symmetric neither objective (i.e, it is affected by rigid body motion). Nominal stress in a plane $\hat{\boldsymbol{n}}^r$ can be calculated by

$$\boldsymbol{\rho}^r = \boldsymbol{P}\boldsymbol{n}^r. \tag{B.5}$$

2nd Piola-Kirchoff tensor ($\boldsymbol{S}$)

This tensor is obtained by applying the inverse transformation $\boldsymbol{F}^{-1}$ on the nominal stress components, as if those vectors performed the same transformation as the continuum fibres (see Figure 52), yielding

$$\hat{\boldsymbol{\rho}}^r = \boldsymbol{F}^{-1}\boldsymbol{\rho}^r = \boldsymbol{F}^{-1}\boldsymbol{P}\boldsymbol{n}^r = \boldsymbol{S}\boldsymbol{n}^r, \tag{B.6}$$

thus,

$$\boldsymbol{S} = \boldsymbol{F}^{-1}\boldsymbol{P}. \tag{B.7}$$

This tensor is always symmetric and objective, so is adequate to formulate constitutive equations.

Marcos Pires Kassab   131

Advances on a kinematically exact rod model for thin-walled open section members: consistent warping function and nonlinear constitutive equation

APPENDIX C.SECTORIAL AREA, PRINCIPAL POLE AND ORIGIN FOR TOP HAT AND STIFFNED C-SECTIONS
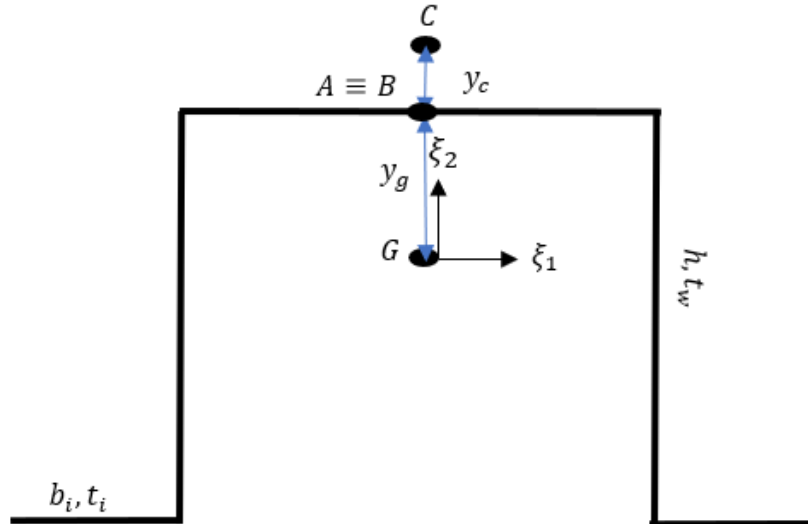
a)
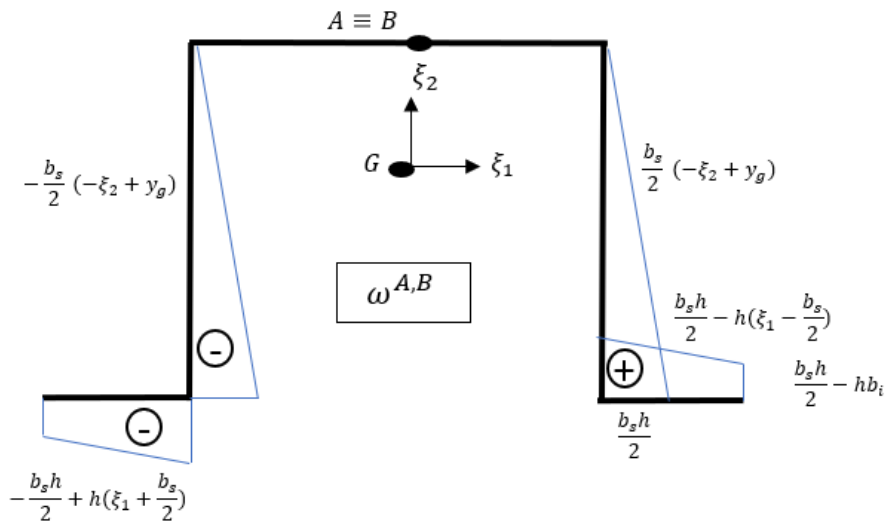
b)

Figure 53 – Geometric attributes; b) Sectorial area for an arbitrary A, B ($\omega^{A,B}$).

This cross-section area is

$$A = 2ht_w + 2b_it_i + b_st_s. \tag{C.1}$$

The position of the centroid can be calculated, by definition, as

$$\left|y_g\right| = \frac{h^2 t_w + 2h t_i b_i}{A}.$$
(C.2)

The moment of inertia I_2 with respect to the centroid is

$$I_2^g = \frac{b_s^3 t_s}{12} + 2\left[\frac{b_i^3 t_i}{12} + \left(\frac{b_s + b_i}{2}\right)^2 b_i t_i\right] + 2\left(\frac{b_s}{2}\right)^2 t_w$$

$$= \frac{b_s^3 t_s}{12} + \frac{b_i^3 t_i}{6} + \frac{(b_s + b_i)^2}{2} b_i t_i + \frac{b_s^2}{2} t_w$$
(C.3)

The sectorial moments of inertia $I_{\omega x_1}^{A,B}$ can be readily obtained, with the aid of symmetry as

$$I_{\omega x_1}^{A,B} = 2\left[\int_{y_g-h}^{y_g} \frac{b_s}{2} t_w (-\xi_2 + y_g) \frac{bs}{2} d\xi_2 + \int_{\frac{b_s}{2}}^{\frac{b_s}{2}+b_i} \frac{b_s h}{2} - \left(\xi_1 - \frac{b_s}{2}\right) h t_i d\xi_1\right].$$
(C.4)

Using the substitutions $u = y_g - \xi_2 \to du = -d\xi_2$ and $v = \xi_1 - \frac{b_s}{2} \to dv = d\xi_1$

$$I_{\omega x_1}^{A,B} = 2\left[\int_0^{b_i} \frac{b_s^2}{4} t_w u(-du) + \int_0^{b_i}\left[\frac{b_s h}{2}\left(v + \frac{b_s}{2}\right) - vh\left(v + \frac{b_s}{2}\right)\right] t_i dv\right] =$$

$$2\left[\frac{b_s^2 h^2 t_w}{8} + \frac{b_s^2 h b_i t_i}{4} - \frac{b_i^3 h t_i}{3}\right] = \frac{b_s^2 h^2 t_w}{4} + \frac{b_s^2 h b_i t_i}{2} - \frac{2 b_i^3 h t_i}{3}.$$
(C.5)

With equation (3.59), and with the aid of symmetry ($I_{12} = 0$), the position of the shear centre is given by

$$y_c = \xi_2^C - \xi_2^A = \frac{I_{\omega x_1}^{A,B}}{I_2^g}$$
(C.6)

Using the symmetry again, it is possible to infer that B coincides with the principal origin. Therefore, the principal sectorial area function is readily obtained (see Figure 54).
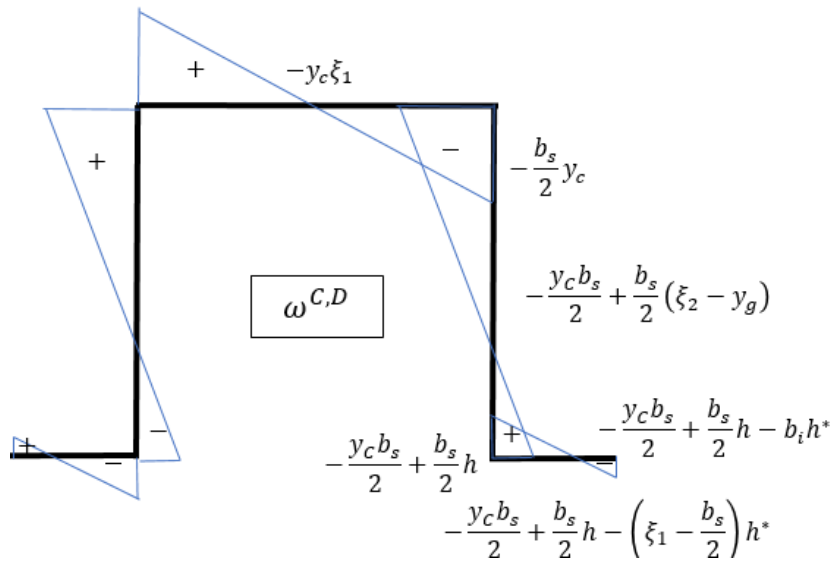
Figure 54 – Principal sectorial area ($\omega^{C,D}$). The expressions of the anti-symmetric part of the diagram were not shown.

Marcos Pires Kassab   133

Advances on a kinematically exact rod model for thin-walled open section members: consistent warping function and nonlinear constitutive equation

Now, it is possible to obtain the principal sectorial moment of inertia, with

$$
I_\omega^{C,D} = 2\left[\int_0^{\frac{b_2}{2}} (-y_c\xi_1)^2 t_s d\xi_1 \right.
$$

$$
+ \int_{y_g-h}^{y_g} \left(-y_c\frac{b_s}{2} + \frac{b_s}{2}(y_g - \xi_2)\right)^2 t_w d\xi_2 \tag{C.7}
$$

$$
\left. + \int_{\frac{b_s}{2}}^{\frac{b_s}{2}+b_i} \left(\frac{b_s h}{2} - \left(\xi_1 - \frac{b_s}{2}\right)h - y_c\right)^2 t_i d\xi_1 \right].
$$

Using the substitutions $u = y_g - \xi_2 \rightarrow du = -d\xi_2$ and $v = \xi_1 - \frac{b_s}{2} \rightarrow dv = d\xi_1$, one gets

$$
I_\omega^{C,D} = 2\left[\frac{b_s^3 t_s y_c^2}{24} + \int_h^0 \left(-\frac{y_c b_s}{2} + \frac{b_s}{2}u\right)^2 t_w(-du)\right.
$$

$$
\left. + \int_0^{b_i} \left(\frac{b_s}{2}(h - y_c) - vh^*\right)^2 t_i dv\right], \tag{C.8}
$$

with $h^* = h + y_c$ and $k = \frac{b_s}{2}(h - y_c)$. Performing other substitutions $p = u - \Delta\xi_2$ and $w = k - vh^*$, and then integrating the polynomials, it is obtained

$$
I_\omega^{C,D} = 2\left[\frac{b_s^3 t_s y_c^2}{24} + \frac{b_s^2 t_w}{4}((h - y_c)^3 - (y_c)^3) - \frac{t_i|b_i|}{3h^*}((k - b_i h^*)^3 - k^3)\right]
$$

$$
= \frac{b_s^3 t_s y_c^2}{12} + \frac{b_s^2}{6}t_w(h^3 - 3h^2 y_c + 3hy_c^2) \tag{C.9}
$$

$$
+ \frac{2|b_i|}{3}(3k^2 - 3kb_i h^* + b_i^2 h^{*2})t_i.
$$

Note that, sometimes, $|b_i|$ is taken is absolute value. This is due to the fact that b_i might be positive (top hat section), negative (stiffened C-section) or zero (standard C-section). Therefore, this adjustment is necessary.

Marcos Pires Kassab 135

Advances on a kinematically exact rod model for thin-walled open section members: consistent warping function and nonlinear constitutive equation

APPENDIX D. SECTORIAL AREA, PRINCIPAL POLE AND ORIGIN FOR STIFFENED V-SECTION

(a)   (b)
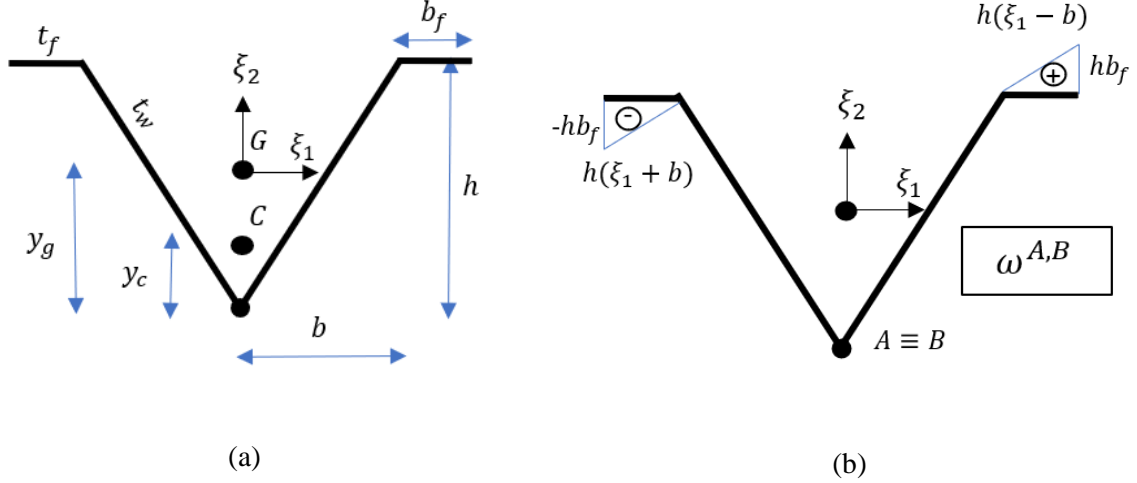
Figure 55 – Geometric attributes; b) Sectorial area for an arbitrary A, B ($\omega^{A,B}$).

First, let us define

$$l = \sqrt{h^2 + b^2}.$$
(D.1)

This cross-section area is

$$A = 2lt_w + 2t_f b_f.$$
(D.2)

The position of the centroid can be calculated, by definition, as

$$y_g = \frac{ht_w l + 2t_f b_f h}{A}.$$
(D.3)

The moment of inertia I_2 with respect to the centroid is

$$I_2^g = 2\int_0^b \xi_1^2 \sqrt{1 + h^2/b^2}\, d\xi_1 + 2\left[\frac{b_f^3 t_f}{12} + \left(b + \frac{b_f}{2}\right)^2 b_f t_f\right]$$

$$= \frac{2}{3}b^2 l t_w + \frac{b_f^3 t_f}{6} + 2\left(b + \frac{b_f}{2}\right)^2 b_f t_f.$$
(D.4)

The sectorial moments of inertia $I_{\omega x_1}^{A,B}$ can be readily obtained, with the aid of symmetry as

$$I_{\omega x_1}^{A,B} = 2\left[\int_b^{b+b_f} h(\xi_1 - b)\xi_1 t_f\, d\xi_1\right].$$
(D.5)

Using the substitutions $u = x - \xi_1 \rightarrow du = -d\xi_1$, one gets

$$I_{\omega x_1}^{A,B} = 2ht_f \int_0^{b_f} u(u + b)\, du = 2ht_f\left(\frac{b_f^3}{3} + \frac{b_f^2 b}{2}\right).$$
(D.6)

With equation (3.59), and with the aid of symmetry ($I_{12} = 0$), the position of the shear centre is given by

$$y_c = \xi_2^C - \xi_2^A = \frac{I_{\omega x_1}^{A,B}}{I_2^g} \tag{D.7}$$

Using the symmetry again, it is possible to infer that B coincides with the principal origin (D). Therefore, the principal sectorial area function is readily obtained (see Figure 56).
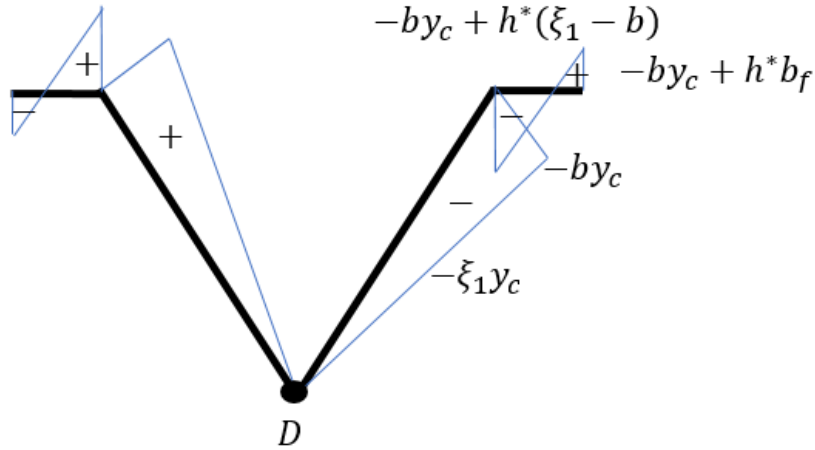
Figure 56 – Principal sectorial area ($\omega^{C,D}$). The expressions of the anti-symmetric part of the diagram were not shown.

Now, it is possible to obtain the principal sectorial moment of inertia, with

$$I_\omega^{C,D} = 2\left[\int_0^b (-\xi_1 y_C)^2 \, t_w \sqrt{1 + h^2/b^2} d\xi_1 \right.$$

$$\left. + \int_b^{b+b_f} \left(-by_c + h^*(\xi_1 - b)\right)^2 t_f d\xi_1\right], \tag{D.8}$$

with $h^* = h - y_c$.

Developing the expression, one gets

$$I_\omega^{C,D} = \frac{2}{3} y_c^2 b^2 l t_w + \frac{2}{3} b_f \left[3b^2 y_c^2 - 3by_c h^* b_f + \left(h^* b_f\right)^2\right] t_f. \tag{D.9}$$

Marcos Pires Kassab 137

Advances on a kinematically exact rod model for thin-walled open section members: consistent warping function and nonlinear constitutive equation

APPENDIX E. EVALUATING THE POSITION OF THE AXIS AND POLE FOR WARPING FUNCTION GENERATION

The first step for every rod model is to determine the axis that will represent the reference for the solid geometry. In the linear analysis, little discussion is made about this topic: the problem is separated in axial/shearing forces and bending moment, taking as reference the centroid, while for the torsion, the axis is taken at the torsion centre (in this context, equivalent to the shear centre and the principal pole). Sometimes, when only the Saint-Venant (uniform) torsion is considered, this discussion is not even approached, since a) it is known that I_T is invariant to the choice of the rod axis; b) for a fixed centre, considering uniform specific rotation, the stress field is not dependent on such choice.

In the kinematically exact context, it is known that the rigid body motion is not affected by the choice of the rod axis, as such transformation can be written in terms of any reference. The only requirement is that normal and shear stresses and its resultants are consistently derived, rendering equivalent models, regardless of the axis choices (at least, if the boundary conditions remain unchanged), as mentioned in Pimenta [22] or Campello [1].

The other problem to be faced is the choice of the pole for the generation of the warping function, which is a more sensitive subject. In the uniform torsion, changing the pole leads to a difference of "only" a rigid body motion along the whole axis, whereas the stress field and the torsional rotation (which is the kinematical quantity of interest) are correctly calculated, and, as consequence, no further discussion is usually carried in this framework.

However, in complex cases with non-uniform torsion (specially kinematically exact 3D rod theories), this subject becomes more sensitive, mainly when the bending/torsion rotations coexist and independent degrees of freedom are added to the model. Usually, one of the two alternatives is chosen:

a) the so-called orthogonality conditions are applied: the pole is taken at the shear centre (principal pole). The idea is to uncouple first order torsion strains from axial and bending strains;

b) the pole is the rod axis itself – no further treatment is done.

This topic is rather underestimated, and sometimes the same author adopts one or another approach in different works without further explanations. However, it will be shown here that this choice is important and is much more than just an option to uncouple or not certain strain components.

Here, it will be shown that the change of the warping pole changes the space of admissible solutions for the model, and therefore it must be treated as a modelling decision that impacts the solution.

Proposition: Consider a generic cross section. Let us consider two warping functions ψ_a and ψ_b generated with different poles A and B. Using equation (3.79), the following relation is valid

$$\psi_b = \psi_a + a\xi_1 + b\xi_2 + c \tag{E.1}$$

Let us prove that the possible deformation fields generated with ψ_a and ψ_b are different.

Proof: Without any loss of generality, let us impose that ψ_a obeys the orthogonality conditions, so that rigid body motions are filtered. Now, let us consider a generic cross-sectional deformation characterized by $\boldsymbol{d}_a = [\boldsymbol{u}_a, \boldsymbol{\theta}_a, p_a]$, that will act with the shape function ψ_a. Now, it is possible to build another set $\boldsymbol{d}_b = [\boldsymbol{u}_b, \boldsymbol{\theta}_b, p_b]$ so that the rigid motion that is embedded in ψ_b (the terms $a\xi_1 + b\xi_2 + c$) is compensated. Formally, it is searched $\boldsymbol{d}_a, \boldsymbol{d}_b$ such that

$$\boldsymbol{u}_a + \boldsymbol{Q}_a \boldsymbol{a}^r \parallel \boldsymbol{u}_b + \boldsymbol{Q}_b \boldsymbol{a}^r + \boldsymbol{p}_b(a\xi_1 + b\xi_2 + c)\boldsymbol{e}_3^b, \qquad \forall\, \boldsymbol{a}^r, \tag{E.2}$$

where the symbol $\parallel$ stands for "parallel to".

Thus, since $(a\xi_1 + b\xi_2)\boldsymbol{e}_3^b$ represents an additional rotation, necessarily $\boldsymbol{\theta}_a \neq \boldsymbol{\theta}_b$. As consequence, it is impossible for the "pure" warping contribution from $p_b(\psi_b - a\xi_1 - b\xi_2 - c)\boldsymbol{e}_3^b = p_b\psi_a\boldsymbol{e}_3^b$ to be equivalent to the one from $p_a\psi_a\boldsymbol{e}_3^a$, because, in general if $\boldsymbol{\theta}_a \neq \boldsymbol{\theta}_b \Rightarrow \boldsymbol{e}_3^a \neq \boldsymbol{e}_3^b$, and therefore it is impossible to exactly convert the solution with pole B into the one with pole A. This means that, physically, if a pole that is not principal is used, one might end up with a warping that is not really orthogonal to the cross-section, since it will be orthogonal to the plane that contains the vectors $\boldsymbol{Q}_b \boldsymbol{a}^r$, instead of $\boldsymbol{Q}_a \boldsymbol{a}^r$. This is better illustrated in Figure 57.
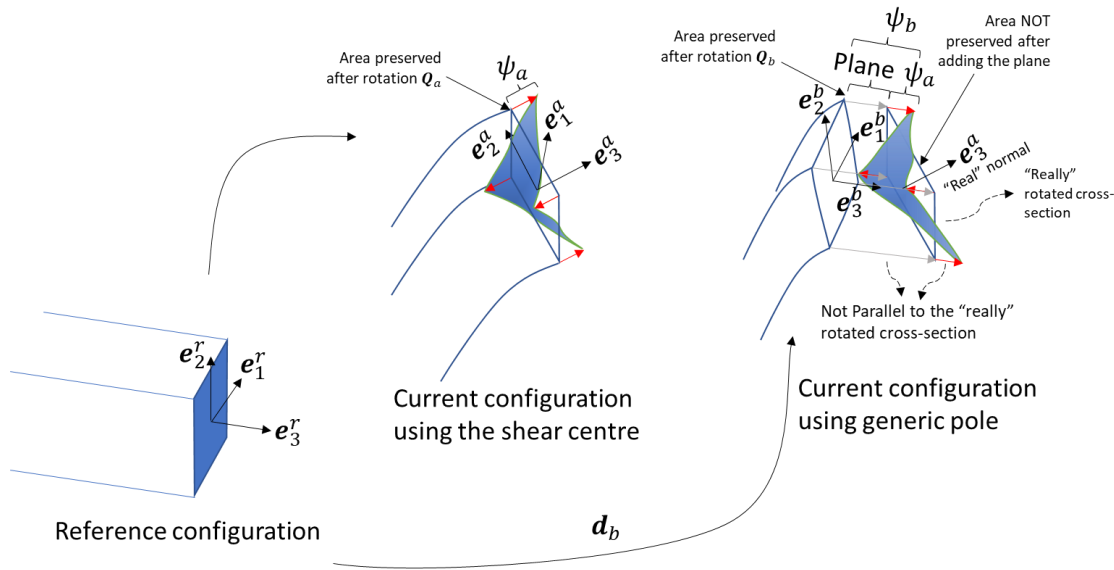
Figure 57 – On the differences of using or not the orthogonality conditions for the shear centre.

Moreover, in the attempt to compensate the rigid body motion, the cross-sectional area before warping is NOT preserved, since, in case b), as the area of the projection is the original cross-section itself, when $\boldsymbol{p}_b(a\xi_1 + b\xi_2 + c)\boldsymbol{e}_3^b$ is added, the final "rotated" area must be greater than the one from the reference configuration.

Thus, the conclusion is that the choice of the pole directly affects the space of admissible solutions, and therefore the model is NOT invariant to its choice, differently from the choice of the rods axis∎.

Marcos Pires Kassab   139

Advances on a kinematically exact rod model for thin-walled open section members: consistent warping function and nonlinear constitutive equation

A question that also arises is how the use of a pole that is different from the axis impacts the stress field. Let us study a linear problem and compare to some results from the kinematically exact theory:

Consider a rod with a generic cross-section, with a torsion rotation $\theta_3(\xi_3)$ and warping intensity $p(\xi_3)$. The geometric characterization of three different cases can be found in Figure 58. In case a), the rotation is around the shear centre, and the principal warping function ψ_a is used. In case b) a generic point is used as rotation centre, and the corresponding warping function ψ_b is used. In case c), the rotation is around the same point as in case b), but ψ_a is used.
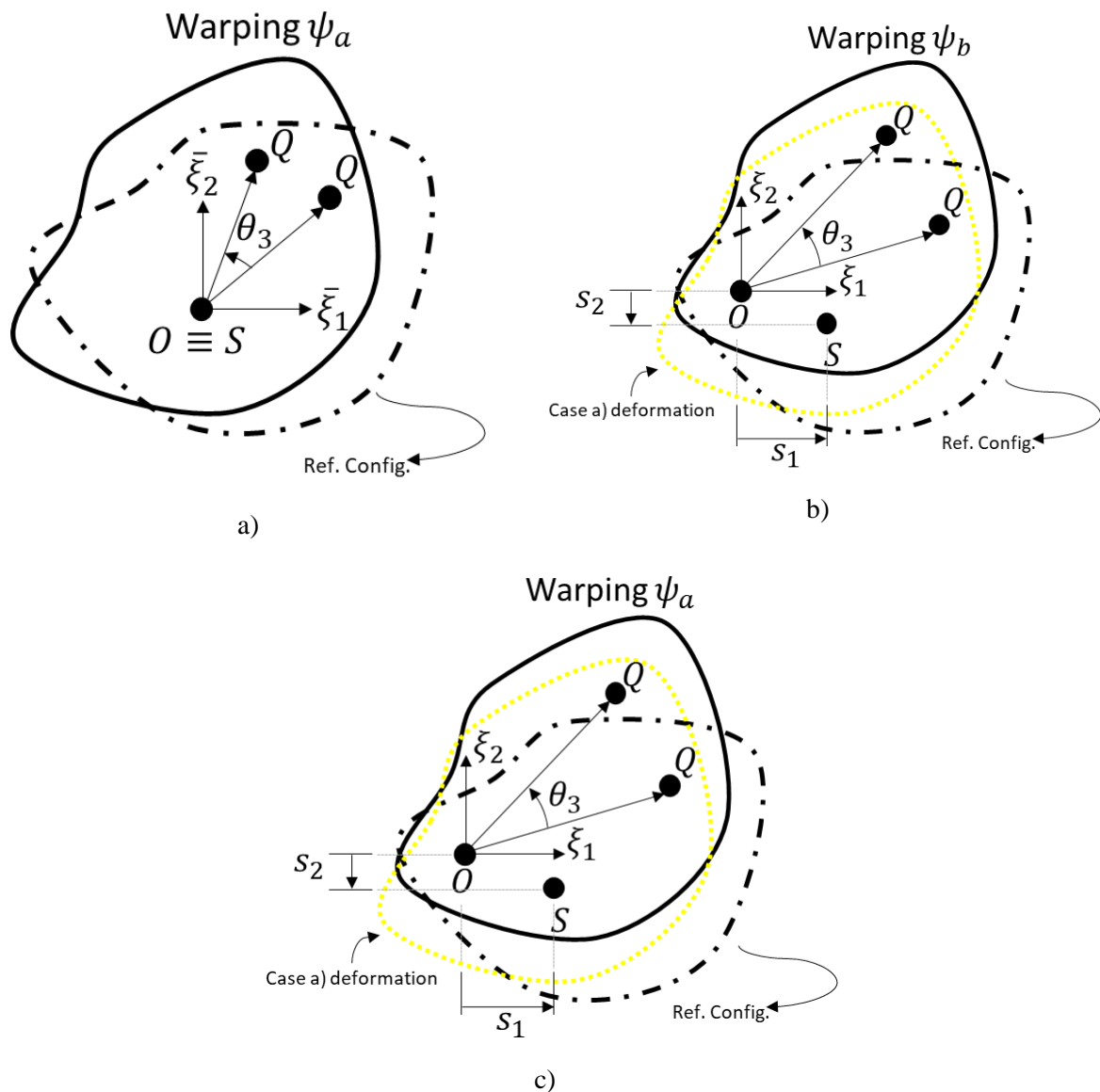
Figure 58 – Three kinematical descriptions for different axial reference and pole. Dash-dot line: reference configuration. Full line: current configuration. a) Axis and pole in the shear centre; b) Axis and pole in generic point; c) Axis in the same point as b) and pole in shear centre.

It is possible to represent the axial reference translation by

$$\bar{\bar{\xi}}_\alpha = \xi_\alpha - s_\alpha \tag{E.3}$$

Let us compare the relevant displacements, strains and stress fields, assuming small displacements and linear elastic materials (Table 10, where u_i is the displacement in direction i, $\varepsilon_i = \frac{\partial u_i}{\partial \xi_i}$ is the axial linear strain in direction i, $\gamma_{ij} = \frac{\partial u_i}{\partial \xi_j} + \frac{\partial u_j}{\partial \xi_i}$ is the shear strain in the i plane at the j direction, τ_{ij} is the stress in the i plane at the j direction, taken from the Cauchy's stress tensor).

Table 10 – Displacement, strain and stress field for cases a), b) and c)

	Case a)	Case b)	Case c)
Displacement	$u_1 = -\theta_3 \bar{\bar{\xi}}_2$ $u_2 = \theta_3 \bar{\bar{\xi}}_1$ $u_3 = p\psi_a(\bar{\bar{\xi}}_1, \bar{\bar{\xi}}_2)$	$u_1 = -\theta_3 \xi_2$ $u_2 = \theta_3 \xi_1$ $u_3 = p\psi_b(\xi_1, \xi_2)$	$u_1 = -\theta_3 \xi_2$ $u_2 = \theta_3 \xi_1$ $u_3 = p\psi_a(\xi_1, \xi_2)$
Strain	$\varepsilon_1 = \varepsilon_2 = \gamma_{12} = 0$ $\varepsilon_3 = p'\psi_a$ $\gamma_{\alpha 3} = e_{\beta\alpha}\theta_3' \bar{\bar{\xi}}_\beta + p\psi_{a,\alpha}$	$\varepsilon_1 = \varepsilon_2 = \gamma_{12} = 0$ $\varepsilon_3 = p'E\psi_b$ $\gamma_{\alpha 3} = e_{\beta\alpha}\theta_3' \xi_\beta + p\psi_{b,\alpha}$	$\varepsilon_1 = \varepsilon_2 = \gamma_{12} = 0$ $\varepsilon_3 = p'E\psi_a$ $\gamma_{\alpha 3} = e_{\beta\alpha}\theta_3' \xi_\beta + p\psi_{a,\alpha}$
Stress	$T_{11} = T_{12} = T_{22} = 0$ $T_{33} = Ep'\psi_a$ $T_{\alpha 3} = G\left(e_{\beta\alpha}\theta_3' \bar{\bar{\xi}}_\beta + p\psi_{a,\alpha}\right)$	$T_{11} = T_{12} = T_{22} = 0$ $T_{33} = Ep'\psi_b$ $T_{\alpha 3} = G\left(e_{\beta\alpha}\theta_3' \xi_\beta + p\psi_{b,\alpha}\right)$	$T_{\alpha 3} = G\gamma_{\alpha 3}$ $T_{33} = Ep'\psi_b$ $T_{\alpha 3} = G\left(e_{\beta\alpha}\theta_3' \xi_\beta + p\psi_{a,\alpha}\right)$

In order to obtain the Saint-Venant's warping function, for the cases a) and b), one can impose the uniform torsion basic assumptions: $\theta_3 = \theta_3'\xi_3$, with $\theta_3' = cte$, $p = \theta_3'$ and traction-free lateral boundary. Therefore, from the traditional Saint-Venant's theory, one gets, for case a)

$$\begin{cases} \psi_{a,\alpha\alpha} = 0 \\ \psi_{a,\alpha}n_\alpha = -e_{\alpha\beta}(\bar{\bar{\xi}}_\alpha)n_\beta = -e_{\alpha\beta}(\xi_\alpha - s_\alpha)n_\beta \end{cases} \tag{E.4}$$

and for case b),

$$\begin{cases} \psi_{b,\alpha\alpha} = 0 \\ \psi_{b,\alpha}n_\alpha = -e_{\alpha\beta}(\xi_\alpha)n_\beta \end{cases} \tag{E.5}$$

where $\boldsymbol{n} = [n_1 \quad n_2 \quad 0]^T$ is the unitary normal to the boundary external vector and $\boldsymbol{e} = \begin{bmatrix} 0 & 1 \\ -1 & 0 \end{bmatrix}$.

As already mentioned throughout the text, for Saint-Venant's warping functions generated from different poles, the following relation is valid

$$\left(\psi_{a,\alpha} - e_{\beta\alpha}s_\beta\right)n_\alpha = \psi_{b,\alpha}n_\alpha \Rightarrow \psi_{a,\alpha}n_\alpha = \left(\psi_{b,\alpha} + e_{\beta\alpha}s_\beta\right)n_\alpha \Rightarrow$$
$$\psi_a = \psi_b - s_2\xi_1 + s_1\xi_2 + c \tag{E.6}$$

Rewriting the tangential strain field from case c) in terms of ψ_b, one gets

$$\gamma_{\alpha 3} = e_{\beta\alpha}\theta_3'\xi_\beta + p(\psi_{b,\alpha} + e_{\beta\alpha}s_\beta) \tag{E.7}$$

Therefore, the tangential stress field become

$$T_{\alpha 3} = G\left(e_{\beta\alpha}\theta_3'\xi_\beta + p\psi_{b,\alpha}\right) + Gpe_{\beta\alpha}s_\beta \tag{E.8}$$

Let us now calculate the stress resultants for those cases, for generic p, θ_z, θ_z' (Table 11). Using the definitions from the linear theory, $N = \int_A T_{33}dA$, $V_\alpha = \int_A T_{\alpha 3}dA$, $M_\alpha = e_{\alpha\beta}\int_A T_{33}\xi_\beta dA$, $T = \int_A e_{\alpha\beta}\xi_\alpha T_{\beta 3}dA$, one gets, (some results concerning the integration of products of the type $\int_A \psi_{,\alpha}dA$, $\int_A \psi_{,\alpha}\xi_\beta dA$, etc are used, see Campello [1] or Gruttmann [18], [48] for details)

Advances on a kinematically exact rod model for thin-walled open section members: consistent warping function and nonlinear constitutive equation

Table 11 – Stress resultants for the proposed problem

Case a)	Case b)	Case c)
$N = p'ES_{\psi_a} = 0$	$N = p'ES_{\psi_b}$	$N = p'ES_{\psi_a} = 0$
$V_1 = (p - \theta_3')GA\bar{g}_2$	$V_1 = (p - \theta_3')GAg_2$	$V_1 = -G\theta_3'Ag_2 - pGA(s_2 - g_2)$
$V_2 = -(p - \theta_3')GA\bar{g}_1$	$V_2 = -(p - \theta_3')GAg_1$	$V_2 = G\theta_3'Ag_1 + pGA(s_1 - g_1)$
$M_1 = p'EI_{\psi_a\bar{2}} = 0$	$M_1 = p'EI_{\psi_b2}$	$M_1 = p'EI_{\psi_a2} = 0$
$M_2 = -p'EI_{\psi_a\bar{1}} = 0$	$M_2 = -p'EI_{\psi_b1}$	$M_2 = -p'EI_{\psi_a1} = 0$
$T = G\theta_3'\bar{I}_0 + GpI_T$	$T = G\theta_3'I_0 + GpI_T$	$T = G\theta_3'I_0 + Gp(I_T - I_0 + Ag_\alpha s_\alpha)$

In Table 11, g_α denotes the position of the centroid and the other symbols are used as defined during the text.

Of course, if $p = \theta_3'$, and $\theta_3 = \theta_3'\xi_3$, case a) and case b) recover the uniform torsion problem, with $N = V_1 = V_2 = M_1 = M_2 = 0$ and $T = G\theta_3'I_T$.

Comparing equations (E.4) and (E.5) with Table 10 for the case b), it is clear that the traction-free boundary condition is not met in case c), even if the torsion was uniform, since there is a discrepancy between the pole and the axis. The practical consequence of this statement for the rod model is that, by integrating the stresses, the shear resultant forces would only be zero in uniform torsion situations if a shear deformation strain were added (proportional to κ_α), in order to counterbalance the term $Gpe_{\beta\alpha}s_\beta$ – this would generate a sideways deflection, i.e. the deformed axis would not remain parallel to the original configuration. This is expected, since, comparing the displacements field from cases a) to c), despite the warping being the same, rigid body lateral and vertical displacements are added. On the other hand, the orthogonality conditions from the warping function eliminates any kind of axial and bending resultants. Only when the shear centre is taken as the rod axis that the traction-free boundary condition is respected and both axial *and* bending resultants remains null.

All those statements are in perfect agreement with the formulation of kinematically exact theories. In Simo [17] (equation (63)), Campello [1] (equation (4.22)), the orthogonality conditions are imposed and the shear resultants $V_1 = pGA(g_2 - s_2)$ and $V_2 = pGA(s_1 - g_1)$ are present (the same happens, implicitly, in 6 DOF models from Pimenta and Yojo [22] (equation (128)) and Gruttmann [48] (equation (45)) and also the bi-shear is modified (becomes function of s_α). In Gruttmann [18](equation (53)), where the pole is fixed as the same as the axis, no shear resultant is present, but the warping contributes to the bending resultants $M_1 = p'EI_{\psi1}$, $M_2 = -p'EI_{\psi2}$ and bi-moment. If bi-moment (depends on the normal stresses, therefore, on $E\psi$) and bi-shears (depends on the shear stresses, therefore, on $G\psi_{,\alpha}$)were also calculated, similar conclusions would hold.

NOTE: merely by inspecting how the bending and torsional moments are defined, one can see that they are axis-dependent, in order to generate a mechanically equivalent system. Analogously, if bi-moment and bi-shear are calculated on various poles, they shall differ among them.

Neither of the approaches for the pole position is wrong *a priori*, but one must acknowledge that they might impact the solution. Therefore, some practical situations were studied, in order to

142   Marcos Pires Kassab

Advances on a kinematically exact rod model for thin-walled open section members: consistent warping function and nonlinear constitutive equation

investigate such influence. Three examples were simulated, and for each one of them, five models are created:

a) Analytic Vlasov's linear model;

b) kinematically exact 7 DOF with linear elastic material – axis and pole at the load point application;

c) kinematically exact 7 DOF with linear elastic material – axis and pole at the shear centre;

d) kinematically exact 7 DOF with linear elastic material – axis at the load point application and pole at the shear centre;

e) *Ansys shell 281* model (with large deformation).

The models b), c) and d) were simulated using PEFSYS, based on the formulation from Pimenta and Yojo [22], and Campello [1].

For cases all the rod models, a homogeneous mesh with 30 linear elements is adopted.

Example C1) I-cantilever, vertically loaded at the top flange

This example is completely equivalent to the one from section 6.2.2. It has as material properties $E = 200\ GPa$ and $G = 80\ GPa$ and the vertical load is incremented up to $40\ kN$. A small lateral perturbation is imposed in order to transpose the bifurcation. One can see in Figure 59 and Figure 60 the geometric characterization of the problem and the adopted warping function, respectively.
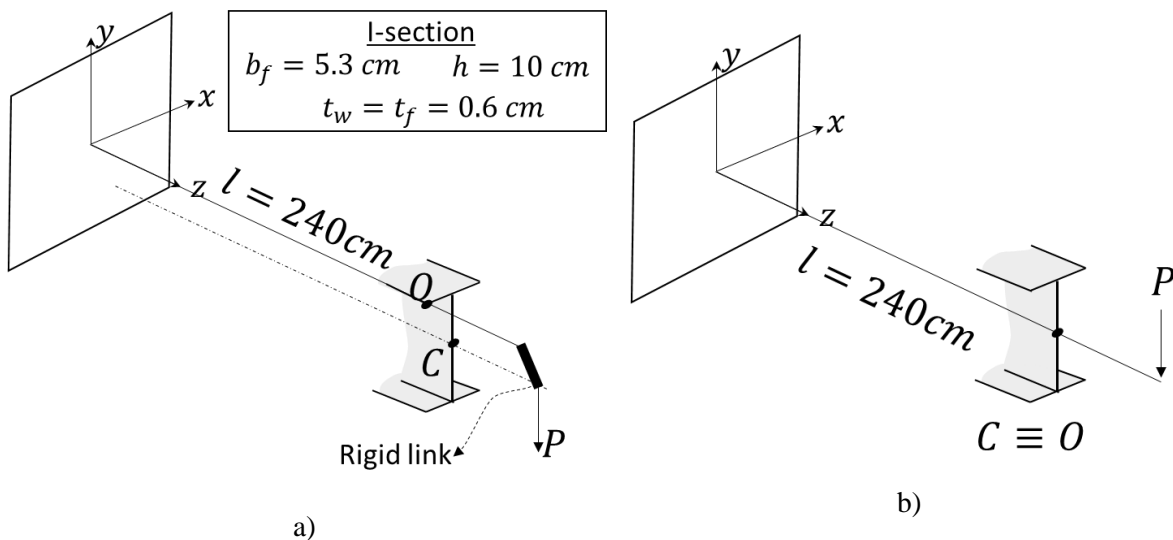
Figure 59 – Geometric description of the example and warping function C1. a) Axis on right-top flange; b) Axis on shear centre.

Advances on a kinematically exact rod model for thin-walled open section members: consistent warping function and nonlinear constitutive equation
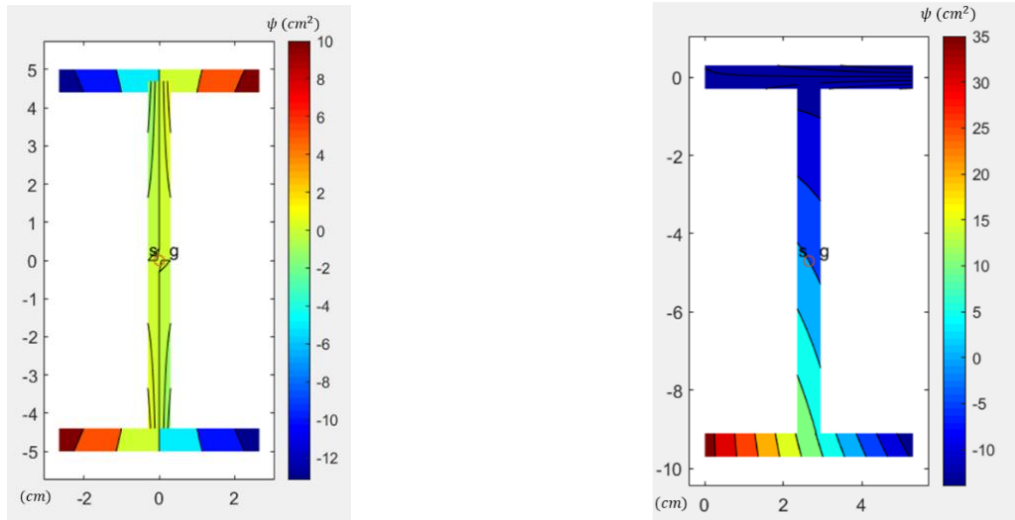
$$S_\psi = 0 \ cm^4$$
$$I_\psi = 330.52 \ cm^6$$
$$I_{\psi x_1} = 0 \ cm^5$$
$$I_{\psi x_2} = 0 \ cm^5$$
$$I_T = 1.40 \ cm^4$$

a)

$$S_\psi = 0 \ cm^4$$
$$I_\psi = 1942.714 \ cm^6$$
$$I_{\psi x_1} = -482.863 \ cm^5$$
$$I_{\psi x_2} = -70.7674 \ cm^5$$
$$I_T = 1.40 \ cm^4$$

b)

Figure 60 – Warping function for pole in a) shear centre; b) rod axis (top flange/web intersection).

In Figure 61, the equilibrium path for vertical and horizontal displacements, torsional rotation and warping intensity were displayed. It was stated that adopting a pole which is not principal has completely changed the solution, when compared to rod models that uses the shear centre as pole. Those differences become more noticeable at higher loadings (after $5.4 \ kN$).

We refer the reader to the 6.2.2 for a broader discussion about this example, since this appendix is only dedicated to the choice of the pole for the warping function.

Advances on a kinematically exact rod model for thin-walled open section members: consistent warping function and nonlinear constitutive equation

a)

b)

c)

d)
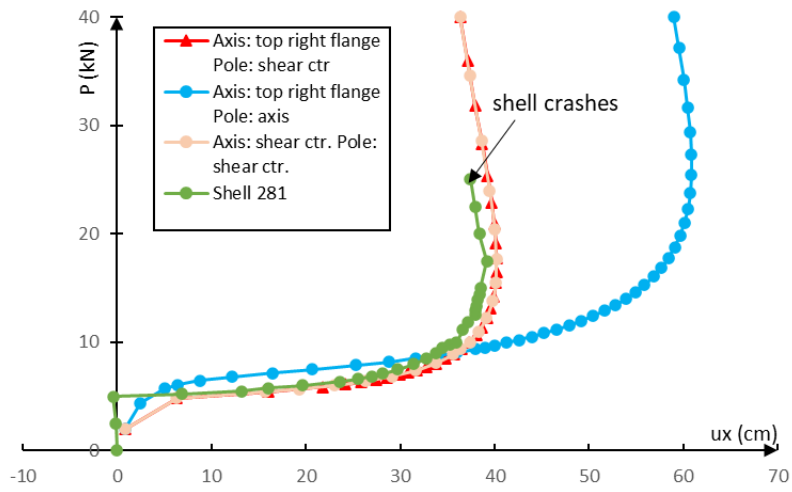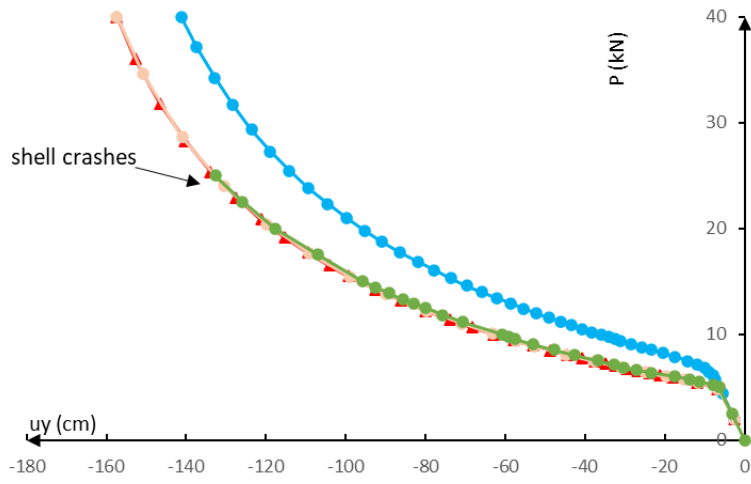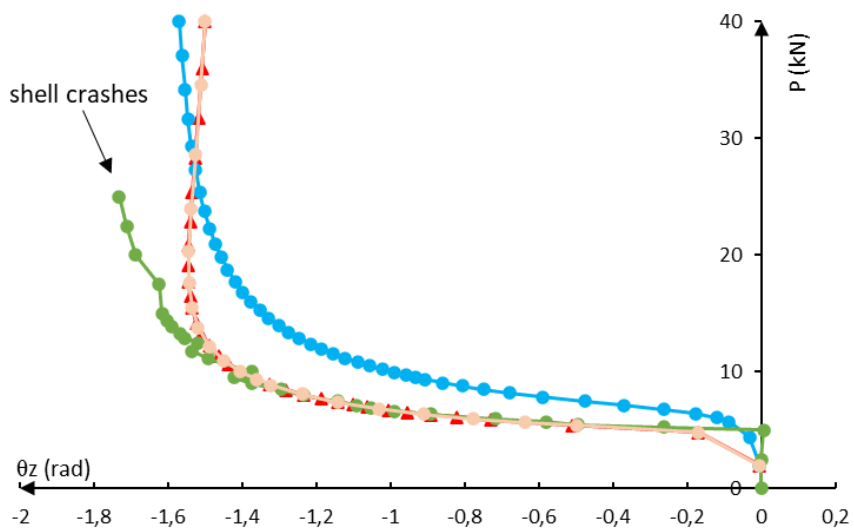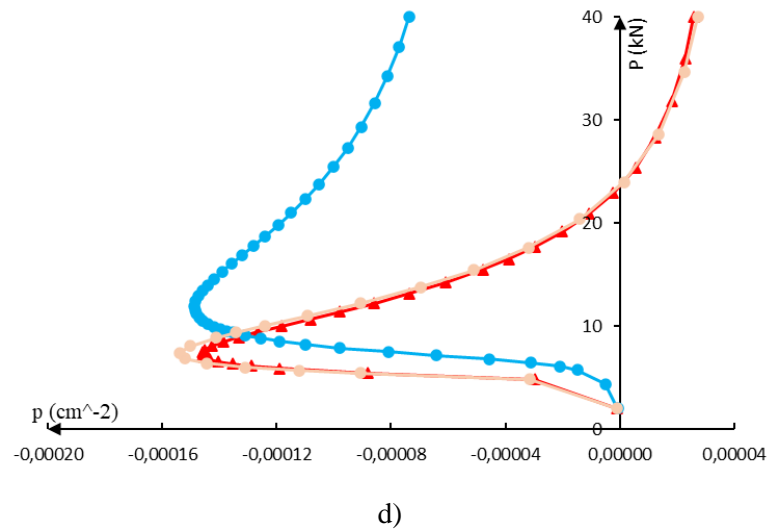
Figure 61 – Equilibrium paths for example E1, at the web mid-height. a) Lateral displacement; b) Vertical displacement; c) Torsional rotation; d) warping intensity.

Example C2) C-channel cantilever, vertically loaded at the top flange/web intersection (same as example 6.1.3)

This example is completely equivalent to the one from section 6.1.3. It has as material parameters $E = 210\ GPa$ and $G = 80\ GPa$. The load is incremented up to $P = 20\ kN$. One can see in

a)   b)
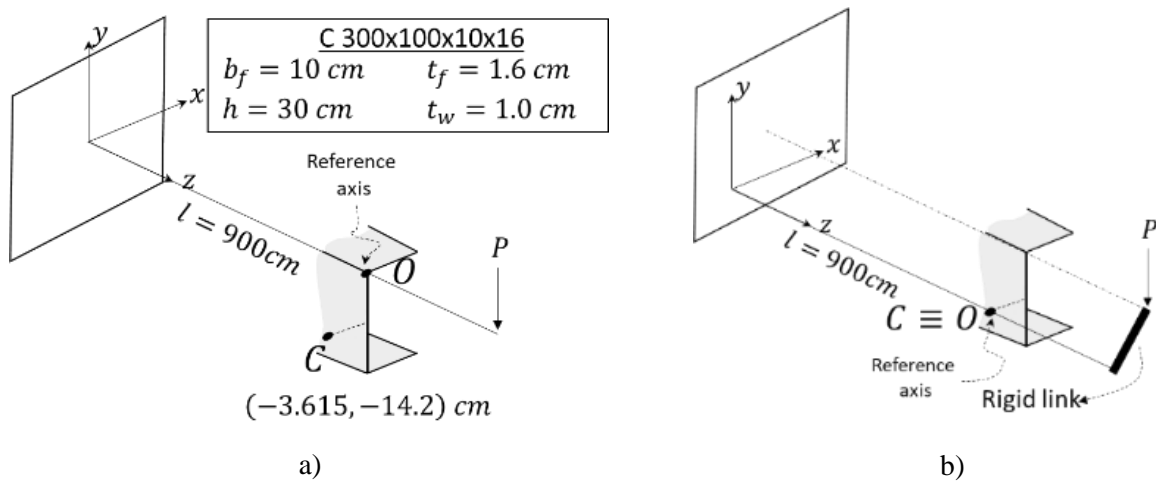
Figure 62 – Geometric description of the example and warping function E.2. a) Axis on the point of load application; b) Axis on shear centre.
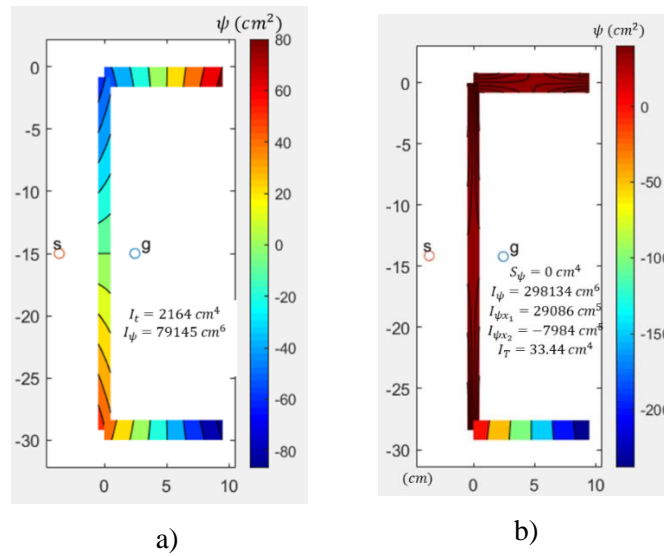
Figure 63 – Warping function for pole in a) shear centre; b) rod axis (top flange/web intersection).

In Figure 64, the equilibrium path for vertical and horizontal displacements, torsional rotation and warping intensity were displayed. It was stated that adopting a pole which is not principal has artificially stiffened the system as a whole, leading to significantly smaller displacements, when compared to rod models that uses the shear centre as pole. Those differences become more noticeable at higher loadings (after $7.7\ kN$).

We refer the reader to the 6.1.3 for a broader discussion about this example, since this appendix is only dedicated to the choice of the pole for the warping function.

a)
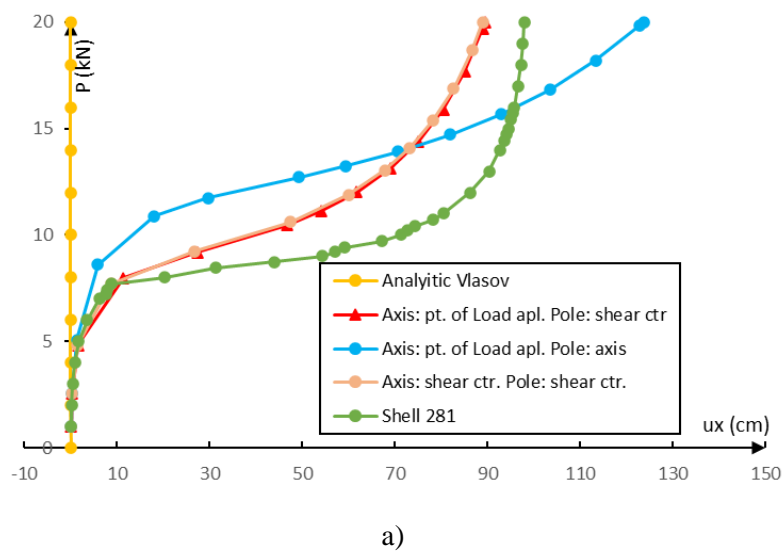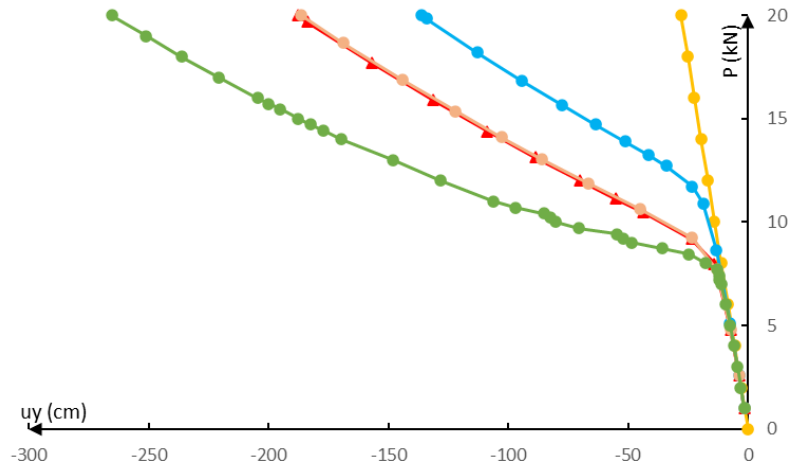
b)
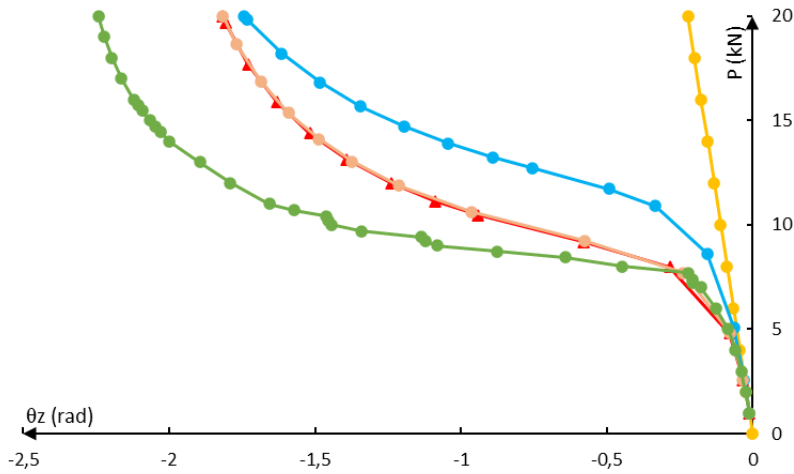
c)
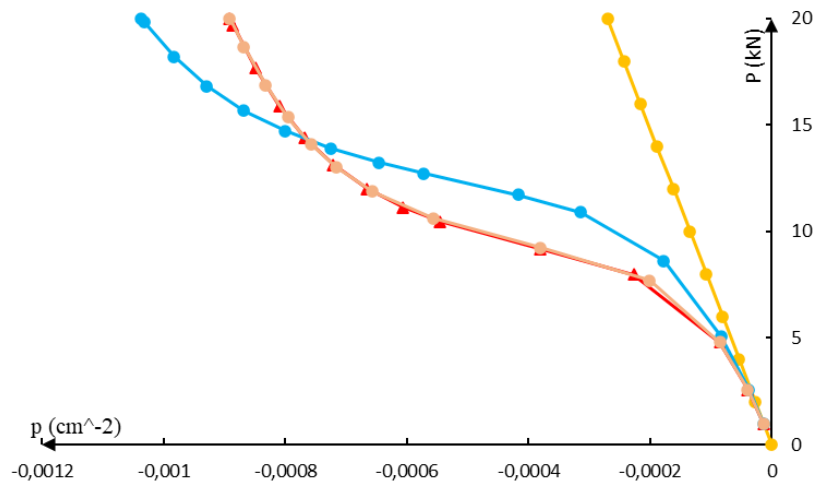
d)

Figure 64 – Equilibrium paths for example E3, at the web mid-height. a) Lateral displacement; b) Vertical displacement; c) Torsional rotation; d) warping intensity.

Example C3) C-channel cantilever, vertically loaded at the top flange/web intersection

This example has the same geometry as the one from section 6.1.3, but the load is now horizontal. It has as material parameters $E = 210\ GPa$ and $G = 80\ GPa$. The load is incremented up to $P = 80\ kN$. One can see in Figure 65 the geometric characterization of the problem. The adopted warping functions are the same as in the previous example.
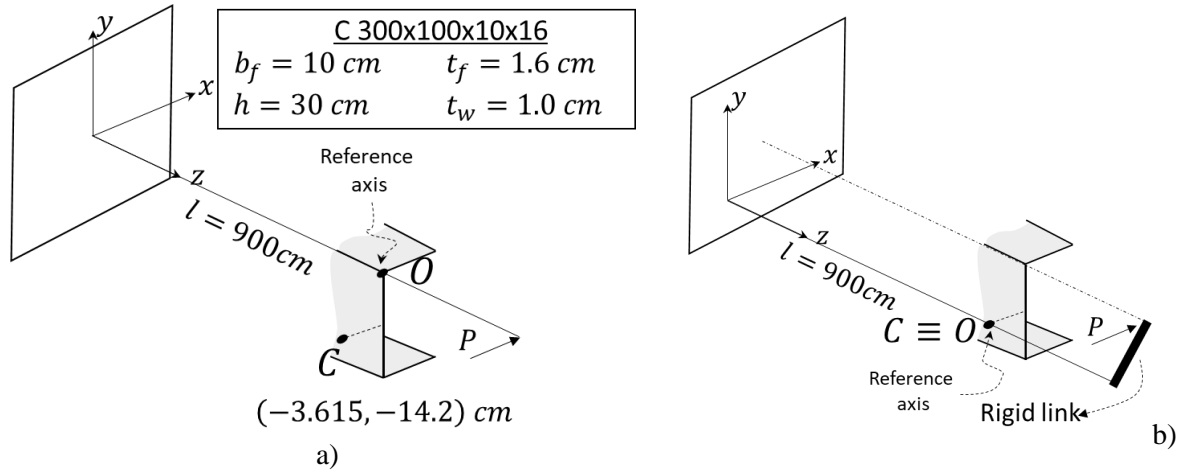
Figure 65 – Geometric description of the example and warping function E.4. a) Axis on the point of load application; b) Axis on shear centre.

In Figure 66, the equilibrium path for vertical and horizontal displacements, torsional rotation and warping intensity are displayed. As in the previous example, it was stated that adopting a pole which is not principal has a major impact on the warping intensity field, whereas the other kinematic quantities are almost not impacted in this example. Those differences become more evident at higher loadings, notably after $20\ kN$. It must be highlighted the invariance of the displacement field with the change of the axis. Comparing to the shell model, at higher loads the displacements are underestimated, probably due to the lack of in-plane distortion modes, such as web local bending.

a)

Marcos Pires Kassab

149

Advances on a kinematically exact rod model for thin-walled open section members: consistent warping function and nonlinear constitutive equation
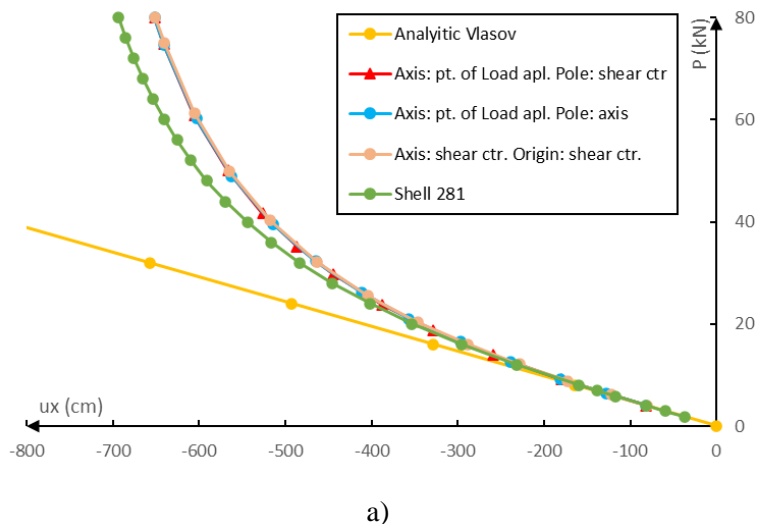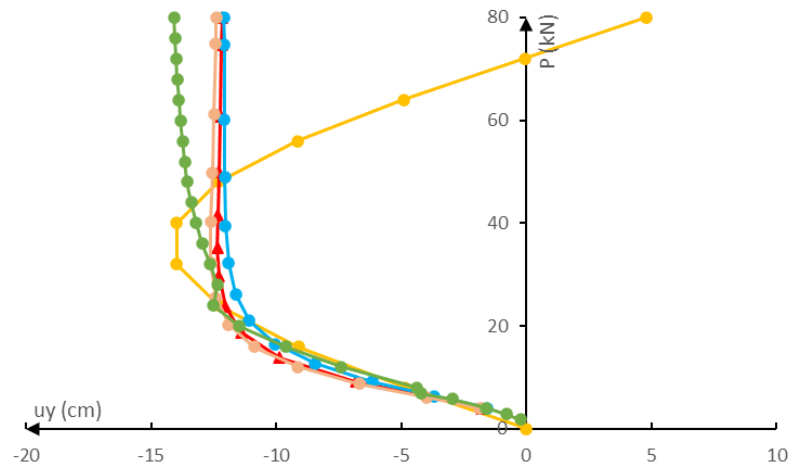
b)
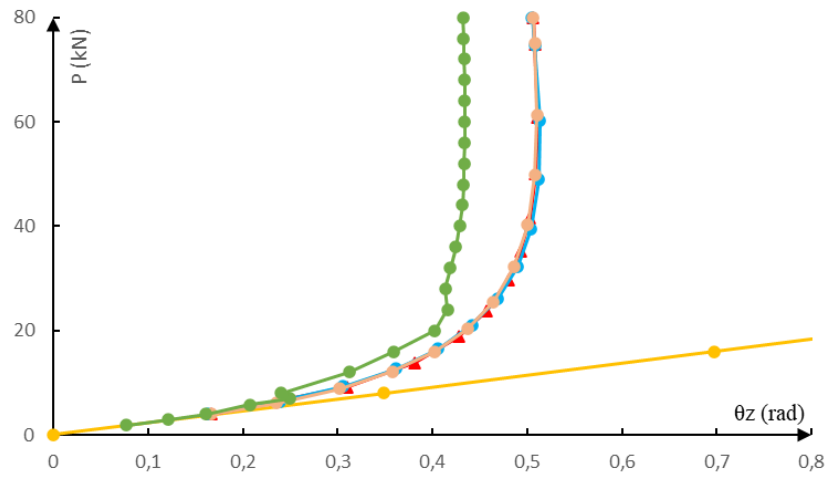
c)
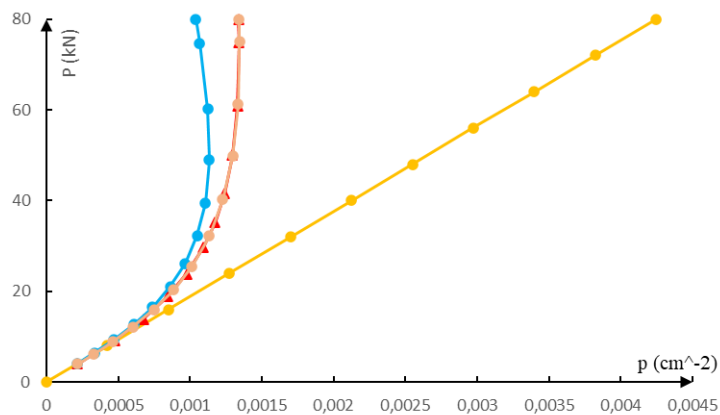
d)

Figure 66 – Equilibrium paths for example E4, at the web mid-height. a) Lateral displacement; b) Vertical displacement; c) Torsional rotation; d) warping intensity.

MODELLING NOTE: the rigid link was imposed through a very stiff rod element. It must be remarked that such element cannot influence the warping field, therefore, one of the following precautions must be adopted: a) link with null warping constant; b) unlink the warping intensity field

150   Marcos Pires Kassab

Advances on a kinematically exact rod model for thin-walled open section members: consistent warping function and nonlinear constitutive equation

of the rigid element from the rest of the structure; c) use other method to impose the link (Lagrange's multiplicator, implementation that allows a buffer on the applied load, etc).

CONCLUSION OF THE APPENDIX

Having in mind the theoretical aspects that were presented in this topic, altogether with the numerical results, the author has chosen to adopt the orthogonality conditions for warping function generation, even if that means that the pole is different from the rod axis. The simulated examples suggests that, by not doing so, a locking effect might be sensed. Also, as already stated in many references, it was seen that the position of the axis does not alter the solutions, and therefore, the modeller is free to choose the one that she/he considers more suitable. Therefore, in all the examples from section 4.5, the rod models were simulated using the shear centre as pole.

The beforementioned posture seems also to be prudent for more advanced formulations that employ a wide array of warping mode: if each one of them carries embedded additional rigid body motion, the "real" rotation of the cross-section is either lost or only recoverable through specific post-processing, which is cumbersome. That said, there is still the risk of artificial stiffening, which is undesirable. It should be noted that in linear Generalized Beam Theory, the warping/distortion modes are always orthogonal to each other, thus it would not be an absurd extrapolation to conceive that equivalent non-linear models should also respect orthogonality conditions.

NOTE: 6 DOF models can be derived from 7 DOF models by imposing $p = \kappa_3$ and ignoring the work that comes from the bi-moment. By doing so, the constitutive equation is no longer function of p' (and usually the "new" warping intensity derivative κ_3' is not calculated), forcing one to adopt as pole the shear centre, in order to not lose information about the bending moment contribution $p'EI_{\psi\alpha}$, which becomes forcingly zero.

Marcos Pires Kassab

151

Advances on a kinematically exact rod model for thin-walled open section members: consistent warping function and nonlinear constitutive equation

APPENDIX F. ROTATION DERIVATIVES

Some important derivatives are deducted here, for didactic purposes. They have already been documented in many classic works, such as [15], [22], [46], and were also deduced in other modern works, such as [25], [26].

Let us consider the time derivative-related tensor $\boldsymbol{\Omega} = \dot{\boldsymbol{Q}}\boldsymbol{Q}^T$. First, let us verificate that $\boldsymbol{\Omega}$ is skew-symmetric:

$$\boldsymbol{Q}\boldsymbol{Q}^T = \boldsymbol{I} \Leftrightarrow \dot{\boldsymbol{Q}}\boldsymbol{Q}^T + \boldsymbol{Q}\dot{\boldsymbol{Q}}^T = \boldsymbol{0} \Leftrightarrow \dot{\boldsymbol{Q}}\boldsymbol{Q}^T = -\boldsymbol{Q}\dot{\boldsymbol{Q}}^T = -\left(\dot{\boldsymbol{Q}}\boldsymbol{Q}^T\right)^T \Leftrightarrow \boldsymbol{\Omega} = -\boldsymbol{\Omega}^T \;\blacksquare \tag{F.9}$$

By definition, and using the fact that $\boldsymbol{Q}$ is skew-symmetric

$$\boldsymbol{\Omega} = (\dot{h}_1\boldsymbol{\Theta} + h_1\dot{\boldsymbol{\Theta}} + \dot{h}_2\boldsymbol{\Theta}^2 + h_2(\boldsymbol{\Theta}\dot{\boldsymbol{\Theta}} + \dot{\boldsymbol{\Theta}}\boldsymbol{\Theta}))(\boldsymbol{I} - h_1\boldsymbol{\Theta} + h_2\boldsymbol{\Theta}^2), \tag{F.10}$$

where h_i was used instead of $h_i(\theta)$ to alleviate the notation.

It is appropriate to introduce some properties of the skew-symmetric operators. For generic skew-symmetric $\boldsymbol{B}, \boldsymbol{C}, \boldsymbol{T}$, with axial vectors $\boldsymbol{b}, \boldsymbol{c}, \boldsymbol{t}$, and a generic vector $\boldsymbol{w}$

$$\boldsymbol{b} \times \boldsymbol{w} = \boldsymbol{B}\boldsymbol{w} \tag{F.11}$$

$$\boldsymbol{T} = \boldsymbol{B}\boldsymbol{C} = \boldsymbol{c} \otimes \boldsymbol{b} - (\boldsymbol{b} \cdot \boldsymbol{c})\boldsymbol{I}, \tag{F.12}$$

$$\boldsymbol{t} = \boldsymbol{b} \times \boldsymbol{c} \Leftrightarrow \boldsymbol{T} = \boldsymbol{B}\boldsymbol{C} - \boldsymbol{C}\boldsymbol{B}, \tag{F.13}$$

$$\boldsymbol{T}^3 = t^2\boldsymbol{T}, \boldsymbol{T}^4 = -t^2\boldsymbol{T}^2, \boldsymbol{T}^5 = +t^4\boldsymbol{T}, \boldsymbol{T}^6 = +t^4\boldsymbol{T}^2. \tag{F.14}$$

A consequence of (F.12) and (F.13) is that, for $\boldsymbol{t} = \boldsymbol{b} \times \boldsymbol{c},$

$$\boldsymbol{T} = skew(\boldsymbol{t}) = skew(\boldsymbol{b} \times \boldsymbol{c}) = \boldsymbol{B}\boldsymbol{C} - \boldsymbol{C}\boldsymbol{B} = \boldsymbol{c} \otimes \boldsymbol{b} - \boldsymbol{b} \otimes \boldsymbol{c} \tag{F.15}$$

The definition of the dyadic product is also useful. Let $\boldsymbol{a}, \boldsymbol{b}, \boldsymbol{x}$ be generic vectors, and $\boldsymbol{T}$ a generic second-order tensor. Thus

$$(\boldsymbol{a} \otimes \boldsymbol{b})\boldsymbol{x} = (\boldsymbol{b} \cdot \boldsymbol{x})\boldsymbol{a}. \tag{F.16}$$

As a consequence of this definition,

$$(\boldsymbol{a} \otimes \boldsymbol{b})\boldsymbol{T}\boldsymbol{x} = (\boldsymbol{b} \cdot \boldsymbol{T}\boldsymbol{x})\boldsymbol{a} = (\boldsymbol{T}^T\boldsymbol{b} \cdot \boldsymbol{x})\boldsymbol{a} = (\boldsymbol{a} \otimes (\boldsymbol{T}^T\boldsymbol{b}))\boldsymbol{x}. \tag{F.17}$$

Thus

$$(\boldsymbol{a} \otimes \boldsymbol{b})\boldsymbol{T} = (\boldsymbol{a} \otimes (\boldsymbol{T}^T\boldsymbol{b})) \tag{F.18}$$

Consider now that

$$\dot{\theta} = \sqrt{\boldsymbol{\theta} \cdot \boldsymbol{\theta}} \Rightarrow \dot{\theta} = \frac{1}{2}\frac{2(\boldsymbol{\theta} \cdot \dot{\boldsymbol{\theta}})}{\sqrt{\boldsymbol{\theta} \cdot \boldsymbol{\theta}}} = \frac{\boldsymbol{\theta} \cdot \dot{\boldsymbol{\theta}}}{\theta}. \tag{F.19}$$

Then

$$\dot{h}_\iota = \frac{dh_i}{d\theta}\dot{\theta} = \frac{dh_i}{d\theta}\frac{\boldsymbol{\theta} \cdot \dot{\boldsymbol{\theta}}}{\theta}, \tag{F.20}$$

and evaluating the derivatives of h_1 and h_2, one gets

$$\frac{dh_1}{d\theta} = \frac{\theta \cos\theta - sen\theta}{\theta^2} = \frac{\cos\theta - h_1}{\theta};$$

$$\frac{dh_2}{d\theta} = \frac{\theta sen\theta - 2 + 2cos\theta}{\theta^3} = \frac{h_1 - 2h_2}{\theta}. \tag{F.21}$$

Applying (F.20) and (F.21) on (F.10), one gets

$$\boldsymbol{\Omega} = h_1\dot{\boldsymbol{\Theta}} + h_2\boldsymbol{\Theta}\dot{\boldsymbol{\Theta}} + (h_1 - h_1^2 - \theta^2 h_2^2)\dot{\boldsymbol{\Theta}}\boldsymbol{\Theta} + \left(\dot{h}_1 + h_1\dot{h}_2\theta^2 - h_2\dot{h}_1\theta^2\right)\boldsymbol{\Theta}$$
$$+ \left(\dot{h}_2 - h_1\dot{h}_1 - h_2\dot{h}_2\theta^2\right)\boldsymbol{\Theta}^2 - h_1 h_2\boldsymbol{\Theta}\dot{\boldsymbol{\Theta}}\boldsymbol{\Theta} + h_2^2\boldsymbol{\Theta}\dot{\boldsymbol{\Theta}}\boldsymbol{\Theta}^2. \tag{F.22}$$

Using the property from equation (F.12),

$$(\boldsymbol{\Theta}\dot{\boldsymbol{\theta}})\boldsymbol{\theta} = (\dot{\boldsymbol{\theta}} \otimes \boldsymbol{\theta})\boldsymbol{\theta} - (\boldsymbol{\theta} \cdot \dot{\boldsymbol{\theta}})\boldsymbol{\theta}, \tag{F.23}$$

and with equation (F.17),

$$(\boldsymbol{\Theta}\dot{\boldsymbol{\theta}})\boldsymbol{\theta} = (\dot{\boldsymbol{\theta}} \otimes \boldsymbol{\Theta}^T\boldsymbol{\theta}) - (\boldsymbol{\theta} \cdot \dot{\boldsymbol{\theta}})\boldsymbol{\theta} = -\left(\dot{\boldsymbol{\theta}} \otimes \underbrace{(\boldsymbol{\theta} \times \boldsymbol{\theta})}_{=0}\right) - (\boldsymbol{\theta} \cdot \dot{\boldsymbol{\theta}})\boldsymbol{\theta}$$
$$= -(\boldsymbol{\theta} \cdot \dot{\boldsymbol{\theta}})\boldsymbol{\theta}. \tag{F.24}$$

Applying (F.24) in (F.22)

$$\boldsymbol{\Omega} = h_1\dot{\boldsymbol{\Theta}} + h_2\boldsymbol{\Theta}\dot{\boldsymbol{\Theta}} + (h_1 - h_1^2 - \theta^2 h_2^2)\dot{\boldsymbol{\Theta}}\boldsymbol{\Theta} + \left(\dot{h}_1 + h_1\dot{h}_2\theta^2 - \right.$$
$$\left. h_2\dot{h}_1\theta^2 + h_1 h_2(\boldsymbol{\theta} \cdot \dot{\boldsymbol{\theta}})\right)\boldsymbol{\Theta} + \left(\dot{h}_2 - h_1\dot{h}_1 - h_2\dot{h}_2\theta^2 - h_2^2(\boldsymbol{\theta} \cdot \dot{\boldsymbol{\theta}})\right)\boldsymbol{\Theta}^2. \tag{F.25}$$

Evaluating the scalar terms, and substituting the derivatives from (F.25),

$$h_1 - h_1^2 - \theta^2 h_2^2 = h_2 - \frac{sen^2\theta}{\theta^2} + \frac{\theta^2}{4} + \frac{(sen^4\theta)}{(\theta/2)^4} = h_2 -$$
$$\frac{4}{\theta^2}sen^2\left(\frac{\theta}{2}\right)\left(cos^2\left(\frac{\theta}{2}\right) + sen^2\left(\frac{\theta}{2}\right)\right) = h_2 - 2h_2 = -h_2, \tag{F.26}$$

$$\dot{h}_1 + h_1\dot{h}_2\theta^2 - h_2\dot{h}_1\theta^2 + h_1 h_2(\boldsymbol{\theta} \cdot \dot{\boldsymbol{\theta}}) = \left(\frac{cos\theta - h_1}{\theta}\frac{1}{\theta} + h_1\frac{h_1 - 2h_2}{\theta}\theta - \right.$$
$$\left. h_2\frac{cos\theta - h_1}{\theta}\theta + h_1 h_2\right)(\boldsymbol{\theta} \cdot \dot{\boldsymbol{\theta}}) = \left(\frac{cos\theta}{\theta^2} - \frac{h_1}{\theta^2} + h_1^2 - 2h_1 h_2 - h_2 cos\theta + \right.$$
$$\left. h_1 h_2 + h_1 h_2\right)(\boldsymbol{\theta} \cdot \dot{\boldsymbol{\theta}}) = \left(-\frac{sen\theta}{\theta^3} + \frac{1}{\theta^3}\right)(\boldsymbol{\theta} \cdot \dot{\boldsymbol{\theta}}) = \left(\frac{1 - h_1}{\theta^2}\right)(\boldsymbol{\theta} \cdot \dot{\boldsymbol{\theta}}) =$$
$$h_3(\boldsymbol{\theta} \cdot \dot{\boldsymbol{\theta}}), \tag{F.27}$$

$$\dot{h}_2 - h_1\dot{h}_1 - h_2\dot{h}_2\theta^2 - h_2^2(\boldsymbol{\theta} \cdot \dot{\boldsymbol{\theta}})$$
$$= \left(\frac{h_1 - 2h_2}{\theta}\frac{1}{\theta} - h_1\frac{cos\theta - h_1}{\theta}\frac{1}{\theta} - h_2\frac{h_1 - 2h_2}{\theta}\theta \right.$$
$$\left. - h_2^2\right)(\boldsymbol{\theta} \cdot \dot{\boldsymbol{\theta}})$$
$$= \left(\frac{h_1}{\theta^2} - \frac{2h_2}{\theta^2} - \frac{h_1 cos\theta}{\theta^2} + \frac{h_1^2}{\theta^2} - h_1 h_2 + h_2^2\right)(\boldsymbol{\theta} \cdot \dot{\boldsymbol{\theta}}) \tag{F.28}$$
$$= \left(\frac{sen\theta}{\theta^3} - \frac{2(1 - cos\theta)}{\theta^4} - \frac{sen\theta cos\theta}{\theta^3} + \frac{sen^2\theta}{\theta^4}\right.$$
$$\left. - \frac{sen\theta(1 - cos\theta)}{\theta^3} + \frac{(1 - 2cos\theta + cos^2\theta)}{\theta^4}\right)(\boldsymbol{\theta} \cdot \dot{\boldsymbol{\theta}}) = 0.$$

Therefore

$$\boldsymbol{\Omega} = h_1\dot{\boldsymbol{\Theta}} + h_2\left(\boldsymbol{\Theta}\dot{\boldsymbol{\Theta}} - \dot{\boldsymbol{\Theta}}\boldsymbol{\Theta}\right) + h_3(\boldsymbol{\theta} \cdot \dot{\boldsymbol{\theta}})\boldsymbol{\Theta}. \tag{F.29}$$

Using the properties from equation (F.13), the axial vector is

$$\boldsymbol{\omega} = h_1\dot{\boldsymbol{\theta}} + h_2(\boldsymbol{\theta} \times \dot{\boldsymbol{\theta}}) + h_3(\boldsymbol{\theta} \cdot \dot{\boldsymbol{\theta}})\boldsymbol{\theta} \tag{F.30}$$

Using the result (F.16) and (F.12)

Marcos Pires Kassab

153

Advances on a kinematically exact rod model for thin-walled open section members: consistent warping function and nonlinear constitutive equation

$$\boldsymbol{\omega} = \left(h_1\boldsymbol{I} + h_2\boldsymbol{\Theta} + h_3(\boldsymbol{\Theta\Theta} + \theta^2\boldsymbol{I})\right)\dot{\boldsymbol{\theta}}. \tag{F.31}$$

Further manipulating,

$$\boldsymbol{\omega} = \left((h_1 + \theta^2 h_3)\boldsymbol{I} + h_2\boldsymbol{\Theta} + h_3\boldsymbol{\Theta}^2\right)\dot{\boldsymbol{\theta}}, \tag{F.32}$$

but

$$h_1 + \theta^2 h_3 = h_1 + (1 - h_1) = 1. \tag{F.33}$$

Thus

$$\boldsymbol{\omega} = (\boldsymbol{I} + h_2\boldsymbol{\Theta} + h_3\boldsymbol{\Theta}^2)\dot{\boldsymbol{\theta}} = \boldsymbol{\Gamma}\dot{\boldsymbol{\theta}}. \tag{F.34}$$

Note that, in equation (F.34) the operator

$$\boldsymbol{\Gamma} = (\boldsymbol{I} + h_2\boldsymbol{\Theta} + h_3\boldsymbol{\Theta}^2) \tag{F.35}$$

is defined and is present throughout the whole work.

The derivative of this tensor with respect to a scalar is also relevant. Let us calculate

$$\dot{\boldsymbol{\Gamma}} = \dot{h}_2\boldsymbol{\Theta} + h_2\dot{\boldsymbol{\Theta}} + \dot{h}_3\boldsymbol{\Theta}^2 + h_3(\boldsymbol{\Theta}\dot{\boldsymbol{\Theta}} + \dot{\boldsymbol{\Theta}}\boldsymbol{\Theta}). \tag{F.36}$$

Since

$$\frac{dh_3}{d\theta} = -\frac{2}{\theta^3} - \left(\frac{\theta^3\cos\theta - 3\theta^2 sen\theta}{\theta^6}\right) = \left(\frac{-3 + 3h_1}{\theta^3}\right) + \left(\frac{1 - \cos\theta}{\theta^3}\right) = \frac{h_2 - 3h_3}{\theta}, \tag{F.37}$$

then, defining

$$h_4 = \frac{dh_2}{d\theta}\frac{1}{\theta} = \frac{\theta sen\theta - 2 + 2\cos\theta}{\theta^4} = \frac{h_1 - 2h_2}{\theta^2},$$

$$h_5 = \frac{h_2 - 3h_3}{\theta^2}, \tag{F.38}$$

one gets

$$\dot{\boldsymbol{\Gamma}} = h_2\dot{\boldsymbol{\Theta}} + h_3(\boldsymbol{\Theta}\dot{\boldsymbol{\Theta}} + \dot{\boldsymbol{\Theta}}\boldsymbol{\Theta}) + h_4(\boldsymbol{\theta}\cdot\dot{\boldsymbol{\theta}})\boldsymbol{\Theta} + h_5(\boldsymbol{\theta}\cdot\dot{\boldsymbol{\theta}})\boldsymbol{\Theta}^2. \tag{F.39}$$

The operator $\boldsymbol{\Gamma}$ has some properties, which will not be demonstrated here:

a) $\boldsymbol{\Gamma}$ and $\boldsymbol{Q}$ are commutative, as they share the same eigenvectors. Ibrahimbegovic shows this in [56];

b) $\boldsymbol{Q}^T\boldsymbol{\Gamma} = \boldsymbol{\Gamma}^T \Leftrightarrow \boldsymbol{\Gamma}^T = \boldsymbol{\Gamma}\boldsymbol{Q}^T$. The left-hand side of this demonstration can be done by simply substituting (2.4), (2.5) and (F.35), and using the property $\boldsymbol{\Theta} = -\boldsymbol{\Theta}^T$ and manipulating the expression in terms of h_i. The right-hand side comes from the fact that $\boldsymbol{Q}\boldsymbol{Q}^T\boldsymbol{\Gamma} = \boldsymbol{\Gamma} = \boldsymbol{Q}\boldsymbol{\Gamma}^T \Rightarrow \boldsymbol{\Gamma}^T = \boldsymbol{\Gamma}\boldsymbol{Q}^T$.

The same expressions can be used to derivate the rotation tensor with respect to any scalar. For example, for the coordinate ζ, that indicates the position along a rod axis becomes

$$\boldsymbol{K} = \boldsymbol{Q}'\boldsymbol{Q}^T, \text{ and } \boldsymbol{\kappa} = axial(\boldsymbol{K}), \tag{F.40}$$

$$\boldsymbol{\Omega} = h_1\boldsymbol{\Theta}' + h_2(\boldsymbol{\Theta}\boldsymbol{\Theta}' - \boldsymbol{\Theta}'\boldsymbol{\Theta}) + h_3(\boldsymbol{\theta}\cdot\boldsymbol{\theta}')\boldsymbol{\Theta} \tag{F.41}$$

$$\boldsymbol{\kappa} = \boldsymbol{\Gamma}\boldsymbol{\theta}' \tag{F.42}$$

$$\boldsymbol{\Gamma}' = h_2\boldsymbol{\Theta}' + h_3(\boldsymbol{\Theta}\boldsymbol{\Theta}' + \boldsymbol{\Theta}'\boldsymbol{\Theta}) + h_4(\boldsymbol{\theta}\cdot\boldsymbol{\theta}')\boldsymbol{\Theta} + h_5(\boldsymbol{\theta}\cdot\boldsymbol{\theta}')\boldsymbol{\Theta}^2 \tag{F.43}$$

and those identities are also present throughout the text.

From now on, let us assume t as a constant vector. Then, using the skew-symmetry of $\boldsymbol{\Theta}$, the product $\dot{\boldsymbol{\Gamma}}^T t$ is

$$\dot{\boldsymbol{\Gamma}}^T t = \left(-h_2\dot{\boldsymbol{\Theta}} + h_3\left(\boldsymbol{\Theta}\dot{\boldsymbol{\Theta}} + \dot{\boldsymbol{\Theta}}\boldsymbol{\Theta}\right) - h_4(\boldsymbol{\theta}\cdot\dot{\boldsymbol{\theta}})\boldsymbol{\Theta} + h_5(\boldsymbol{\theta}\cdot\dot{\boldsymbol{\theta}})\boldsymbol{\Theta}^2\right)t. \tag{F.44}$$

Transforming term $\dot{\boldsymbol{\Theta}}t$ in a cross product, and manipulating it

$$\dot{\boldsymbol{\Theta}}t = \dot{\boldsymbol{\theta}}\times t = -t\times\dot{\boldsymbol{\theta}} = -T\dot{\boldsymbol{\theta}}. \tag{F.45}$$

With equations (F.13) and (F.45), the product

$$\left(\boldsymbol{\Theta}\dot{\boldsymbol{\Theta}} + \dot{\boldsymbol{\Theta}}\boldsymbol{\Theta}\right)t = \dot{\boldsymbol{\theta}}\times(\boldsymbol{\Theta}t) - \boldsymbol{\Theta}T\dot{\boldsymbol{\theta}} = -skew(\boldsymbol{\theta}\times t)\dot{\boldsymbol{\theta}} - \boldsymbol{\Theta}T\dot{\boldsymbol{\theta}}$$
$$= -2\boldsymbol{\Theta}T\dot{\boldsymbol{\theta}} - T\boldsymbol{\Theta}\dot{\boldsymbol{\theta}}, \tag{F.46}$$

and with the definition of dyadic product from equation (F.16)

$$\left(\boldsymbol{\theta}\cdot\dot{\boldsymbol{\theta}}\right)\boldsymbol{\Theta}t = (\boldsymbol{\Theta}t\otimes\boldsymbol{\theta})\dot{\boldsymbol{\theta}}$$
$$\left(\boldsymbol{\theta}\cdot\dot{\boldsymbol{\theta}}\right)\boldsymbol{\Theta}^2 t = (\boldsymbol{\Theta}^2 t\otimes\boldsymbol{\theta})\dot{\boldsymbol{\theta}} \tag{F.47}$$

the equation (F.44) becomes

$$\dot{\boldsymbol{\Gamma}}^T t = V(\boldsymbol{\theta},t)\dot{\boldsymbol{\theta}}, \tag{F.48}$$

by defining

$$V(\boldsymbol{\theta},t) = h_2 T + h_3(T\boldsymbol{\Theta} - 2\boldsymbol{\Theta}T) - h_4(\boldsymbol{\Theta}t\otimes\boldsymbol{\theta}) + h_5(\boldsymbol{\Theta}^2 t\otimes\boldsymbol{\theta}) \tag{F.49}$$

An important property used to demonstrate that the geometric tangent operator is symmetric is that

$$V(\boldsymbol{\theta},t) - V^T(\boldsymbol{\theta},t) = \boldsymbol{\Gamma}^T T\boldsymbol{\Gamma} \tag{F.50}$$

since

$$V^T(\boldsymbol{\theta},t) = -h_2 T + h_3(\boldsymbol{\Theta}T - 2T\boldsymbol{\Theta}) - h_4(\boldsymbol{\theta}\otimes\boldsymbol{\Theta}t) + h_5(\boldsymbol{\theta}\otimes\boldsymbol{\Theta}^2 t), \tag{F.51}$$

and, consequently

$$V(\boldsymbol{\theta},t) - V^T(\boldsymbol{\theta},t)$$
$$= 2h_2 T - h_4(\boldsymbol{\Theta}t\otimes\boldsymbol{\theta} - \boldsymbol{\theta}\otimes\boldsymbol{\Theta}t) \tag{F.52}$$
$$+ h_5(\boldsymbol{\Theta}^2 t\otimes\boldsymbol{\theta} - \boldsymbol{\theta}\otimes\boldsymbol{\Theta}^2 t) + 3h_3(T\boldsymbol{\Theta} - \boldsymbol{\Theta}T).$$

Using the identities (F.14) and (F.15),

$$\boldsymbol{\Theta}^2 t\otimes\boldsymbol{\theta} - \boldsymbol{\theta}\otimes\boldsymbol{\Theta}^2 t = skew(\boldsymbol{\theta}\times\boldsymbol{\Theta}^2 t) = skew(\boldsymbol{\Theta}^3 t) = -\theta^2 skew(\boldsymbol{\Theta}t). \tag{F.53}$$

Also, with equation (F.15)

$$\boldsymbol{\Theta}t\otimes\boldsymbol{\theta} - \boldsymbol{\theta}\otimes\boldsymbol{\Theta}t = skew(\boldsymbol{\theta}\times\boldsymbol{\Theta}t) = skew(\boldsymbol{\Theta}^2 t), \tag{F.54}$$

thus

$$V(\boldsymbol{\theta},t) - V^T(\boldsymbol{\theta},t) = 2h_2 T - (3h_3 + \theta^2 h_5)skew(\boldsymbol{\Theta}t) - h_4 skew(\boldsymbol{\Theta}^2 t). \tag{F.55}$$

However, using (F.27) and (F.38), $3h_3 + \theta^2 h_5 = h_2$, and, therefore

$$V(\boldsymbol{\theta},t) - V^T(\boldsymbol{\theta},t) = 2h_2 T - h_2 skew(\boldsymbol{\Theta}t) - h_4 skew(\boldsymbol{\Theta}^2 t), \tag{F.56}$$

which can be rewrite as

Marcos Pires Kassab   155

Advances on a kinematically exact rod model for thin-walled open section members: consistent warping function and nonlinear constitutive equation

$$V(\boldsymbol{\theta}, \boldsymbol{t}) - V^T(\boldsymbol{\theta}, \boldsymbol{t}) = 2h_2 \left[skew(\boldsymbol{t}) - \frac{1}{2} skew(\boldsymbol{\Theta t}) - \frac{h_4}{2h_2} skew(\boldsymbol{\Theta}^2 \boldsymbol{t}) \right]$$

$$= 2h_2 skew \left[\left(\boldsymbol{I} - \frac{1}{2} \boldsymbol{\Theta} - \frac{h_4}{2h_2} \boldsymbol{\Theta}^2 \right) \boldsymbol{t} \right].$$

(F.57)

Using the results of the determinant and inverse of $\boldsymbol{\Gamma}$ (from Ibrahimbegovic [56])

$$det\boldsymbol{\Gamma} = \frac{2(1-cos\theta)}{\theta^2} \text{ and } \boldsymbol{\Gamma}^{-1} = \boldsymbol{I} - \frac{1}{2}\boldsymbol{\Theta} - \frac{h_4}{2h_2}\boldsymbol{\Theta}^2,$$

(F.58)

one gets

$$V(\boldsymbol{\theta}, \boldsymbol{t}) - V^T(\boldsymbol{\theta}, \boldsymbol{t}) = det\boldsymbol{\Gamma} skew(\boldsymbol{\Gamma}^{-1}\boldsymbol{t}).$$

(F.59)

Deducing the Nanson's rule from the Euler's relation for a tensor $\boldsymbol{K}$, with linear independent vectors $\boldsymbol{a}, \boldsymbol{b}, \boldsymbol{c}$

$$det\boldsymbol{K} = \frac{[\boldsymbol{Ka}, \boldsymbol{Kb}, \boldsymbol{Kc}]}{[\boldsymbol{a}, \boldsymbol{b}, \boldsymbol{c}]} \Leftrightarrow det\boldsymbol{K}(\boldsymbol{a} \times \boldsymbol{b}) \cdot \boldsymbol{c} = (\boldsymbol{Ka} \times \boldsymbol{Kb}) \cdot \boldsymbol{Tc} =$$

$$\boldsymbol{K}^T(\boldsymbol{Ka} \times \boldsymbol{Kb}) \cdot \boldsymbol{c} \Rightarrow \boldsymbol{K}^T(\boldsymbol{Ka} \times \boldsymbol{Kb}) = det\boldsymbol{K}(\boldsymbol{a} \times \boldsymbol{b}) \Leftrightarrow skew(\boldsymbol{Ka})\boldsymbol{Kb} =$$

$$det\boldsymbol{K}(\boldsymbol{K}^{-T}\boldsymbol{A})\boldsymbol{b} \Leftrightarrow skew(\boldsymbol{Ka})\boldsymbol{K} = det\boldsymbol{K}(\boldsymbol{K}^{-T}\boldsymbol{A}),$$

(F.60)

and taking $\boldsymbol{\Gamma}^{-1}$ as $\boldsymbol{K}$ and $\boldsymbol{t}$ as $\boldsymbol{A}$, and remembering that $det\boldsymbol{\Gamma}^{-1} = (det\boldsymbol{\Gamma})^{-1}$, equation (F.60) becomes

$$skew(\boldsymbol{\Gamma}^{-1}\boldsymbol{t})\boldsymbol{\Gamma}^{-1} = det\boldsymbol{\Gamma}^{-1}((\boldsymbol{\Gamma}^{-1})^{-T}\boldsymbol{T}) \Rightarrow det\boldsymbol{\Gamma} skew(\boldsymbol{\Gamma}^{-1}\boldsymbol{t}) = \boldsymbol{\Gamma}^T\boldsymbol{T}\boldsymbol{\Gamma},$$

(F.61)

and finally substituting (F.61) in (F.59),

$$V(\boldsymbol{\theta}, \boldsymbol{t}) - V^T(\boldsymbol{\theta}, \boldsymbol{t}) = \boldsymbol{\Gamma}^T\boldsymbol{T}\boldsymbol{\Gamma} \quad \blacksquare.$$

(F.62)

Now, it is of interest to find the derivative of (F.49) along the rod axis

$$\left(\dot{\boldsymbol{\Gamma}}^T \boldsymbol{t} \right)' = V(\boldsymbol{\theta}, \boldsymbol{t})' \dot{\theta} + V(\boldsymbol{\theta}, \boldsymbol{t})\dot{\theta}',$$

(F.63)

with

$$V'(\boldsymbol{\theta}, \boldsymbol{t}) = h_2' \boldsymbol{T} + h_3'(\boldsymbol{T}\boldsymbol{\Theta} - 2\boldsymbol{\Theta}\boldsymbol{T}) + h_3(\boldsymbol{T}\boldsymbol{\Theta}' - 2\boldsymbol{\Theta}'\boldsymbol{T}) - h_4'(\boldsymbol{\Theta t} \otimes \boldsymbol{\theta})$$

$$- h_4(\boldsymbol{\Theta}'\boldsymbol{t} \otimes \boldsymbol{\theta} + \boldsymbol{\Theta t} \otimes \boldsymbol{\theta}') + h_5'(\boldsymbol{\Theta}^2 \boldsymbol{t} \otimes \boldsymbol{\theta})$$

$$+ h_5((\boldsymbol{\Theta}^2)'\boldsymbol{t} \otimes \boldsymbol{\theta} + \boldsymbol{\Theta}^2\boldsymbol{t} \otimes \boldsymbol{\theta}'),$$

(F.64)

and, using the definitions of h_4 and h_5 from (F.38), and further defining another two quantities

$$h_6 = \frac{dh_4}{d\theta}\frac{1}{\theta} = \frac{1}{\theta}\left[\frac{\left(\frac{dh_1}{d\theta} - 2\frac{dh_2}{d\theta} \right)\theta^2 - 2\theta(h_1 - 2h_2)}{\theta^4} \right]$$

$$= \frac{1}{\theta^2}\left[\frac{1 - 5h_1 + 7h_2}{\theta^2} \right] = \frac{1}{\theta^2}[h_3 - h_2 - 4h_4],$$

(F.65)

$$h_7 = \frac{dh_5}{d\theta}\frac{1}{\theta} = \frac{1}{\theta}\left[\frac{\left(\frac{dh_2}{d\theta} - 3\frac{dh_3}{d\theta} \right)\theta^2 - 2\theta(h_2 - 3h_2)}{\theta^4} \right]$$

$$= \frac{1}{\theta^2}\left[\frac{h_1 - 7h_2 - 15h_3}{\theta^2} \right] = \frac{1}{\theta^2}[h_4 - 5h_5],$$

(F.66)

one gets

$$V'(\boldsymbol{\theta}, t) = h_4(\boldsymbol{\theta} \cdot \boldsymbol{\theta}')T + h_3(T\boldsymbol{\Theta}' - 2\boldsymbol{\Theta}'T) + h_5(\boldsymbol{\theta} \cdot \boldsymbol{\theta}')(T\boldsymbol{\Theta} - 2\boldsymbol{\Theta}T)$$
$$- h_4(\boldsymbol{\Theta}'t \otimes \boldsymbol{\theta} + \boldsymbol{\Theta}t \otimes \boldsymbol{\theta}') - h_6(\boldsymbol{\theta} \cdot \boldsymbol{\theta}')(\boldsymbol{\Theta}t \otimes \boldsymbol{\theta})$$
$$+ h_5((\boldsymbol{\Theta}'\boldsymbol{\Theta} + \boldsymbol{\Theta}\boldsymbol{\Theta}')t \otimes \boldsymbol{\theta} + \boldsymbol{\Theta}^2 t \otimes \boldsymbol{\theta}')$$
$$+ h_7(\boldsymbol{\theta} \cdot \boldsymbol{\theta}')(\boldsymbol{\Theta}^2 t \otimes \boldsymbol{\theta}) \tag{F.67}$$

Equation (F.67) can be rewritten as

$$V'(\boldsymbol{\theta}, t) = h_3(T\boldsymbol{\Theta}' - 2\boldsymbol{\Theta}'T) - h_4(\boldsymbol{\Theta}'t \otimes \boldsymbol{\theta} + \boldsymbol{\Theta}t \otimes \boldsymbol{\theta}')$$
$$+ h_5((\boldsymbol{\Theta}'\boldsymbol{\Theta} + \boldsymbol{\Theta}\boldsymbol{\Theta}')t \otimes \boldsymbol{\theta} + \boldsymbol{\Theta}^2 t \otimes \boldsymbol{\theta}')$$
$$+ (\boldsymbol{\theta} \cdot \boldsymbol{\theta}')[h_4 T + h_5(T\boldsymbol{\Theta} - 2\boldsymbol{\Theta}T) - h_6(\boldsymbol{\Theta}t \otimes \boldsymbol{\theta})$$
$$+ h_7(\boldsymbol{\Theta}^2 t \otimes \boldsymbol{\theta})] \tag{F.68}$$

The relation of $V'(\boldsymbol{\theta}, t)$ and $V'^T(\boldsymbol{\theta}, t)$ directly comes from (F.50)

$$V'^T(\boldsymbol{\theta}, t) = V'(\boldsymbol{\theta}, t) - \Gamma'^T T\Gamma - \Gamma^T T\Gamma' \tag{F.69}$$

Advances on a kinematically exact rod model for thin-walled open section members: consistent warping function and nonlinear constitutive equation

APPENDIX G.   DEDUCTION OF THE TANGENT OPERATOR

The tangent operator can be consistently deduced by taking the variation of the equilibrium weak form (linearization), represented by the virtual work theorem for rod (equation (3.39)). Therefore, this operator is the second variation of the work, and can be found with the aid of the derivative of (3.39) with respect to a scalar. For the sake of simplicity, the virtual work from concentrated loads will be neglected, but by using the Dirac delta, its insertion is trivial. Let us perform the derivative with respect to the scalar time:

$$\frac{d}{dt}(\delta W) = \frac{d}{dt}\left(\int_0^L (\boldsymbol{\sigma}^r \cdot \delta\boldsymbol{\varepsilon}^r - \overline{\boldsymbol{q}} \cdot \delta\boldsymbol{d}_\theta)d\zeta\right), \delta\boldsymbol{d}_\theta(\zeta) \in \mathcal{H}_1^0(\Omega) \tag{G.1}$$

Using the product rule,

$$\frac{d}{dt}(\delta W) = \int_0^L (\dot{\boldsymbol{\sigma}}^r \cdot \delta\boldsymbol{\varepsilon}^r + \boldsymbol{\sigma}^r \cdot \delta\dot{\boldsymbol{\varepsilon}}^r - (\dot{\overline{\boldsymbol{q}}}) \cdot \delta\boldsymbol{d}_\theta)d\zeta \tag{G.2}$$

Using the chain rule in the first term

$$\dot{\boldsymbol{\sigma}}^r \cdot \delta\boldsymbol{\varepsilon}^r = \frac{\partial\boldsymbol{\sigma}^r}{\partial\boldsymbol{\varepsilon}^r}\dot{\boldsymbol{\varepsilon}}^r \cdot \delta\boldsymbol{\varepsilon}^r = \boldsymbol{D}\dot{\boldsymbol{\varepsilon}}^r \cdot \delta\boldsymbol{\varepsilon}^r = \boldsymbol{\Psi}\boldsymbol{\Delta}\delta\boldsymbol{d}_\theta \cdot \boldsymbol{D}\boldsymbol{\Psi}\boldsymbol{\Delta}\dot{\boldsymbol{d}}_\theta \tag{G.3}$$

The composition of $\boldsymbol{D}$ was discussed throughout the text, and here, this representation is sufficient. However, the second term must be more carefully treated here. Using the definition $\delta\boldsymbol{\varepsilon}^r = [\delta\boldsymbol{\eta}^r \quad \delta\boldsymbol{\kappa}^r \quad \delta p \quad \delta p']^T$,

$$\boldsymbol{\sigma}^r \cdot \delta\dot{\boldsymbol{\varepsilon}}^r = \boldsymbol{\sigma}^r \cdot \dot{\boldsymbol{\Psi}}\boldsymbol{\Delta}\delta\boldsymbol{d}_\theta = \begin{bmatrix} \boldsymbol{n}^r \\ \boldsymbol{m}^r \\ Q \\ B \end{bmatrix} \cdot \begin{bmatrix} \dot{\boldsymbol{Q}}^T\delta\boldsymbol{u}' + \frac{d}{dt}(\boldsymbol{Q}^T\boldsymbol{Z}'\boldsymbol{\Gamma})\delta\boldsymbol{\theta} \\ \frac{d}{dt}(\boldsymbol{Q}^T\boldsymbol{\Gamma}')\delta\boldsymbol{\theta} + \frac{d}{dt}(\boldsymbol{Q}^T\boldsymbol{\Gamma})\delta\boldsymbol{\theta}' \\ 0 \\ 0 \end{bmatrix}. \tag{G.4}$$

Each one of the components are now expanded. The first one of them is, using the fact that $\boldsymbol{\Omega} = \dot{\boldsymbol{Q}}\boldsymbol{Q}^T = skew(\boldsymbol{\Gamma}\dot{\boldsymbol{\theta}})$

$$\boldsymbol{n}^r \cdot \dot{\boldsymbol{Q}}^T\delta\boldsymbol{u}' = \dot{\boldsymbol{Q}}\boldsymbol{n}^r \cdot \delta\boldsymbol{u}' = skew(\boldsymbol{\Gamma}\dot{\boldsymbol{\theta}})\boldsymbol{Q}\boldsymbol{n}^r \cdot \delta\boldsymbol{u}' = \boldsymbol{\Gamma}\dot{\boldsymbol{\theta}} \times \boldsymbol{n} \cdot \delta\boldsymbol{u}'$$
$$= -\boldsymbol{N}\boldsymbol{\Gamma}\dot{\boldsymbol{\theta}} \cdot \delta\boldsymbol{u}'. \tag{G.5}$$

The second one is

$$\boldsymbol{n}^r \cdot \frac{d}{dt}(\boldsymbol{Q}^T\boldsymbol{Z}'\boldsymbol{\Gamma})\delta\boldsymbol{\theta} = \boldsymbol{n}^r \cdot \left(\dot{\boldsymbol{Q}}^T\boldsymbol{Z}'\boldsymbol{\Gamma} + \boldsymbol{Q}^T\dot{\boldsymbol{Z}}'\boldsymbol{\Gamma} + \boldsymbol{Q}^T\boldsymbol{Z}'\dot{\boldsymbol{\Gamma}}\right)\delta\boldsymbol{\theta}, \tag{G.6}$$

with aid of the equation (F.34), and the definition of $\boldsymbol{\Omega}$,

$$\boldsymbol{n}^r \cdot \dot{\boldsymbol{Q}}^T\boldsymbol{Z}'\boldsymbol{\Gamma}\delta\boldsymbol{\theta} = \boldsymbol{n}^r \cdot \left(skew(\boldsymbol{\Gamma}\dot{\boldsymbol{\theta}})\boldsymbol{Q}\right)^T\boldsymbol{Z}'\boldsymbol{\Gamma}\delta\boldsymbol{\theta} = \boldsymbol{n} \cdot skew(\boldsymbol{\Gamma}\dot{\boldsymbol{\theta}})^T\boldsymbol{Z}'\boldsymbol{\Gamma}\delta\boldsymbol{\theta}$$
$$= \boldsymbol{n} \cdot \left(-\boldsymbol{\Gamma}\dot{\boldsymbol{\theta}} \times \boldsymbol{Z}'\boldsymbol{\Gamma}\delta\boldsymbol{\theta}\right) = -\boldsymbol{Z}'\boldsymbol{\Gamma}\delta\boldsymbol{\theta} \cdot \left(\boldsymbol{n} \times \boldsymbol{\Gamma}\dot{\boldsymbol{\theta}}\right) \tag{G.7}$$
$$= \boldsymbol{\Gamma}^T\boldsymbol{Z}'\boldsymbol{N}\boldsymbol{\Gamma}\dot{\boldsymbol{\theta}} \cdot \delta\boldsymbol{\theta},$$

$$\boldsymbol{n}^r \cdot \boldsymbol{Q}^T\dot{\boldsymbol{Z}}'\boldsymbol{\Gamma}\delta\boldsymbol{\theta} = \boldsymbol{n} \cdot \dot{\boldsymbol{u}}' \times \boldsymbol{\Gamma}\delta\boldsymbol{\theta} = \boldsymbol{\Gamma}^T\boldsymbol{N}\dot{\boldsymbol{u}}' \cdot \delta\boldsymbol{\theta} = -(\boldsymbol{N}\boldsymbol{\Gamma})^T\dot{\boldsymbol{u}}' \cdot \delta\boldsymbol{\theta} \tag{G.8}$$

$$\boldsymbol{n}^r \cdot \boldsymbol{Q}^T\boldsymbol{Z}'\dot{\boldsymbol{\Gamma}}\delta\boldsymbol{\theta} = -\dot{\boldsymbol{\Gamma}}^T\boldsymbol{Z}'\boldsymbol{n} \cdot \delta\boldsymbol{\theta} = -\boldsymbol{V}(\boldsymbol{\theta}, \boldsymbol{z}' \times \boldsymbol{n}) \cdot \delta\boldsymbol{\theta}, \tag{G.9}$$

rendering

$$\boldsymbol{n}^r \cdot \frac{d}{dt}(\boldsymbol{Q}^T\boldsymbol{Z}'\boldsymbol{\Gamma})\delta\boldsymbol{\theta} = \left[\boldsymbol{\Gamma}^T\boldsymbol{Z}'\boldsymbol{N}\boldsymbol{\Gamma}\dot{\boldsymbol{\theta}} - (\boldsymbol{N}\boldsymbol{\Gamma})^T\dot{\boldsymbol{u}}' - \boldsymbol{V}(\boldsymbol{\theta}, \boldsymbol{z}' \times \boldsymbol{n})\right] \cdot \delta\boldsymbol{\theta}. \tag{G.10}$$

158   Marcos Pires Kassab

Advances on a kinematically exact rod model for thin-walled open section members: consistent warping function and nonlinear constitutive equation

The third term is, with the aid of equations (F.34),(F.48), the definition of $\boldsymbol{\Omega}$, and using the property of permutation for triple products,

$$
\begin{aligned}
&\boldsymbol{m}^r \cdot \frac{d}{dt}(\boldsymbol{Q}^T \boldsymbol{\Gamma}') \delta\boldsymbol{\theta} = \boldsymbol{m}^r \cdot \left(\dot{\boldsymbol{Q}}^T \boldsymbol{\Gamma}' + \boldsymbol{Q}^T \dot{\boldsymbol{\Gamma}}'\right) \delta\boldsymbol{\theta} = \boldsymbol{m} \cdot \left(-\boldsymbol{\Gamma}\dot{\boldsymbol{\theta}} \times \boldsymbol{\Gamma}'\delta\boldsymbol{\theta}\right) + \\
&\dot{\boldsymbol{\Gamma}}'^T \boldsymbol{m} \cdot \delta\boldsymbol{\theta} = \left(-\boldsymbol{\Gamma}'\boldsymbol{M}\boldsymbol{\Gamma}\dot{\boldsymbol{\theta}}\right) \cdot \delta\boldsymbol{\theta} + \left(\boldsymbol{V}'(\boldsymbol{\theta},\boldsymbol{m})\dot{\boldsymbol{\theta}} + \boldsymbol{V}(\boldsymbol{\theta},\boldsymbol{m})\dot{\boldsymbol{\theta}}'\right) \cdot \delta\boldsymbol{\theta}.
\end{aligned}
\tag{G.11}
$$

The last term is

$$
\begin{aligned}
&\boldsymbol{m}^r \cdot \frac{d}{dt}(\boldsymbol{Q}^T \boldsymbol{\Gamma}) \delta\boldsymbol{\theta}' = \boldsymbol{m}^r \cdot \left(\dot{\boldsymbol{Q}}^T \boldsymbol{\Gamma} + \boldsymbol{Q}^T \dot{\boldsymbol{\Gamma}}\right) \delta\boldsymbol{\theta}' = \boldsymbol{m} \cdot skew(\boldsymbol{\Gamma}\dot{\boldsymbol{\theta}})^T \boldsymbol{\Gamma}\delta\boldsymbol{\theta}' + \\
&\dot{\boldsymbol{\Gamma}}^T \boldsymbol{m} \cdot \delta\boldsymbol{\theta}' = \left(-\boldsymbol{\Gamma}^T \boldsymbol{M}\boldsymbol{\Gamma}\dot{\boldsymbol{\theta}} + \boldsymbol{V}(\boldsymbol{\theta},\boldsymbol{m})\dot{\boldsymbol{\theta}}\right) \cdot \delta\boldsymbol{\theta}'.
\end{aligned}
\tag{G.12}
$$

Using the result from equations (F.34),(F.48), the definition of $\boldsymbol{\Omega}$, and using the property of permutation for triple products, one gets

$$
\begin{aligned}
\boldsymbol{\sigma}^r \cdot \boldsymbol{\Psi}\boldsymbol{\Delta}\delta\boldsymbol{d}_{\boldsymbol{\theta}} &= -\boldsymbol{N}\boldsymbol{\Gamma}\dot{\boldsymbol{\theta}} \cdot \delta\boldsymbol{u}' - (\boldsymbol{N}\boldsymbol{\Gamma})^T \dot{\boldsymbol{u}}' \cdot \delta\boldsymbol{\theta} + [\boldsymbol{\Gamma}^T \boldsymbol{Z}'\boldsymbol{N}\boldsymbol{\Gamma} - \boldsymbol{V}(\boldsymbol{\theta}, \boldsymbol{z}' \times \boldsymbol{n})]\dot{\boldsymbol{\theta}} \\
&\quad \cdot \delta\boldsymbol{\theta} + (\boldsymbol{V}'(\boldsymbol{\theta},\boldsymbol{m}) - \boldsymbol{\Gamma}'\boldsymbol{M}\boldsymbol{\Gamma})\dot{\boldsymbol{\theta}} \cdot \delta\boldsymbol{\theta} + \boldsymbol{V}(\boldsymbol{\theta},\boldsymbol{m})\dot{\boldsymbol{\theta}}' \cdot \delta\boldsymbol{\theta} \\
&\quad + \left(-\boldsymbol{\Gamma}^T \boldsymbol{M}\boldsymbol{\Gamma} + \boldsymbol{V}(\boldsymbol{\theta},\boldsymbol{m})\right)\dot{\boldsymbol{\theta}} \cdot \delta\boldsymbol{\theta}' = \\
&= -\boldsymbol{N}\boldsymbol{\Gamma}\dot{\boldsymbol{\theta}} \cdot \delta\boldsymbol{u}' + (-\boldsymbol{N}\boldsymbol{\Gamma})^T \dot{\boldsymbol{u}}' \cdot \delta\boldsymbol{\theta} \\
&\quad + [\boldsymbol{\Gamma}^T \boldsymbol{Z}'\boldsymbol{N}\boldsymbol{\Gamma} - \boldsymbol{V}(\boldsymbol{\theta}, \boldsymbol{z}' \times \boldsymbol{n})]\dot{\boldsymbol{\theta}} \cdot \delta\boldsymbol{\theta} + (\boldsymbol{V}'(\boldsymbol{\theta},\boldsymbol{m}) - \boldsymbol{\Gamma}'\boldsymbol{M}\boldsymbol{\Gamma})\dot{\boldsymbol{\theta}} \\
&\quad \cdot \delta\boldsymbol{\theta} + \boldsymbol{V}(\boldsymbol{\theta},\boldsymbol{m})\dot{\boldsymbol{\theta}}' \cdot \delta\boldsymbol{\theta} + \boldsymbol{V}^T(\boldsymbol{\theta},\boldsymbol{m})\dot{\boldsymbol{\theta}} \cdot \delta\boldsymbol{\theta}'
\end{aligned}
\tag{G.13}
$$

Rewriting this expression in a compactly

$$
\boldsymbol{\sigma}^r \cdot \boldsymbol{\Psi}\boldsymbol{\Delta}\delta\boldsymbol{d}_{\boldsymbol{\theta}} = \begin{bmatrix} \delta\boldsymbol{u}' \\ \delta\boldsymbol{\theta} \\ \delta\boldsymbol{\theta}' \\ \delta p \\ \delta p' \end{bmatrix} \cdot \begin{bmatrix} \boldsymbol{O} & \boldsymbol{G}_{u'\theta} & \boldsymbol{O} & \boldsymbol{o} & \boldsymbol{o} \\ \boldsymbol{G}_{\theta u'} & \boldsymbol{G}_{\theta\theta} & \boldsymbol{G}_{\theta\theta'} & \boldsymbol{o} & \boldsymbol{o} \\ \boldsymbol{O} & \boldsymbol{G}_{\theta'\theta} & \boldsymbol{O} & \boldsymbol{o} & \boldsymbol{o} \\ \boldsymbol{o}^T & \boldsymbol{o}^T & \boldsymbol{o}^T & 0 & 0 \\ \boldsymbol{o}^T & \boldsymbol{o}^T & \boldsymbol{o}^T & 0 & 0 \end{bmatrix} \begin{bmatrix} \dot{\boldsymbol{u}}' \\ \dot{\boldsymbol{\theta}} \\ \dot{\boldsymbol{\theta}}' \\ \dot{p} \\ \dot{p}' \end{bmatrix} = \boldsymbol{\Delta}\delta\boldsymbol{d}_{\boldsymbol{\theta}} \cdot
\tag{G.14}
$$

$$
\boldsymbol{G}\boldsymbol{\Delta}\dot{\boldsymbol{d}}_{\boldsymbol{\theta}},
$$

with

$$
\boldsymbol{G}_{u'\theta} = \boldsymbol{G}_{u'\theta}^T = -\boldsymbol{N}\boldsymbol{\Gamma},
$$

$$
\boldsymbol{G}_{\theta\theta'} = \boldsymbol{G}_{\theta'\theta}^T = \boldsymbol{V}(\boldsymbol{\theta},\boldsymbol{m})
\tag{G.15}
$$

$$
\boldsymbol{G}_{\theta\theta} = \boldsymbol{\Gamma}^T \boldsymbol{Z}'\boldsymbol{N}\boldsymbol{\Gamma} - \boldsymbol{V}(\boldsymbol{\theta}, \boldsymbol{z}' \times \boldsymbol{n}) + \boldsymbol{V}'(\boldsymbol{\theta},\boldsymbol{m}) - \boldsymbol{\Gamma}'\boldsymbol{M}\boldsymbol{\Gamma}
$$

Let us now prove that $\boldsymbol{G}_{\theta\theta}$ is symmetric, by analysing $skew(\boldsymbol{G}_{\theta\theta}) = \frac{1}{2}(\boldsymbol{G}_{\theta\theta} - \boldsymbol{G}_{\theta\theta}^T)$. Using equations (F.50), (F.69) and (G.15), and remembering that $skew(\boldsymbol{z}' \times \boldsymbol{n}) = \boldsymbol{Z}'\boldsymbol{N} - \boldsymbol{N}\boldsymbol{Z}'$,

$$
\begin{aligned}
skew(\boldsymbol{G}_{\theta\theta}) &= \frac{1}{2}\big[\boldsymbol{\Gamma}^T \boldsymbol{Z}'\boldsymbol{N}\boldsymbol{\Gamma} - \boldsymbol{V}(\boldsymbol{\theta}, \boldsymbol{z}' \times \boldsymbol{n}) + \boldsymbol{V}'(\boldsymbol{\theta},\boldsymbol{m}) - \boldsymbol{\Gamma}'\boldsymbol{M}\boldsymbol{\Gamma} \\
&\quad - \left(\boldsymbol{\Gamma}^T \boldsymbol{N}\boldsymbol{Z}'\boldsymbol{\Gamma} - \boldsymbol{V}^T(\boldsymbol{\theta}, \boldsymbol{z}' \times \boldsymbol{n}) + \boldsymbol{V}'^T(\boldsymbol{\theta},\boldsymbol{m}) + \boldsymbol{\Gamma}^T \boldsymbol{M}\boldsymbol{\Gamma}'^T\right)\big] \\
&= \frac{1}{2}\big[\left(\boldsymbol{V}^T(\boldsymbol{\theta}, \boldsymbol{z}' \times \boldsymbol{n}) + \boldsymbol{\Gamma}^T(\boldsymbol{Z}'\boldsymbol{N} - \boldsymbol{N}\boldsymbol{Z}')\boldsymbol{\Gamma} - \boldsymbol{V}(\boldsymbol{\theta}, \boldsymbol{z}' \times \boldsymbol{n})\right) \\
&\quad + \boldsymbol{V}'(\boldsymbol{\theta},\boldsymbol{m}) - \left(\boldsymbol{V}'^T(\boldsymbol{\theta},\boldsymbol{m}) + \boldsymbol{\Gamma}'\boldsymbol{M}\boldsymbol{\Gamma} + \boldsymbol{\Gamma}^T \boldsymbol{M}\boldsymbol{\Gamma}'^T\right)\big] = 0.
\end{aligned}
\tag{G.16}
$$

Having proven that $\boldsymbol{G}_{\theta\theta}$ is symmetric, it is now evident that $\boldsymbol{G}$ also is.

Marcos Pires Kassab 159

Advances on a kinematically exact rod model for thin-walled open section members: consistent warping function and nonlinear constitutive equation

Now, it is only left the external loading contribution. Using the chain rule

$$-(\dot{\bar{q}}) \cdot \delta \boldsymbol{d}_\theta = -\delta \boldsymbol{d}_\theta \cdot \frac{\partial \bar{\boldsymbol{q}}}{\partial \boldsymbol{d}_\theta} \dot{\boldsymbol{d}}_\theta = -\delta \boldsymbol{d}_\theta \cdot \boldsymbol{L}_\theta \dot{\boldsymbol{d}}_\theta. \tag{G.17}$$

The structure of $\boldsymbol{L}_\theta$ is as follows

$$\boldsymbol{L}_\theta = \begin{bmatrix} \boldsymbol{L}_{uu} & \boldsymbol{L}_{u\theta} & \boldsymbol{L}_{up} \\ \boldsymbol{L}_{\theta u} & \boldsymbol{L}_{\theta\theta} & \boldsymbol{L}_{p\theta} \\ \boldsymbol{L}_{pu} & \boldsymbol{L}_{p\theta} & \boldsymbol{L}_{pp} \end{bmatrix}, \tag{G.18}$$

with

$$\boldsymbol{L}_{uu} = \frac{\partial \bar{\boldsymbol{n}}}{\partial \boldsymbol{u}} \qquad \boldsymbol{L}_{u\theta} = \frac{\partial \bar{\boldsymbol{n}}}{\partial \boldsymbol{\theta}} \qquad \boldsymbol{L}_{up} = \frac{\partial \bar{\boldsymbol{n}}}{\partial p}$$

$$\boldsymbol{L}_{\theta u} = \frac{\partial \boldsymbol{\Gamma}^T \bar{\boldsymbol{m}}}{\partial \boldsymbol{u}} \qquad \boldsymbol{L}_{\theta\theta} = \frac{\partial \boldsymbol{\Gamma}^T \bar{\boldsymbol{m}}}{\partial \boldsymbol{\theta}} \qquad \boldsymbol{L}_{p\theta} = \frac{\partial \boldsymbol{\Gamma}^T \bar{\boldsymbol{m}}}{\partial p} \tag{G.19}$$

$$\boldsymbol{L}_{pu} = \frac{\partial \bar{B}}{\partial \boldsymbol{u}} \qquad \boldsymbol{L}_{p\theta} = \frac{\partial \bar{B}}{\partial \boldsymbol{\theta}} \qquad \boldsymbol{L}_{pp} = \frac{\partial \bar{B}}{\partial p}$$

Note that the $\boldsymbol{L}_\theta$ is not necessarily symmetric. There is a broad discussion about specific cases for which it might be symmetric, for example, when the load is conservative. It is suggested that the reader sees [22], [1]or [26] for more information.

With the results from equations (G.3), (G.14) and (G.18) it is possible to write the Fréchet derivative of the virtual work in the bilinear form,

$$\delta^2 W = \int_0^L (\boldsymbol{\Psi} \Delta \delta \boldsymbol{d}_\theta \cdot \boldsymbol{D} \boldsymbol{\Psi} \Delta \delta \boldsymbol{d}_\theta + \Delta \delta \boldsymbol{d}_\theta \cdot \boldsymbol{G} \Delta \delta \boldsymbol{d}_\theta - \delta \boldsymbol{d}_\theta \cdot \boldsymbol{L}_\theta \delta \boldsymbol{d}_\theta) d\zeta. \tag{G.20}$$

Due to how each of these contributions is built, the tensors $\boldsymbol{D}, \boldsymbol{G}, \boldsymbol{L}_\theta$ are named, respectively the material, geometric and external loading tangent contributions for the tangent operator.

Marcos Pires Kassab

161

Advances on a kinematically exact rod model for thin-walled open section members: consistent warping function and nonlinear constitutive equation

APPENDIX H.   DEDUCTION OF DERIVATIVES OF THE STRAIN INVARIANTS

The derivatives of the first and second invariants w.r.t to $\boldsymbol{C}$ is easy

$$\frac{\partial I_1}{\partial \boldsymbol{C}} = \frac{\partial (\boldsymbol{I}:\boldsymbol{C})}{\partial \boldsymbol{C}} = \frac{\partial (tr\boldsymbol{C})}{\partial \boldsymbol{C}} = \frac{\partial (C_{kk})}{\partial C_{ij}} e_i^r \otimes e_j^r = 1 e_k^r \otimes e_k^r = \boldsymbol{I} \tag{H.1}$$

$$\frac{\partial I_2}{\partial \boldsymbol{C}} = \frac{1}{2}\frac{\partial (\boldsymbol{I}:\boldsymbol{C}^2)}{\partial \boldsymbol{C}} = \frac{1}{2}\frac{\partial (tr\boldsymbol{C}^2)}{\partial \boldsymbol{C}} = \frac{1}{2}\frac{\partial ((\boldsymbol{C}^2)_{kk})}{\partial C_{ij}} e_i^r \otimes e_j^r = \frac{1}{2}\frac{\partial (C_{kl}C_{lk})}{\partial C_{ij}} e_i^r \otimes e_j^r$$

$$= \frac{1}{2}\left(\frac{\partial (C_{kl})}{\partial C_{ij}}C_{lk} + C_{kl}\frac{\partial (C_{lk})}{\partial C_{ij}}\right) e_i^r \otimes e_j^r \tag{H.2}$$

$$= \frac{1}{2}\left(C_{ji}e_i^r \otimes e_j^r + C_{ji}e_i^r \otimes e_j^r\right) = C_{ji}e_i^r \otimes e_j^r = \boldsymbol{C}^T$$

$$= \boldsymbol{C} \ (\boldsymbol{C} \text{ is symmetric})$$

In order to find the derivatives of I_3, some auxiliar results are needed.

First, let us remember that

$$J = \frac{\boldsymbol{F}v_1 \cdot \boldsymbol{F}v_2 \times \boldsymbol{F}v_3}{v_1 \cdot v_2 \times v_3}. \tag{H.3}$$

Deriving w.r.t a scalar (time, for example). Using the Nanson's rule, for a linear independent constant triplet $\boldsymbol{v}_1, \boldsymbol{v}_2, \boldsymbol{v}_3$

$$\frac{\partial J}{\partial t} = \dot{J} = \frac{\dot{\boldsymbol{F}}v_1 \cdot \boldsymbol{F}v_2 \times \boldsymbol{F}v_3}{v_1 \cdot v_2 \times v_3} + \frac{\boldsymbol{F}v_1 \cdot \dot{\boldsymbol{F}}v_2 \times \boldsymbol{F}v_3}{v_1 \cdot v_2 \times v_3} + \frac{\boldsymbol{F}v_1 \cdot \boldsymbol{F}v_2 \times \dot{\boldsymbol{F}}v_3}{v_1 \cdot v_2 \times v_3} =$$

$$\frac{\dot{\boldsymbol{F}}v_1 \cdot J\boldsymbol{F}^{-T}(v_2 \times v_3) + \dot{\boldsymbol{F}}v_2 \cdot J\boldsymbol{F}^{-T}(v_3 \times v_1) + \dot{\boldsymbol{F}}v_3 \cdot J\boldsymbol{F}^{-T}(v_1 \times v_2)}{v_1 \cdot v_2 \times v_3}. \tag{H.4}$$

Taking $\boldsymbol{v}_i = \boldsymbol{e}_i^r$

$$\frac{\partial J}{\partial t} = \dot{J} = J\left(\dot{\boldsymbol{F}}e_i^r \cdot \boldsymbol{F}^{-T}e_i^r\right) = J\boldsymbol{F}^{-1}\dot{\boldsymbol{F}}(e_i^r \cdot e_i^r) = Jtr\left(\boldsymbol{F}^{-1}\dot{\boldsymbol{F}}\right) =$$

$$J\left(\boldsymbol{I}:\boldsymbol{F}^{-1}\dot{\boldsymbol{F}}\right) = J\left(\boldsymbol{F}^{-T}:\dot{\boldsymbol{F}}\right). \tag{H.5}$$

Now, let us evaluate the following expression

$$\dot{\boldsymbol{C}} = \dot{\boldsymbol{F}}^T\boldsymbol{F} + \boldsymbol{F}^T\dot{\boldsymbol{F}}. \tag{H.6}$$

Using this result,

$$\frac{1}{2}\boldsymbol{C}^{-1}:\dot{\boldsymbol{C}} = \frac{1}{2}\left((\boldsymbol{F}^T\boldsymbol{F})^{-1}:\dot{\boldsymbol{F}}^T\boldsymbol{F} + (\boldsymbol{F}^T\boldsymbol{F})^{-1}:\boldsymbol{F}^T\dot{\boldsymbol{F}}\right) = \frac{1}{2}\left(\boldsymbol{F}^{-1}\boldsymbol{F}^{-T}:\boldsymbol{F}^T\dot{\boldsymbol{F}} + \boldsymbol{F}^{-T}:\dot{\boldsymbol{F}}\right) = \boldsymbol{F}^{-T}:\dot{\boldsymbol{F}}. \tag{H.7}$$

Comparing (H.5) with (H.7), one gets

$$\dot{J} = \left(\frac{J}{2}\boldsymbol{C}^{-1}:\dot{\boldsymbol{C}}\right). \tag{H.8}$$

Revaluating (H.5) using the chain rule, and comparing with (H.8)

$$\dot{J} = \frac{\partial J}{\partial \boldsymbol{C}}:\frac{\partial \boldsymbol{C}}{\partial t} = \left(\frac{J}{2}\boldsymbol{C}^{-1}:\dot{\boldsymbol{C}}\right) \Rightarrow \frac{\partial J}{\partial \boldsymbol{C}} = \frac{J}{2}\boldsymbol{C}^{-1}, \tag{H.9}$$

thus

$$\frac{\partial I_3}{\partial \boldsymbol{C}} = \frac{J}{2}\left(F^{r-1}F^{r-T}\right). \tag{H.10}$$

Marcos Pires Kassab   163

Advances on a kinematically exact rod model for thin-walled open section members: consistent warping function and nonlinear constitutive equation

APPENDIX I. EXACT CONSTITUTIVE EQUATION FOR SAINT-VENANT'S MATERIAL: DEDUCTION FROM [2]

This approach is the one that is actually implemented in PEFSYS, despite being less compact to write in reports.

Let us consider the basic potential expression

$$\psi_h(\boldsymbol{E}) = \tfrac{1}{2}\lambda I_1^2 + 2\mu I_2, \tag{I.1}$$

where I_i are the Green-Lagrange tensor invariants

$$I_1 = tr\boldsymbol{E} = (\boldsymbol{I}:\boldsymbol{E}); \ I_2 = \tfrac{1}{2}tr(\boldsymbol{E}^2); \ I_3 = \tfrac{1}{3}tr(\boldsymbol{E}^3). \tag{I.2}$$

Using the definition (4.1),

$$\boldsymbol{S} = \mathbb{D}\boldsymbol{E} = \lambda(\boldsymbol{I}:\boldsymbol{E})\boldsymbol{I} + 2\mu\boldsymbol{E}, \tag{I.3}$$

where $\boldsymbol{E}$ is Green-Lagrange strain tensor.

Using the definitions of the first ($\boldsymbol{P}$) and second ($\boldsymbol{S}$) Piola-Kirchoff stress tensor

$$\boldsymbol{P} = \boldsymbol{F}\boldsymbol{S} \tag{I.4}$$

and calculating the back-rotated stresses $\boldsymbol{P}^r$, one gets

$$\boldsymbol{P}^r = \boldsymbol{Q}^T\boldsymbol{F}\boldsymbol{S} = \boldsymbol{F}^r\boldsymbol{S} = \boldsymbol{F}^r\{\lambda(\boldsymbol{I}:\boldsymbol{E})\boldsymbol{I} + 2\mu\boldsymbol{E}\}. \tag{I.5}$$

The Green-Lagrange strain tensor ($\boldsymbol{E}$) is computed with the aid of the right Cauchy-Green strain tensor ($\boldsymbol{C} = \boldsymbol{F}^T\boldsymbol{F}$), as

$$\boldsymbol{E} = \tfrac{1}{2}(\boldsymbol{C} - \boldsymbol{I}) = \tfrac{1}{2}\boldsymbol{c}_\alpha \otimes \boldsymbol{e}_\alpha^r + \tfrac{1}{2}\boldsymbol{c}_3 \otimes \boldsymbol{e}_3^r, \tag{I.6}$$

where the vectors $\boldsymbol{c}_i$ are defined in such a way that

$$\begin{aligned}\boldsymbol{C} = \boldsymbol{F}^T\boldsymbol{F} = (\boldsymbol{Q}\boldsymbol{F}^r)^T(\boldsymbol{Q}\boldsymbol{F}^r) = \boldsymbol{F}^{rT}\boldsymbol{Q}^T\boldsymbol{Q}\boldsymbol{F}^r = \boldsymbol{F}^{rT}\boldsymbol{F}^r \\ = \boldsymbol{I} + \boldsymbol{c}_\alpha \otimes \boldsymbol{e}_\alpha^r + \boldsymbol{c}_3 \otimes \boldsymbol{e}_3^r.\end{aligned} \tag{I.7}$$

Let us compute $\boldsymbol{C}$ in terms of the generalised strain measures from equation (3.5). Performing the multiplications

$$\begin{aligned}\boldsymbol{C} = \left(\boldsymbol{I} + p\psi_{,\alpha}\boldsymbol{e}_\alpha^r \otimes \boldsymbol{e}_3^r + \boldsymbol{e}_3^r \otimes \boldsymbol{\gamma}^r\right)\left(\boldsymbol{I} + p\psi_{,\beta}\boldsymbol{e}_3^r \otimes \boldsymbol{e}_\beta^r + \boldsymbol{\gamma}^r \otimes \boldsymbol{e}_3^r\right) = \\ = \boldsymbol{I} + p\psi_{,\beta}\boldsymbol{e}_3^r \otimes \boldsymbol{e}_\beta^r + \boldsymbol{\gamma}^r \otimes \boldsymbol{e}_3^r + p\psi_{,\alpha}\boldsymbol{e}_\alpha^r \otimes \boldsymbol{e}_3^r + p^2\psi_{,\alpha}\psi_{,\beta}\boldsymbol{e}_\alpha^r \otimes \boldsymbol{e}_\beta^r + \\ p\psi_{,\alpha}(\boldsymbol{\gamma}^r \cdot \boldsymbol{e}_3^r)\boldsymbol{e}_\alpha^r \otimes \boldsymbol{e}_3^r + \boldsymbol{e}_3^r \otimes \boldsymbol{\gamma}^r + p\psi_{,\beta}(\boldsymbol{\gamma}^r \cdot \boldsymbol{e}_3^r)\boldsymbol{e}_3^r \otimes \boldsymbol{e}_\beta^r + (\boldsymbol{\gamma}^r \cdot \boldsymbol{\gamma}^r)\boldsymbol{e}_3^r \otimes \boldsymbol{e}_3^r.\end{aligned} \tag{I.8}$$

Rewriting $\boldsymbol{\gamma}^r = (\boldsymbol{\gamma}^r \cdot \boldsymbol{e}_\beta^r)\boldsymbol{e}_\beta^r + (\boldsymbol{\gamma}^r \cdot \boldsymbol{e}_3^r)\boldsymbol{e}_3^r$, then grouping the terms

$$\begin{aligned}\boldsymbol{C} = \boldsymbol{I} + \left(p\psi_{,\alpha}\boldsymbol{e}_3^r + (\boldsymbol{\gamma}^r \cdot \boldsymbol{e}_\beta^r)\boldsymbol{e}_3^r + p\psi_{,\alpha}(\boldsymbol{\gamma}^r \cdot \boldsymbol{e}_3^r)\boldsymbol{e}_3^r + p^2\psi_{,\alpha}\psi_{,\beta}\boldsymbol{e}_\beta^r\right) \otimes \\ \boldsymbol{e}_\alpha^r + \left(\boldsymbol{\gamma}^r + (\boldsymbol{\gamma}^r \cdot \boldsymbol{e}_3^r)\boldsymbol{e}_3^r + (\boldsymbol{\gamma}^r \cdot \boldsymbol{\gamma}^r)\boldsymbol{e}_3^r + p\psi_{,\alpha}\boldsymbol{e}_\alpha^r + p\psi_{,\alpha}(\boldsymbol{\gamma}^r \cdot \boldsymbol{e}_3^r)\boldsymbol{e}_\alpha^r\right) \otimes \boldsymbol{e}_3^r.\end{aligned} \tag{I.9}$$

It is now possible to put in evidence the quantities

$$\begin{aligned}\boldsymbol{c}_\alpha = p\psi_{,\alpha}\boldsymbol{e}_3^r + (\boldsymbol{\gamma}^r \cdot \boldsymbol{e}_\beta^r)\boldsymbol{e}_3^r + p\psi_{,\alpha}(\boldsymbol{\gamma}^r \cdot \boldsymbol{e}_3^r)\boldsymbol{e}_3^r + p^2\psi_{,\alpha}\psi_{,\beta}\boldsymbol{e}_\beta^r \\ \boldsymbol{c}_3 = \boldsymbol{\gamma}^r + (\boldsymbol{\gamma}^r \cdot \boldsymbol{e}_3^r)\boldsymbol{e}_3^r + (\boldsymbol{\gamma}^r \cdot \boldsymbol{\gamma}^r)\boldsymbol{e}_3^r + p\psi_{,\alpha}\boldsymbol{e}_\alpha^r + p\psi_{,\alpha}(\boldsymbol{\gamma}^r \cdot \boldsymbol{e}_3^r)\boldsymbol{e}_\alpha^r.\end{aligned} \tag{I.10}$$

Introducing (3.70) and (3.74) in (3.68)

$$\boldsymbol{P}^r = \lambda(\boldsymbol{I}:\boldsymbol{E})\boldsymbol{I} + \mu \boldsymbol{c}_\alpha \otimes \boldsymbol{e}_\alpha^r + \mu \boldsymbol{c_3} \otimes \boldsymbol{e_3^r} + \lambda(\boldsymbol{I}:\boldsymbol{E})\boldsymbol{\gamma}^r \otimes \boldsymbol{e_3^r} +$$
$$\mu(\boldsymbol{c}_\alpha \cdot \boldsymbol{e_3^r})\boldsymbol{\gamma}^r \otimes \boldsymbol{e}_\alpha^r + \mu(\boldsymbol{c_3} \cdot \boldsymbol{e_3^r})\boldsymbol{\gamma}^r \otimes \boldsymbol{e_3^r} + \lambda(\boldsymbol{I}:\boldsymbol{E})p\psi_{,\alpha}\boldsymbol{e_3^r} \otimes \boldsymbol{e}_\alpha^r + \qquad \text{(I.11)}$$
$$\mu p\psi_{,\beta}(\boldsymbol{c}_\alpha \cdot \boldsymbol{e}_\beta^r)\boldsymbol{e_3^r} \otimes \boldsymbol{e}_\alpha^r + \mu p\psi_{,\alpha}(\boldsymbol{c_3} \cdot \boldsymbol{e}_\alpha^r)\boldsymbol{e_3^r} \otimes \boldsymbol{e_3^r}.$$

Grouping the terms in columns

$$\boldsymbol{P}^r = \lambda(\boldsymbol{I}:\boldsymbol{E})\boldsymbol{e}_i^r \otimes \boldsymbol{e}_i^r + [\mu \boldsymbol{c}_\alpha + \mu(\boldsymbol{c}_\alpha \cdot \boldsymbol{e_3^r})\boldsymbol{\gamma}^r + \lambda(\boldsymbol{I}:\boldsymbol{E})p\psi_{,\alpha}\boldsymbol{e_3^r} +$$
$$\mu p\psi_{,\beta}(\boldsymbol{c}_\alpha \cdot \boldsymbol{e}_\beta^r)\boldsymbol{e_3^r}] \otimes \boldsymbol{e}_\alpha^r + [\mu \boldsymbol{c_3} + \lambda(\boldsymbol{I}:\boldsymbol{E})\boldsymbol{\gamma}^r + \mu(\boldsymbol{c_3} \cdot \boldsymbol{e_3^r})\boldsymbol{\gamma}^r + \qquad \text{(I.12)}$$
$$\mu p\psi_{,\alpha}(\boldsymbol{c_3} \cdot \boldsymbol{e}_\alpha^r)\boldsymbol{e_3^r}] \otimes \boldsymbol{e_3^r},$$

yielding

$$\boldsymbol{\tau}_\alpha^r = \lambda(\boldsymbol{I}:\boldsymbol{E})\boldsymbol{e}_\alpha^r + \mu \boldsymbol{c}_\alpha + \mu(\boldsymbol{c}_\alpha \cdot \boldsymbol{e_3^r})\boldsymbol{\gamma}^r + \lambda(\boldsymbol{I}:\boldsymbol{E})p\psi_{,\alpha}\boldsymbol{e_3^r}$$
$$+ \mu p\psi_{,\beta}(\boldsymbol{c}_\alpha \cdot \boldsymbol{e}_\beta^r)\boldsymbol{e_3^r} \qquad \text{(I.13)}$$
$$\boldsymbol{\tau_3^r} = \lambda(\boldsymbol{I}:\boldsymbol{E})\boldsymbol{e_3^r} + \mu \boldsymbol{c_3} + \lambda(\boldsymbol{I}:\boldsymbol{E})\boldsymbol{\gamma}^r + \mu(\boldsymbol{c_3} \cdot \boldsymbol{e_3^r})\boldsymbol{\gamma}^r + \mu p\psi_{,\alpha}(\boldsymbol{c_3} \cdot \boldsymbol{e}_\alpha^r)\boldsymbol{e_3^r}.$$

The expressions in equation (I.13) are precisely the ones that are employed for obtaining the stress resultants (equation (3.28)) and the constitutive contribution to the tangent stiffness matrix (equation (3.48)) of the rod model. Despite being compactly written, they are in fact enormous expressions with many high order strain terms (of third order), with a wide array of products, not only with the axial, bending, torsion and warping strains, but also with the warping function and its derivatives. Therefore, when those stress vectors are in the integrand of any expression, usually numeric integration is more convenient.

The internal product $\boldsymbol{I}:\boldsymbol{E}$ is

$$\boldsymbol{I}:\boldsymbol{E} = tr(\boldsymbol{E}) = \frac{1}{2}(\boldsymbol{c}_i \cdot \boldsymbol{e}_i^r) = (\boldsymbol{\gamma}^r \cdot \boldsymbol{e_3^r}) + \frac{1}{2}(\boldsymbol{\gamma}^r \cdot \boldsymbol{\gamma}^r) + \frac{1}{2}p^2\psi_{,\beta}^2. \qquad \text{(I.14)}$$

In [2], the stress vectors were further dissected, being then represented by more elemental scalar values that constitute the generalized strain quantities, in order to emphasize the highly non-linear behaviour of this equation. Many of the so-called "Wagner terms" were put into evidence, highlighting the important coupling effects among different strain measures. This will not be done here, since it just represents equation (I.14) (and, consequently, (I.13)) in a less compact manner.

The operators $\boldsymbol{C}_{33}$, $\boldsymbol{c}$, $\boldsymbol{d}$, b_α and d_α for the Saint-Venant's material are defined as

$$\boldsymbol{C}_{33} = \frac{\partial \boldsymbol{\tau_3^r}}{\partial \boldsymbol{\gamma}^r} = \lambda \boldsymbol{e_3^r} \otimes (\boldsymbol{e_3^r} + \boldsymbol{\gamma}^r) + \mu(\boldsymbol{I} + \boldsymbol{e_3^r} \otimes \boldsymbol{e_3^r} + 2\boldsymbol{e_3^r} \otimes \boldsymbol{\gamma}^r +$$
$$p\psi_{,\alpha}\boldsymbol{e}_\alpha^r \otimes \boldsymbol{e_3^r}) + \lambda[\boldsymbol{\gamma}^r \otimes (\boldsymbol{e_3^r} + \boldsymbol{\gamma}^r) + (\boldsymbol{I}:\boldsymbol{E})\boldsymbol{I}] + \mu[\boldsymbol{\gamma}^r \otimes (2\boldsymbol{e_3^r} + 2\boldsymbol{\gamma}^r) +$$
$$(\boldsymbol{c_3} \cdot \boldsymbol{e_3^r})\boldsymbol{I}] + \mu p\psi_{,\alpha}(\boldsymbol{e_3^r} \otimes \boldsymbol{e}_\alpha^r + p\psi_{,\alpha}\boldsymbol{e_3^r} \otimes \boldsymbol{e_3^r}),$$

$$\text{(I.15)}$$

$$\boldsymbol{c} = \frac{\partial \boldsymbol{\tau_3^r}}{\partial p} = \lambda[\boldsymbol{\gamma}^r \cdot (\psi\boldsymbol{\kappa}^r \times \boldsymbol{e_3^r}) + p\psi_{,\beta}^2]\boldsymbol{e_3^r} + \mu[\psi\boldsymbol{\kappa}^r \times \boldsymbol{e_3^r} + 2\psi(\boldsymbol{\gamma}^r \cdot$$
$$(\boldsymbol{\kappa}^r \times \boldsymbol{e_3^r}))\boldsymbol{e_3^r} + \psi_{,\alpha}(1 + \boldsymbol{\gamma}^r \cdot \boldsymbol{e_3^r})\boldsymbol{e}_\alpha^r] + \lambda[(\boldsymbol{\gamma}^r \cdot (\psi\boldsymbol{\kappa}^r \times \boldsymbol{e_3^r}) + p\psi_{,\beta}^2)\boldsymbol{\gamma}^r +$$
$$(\boldsymbol{I}:\boldsymbol{E})\psi\boldsymbol{\kappa}^r \times \boldsymbol{e_3^r}] + \mu[(2\boldsymbol{\gamma}^r \cdot (\psi\boldsymbol{\kappa}^r \times \boldsymbol{e_3^r}))\boldsymbol{\gamma}^r + (\boldsymbol{c_3} \cdot \boldsymbol{e_3^r})(\psi\boldsymbol{\kappa}^r \times \boldsymbol{e_3^r})] +$$

Marcos Pires Kassab 165

Advances on a kinematically exact rod model for thin-walled open section members: consistent warping function and nonlinear constitutive equation

$$\mu\big[\psi_{,\alpha}(\boldsymbol{c}_3 \cdot \boldsymbol{e}_\alpha^r)\boldsymbol{e}_3^r + p\psi_{,\alpha}\big(\boldsymbol{e}_\alpha^r \cdot (\psi\boldsymbol{\kappa}^r \times \boldsymbol{e}_3^r) + 2\boldsymbol{\gamma}^r \cdot (\psi\boldsymbol{\kappa}^r \times \boldsymbol{e}_3^r)\boldsymbol{e}_3^r + \psi_{,\alpha}\boldsymbol{e}_\alpha^r +$$
$$\psi_{,\alpha}(\boldsymbol{\gamma}^r \cdot \boldsymbol{e}_3^r)\boldsymbol{e}_3^r \big)\big],$$

$$\boldsymbol{d} = \frac{\partial \boldsymbol{\tau}_3^r}{\partial p'} = \lambda(\psi + \psi\boldsymbol{\gamma}^r \cdot \boldsymbol{e}_3^r)\boldsymbol{e}_3^r + \mu\big[2\psi\boldsymbol{e}_3^r + 2\psi(\boldsymbol{\gamma}^r \cdot \boldsymbol{e}_3^r)\boldsymbol{e}_3^r +$$
$$p\psi_{,\alpha}\psi\boldsymbol{e}_\alpha^r\big] + \lambda\big[(\psi + \psi\boldsymbol{\gamma}^r \cdot \boldsymbol{e}_3^r)\boldsymbol{\gamma}^r + (\boldsymbol{I}\!:\!\boldsymbol{E})\psi\boldsymbol{e}_3^r\big] + \mu\big[(2\psi + 2\psi\boldsymbol{\gamma}^r \cdot \boldsymbol{e}_3^r)\boldsymbol{\gamma}^r +$$
$$(\boldsymbol{c}_3 \cdot \boldsymbol{e}_3^r)\psi\boldsymbol{e}_3^r\big] + \mu p^2\psi_{,\alpha}^2\psi\boldsymbol{e}_3^r,$$

$$b_\alpha = \frac{\partial(\boldsymbol{\tau}_\alpha^r \cdot \boldsymbol{e}_3^r)}{\partial p} = \mu\big[\psi_{,\alpha} + \boldsymbol{e}_\alpha^r \cdot (\psi\boldsymbol{\kappa}^r \times \boldsymbol{e}_3^r) + \psi_{,\alpha}(\boldsymbol{\gamma}^r \cdot \boldsymbol{e}_3^r)\big] +$$
$$\mu\big[\psi_{,\alpha} + \psi(\boldsymbol{\kappa}^r \times \boldsymbol{e}_3^r) \cdot \boldsymbol{e}_\alpha^r + \psi_{,\alpha}(\boldsymbol{\gamma}^r \cdot \boldsymbol{e}_3^r)\big](\boldsymbol{\gamma}^r \cdot \boldsymbol{e}_3^r) + \lambda\big[\boldsymbol{\gamma}^r \cdot (\psi\boldsymbol{\kappa}^r \times \boldsymbol{e}_3^r) +$$
$$p\psi_{,\beta}^2\big]p\psi_{,\alpha} + \lambda(\boldsymbol{I}\!:\!\boldsymbol{E})\psi_{,\alpha} + \mu\psi_{,\beta}\big[(c_\alpha \cdot e_\beta^r) + 2p^2\psi_{,\beta}\psi_{,\alpha}\big],$$

$$d_\alpha = \frac{\partial(\boldsymbol{\tau}_\alpha^r \cdot \boldsymbol{e}_3^r)}{\partial p'} = \mu\big[p\psi_{,\alpha}\psi\big] + \mu\big[p\psi_{,\alpha}\psi(\boldsymbol{\gamma}^r \cdot \boldsymbol{e}_3^r) + (\boldsymbol{c}_\alpha \cdot \boldsymbol{e}_3^r)\psi\big] +$$
$$\lambda\big[(\psi + \psi\boldsymbol{\gamma}^r \cdot \boldsymbol{e}_3^r)p\psi_{,\alpha}\big].$$

Note that, since $\boldsymbol{\tau}_i^r$ are also polynomials in $\boldsymbol{\varepsilon}^r$, the expressions from (I.15) can also be represented as polynomials in $\boldsymbol{\varepsilon}^r$, having as coefficients products of the material properties and geometric properties (powers of $a_1, a_2, \psi, \psi_{,1}, \psi_{,2}$). Thus, generically speaking, for the Saint-Venant's material, each entry of $\boldsymbol{\sigma}^r$ can be represented by

$$\sigma_i^r = \sum_{j=1}^{k_i} c_j\big(m_j E + n_j G\big) *$$
$$\int_{A^r} F\left(a_1^{r\,(p_1)_j} a_2^{r\,(p_2)_j} \psi^{(p_3)_j} \psi_{,1}^{(p_4)_j} \psi_{,2}^{(p_5)_j}\right) dA^r * \tag{I.16}$$
$$\left(\eta_1^{r\,(w_1)_j} \eta_2^{r\,(w_2)_j} \eta_3^{r\,(w_3)_j} \kappa_1^{r\,(w_4)_j} \kappa_2^{r\,(w_5)_j} \kappa_3^{r\,(w_6)_j} p^{(w_7)_j} p'^{(w_8)_j}\right).$$

with $m_j, n_j, c_j \in \mathbb{R}$ and $(p_i)_j, (w_i)_j \in \mathbb{N}$. Note that $\int_{A^r} F\big(a_1^{p_1} a_2^{p_2} \psi^{p_3} \psi_{,1}^{p_4} \psi_{,2}^{p_5}\big) dA^r$ can be interpreted as a generalized geometric property, which can be calculated only once beforehand. Due to this structure, equation (I.16) is easy to procedurally differentiate, for obtention of the integrands of $\boldsymbol{D}$ (differentiation directly w.r.t η_i^r, κ_i^r, p or p'). By arranging those terms conveniently, the integration of $\boldsymbol{\sigma}^r$ and $\boldsymbol{D}$ can be sped up, since several repeated terms arise. In Table 12, the values for $m_j, n_j, (p_i)_j, (w_i)_j$ are shown, for each of the stress resultants.

Table 12 – Coefficients of equation (I.16) for the Saint-Venant's material

	p_1	p_2	p_3	p_4	p_5	w_1	w_2	w_3	w_4	w_5	w_6	w_7	w_8	ORDER	m_j	n_j	c_j
								Monomials for n_1^r									
1	0	0	0	0	0	1	0	0	0	0	0	0	0	1	0	1	1
2	0	1	0	0	0	0	0	0	0	0	1	0	0	1	0	1	-1
3	0	0	0	1	0	0	0	0	0	0	0	1	0	1	0	1	1
4	0	0	0	0	0	1	0	1	0	0	0	0	0	2	1	0	1

To be continued

Advances on a kinematically exact rod model for thin-walled open section members: consistent warping function and nonlinear constitutive equation

Continued

5	0	1	0	0	0	1	0	0	1	0	0	0	0	2	1	0	1
6	1	0	0	0	0	1	0	0	0	1	0	0	0	2	1	0	-1
7	0	0	1	0	0	1	0	0	0	0	0	0	1	2	1	0	1
8	0	1	0	0	0	0	0	1	0	0	1	0	0	2	1	0	-1
9	0	0	0	1	0	0	0	1	0	0	0	1	0	2	0	1	1
10	0	2	0	0	0	0	0	0	1	0	1	0	0	2	1	0	-1
11	0	1	0	1	0	0	0	0	1	0	0	1	0	2	0	1	1
12	1	1	0	0	0	0	0	0	0	1	1	0	0	2	1	0	1
13	1	0	0	1	0	0	0	0	0	1	0	1	0	2	0	1	-1
14	0	0	1	0	0	0	0	0	0	1	0	1	0	2	0	1	1
15	0	1	1	0	0	0	0	0	0	0	1	0	1	2	1	0	-1
16	0	0	1	1	0	0	0	0	0	0	0	1	1	2	0	1	1
17	0	0	0	0	0	3	0	0	0	0	0	0	0	3	1	0	0,5
18	0	1	0	0	0	2	0	0	0	0	1	0	0	3	1	0	-1,5
19	0	0	0	0	0	1	2	0	0	0	0	0	0	3	1	0	0,5
20	1	0	0	0	0	1	1	0	0	0	1	0	0	3	1	0	1
21	0	0	0	0	0	1	0	2	0	0	0	0	0	3	1	0	0,5
22	0	1	0	0	0	1	0	1	1	0	0	0	0	3	1	0	1
23	1	0	0	0	0	1	0	1	0	1	0	0	0	3	1	0	-1
24	0	0	1	0	0	1	0	1	0	0	0	0	1	3	1	0	1
25	0	2	0	0	0	1	0	0	2	0	0	0	0	3	1	0	0,5
26	1	1	0	0	0	1	0	0	1	1	0	0	0	3	1	0	-1
27	0	1	1	0	0	1	0	0	1	0	0	0	1	3	1	0	1
28	2	0	0	0	0	1	0	0	0	2	0	0	0	3	1	0	0,5
29	1	0	1	0	0	1	0	0	0	1	0	0	1	3	1	0	-1
30	2	0	0	0	0	1	0	0	0	0	2	0	0	3	1	0	0,5
31	0	2	0	0	0	1	0	0	0	0	2	0	0	3	1	0	1,5
32	0	0	0	2	0	1	0	0	0	0	0	2	0	3	1	0	0,5
33	0	0	0	2	0	1	0	0	0	0	0	2	0	3	0	1	-1
34	0	0	0	0	2	1	0	0	0	0	0	2	0	3	1	0	0,5
35	0	0	0	0	2	1	0	0	0	0	0	2	0	3	0	1	-1
36	0	0	2	0	0	1	0	0	0	0	0	0	2	3	1	0	0,5
37	0	1	0	0	0	0	2	0	0	0	1	0	0	3	1	0	-0,5
38	1	1	0	0	0	0	1	0	0	0	2	0	0	3	1	0	-1
39	0	1	0	0	0	0	0	2	0	0	1	0	0	3	1	0	-0,5
40	0	2	0	0	0	0	0	1	1	0	1	0	0	3	1	0	-1
41	1	1	0	0	0	0	0	1	0	1	1	0	0	3	1	0	1
42	0	0	1	0	0	0	0	1	0	1	0	1	0	3	1	0	1
43	0	1	1	0	0	0	0	1	0	0	1	0	1	3	1	0	-1
44	0	3	0	0	0	0	0	0	2	0	1	0	0	3	1	0	-0,5
45	1	2	0	0	0	0	0	0	1	1	1	0	0	3	1	0	1
46	0	1	1	0	0	0	0	0	1	1	0	1	0	3	1	0	1
47	0	2	1	0	0	0	0	0	1	0	1	0	1	3	1	0	-1
48	2	1	0	0	0	0	0	0	0	2	1	0	0	3	1	0	-0,5
49	1	0	1	0	0	0	0	0	0	2	0	1	0	3	1	0	-1

Advances on a kinematically exact rod model for thin-walled open section members: consistent warping function and nonlinear constitutive equation

Continued

50	1	1	1	0	0	0	0	0	0	1	1	0	1	3	1	0	1
51	0	0	2	0	0	0	0	0	0	1	0	1	1	3	1	0	1
52	2	1	0	0	0	0	0	0	0	0	3	0	0	3	1	0	-0,5
53	0	3	0	0	0	0	0	0	0	0	3	0	0	3	1	0	-0,5
54	0	1	0	2	0	0	0	0	0	0	1	2	0	3	1	0	-0,5
55	0	1	0	2	0	0	0	0	0	0	1	2	0	3	0	1	1
56	0	1	0	0	2	0	0	0	0	0	1	2	0	3	1	0	-0,5
57	0	1	0	0	2	0	0	0	0	0	1	2	0	3	0	1	1
58	0	1	2	0	0	0	0	0	0	0	1	0	2	3	1	0	-0,5
59	0	0	1	0	0	2	0	0	0	1	0	1	0	4	1	0	1,5
60	0	0	1	0	0	1	1	0	1	0	0	1	0	4	1	0	-1
61	1	0	1	0	0	1	0	0	1	0	1	1	0	4	1	0	-1
62	0	1	1	0	0	1	0	0	0	1	1	1	0	4	1	0	-3
63	0	0	1	0	0	0	2	0	0	1	0	1	0	4	1	0	0,5
64	0	1	1	0	0	0	1	0	1	0	1	1	0	4	1	0	1
65	1	0	1	0	0	0	1	0	0	1	1	1	0	4	1	0	1
66	0	0	1	0	0	0	0	2	0	1	0	1	0	4	1	0	0,5
67	0	1	1	0	0	0	0	1	1	1	0	1	0	4	1	0	1
68	1	0	1	0	0	0	0	1	0	2	0	1	0	4	1	0	-1
69	0	0	2	0	0	0	0	1	0	1	0	1	1	4	1	0	1
70	0	2	1	0	0	0	0	0	2	1	0	1	0	4	1	0	0,5
71	1	1	1	0	0	0	0	0	1	2	0	1	0	4	1	0	-1
72	0	1	2	0	0	0	0	0	1	1	0	1	1	4	1	0	1
73	1	1	1	0	0	0	0	0	1	0	2	1	0	4	1	0	1
74	2	0	1	0	0	0	0	0	0	3	0	1	0	4	1	0	0,5
75	1	0	2	0	0	0	0	0	0	2	0	1	1	4	1	0	-1
76	2	0	1	0	0	0	0	0	0	1	2	1	0	4	1	0	0,5
77	0	2	1	0	0	0	0	0	0	1	2	1	0	4	1	0	1,5
78	0	0	1	2	0	0	0	0	0	1	0	3	0	4	1	0	0,5
79	0	0	1	2	0	0	0	0	0	1	0	3	0	4	0	1	-1
80	0	0	1	0	2	0	0	0	0	1	0	3	0	4	1	0	0,5
81	0	0	1	0	2	0	0	0	0	1	0	3	0	4	0	1	-1
82	0	0	3	0	0	0	0	0	0	1	0	1	2	4	1	0	0,5
83	0	0	2	0	0	1	0	0	2	0	0	2	0	5	1	0	0,5
84	0	0	2	0	0	1	0	0	0	2	0	2	0	5	1	0	1,5
85	0	0	2	0	0	0	1	0	1	1	0	2	0	5	1	0	-1
86	0	1	2	0	0	0	0	0	2	0	1	2	0	5	1	0	-0,5
87	1	0	2	0	0	0	0	0	1	1	1	2	0	5	1	0	-1
88	0	1	2	0	0	0	0	0	0	2	1	2	0	5	1	0	-1,5
89	0	0	3	0	0	0	0	0	2	1	0	3	0	6	1	0	0,5
90	0	0	3	0	0	0	0	0	0	3	0	3	0	6	1	0	0,5
Monomials for n_2^r																	
1	0	0	0	0	0	0	1	0	0	0	0	0	0	1	0,00	1,00	1,00
2	1	0	0	0	0	0	0	0	0	0	1	0	0	1	0	1,00	1,00
3	0	0	0	0	1	0	0	0	0	0	0	1	0	1	0	1,00	1,00

Advances on a kinematically exact rod model for thin-walled open section members: consistent warping function and nonlinear constitutive equation

Continued

4	0	0	0	0	0	0	1	1	0	0	0	0	0	2	1	0,00	1,00
5	0	1	0	0	0	0	1	0	1	0	0	0	0	2	1	0,00	1,00
6	1	0	0	0	0	0	1	0	0	1	0	0	0	2	1	0,00	-1,00
7	0	0	1	0	0	0	1	0	0	0	0	0	1	2	1	0,00	1,00
8	1	0	0	0	0	0	0	1	0	0	1	0	0	2	1	0,00	1,00
9	0	0	0	0	1	0	0	1	0	0	0	1	0	2	0	1,00	1,00
10	1	1	0	0	0	0	0	0	1	0	1	0	0	2	1	0,00	1,00
11	0	0	1	0	0	0	0	0	1	0	0	1	0	2	0	1,00	-1,00
12	0	1	0	0	1	0	0	0	1	0	0	1	0	2	0	1,00	1,00
13	2	0	0	0	0	0	0	0	0	1	1	0	0	2	1	0,00	-1,00
14	1	0	0	0	1	0	0	0	0	1	0	1	0	2	0	1,00	-1,00
15	1	0	1	0	0	0	0	0	0	0	1	0	1	2	1	0,00	1,00
16	0	0	1	0	1	0	0	0	0	0	0	1	1	2	0	1,00	1,00
17	0	0	0	0	0	2	1	0	0	0	0	0	0	3	1	0,00	0,50
18	1	0	0	0	0	2	0	0	0	0	1	0	0	3	1	0,00	0,50
19	0	1	0	0	0	1	1	0	0	0	1	0	0	3	1	0,00	-1,00
20	1	1	0	0	0	1	0	0	0	0	2	0	0	3	1	0,00	-1,00
21	0	0	0	0	0	0	3	0	0	0	0	0	0	3	1	0,00	0,50
22	1	0	0	0	0	0	2	0	0	0	1	0	0	3	1	0,00	1,50
23	0	0	0	0	0	0	1	2	0	0	0	0	0	3	1	0,00	0,50
24	0	1	0	0	0	0	1	1	1	0	0	0	0	3	1	0,00	1,00
25	1	0	0	0	0	0	1	1	0	1	0	0	0	3	1	0,00	-1,00
26	0	0	1	0	0	0	1	1	0	0	0	0	1	3	1	0,00	1,00
27	0	2	0	0	0	0	1	0	2	0	0	0	0	3	1	0,00	0,50
28	1	1	0	0	0	0	1	0	1	1	0	0	0	3	1	0,00	-1,00
29	0	1	1	0	0	0	1	0	1	0	0	0	1	3	1	0,00	1,00
30	2	0	0	0	0	0	1	0	0	2	0	0	0	3	1	0,00	0,50
31	1	0	1	0	0	0	1	0	0	1	0	0	1	3	1	0,00	-1,00
32	2	0	0	0	0	0	1	0	0	0	2	0	0	3	1	0,00	1,50
33	0	2	0	0	0	0	1	0	0	0	2	0	0	3	1	0,00	0,50
34	0	0	0	2	0	0	1	0	0	0	0	2	0	3	1	0,00	0,50
35	0	0	0	2	0	0	1	0	0	0	0	2	0	3	0	1,00	-1,00
36	0	0	0	0	2	0	1	0	0	0	0	2	0	3	1	0,00	0,50
37	0	0	0	0	2	0	1	0	0	0	0	2	0	3	0	1,00	-1,00
38	0	0	2	0	0	0	1	0	0	0	0	0	2	3	1	0,00	0,50
39	1	0	0	0	0	0	0	2	0	0	1	0	0	3	1	0,00	0,50
40	1	1	0	0	0	0	0	1	1	0	1	0	0	3	1	0,00	1,00
41	0	0	1	0	0	0	0	1	1	0	0	1	0	3	1	0,00	-1,00
42	2	0	0	0	0	0	0	1	0	1	1	0	0	3	1	0,00	-1,00
43	1	0	1	0	0	0	0	1	0	0	1	0	1	3	1	0,00	1,00
44	1	2	0	0	0	0	0	0	2	0	1	0	0	3	1	0,00	0,50
45	0	1	1	0	0	0	0	0	2	0	0	1	0	3	1	0,00	-1,00
46	2	1	0	0	0	0	0	0	1	1	1	0	0	3	1	0,00	-1,00
47	1	0	1	0	0	0	0	0	1	1	0	1	0	3	1	0,00	1,00
48	1	1	1	0	0	0	0	0	1	0	1	0	1	3	1	0,00	1,00

Continued

49	0	0	2	0	0	0	0	0	1	0	0	1	1	3	1	0,00	-1,00
50	3	0	0	0	0	0	0	0	0	2	1	0	0	3	1	0,00	0,50
51	2	0	1	0	0	0	0	0	0	1	1	0	1	3	1	0,00	-1,00
52	3	0	0	0	0	0	0	0	0	0	3	0	0	3	1	0,00	0,50
53	1	2	0	0	0	0	0	0	0	0	3	0	0	3	1	0,00	0,50
54	1	0	0	2	0	0	0	0	0	0	1	2	0	3	1	0,00	0,50
55	1	0	0	2	0	0	0	0	0	0	1	2	0	3	0	1,00	-1,00
56	1	0	0	0	2	0	0	0	0	0	1	2	0	3	1	0,00	0,50
57	1	0	0	0	2	0	0	0	0	0	1	2	0	3	0	1,00	-1,00
58	1	0	2	0	0	0	0	0	0	0	1	0	2	3	1	0,00	0,50
59	0	0	1	0	0	2	0	0	1	0	0	1	0	4	1	0,00	-0,50
60	0	0	1	0	0	1	1	0	0	1	0	1	0	4	1	0,00	1,00
61	0	1	1	0	0	1	0	0	1	0	1	1	0	4	1	0,00	1,00
62	1	0	1	0	0	1	0	0	0	1	1	1	0	4	1	0,00	1,00
63	0	0	1	0	0	0	2	0	1	0	0	1	0	4	1	0,00	-1,50
64	1	0	1	0	0	0	1	0	1	0	1	1	0	4	1	0,00	-3,00
65	0	1	1	0	0	0	1	0	0	1	1	1	0	4	1	0,00	-1,00
66	0	0	1	0	0	0	0	2	1	0	0	1	0	4	1	0,00	-0,50
67	0	1	1	0	0	0	0	1	2	0	0	1	0	4	1	0,00	-1,00
68	1	0	1	0	0	0	0	1	1	1	0	1	0	4	1	0,00	1,00
69	0	0	2	0	0	0	0	1	1	0	0	1	1	4	1	0,00	-1,00
70	0	2	1	0	0	0	0	0	3	0	0	1	0	4	1	0,00	-0,50
71	1	1	1	0	0	0	0	0	2	1	0	1	0	4	1	0,00	1,00
72	0	1	2	0	0	0	0	0	2	0	0	1	1	4	1	0,00	-1,00
73	2	0	1	0	0	0	0	0	1	2	0	1	0	4	1	0,00	-0,50
74	1	0	2	0	0	0	0	0	1	1	0	1	1	4	1	0,00	1,00
75	2	0	1	0	0	0	0	0	1	0	2	1	0	4	1	0,00	-1,50
76	0	2	1	0	0	0	0	0	1	0	2	1	0	4	1	0,00	-0,50
77	0	0	1	2	0	0	0	0	1	0	0	3	0	4	1	0,00	-0,50
78	0	0	1	2	0	0	0	0	1	0	0	3	0	4	0	1,00	1,00
79	0	0	1	0	2	0	0	0	1	0	0	3	0	4	1	0,00	-0,50
80	0	0	1	0	2	0	0	0	1	0	0	3	0	4	0	1,00	1,00
81	0	0	3	0	0	0	0	0	1	0	0	1	2	4	1	0,00	-0,50
82	1	1	1	0	0	0	0	0	0	1	2	1	0	4	1	0,00	-1,00
83	0	0	2	0	0	1	0	0	1	1	0	2	0	5	1	0,00	-1,00
84	0	0	2	0	0	0	1	0	2	0	0	2	0	5	1	0,00	1,50
85	0	0	2	0	0	0	1	0	0	2	0	2	0	5	1	0,00	0,50
86	1	0	2	0	0	0	0	0	2	0	1	2	0	5	1	0,00	1,50
87	0	1	2	0	0	0	0	0	1	1	1	2	0	5	1	0,00	1,00
88	1	0	2	0	0	0	0	0	0	2	1	2	0	5	1	0,00	0,50
89	0	0	3	0	0	0	0	0	3	0	0	3	0	6	1	0,00	-0,50
90	0	0	3	0	0	0	0	0	1	2	0	3	0	6	1	0,00	-0,50

Monomials for n_3^r

1	0	0	0	0	0	0	0	1	0	0	0	0	0	1	1	0	1
2	0	1	0	0	0	0	0	0	1	0	0	0	0	1	1	0	1

Advances on a kinematically exact rod model for thin-walled open section members: consistent warping function and nonlinear constitutive equation

Continued

3	1	0	0	0	0	0	0	0	0	1	0	0	0	1	1	0	-1
4	0	0	1	0	0	0	0	0	0	0	0	0	1	1	1	0	1
5	0	0	0	0	0	2	0	0	0	0	0	0	0	2	1	0	0,5
6	0	1	0	0	0	1	0	0	0	0	1	0	0	2	1	0	-1
7	0	0	0	1	0	1	0	0	0	0	0	1	0	2	0	1	1
8	0	0	0	0	0	0	2	0	0	0	0	0	0	2	1	0	0,5
9	1	0	0	0	0	0	1	0	0	0	1	0	0	2	1	0	1
10	0	0	0	0	1	0	1	0	0	0	0	1	0	2	0	1	1
11	0	0	0	0	0	0	0	2	0	0	0	0	0	2	1	0	1,5
12	0	1	0	0	0	0	0	1	1	0	0	0	0	2	1	0	3
13	1	0	0	0	0	0	0	1	0	1	0	0	0	2	1	0	-3
14	0	0	1	0	0	0	0	1	0	0	0	0	1	2	1	0	3
15	0	2	0	0	0	0	0	0	2	0	0	0	0	2	1	0	1,5
16	1	1	0	0	0	0	0	0	1	1	0	0	0	2	1	0	-3
17	0	1	1	0	0	0	0	0	1	0	0	0	1	2	1	0	3
18	2	0	0	0	0	0	0	0	0	2	0	0	0	2	1	0	1,5
19	1	0	1	0	0	0	0	0	0	1	0	0	1	2	1	0	-3
20	2	0	0	0	0	0	0	0	0	0	2	0	0	2	1	0	0,5
21	0	2	0	0	0	0	0	0	0	0	2	0	0	2	1	0	0,5
22	1	0	0	0	1	0	0	0	0	0	1	1	0	2	0	1	1
23	0	1	0	1	0	0	0	0	0	0	1	1	0	2	0	1	-1
24	0	0	0	2	0	0	0	0	0	0	0	2	0	2	1	0	0,5
25	0	0	0	0	2	0	0	0	0	0	0	2	0	2	1	0	0,5
26	0	0	2	0	0	0	0	0	0	0	0	0	2	2	1	0	1,5
27	0	0	0	0	0	2	0	1	0	0	0	0	0	3	1	0	0,5
28	0	1	0	0	0	2	0	0	1	0	0	0	0	3	1	0	0,5
29	1	0	0	0	0	2	0	0	0	1	0	0	0	3	1	0	-0,5
30	0	0	1	0	0	2	0	0	0	0	0	0	1	3	1	0	0,5
31	0	1	0	0	0	1	0	1	0	0	1	0	0	3	1	0	-1
32	0	2	0	0	0	1	0	0	1	0	1	0	0	3	1	0	-1
33	1	1	0	0	0	1	0	0	0	1	1	0	0	3	1	0	1
34	0	0	1	0	0	1	0	0	0	1	0	1	0	3	1	0	1
35	0	1	1	0	0	1	0	0	0	0	1	0	1	3	1	0	-1
36	0	0	0	0	0	0	2	1	0	0	0	0	0	3	1	0	0,5
37	0	1	0	0	0	0	2	0	1	0	0	0	0	3	1	0	0,5
38	1	0	0	0	0	0	2	0	0	1	0	0	0	3	1	0	-0,5
39	0	0	1	0	0	0	2	0	0	0	0	0	1	3	1	0	0,5
40	1	0	0	0	0	0	1	1	0	0	1	0	0	3	1	0	1
41	1	1	0	0	0	0	1	0	1	0	1	0	0	3	1	0	1
42	0	0	1	0	0	0	1	0	1	0	0	1	0	3	1	0	-1
43	2	0	0	0	0	0	1	0	0	1	1	0	0	3	1	0	-1
44	1	0	1	0	0	0	1	0	0	0	1	0	1	3	1	0	1
45	0	0	0	0	0	0	0	3	0	0	0	0	0	3	1	0	0,5
46	0	1	0	0	0	0	0	2	1	0	0	0	0	3	1	0	1,5
47	1	0	0	0	0	0	0	2	0	1	0	0	0	3	1	0	-1,5

Marcos Pires Kassab 171

Advances on a kinematically exact rod model for thin-walled open section members: consistent warping function and nonlinear constitutive equation

Continued

48	0	0	1	0	0	0	0	2	0	0	0	0	1	3	1	0	1,5
49	0	2	0	0	0	0	0	1	2	0	0	0	0	3	1	0	1,5
50	1	1	0	0	0	0	0	1	1	1	0	0	0	3	1	0	-3
51	0	1	1	0	0	0	0	1	1	0	0	0	1	3	1	0	3
52	2	0	0	0	0	0	0	1	0	2	0	0	0	3	1	0	1,5
53	1	0	1	0	0	0	0	1	0	1	0	0	1	3	1	0	-3
54	2	0	0	0	0	0	0	1	0	0	2	0	0	3	1	0	0,5
55	0	2	0	0	0	0	0	1	0	0	2	0	0	3	1	0	0,5
56	0	0	0	2	0	0	0	1	0	0	0	2	0	3	1	0	0,5
57	0	0	0	0	2	0	0	1	0	0	0	2	0	3	1	0	0,5
58	0	0	2	0	0	0	0	1	0	0	0	0	2	3	1	0	1,5
59	0	3	0	0	0	0	0	0	3	0	0	0	0	3	1	0	0,5
60	1	2	0	0	0	0	0	0	2	1	0	0	0	3	1	0	-1,5
61	0	2	1	0	0	0	0	0	2	0	0	0	1	3	1	0	1,5
62	2	1	0	0	0	0	0	0	1	2	0	0	0	3	1	0	1,5
63	1	1	1	0	0	0	0	0	1	1	0	0	1	3	1	0	-3
64	2	1	0	0	0	0	0	0	1	0	2	0	0	3	1	0	0,5
65	0	3	0	0	0	0	0	0	1	0	2	0	0	3	1	0	0,5
66	1	0	1	0	0	0	0	0	1	0	1	1	0	3	1	0	-1
67	0	0	1	0	1	0	0	0	1	0	0	2	0	3	0	1	-1
68	0	1	0	2	0	0	0	0	1	0	0	2	0	3	1	0	0,5
69	0	1	0	0	2	0	0	0	1	0	0	2	0	3	1	0	0,5
70	0	1	2	0	0	0	0	0	1	0	0	0	2	3	1	0	1,5
71	3	0	0	0	0	0	0	0	0	3	0	0	0	3	1	0	-0,5
72	2	0	1	0	0	0	0	0	0	2	0	0	1	3	1	0	1,5
73	3	0	0	0	0	0	0	0	0	1	2	0	0	3	1	0	-0,5
74	1	2	0	0	0	0	0	0	0	1	2	0	0	3	1	0	-0,5
75	0	1	1	0	0	0	0	0	0	1	1	1	0	3	1	0	-1
76	0	0	1	1	0	0	0	0	0	1	0	2	0	3	0	1	1
77	1	0	0	2	0	0	0	0	0	1	0	2	0	3	1	0	-0,5
78	1	0	0	0	2	0	0	0	0	1	0	2	0	3	1	0	-0,5
79	1	0	2	0	0	0	0	0	0	1	0	0	2	3	1	0	-1,5
80	2	0	1	0	0	0	0	0	0	0	2	0	1	3	1	0	0,5
81	0	2	1	0	0	0	0	0	0	0	2	0	1	3	1	0	0,5
82	0	0	1	2	0	0	0	0	0	0	0	2	1	3	1	0	0,5
83	0	0	1	0	2	0	0	0	0	0	0	2	1	3	1	0	0,5
84	0	0	3	0	0	0	0	0	0	0	0	0	3	3	1	0	0,5
85	0	0	1	0	0	1	0	1	0	1	0	1	0	4	1	0	1
86	0	1	1	0	0	1	0	0	1	1	0	1	0	4	1	0	1
87	1	0	1	0	0	1	0	0	0	2	0	1	0	4	1	0	-1
88	0	0	2	0	0	1	0	0	0	1	0	1	1	4	1	0	1
89	0	0	1	0	0	0	1	1	1	0	0	1	0	4	1	0	-1
90	0	1	1	0	0	0	1	0	2	0	0	1	0	4	1	0	-1
91	1	0	1	0	0	0	1	0	1	1	0	1	0	4	1	0	1
92	0	0	2	0	0	0	1	0	1	0	0	1	1	4	1	0	-1

Advances on a kinematically exact rod model for thin-walled open section members: consistent warping function and nonlinear constitutive equation

Continued

93	1	0	1	0	0	0	0	1	1	0	1	1	0	4	1	0	-1
94	0	1	1	0	0	0	0	1	0	1	1	1	0	4	1	0	-1
95	1	1	1	0	0	0	0	0	2	0	1	1	0	4	1	0	-1
96	0	0	2	0	0	0	0	0	2	0	0	2	0	4	1	0	0,5
97	2	0	1	0	0	0	0	0	1	1	1	1	0	4	1	0	1
98	0	2	1	0	0	0	0	0	1	1	1	1	0	4	1	0	-1
99	1	0	2	0	0	0	0	0	1	0	1	1	1	4	1	0	-1
100	1	1	1	0	0	0	0	0	0	2	1	1	0	4	1	0	1
101	0	0	2	0	0	0	0	0	0	2	0	2	0	4	1	0	0,5
102	0	1	2	0	0	0	0	0	0	1	1	1	1	4	1	0	-1
103	0	0	2	0	0	0	0	1	2	0	0	2	0	5	1	0	0,5
104	0	0	2	0	0	0	0	1	0	2	0	2	0	5	1	0	0,5
105	0	1	2	0	0	0	0	0	3	0	0	2	0	5	1	0	0,5
106	1	0	2	0	0	0	0	0	2	1	0	2	0	5	1	0	-0,5
107	0	0	3	0	0	0	0	0	2	0	0	2	1	5	1	0	0,5
108	0	1	2	0	0	0	0	0	1	2	0	2	0	5	1	0	0,5
109	1	0	2	0	0	0	0	0	0	3	0	2	0	5	1	0	-0,5
110	0	0	3	0	0	0	0	0	0	2	0	2	1	5	1	0	0,5
	Monomials for m_1^r																
1	0	1	0	0	0	0	0	1	0	0	0	0	0	1	1	0	1
2	0	2	0	0	0	0	0	0	1	0	0	0	0	1	1	0	1
3	1	1	0	0	0	0	0	0	0	1	0	0	0	1	1	0	-1
4	0	1	1	0	0	0	0	0	0	0	0	0	1	1	1	0	1
5	0	1	0	0	0	2	0	0	0	0	0	0	0	2	1	0	0,5
6	0	2	0	0	0	1	0	0	0	0	1	0	0	2	1	0	-1
7	0	1	0	1	0	1	0	0	0	0	0	1	0	2	0	1	1
8	0	1	0	0	0	0	2	0	0	0	0	0	0	2	1	0	0,5
9	1	1	0	0	0	0	1	0	0	0	1	0	0	2	1	0	1
10	0	0	1	0	0	0	1	0	0	0	0	1	0	2	0	1	-1
11	0	1	0	0	1	0	1	0	0	0	0	1	0	2	0	1	1
12	0	1	0	0	0	0	0	2	0	0	0	0	0	2	1	0	1,5
13	0	2	0	0	0	0	0	1	1	0	0	0	0	2	1	0	3
14	1	1	0	0	0	0	0	1	0	1	0	0	0	2	1	0	-3
15	0	1	1	0	0	0	0	1	0	0	0	0	1	2	1	0	3
16	0	3	0	0	0	0	0	0	2	0	0	0	0	2	1	0	1,5
17	1	2	0	0	0	0	0	0	1	1	0	0	0	2	1	0	-3
18	0	2	1	0	0	0	0	0	1	0	0	0	1	2	1	0	3
19	2	1	0	0	0	0	0	0	0	2	0	0	0	2	1	0	1,5
20	1	1	1	0	0	0	0	0	0	1	0	0	1	2	1	0	-3
21	2	1	0	0	0	0	0	0	0	0	2	0	0	2	1	0	0,5
22	0	3	0	0	0	0	0	0	0	0	2	0	0	2	1	0	0,5
23	1	0	1	0	0	0	0	0	0	0	1	1	0	2	0	1	-1
24	1	1	0	0	1	0	0	0	0	0	1	1	0	2	0	1	1
25	0	2	0	1	0	0	0	0	0	0	1	1	0	2	0	1	-1
26	0	0	1	0	1	0	0	0	0	0	0	2	0	2	0	1	-1

Advances on a kinematically exact rod model for thin-walled open section members: consistent warping function and nonlinear constitutive equation

Continued

27	0	1	0	2	0	0	0	0	0	0	0	2	0	2	1	0	0,5
28	0	1	0	0	2	0	0	0	0	0	0	2	0	2	1	0	0,5
29	0	1	2	0	0	0	0	0	0	0	0	0	2	2	1	0	1,5
30	0	1	0	0	0	2	0	1	0	0	0	0	0	3	1	0	0,5
31	0	2	0	0	0	2	0	0	1	0	0	0	0	3	1	0	0,5
32	1	1	0	0	0	2	0	0	0	1	0	0	0	3	1	0	-0,5
33	0	1	1	0	0	2	0	0	0	0	0	0	1	3	1	0	0,5
34	0	2	0	0	0	1	0	1	0	0	1	0	0	3	1	0	-1
35	0	3	0	0	0	1	0	0	1	0	1	0	0	3	1	0	-1
36	1	2	0	0	0	1	0	0	0	1	1	0	0	3	1	0	1
37	0	1	1	0	0	1	0	0	0	1	0	1	0	3	1	0	1
38	0	2	1	0	0	1	0	0	0	0	1	0	1	3	1	0	-1
39	0	1	0	0	0	0	2	1	0	0	0	0	0	3	1	0	0,5
40	0	2	0	0	0	0	2	0	1	0	0	0	0	3	1	0	0,5
41	1	1	0	0	0	0	2	0	0	1	0	0	0	3	1	0	-0,5
42	0	1	1	0	0	0	2	0	0	0	0	0	1	3	1	0	0,5
43	1	1	0	0	0	0	1	1	0	0	1	0	0	3	1	0	1
44	0	0	1	0	0	0	1	1	0	0	0	1	0	3	1	0	1
45	1	2	0	0	0	0	1	0	1	0	1	0	0	3	1	0	1
46	0	1	1	0	0	0	1	0	1	0	0	1	0	3	1	0	-2
47	2	1	0	0	0	0	1	0	0	1	1	0	0	3	1	0	-1
48	1	0	1	0	0	0	1	0	0	1	0	1	0	3	1	0	1
49	1	1	1	0	0	0	1	0	0	0	1	0	1	3	1	0	1
50	0	0	2	0	0	0	1	0	0	0	0	1	1	3	1	0	-1
51	0	1	0	0	0	0	0	3	0	0	0	0	0	3	1	0	0,5
52	0	2	0	0	0	0	0	2	1	0	0	0	0	3	1	0	1,5
53	1	1	0	0	0	0	0	2	0	1	0	0	0	3	1	0	-1,5
54	0	1	1	0	0	0	0	2	0	0	0	0	1	3	1	0	1,5
55	0	3	0	0	0	0	0	1	2	0	0	0	0	3	1	0	1,5
56	1	2	0	0	0	0	0	1	1	1	0	0	0	3	1	0	-3
57	0	2	1	0	0	0	0	1	1	0	0	0	1	3	1	0	3
58	2	1	0	0	0	0	0	1	0	2	0	0	0	3	1	0	1,5
59	1	1	1	0	0	0	0	1	0	1	0	0	1	3	1	0	-3
60	2	1	0	0	0	0	0	1	0	0	2	0	0	3	1	0	0,5
61	0	3	0	0	0	0	0	1	0	0	2	0	0	3	1	0	0,5
62	1	0	1	0	0	0	0	1	0	0	1	1	0	3	1	0	-1
63	0	0	1	0	1	0	0	1	0	0	0	2	0	3	0	1	-1
64	0	1	0	2	0	0	0	1	0	0	0	2	0	3	1	0	0,5
65	0	1	0	0	2	0	0	1	0	0	0	2	0	3	1	0	0,5
66	0	1	2	0	0	0	0	1	0	0	0	0	2	3	1	0	1,5
67	0	4	0	0	0	0	0	0	3	0	0	0	0	3	1	0	0,5
68	1	3	0	0	0	0	0	0	2	1	0	0	0	3	1	0	-1,5
69	0	3	1	0	0	0	0	0	2	0	0	0	1	3	1	0	1,5
70	2	2	0	0	0	0	0	0	1	2	0	0	0	3	1	0	1,5
71	1	2	1	0	0	0	0	0	1	1	0	0	1	3	1	0	-3

Advances on a kinematically exact rod model for thin-walled open section members: consistent warping function and nonlinear constitutive equation

Continued

72	2	2	0	0	0	0	0	0	1	0	2	0	0	3	1	0	0,5
73	0	4	0	0	0	0	0	0	1	0	2	0	0	3	1	0	0,5
74	1	1	1	0	0	0	0	0	1	0	1	1	0	3	1	0	-2
75	0	0	2	0	0	0	0	0	1	0	0	2	0	3	0	1	1
76	0	1	1	0	1	0	0	0	1	0	0	2	0	3	0	1	-2
77	0	2	0	2	0	0	0	0	1	0	0	2	0	3	1	0	0,5
78	0	2	0	0	2	0	0	0	1	0	0	2	0	3	1	0	0,5
79	0	2	2	0	0	0	0	0	1	0	0	0	2	3	1	0	1,5
80	3	1	0	0	0	0	0	0	0	3	0	0	0	3	1	0	-0,5
81	2	1	1	0	0	0	0	0	0	2	0	0	1	3	1	0	1,5
82	3	1	0	0	0	0	0	0	0	1	2	0	0	3	1	0	-0,5
83	1	3	0	0	0	0	0	0	0	1	2	0	0	3	1	0	-0,5
84	2	0	1	0	0	0	0	0	0	1	1	1	0	3	1	0	1
85	0	2	1	0	0	0	0	0	0	1	1	1	0	3	1	0	-1
86	1	0	1	0	1	0	0	0	0	1	0	2	0	3	0	1	1
87	0	1	1	1	0	0	0	0	0	1	0	2	0	3	0	1	1
88	1	1	0	2	0	0	0	0	0	1	0	2	0	3	1	0	-0,5
89	1	1	0	0	2	0	0	0	0	1	0	2	0	3	1	0	-0,5
90	1	1	2	0	0	0	0	0	0	1	0	0	2	3	1	0	-1,5
91	2	1	1	0	0	0	0	0	0	0	2	0	1	3	1	0	0,5
92	0	3	1	0	0	0	0	0	0	0	2	0	1	3	1	0	0,5
93	1	0	2	0	0	0	0	0	0	0	1	1	1	3	1	0	-1
94	0	0	2	0	1	0	0	0	0	0	0	2	1	3	0	1	-1
95	0	1	1	2	0	0	0	0	0	0	0	2	1	3	1	0	0,5
96	0	1	1	0	2	0	0	0	0	0	0	2	1	3	1	0	0,5
97	0	1	3	0	0	0	0	0	0	0	0	0	3	3	1	0	0,5
98	0	0	1	0	0	2	1	0	0	0	0	1	0	4	1	0	-0,5
99	1	0	1	0	0	2	0	0	0	0	1	1	0	4	1	0	-0,5
100	0	1	1	0	0	1	1	0	0	0	1	1	0	4	1	0	1
101	0	1	1	0	0	1	0	1	0	1	0	1	0	4	1	0	1
102	0	2	1	0	0	1	0	0	1	1	0	1	0	4	1	0	1
103	1	1	1	0	0	1	0	0	0	2	0	1	0	4	1	0	-1
104	0	1	2	0	0	1	0	0	0	1	0	1	1	4	1	0	1
105	1	1	1	0	0	1	0	0	0	0	2	1	0	4	1	0	1
106	0	0	1	0	0	0	3	0	0	0	0	1	0	4	1	0	-0,5
107	1	0	1	0	0	0	2	0	0	0	1	1	0	4	1	0	-1,5
108	0	0	1	0	0	0	1	2	0	0	0	1	0	4	1	0	-0,5
109	0	1	1	0	0	0	1	1	1	0	0	1	0	4	1	0	-2
110	1	0	1	0	0	0	1	1	0	1	0	1	0	4	1	0	1
111	0	0	2	0	0	0	1	1	0	0	0	1	1	4	1	0	-1
112	0	2	1	0	0	0	1	0	2	0	0	1	0	4	1	0	-1,5
113	1	1	1	0	0	0	1	0	1	1	0	1	0	4	1	0	2
114	0	1	2	0	0	0	1	0	1	0	0	1	1	4	1	0	-2
115	2	0	1	0	0	0	1	0	0	2	0	1	0	4	1	0	-0,5
116	1	0	2	0	0	0	1	0	0	1	0	1	1	4	1	0	1

Marcos Pires Kassab 175

Advances on a kinematically exact rod model for thin-walled open section members: consistent warping function and nonlinear constitutive equation

Continued

117	2	0	1	0	0	0	1	0	0	0	2	1	0	4	1	0	-1,5
118	0	2	1	0	0	0	1	0	0	0	2	1	0	4	1	0	-0,5
119	0	0	1	2	0	0	1	0	0	0	0	3	0	4	1	0	-0,5
120	0	0	1	2	0	0	1	0	0	0	0	3	0	4	0	1	1
121	0	0	1	0	2	0	1	0	0	0	0	3	0	4	1	0	-0,5
122	0	0	1	0	2	0	1	0	0	0	0	3	0	4	0	1	1
123	0	0	3	0	0	0	1	0	0	0	0	1	2	4	1	0	-0,5
124	1	0	1	0	0	0	0	2	0	0	1	1	0	4	1	0	-0,5
125	1	1	1	0	0	0	0	1	1	0	1	1	0	4	1	0	-2
126	0	0	2	0	0	0	0	1	1	0	0	2	0	4	1	0	1
127	2	0	1	0	0	0	0	1	0	1	1	1	0	4	1	0	1
128	0	2	1	0	0	0	0	1	0	1	1	1	0	4	1	0	-1
129	1	0	2	0	0	0	0	1	0	0	1	1	1	4	1	0	-1
130	1	2	1	0	0	0	0	0	2	0	1	1	0	4	1	0	-1,5
131	0	1	2	0	0	0	0	0	2	0	0	2	0	4	1	0	1,5
132	2	1	1	0	0	0	0	0	1	1	1	1	0	4	1	0	2
133	0	3	1	0	0	0	0	0	1	1	1	1	0	4	1	0	-1
134	1	0	2	0	0	0	0	0	1	1	0	2	0	4	1	0	-1
135	1	1	2	0	0	0	0	0	1	0	1	1	1	4	1	0	-2
136	0	0	3	0	0	0	0	0	1	0	0	2	1	4	1	0	1
137	3	0	1	0	0	0	0	0	0	2	1	1	0	4	1	0	-0,5
138	1	2	1	0	0	0	0	0	0	2	1	1	0	4	1	0	1
139	0	1	2	0	0	0	0	0	0	2	0	2	0	4	1	0	0,5
140	2	0	2	0	0	0	0	0	0	1	1	1	1	4	1	0	1
141	0	2	2	0	0	0	0	0	0	1	1	1	1	4	1	0	-1
142	3	0	1	0	0	0	0	0	0	0	3	1	0	4	1	0	-0,5
143	1	2	1	0	0	0	0	0	0	0	3	1	0	4	1	0	-0,5
144	1	0	1	2	0	0	0	0	0	0	1	3	0	4	1	0	-0,5
145	1	0	1	2	0	0	0	0	0	0	1	3	0	4	0	1	1
146	1	0	1	0	2	0	0	0	0	0	1	3	0	4	1	0	-0,5
147	1	0	1	0	2	0	0	0	0	0	1	3	0	4	0	1	1
148	1	0	3	0	0	0	0	0	0	0	1	1	2	4	1	0	-0,5
149	0	0	2	0	0	2	0	0	1	0	0	2	0	5	1	0	0,5
150	0	0	2	0	0	1	1	0	0	1	0	2	0	5	1	0	-1
151	0	1	2	0	0	1	0	0	1	0	1	2	0	5	1	0	-1
152	1	0	2	0	0	1	0	0	0	1	1	2	0	5	1	0	-1
153	0	0	2	0	0	0	2	0	1	0	0	2	0	5	1	0	1,5
154	1	0	2	0	0	0	1	0	1	0	1	2	0	5	1	0	3
155	0	1	2	0	0	0	1	0	0	1	1	2	0	5	1	0	1
156	0	0	2	0	0	0	0	2	1	0	0	2	0	5	1	0	0,5
157	0	1	2	0	0	0	0	1	2	0	0	2	0	5	1	0	1,5
158	1	0	2	0	0	0	0	1	1	1	0	2	0	5	1	0	-1
159	0	0	3	0	0	0	0	1	1	0	0	2	1	5	1	0	1
160	0	1	2	0	0	0	0	1	0	2	0	2	0	5	1	0	0,5
161	0	2	2	0	0	0	0	0	3	0	0	2	0	5	1	0	1

Continued

162	1	1	2	0	0	0	0	0	2	1	0	2	0	5	1	0	-1,5
163	0	1	3	0	0	0	0	0	2	0	0	2	1	5	1	0	1,5
164	2	0	2	0	0	0	0	0	1	2	0	2	0	5	1	0	0,5
165	0	2	2	0	0	0	0	0	1	2	0	2	0	5	1	0	0,5
166	1	0	3	0	0	0	0	0	1	1	0	2	1	5	1	0	-1
167	2	0	2	0	0	0	0	0	1	0	2	2	0	5	1	0	1,5
168	0	2	2	0	0	0	0	0	1	0	2	2	0	5	1	0	0,5
169	0	0	2	2	0	0	0	0	1	0	0	4	0	5	1	0	0,5
170	0	0	2	2	0	0	0	0	1	0	0	4	0	5	0	1	-1
171	0	0	2	0	2	0	0	0	1	0	0	4	0	5	1	0	0,5
172	0	0	2	0	2	0	0	0	1	0	0	4	0	5	0	1	-1
173	0	0	4	0	0	0	0	0	1	0	0	2	2	5	1	0	0,5
174	1	1	2	0	0	0	0	0	0	3	0	2	0	5	1	0	-0,5
175	0	1	3	0	0	0	0	0	0	2	0	2	1	5	1	0	0,5
176	1	1	2	0	0	0	0	0	0	1	2	2	0	5	1	0	1
177	0	0	3	0	0	1	0	0	1	1	0	3	0	6	1	0	1
178	0	0	3	0	0	0	1	0	2	0	0	3	0	6	1	0	-1,5
179	0	0	3	0	0	0	1	0	0	2	0	3	0	6	1	0	-0,5
180	1	0	3	0	0	0	0	0	2	0	1	3	0	6	1	0	-1,5
181	0	1	3	0	0	0	0	0	1	1	1	3	0	6	1	0	-1
182	1	0	3	0	0	0	0	0	0	2	1	3	0	6	1	0	-0,5
183	0	0	4	0	0	0	0	0	3	0	0	4	0	7	1	0	0,5
184	0	0	4	0	0	0	0	0	1	2	0	4	0	7	1	0	0,5
	Monomials for m_2^r																
1	1	0	0	0	0	0	0	1	0	0	0	0	0	1	1	0	-1
2	1	1	0	0	0	0	0	0	1	0	0	0	0	1	1	0	-1
3	2	0	0	0	0	0	0	0	0	1	0	0	0	1	1	0	1
4	1	0	1	0	0	0	0	0	0	0	0	0	1	1	1	0	-1
5	1	0	0	0	0	2	0	0	0	0	0	0	0	2	1	0	-0,5
6	1	1	0	0	0	1	0	0	0	0	1	0	0	2	1	0	1
7	0	0	1	0	0	1	0	0	0	0	0	1	0	2	0	1	1
8	1	0	0	1	0	1	0	0	0	0	0	1	0	2	0	1	-1
9	1	0	0	0	0	0	2	0	0	0	0	0	0	2	1	0	-0,5
10	2	0	0	0	0	0	1	0	0	0	1	0	0	2	1	0	-1
11	1	0	0	0	1	0	1	0	0	0	0	1	0	2	0	1	-1
12	1	0	0	0	0	0	0	2	0	0	0	0	0	2	1	0	-1,5
13	1	1	0	0	0	0	0	1	1	0	0	0	0	2	1	0	-3
14	2	0	0	0	0	0	0	1	0	1	0	0	0	2	1	0	3
15	1	0	1	0	0	0	0	1	0	0	0	0	1	2	1	0	-3
16	1	2	0	0	0	0	0	0	2	0	0	0	0	2	1	0	-1,5
17	2	1	0	0	0	0	0	0	1	1	0	0	0	2	1	0	3
18	1	1	1	0	0	0	0	0	1	0	0	0	1	2	1	0	-3
19	3	0	0	0	0	0	0	0	0	2	0	0	0	2	1	0	-1,5
20	2	0	1	0	0	0	0	0	0	1	0	0	1	2	1	0	3
21	3	0	0	0	0	0	0	0	0	0	2	0	0	2	1	0	-0,5

Continued

22	1	2	0	0	0	0	0	0	0	0	2	0	0	2	1	0	-0,5
23	0	1	1	0	0	0	0	0	0	0	1	1	0	2	0	1	-1
24	2	0	0	0	1	0	0	0	0	0	1	1	0	2	0	1	-1
25	1	1	0	1	0	0	0	0	0	0	1	1	0	2	0	1	1
26	0	0	1	1	0	0	0	0	0	0	0	2	0	2	0	1	1
27	1	0	0	2	0	0	0	0	0	0	0	2	0	2	1	0	-0,5
28	1	0	0	0	2	0	0	0	0	0	0	2	0	2	1	0	-0,5
29	1	0	2	0	0	0	0	0	0	0	0	0	2	2	1	0	-1,5
30	1	0	0	0	0	2	0	1	0	0	0	0	0	3	1	0	-0,5
31	1	1	0	0	0	2	0	0	1	0	0	0	0	3	1	0	-0,5
32	2	0	0	0	0	2	0	0	0	1	0	0	0	3	1	0	0,5
33	1	0	1	0	0	2	0	0	0	0	0	0	1	3	1	0	-0,5
34	1	1	0	0	0	1	0	1	0	0	1	0	0	3	1	0	1
35	0	0	1	0	0	1	0	1	0	0	0	1	0	3	1	0	1
36	1	2	0	0	0	1	0	0	1	0	1	0	0	3	1	0	1
37	0	1	1	0	0	1	0	0	1	0	0	1	0	3	1	0	1
38	2	1	0	0	0	1	0	0	0	1	1	0	0	3	1	0	-1
39	1	0	1	0	0	1	0	0	0	1	0	1	0	3	1	0	-2
40	1	1	1	0	0	1	0	0	0	0	1	0	1	3	1	0	1
41	0	0	2	0	0	1	0	0	0	0	0	1	1	3	1	0	1
42	1	0	0	0	0	0	2	1	0	0	0	0	0	3	1	0	-0,5
43	1	1	0	0	0	0	2	0	1	0	0	0	0	3	1	0	-0,5
44	2	0	0	0	0	0	2	0	0	1	0	0	0	3	1	0	0,5
45	1	0	1	0	0	0	2	0	0	0	0	0	1	3	1	0	-0,5
46	2	0	0	0	0	0	1	1	0	0	1	0	0	3	1	0	-1
47	2	1	0	0	0	0	1	0	1	0	1	0	0	3	1	0	-1
48	1	0	1	0	0	0	1	0	1	0	0	1	0	3	1	0	1
49	3	0	0	0	0	0	1	0	0	1	1	0	0	3	1	0	1
50	2	0	1	0	0	0	1	0	0	0	1	0	1	3	1	0	-1
51	1	0	0	0	0	0	0	3	0	0	0	0	0	3	1	0	-0,5
52	1	1	0	0	0	0	0	2	1	0	0	0	0	3	1	0	-1,5
53	2	0	0	0	0	0	0	2	0	1	0	0	0	3	1	0	1,5
54	1	0	1	0	0	0	0	2	0	0	0	0	1	3	1	0	-1,5
55	1	2	0	0	0	0	0	1	2	0	0	0	0	3	1	0	-1,5
56	2	1	0	0	0	0	0	1	1	1	0	0	0	3	1	0	3
57	1	1	1	0	0	0	0	1	1	0	0	0	1	3	1	0	-3
58	3	0	0	0	0	0	0	1	0	2	0	0	0	3	1	0	-1,5
59	2	0	1	0	0	0	0	1	0	1	0	0	1	3	1	0	3
60	3	0	0	0	0	0	0	1	0	0	2	0	0	3	1	0	-0,5
61	1	2	0	0	0	0	0	1	0	0	2	0	0	3	1	0	-0,5
62	0	1	1	0	0	0	0	1	0	0	1	1	0	3	1	0	-1
63	0	0	1	1	0	0	0	1	0	0	0	2	0	3	0	1	1
64	1	0	0	2	0	0	0	1	0	0	0	2	0	3	1	0	-0,5
65	1	0	0	0	2	0	0	1	0	0	0	2	0	3	1	0	-0,5
66	1	0	2	0	0	0	0	1	0	0	0	0	2	3	1	0	-1,5

Advances on a kinematically exact rod model for thin-walled open section members: consistent warping function and nonlinear constitutive equation

Continued

67	1	3	0	0	0	0	0	0	3	0	0	0	0	3	1	0	-0,5
68	2	2	0	0	0	0	0	0	2	1	0	0	0	3	1	0	1,5
69	1	2	1	0	0	0	0	0	2	0	0	0	1	3	1	0	-1,5
70	3	1	0	0	0	0	0	0	1	2	0	0	0	3	1	0	-1,5
71	2	1	1	0	0	0	0	0	1	1	0	0	1	3	1	0	3
72	3	1	0	0	0	0	0	0	1	0	2	0	0	3	1	0	-0,5
73	1	3	0	0	0	0	0	0	1	0	2	0	0	3	1	0	-0,5
74	2	0	1	0	0	0	0	0	1	0	1	1	0	3	1	0	1
75	0	2	1	0	0	0	0	0	1	0	1	1	0	3	1	0	-1
76	1	0	1	0	1	0	0	0	1	0	0	2	0	3	0	1	1
77	0	1	1	1	0	0	0	0	1	0	0	2	0	3	0	1	1
78	1	1	0	2	0	0	0	0	1	0	0	2	0	3	1	0	-0,5
79	1	1	0	0	2	0	0	0	1	0	0	2	0	3	1	0	-0,5
80	1	1	2	0	0	0	0	0	1	0	0	0	2	3	1	0	-1,5
81	4	0	0	0	0	0	0	0	0	3	0	0	0	3	1	0	0,5
82	3	0	1	0	0	0	0	0	0	2	0	0	1	3	1	0	-1,5
83	4	0	0	0	0	0	0	0	0	1	2	0	0	3	1	0	0,5
84	2	2	0	0	0	0	0	0	0	1	2	0	0	3	1	0	0,5
85	1	1	1	0	0	0	0	0	0	1	1	1	0	3	1	0	2
86	0	0	2	0	0	0	0	0	0	1	0	2	0	3	0	1	1
87	1	0	1	1	0	0	0	0	0	1	0	2	0	3	0	1	-2
88	2	0	0	2	0	0	0	0	0	1	0	2	0	3	1	0	0,5
89	2	0	0	0	2	0	0	0	0	1	0	2	0	3	1	0	0,5
90	2	0	2	0	0	0	0	0	0	1	0	0	2	3	1	0	1,5
91	3	0	1	0	0	0	0	0	0	0	2	0	1	3	1	0	-0,5
92	1	2	1	0	0	0	0	0	0	0	2	0	1	3	1	0	-0,5
93	0	1	2	0	0	0	0	0	0	0	1	1	1	3	1	0	-1
94	0	0	2	1	0	0	0	0	0	0	0	2	1	3	0	1	1
95	1	0	1	2	0	0	0	0	0	0	0	2	1	3	1	0	-0,5
96	1	0	1	0	2	0	0	0	0	0	0	2	1	3	1	0	-0,5
97	1	0	3	0	0	0	0	0	0	0	0	0	3	3	1	0	-0,5
98	0	0	1	0	0	3	0	0	0	0	0	1	0	4	1	0	0,5
99	0	1	1	0	0	2	0	0	0	0	1	1	0	4	1	0	-1,5
100	0	0	1	0	0	1	2	0	0	0	0	1	0	4	1	0	0,5
101	1	0	1	0	0	1	1	0	0	0	1	1	0	4	1	0	1
102	0	0	1	0	0	1	0	2	0	0	0	1	0	4	1	0	0,5
103	0	1	1	0	0	1	0	1	1	0	0	1	0	4	1	0	1
104	1	0	1	0	0	1	0	1	0	1	0	1	0	4	1	0	-2
105	0	0	2	0	0	1	0	1	0	0	0	1	1	4	1	0	1
106	0	2	1	0	0	1	0	0	2	0	0	1	0	4	1	0	0,5
107	1	1	1	0	0	1	0	0	1	1	0	1	0	4	1	0	-2
108	0	1	2	0	0	1	0	0	1	0	0	1	1	4	1	0	1
109	2	0	1	0	0	1	0	0	0	2	0	1	0	4	1	0	1,5
110	1	0	2	0	0	1	0	0	0	1	0	1	1	4	1	0	-2
111	2	0	1	0	0	1	0	0	0	0	2	1	0	4	1	0	0,5

Marcos Pires Kassab 179

Advances on a kinematically exact rod model for thin-walled open section members: consistent warping function and nonlinear constitutive equation

Continued

112	0	2	1	0	0	1	0	0	0	0	2	1	0	4	1	0	1,5
113	0	0	1	2	0	1	0	0	0	0	0	3	0	4	1	0	0,5
114	0	0	1	2	0	1	0	0	0	0	0	3	0	4	0	1	-1
115	0	0	1	0	2	1	0	0	0	0	0	3	0	4	1	0	0,5
116	0	0	1	0	2	1	0	0	0	0	0	3	0	4	0	1	-1
117	0	0	3	0	0	1	0	0	0	0	0	1	2	4	1	0	0,5
118	0	1	1	0	0	0	2	0	0	0	1	1	0	4	1	0	-0,5
119	1	0	1	0	0	0	1	1	1	0	0	1	0	4	1	0	1
120	1	1	1	0	0	0	1	0	2	0	0	1	0	4	1	0	1
121	2	0	1	0	0	0	1	0	1	1	0	1	0	4	1	0	-1
122	1	0	2	0	0	0	1	0	1	0	0	1	1	4	1	0	1
123	1	1	1	0	0	0	1	0	0	0	2	1	0	4	1	0	-1
124	0	1	1	0	0	0	0	2	0	0	1	1	0	4	1	0	-0,5
125	2	0	1	0	0	0	0	1	1	0	1	1	0	4	1	0	1
126	0	2	1	0	0	0	0	1	1	0	1	1	0	4	1	0	-1
127	1	1	1	0	0	0	0	1	0	1	1	1	0	4	1	0	2
128	0	0	2	0	0	0	0	1	0	1	0	2	0	4	1	0	1
129	0	1	2	0	0	0	0	1	0	0	1	1	1	4	1	0	-1
130	2	1	1	0	0	0	0	0	2	0	1	1	0	4	1	0	1
131	0	3	1	0	0	0	0	0	2	0	1	1	0	4	1	0	-0,5
132	1	0	2	0	0	0	0	0	2	0	0	2	0	4	1	0	-0,5
133	3	0	1	0	0	0	0	0	1	1	1	1	0	4	1	0	-1
134	1	2	1	0	0	0	0	0	1	1	1	1	0	4	1	0	2
135	0	1	2	0	0	0	0	0	1	1	0	2	0	4	1	0	1
136	2	0	2	0	0	0	0	0	1	0	1	1	1	4	1	0	1
137	0	2	2	0	0	0	0	0	1	0	1	1	1	4	1	0	-1
138	2	1	1	0	0	0	0	0	0	2	1	1	0	4	1	0	-1,5
139	1	0	2	0	0	0	0	0	0	2	0	2	0	4	1	0	-1,5
140	1	1	2	0	0	0	0	0	0	1	1	1	1	4	1	0	2
141	0	0	3	0	0	0	0	0	0	1	0	2	1	4	1	0	1
142	2	1	1	0	0	0	0	0	0	0	3	1	0	4	1	0	-0,5
143	0	3	1	0	0	0	0	0	0	0	3	1	0	4	1	0	-0,5
144	0	1	1	2	0	0	0	0	0	0	1	3	0	4	1	0	-0,5
145	0	1	1	2	0	0	0	0	0	0	1	3	0	4	0	1	1
146	0	1	1	0	2	0	0	0	0	0	1	3	0	4	1	0	-0,5
147	0	1	1	0	2	0	0	0	0	0	1	3	0	4	0	1	1
148	0	1	3	0	0	0	0	0	0	0	1	1	2	4	1	0	-0,5
149	0	0	2	0	0	2	0	0	0	1	0	2	0	5	1	0	1,5
150	0	0	2	0	0	1	1	0	1	0	0	2	0	5	1	0	-1
151	1	0	2	0	0	1	0	0	1	0	1	2	0	5	1	0	-1
152	0	1	2	0	0	1	0	0	0	1	1	2	0	5	1	0	-3
153	0	0	2	0	0	0	2	0	0	1	0	2	0	5	1	0	0,5
154	0	1	2	0	0	0	1	0	1	0	1	2	0	5	1	0	1
155	1	0	2	0	0	0	1	0	0	1	1	2	0	5	1	0	1
156	0	0	2	0	0	0	0	2	0	1	0	2	0	5	1	0	0,5

Advances on a kinematically exact rod model for thin-walled open section members: consistent warping function and nonlinear constitutive equation

Continued

157	1	0	2	0	0	0	0	1	2	0	0	2	0	5	1	0	-0,5
158	0	1	2	0	0	0	0	1	1	1	0	2	0	5	1	0	1
159	1	0	2	0	0	0	0	1	0	2	0	2	0	5	1	0	-1,5
160	0	0	3	0	0	0	0	1	0	1	0	2	1	5	1	0	1
161	1	1	2	0	0	0	0	0	3	0	0	2	0	5	1	0	-0,5
162	2	0	2	0	0	0	0	0	2	1	0	2	0	5	1	0	0,5
163	0	2	2	0	0	0	0	0	2	1	0	2	0	5	1	0	0,5
164	1	0	3	0	0	0	0	0	2	0	0	2	1	5	1	0	-0,5
165	1	1	2	0	0	0	0	0	1	2	0	2	0	5	1	0	-1,5
166	0	1	3	0	0	0	0	0	1	1	0	2	1	5	1	0	1
167	1	1	2	0	0	0	0	0	1	0	2	2	0	5	1	0	1
168	2	0	2	0	0	0	0	0	0	3	0	2	0	5	1	0	1
169	1	0	3	0	0	0	0	0	0	2	0	2	1	5	1	0	-1,5
170	2	0	2	0	0	0	0	0	0	1	2	2	0	5	1	0	0,5
171	0	2	2	0	0	0	0	0	0	1	2	2	0	5	1	0	1,5
172	0	0	2	2	0	0	0	0	0	1	0	4	0	5	1	0	0,5
173	0	0	2	2	0	0	0	0	0	1	0	4	0	5	0	1	-1
174	0	0	2	0	2	0	0	0	0	1	0	4	0	5	1	0	0,5
175	0	0	2	0	2	0	0	0	0	1	0	4	0	5	0	1	-1
176	0	0	4	0	0	0	0	0	0	1	0	2	2	5	1	0	0,5
177	0	0	3	0	0	1	0	0	2	0	0	3	0	6	1	0	0,5
178	0	0	3	0	0	1	0	0	0	2	0	3	0	6	1	0	1,5
179	0	0	3	0	0	0	1	0	1	1	0	3	0	6	1	0	-1
180	0	1	3	0	0	0	0	0	2	0	1	3	0	6	1	0	-0,5
181	1	0	3	0	0	0	0	0	1	1	1	3	0	6	1	0	-1
182	0	1	3	0	0	0	0	0	0	2	1	3	0	6	1	0	-1,5
183	0	0	4	0	0	0	0	0	2	1	0	4	0	7	1	0	0,5
184	0	0	4	0	0	0	0	0	0	3	0	4	0	7	1	0	0,5

Monomials for m_3^r

1	0	1	0	0	0	1	0	0	0	0	0	0	0	1	0	1	-1
2	1	0	0	0	0	0	1	0	0	0	0	0	0	1	0	1	1
3	2	0	0	0	0	0	0	0	0	0	1	0	0	1	0	1	1
4	0	2	0	0	0	0	0	0	0	0	1	0	0	1	0	1	1
5	1	0	0	0	1	0	0	0	0	0	0	1	0	1	0	1	1
6	0	1	0	1	0	0	0	0	0	0	0	1	0	1	0	1	-1
7	0	1	0	0	0	1	0	1	0	0	0	0	0	2	1	0	-1
8	0	2	0	0	0	1	0	0	1	0	0	0	0	2	1	0	-1
9	1	1	0	0	0	1	0	0	0	1	0	0	0	2	1	0	1
10	0	1	1	0	0	1	0	0	0	0	0	0	1	2	1	0	-1
11	1	0	0	0	0	0	1	1	0	0	0	0	0	2	1	0	1
12	1	1	0	0	0	0	1	0	1	0	0	0	0	2	1	0	1
13	2	0	0	0	0	0	1	0	0	1	0	0	0	2	1	0	-1
14	1	0	1	0	0	0	1	0	0	0	0	0	1	2	1	0	1
15	2	0	0	0	0	0	0	1	0	0	1	0	0	2	1	0	1
16	0	2	0	0	0	0	0	1	0	0	1	0	0	2	1	0	1

Marcos Pires Kassab

181

Advances on a kinematically exact rod model for thin-walled open section members: consistent warping function and nonlinear constitutive equation

Continued

17	1	0	0	0	1	0	0	1	0	0	0	1	0	2	0	1	1
18	0	1	0	1	0	0	0	1	0	0	0	1	0	2	0	1	-1
19	2	1	0	0	0	0	0	0	1	0	1	0	0	2	1	0	1
20	0	3	0	0	0	0	0	0	1	0	1	0	0	2	1	0	1
21	1	0	1	0	0	0	0	0	1	0	0	1	0	2	0	1	-1
22	1	1	0	0	1	0	0	0	1	0	0	1	0	2	0	1	1
23	0	2	0	1	0	0	0	0	1	0	0	1	0	2	0	1	-1
24	3	0	0	0	0	0	0	0	0	1	1	0	0	2	1	0	-1
25	1	2	0	0	0	0	0	0	0	1	1	0	0	2	1	0	-1
26	0	1	1	0	0	0	0	0	0	1	0	1	0	2	0	1	-1
27	2	0	0	0	1	0	0	0	0	1	0	1	0	2	0	1	-1
28	1	1	0	1	0	0	0	0	0	1	0	1	0	2	0	1	1
29	2	0	1	0	0	0	0	0	0	0	1	0	1	2	1	0	1
30	0	2	1	0	0	0	0	0	0	0	1	0	1	2	1	0	1
31	1	0	1	0	1	0	0	0	0	0	0	1	1	2	0	1	1
32	0	1	1	1	0	0	0	0	0	0	0	1	1	2	0	1	-1
33	0	1	0	0	0	3	0	0	0	0	0	0	0	3	1	0	-0,5
34	1	0	0	0	0	2	1	0	0	0	0	0	0	3	1	0	0,5
35	2	0	0	0	0	2	0	0	0	0	1	0	0	3	1	0	0,5
36	0	2	0	0	0	2	0	0	0	0	1	0	0	3	1	0	1,5
37	0	1	0	0	0	1	2	0	0	0	0	0	0	3	1	0	-0,5
38	1	1	0	0	0	1	1	0	0	0	1	0	0	3	1	0	-2
39	0	1	0	0	0	1	0	2	0	0	0	0	0	3	1	0	-0,5
40	0	2	0	0	0	1	0	1	1	0	0	0	0	3	1	0	-1
41	1	1	0	0	0	1	0	1	0	1	0	0	0	3	1	0	1
42	0	1	1	0	0	1	0	1	0	0	0	0	1	3	1	0	-1
43	0	3	0	0	0	1	0	0	2	0	0	0	0	3	1	0	-0,5
44	1	2	0	0	0	1	0	0	1	1	0	0	0	3	1	0	1
45	0	2	1	0	0	1	0	0	1	0	0	0	1	3	1	0	-1
46	2	1	0	0	0	1	0	0	0	2	0	0	0	3	1	0	-0,5
47	1	1	1	0	0	1	0	0	0	1	0	0	1	3	1	0	1
48	2	1	0	0	0	1	0	0	0	0	2	0	0	3	1	0	-1,5
49	0	3	0	0	0	1	0	0	0	0	2	0	0	3	1	0	-1,5
50	0	1	0	2	0	1	0	0	0	0	0	2	0	3	1	0	-0,5
51	0	1	0	2	0	1	0	0	0	0	0	2	0	3	0	1	1
52	0	1	0	0	2	1	0	0	0	0	0	2	0	3	1	0	-0,5
53	0	1	0	0	2	1	0	0	0	0	0	2	0	3	0	1	1
54	0	1	2	0	0	1	0	0	0	0	0	0	2	3	1	0	-0,5
55	1	0	0	0	0	0	3	0	0	0	0	0	0	3	1	0	0,5
56	2	0	0	0	0	0	2	0	0	0	1	0	0	3	1	0	1,5
57	0	2	0	0	0	0	2	0	0	0	1	0	0	3	1	0	0,5
58	1	0	0	0	0	0	1	2	0	0	0	0	0	3	1	0	0,5
59	1	1	0	0	0	0	1	1	1	0	0	0	0	3	1	0	1
60	2	0	0	0	0	0	1	1	0	1	0	0	0	3	1	0	-1
61	1	0	1	0	0	0	1	1	0	0	0	0	1	3	1	0	1

Continued

62	1	2	0	0	0	0	1	0	2	0	0	0	0	3	1	0	0,5
63	2	1	0	0	0	0	1	0	1	1	0	0	0	3	1	0	-1
64	1	1	1	0	0	0	1	0	1	0	0	0	1	3	1	0	1
65	3	0	0	0	0	0	1	0	0	2	0	0	0	3	1	0	0,5
66	2	0	1	0	0	0	1	0	0	1	0	0	1	3	1	0	-1
67	3	0	0	0	0	0	1	0	0	0	2	0	0	3	1	0	1,5
68	1	2	0	0	0	0	1	0	0	0	2	0	0	3	1	0	1,5
69	1	0	0	2	0	0	1	0	0	0	0	2	0	3	1	0	0,5
70	1	0	0	2	0	0	1	0	0	0	0	2	0	3	0	1	-1
71	1	0	0	0	2	0	1	0	0	0	0	2	0	3	1	0	0,5
72	1	0	0	0	2	0	1	0	0	0	0	2	0	3	0	1	-1
73	1	0	2	0	0	0	1	0	0	0	0	0	2	3	1	0	0,5
74	2	0	0	0	0	0	0	2	0	0	1	0	0	3	1	0	0,5
75	0	2	0	0	0	0	0	2	0	0	1	0	0	3	1	0	0,5
76	2	1	0	0	0	0	0	1	1	0	1	0	0	3	1	0	1
77	0	3	0	0	0	0	0	1	1	0	1	0	0	3	1	0	1
78	1	0	1	0	0	0	0	1	1	0	0	1	0	3	1	0	-1
79	3	0	0	0	0	0	0	1	0	1	1	0	0	3	1	0	-1
80	1	2	0	0	0	0	0	1	0	1	1	0	0	3	1	0	-1
81	0	1	1	0	0	0	0	1	0	1	0	1	0	3	1	0	-1
82	2	0	1	0	0	0	0	1	0	0	1	0	1	3	1	0	1
83	0	2	1	0	0	0	0	1	0	0	1	0	1	3	1	0	1
84	2	2	0	0	0	0	0	0	2	0	1	0	0	3	1	0	0,5
85	0	4	0	0	0	0	0	0	2	0	1	0	0	3	1	0	0,5
86	1	1	1	0	0	0	0	0	2	0	0	1	0	3	1	0	-1
87	3	1	0	0	0	0	0	0	1	1	1	0	0	3	1	0	-1
88	1	3	0	0	0	0	0	0	1	1	1	0	0	3	1	0	-1
89	2	0	1	0	0	0	0	0	1	1	0	1	0	3	1	0	1
90	0	2	1	0	0	0	0	0	1	1	0	1	0	3	1	0	-1
91	2	1	1	0	0	0	0	0	1	0	1	0	1	3	1	0	1
92	0	3	1	0	0	0	0	0	1	0	1	0	1	3	1	0	1
93	1	0	2	0	0	0	0	0	1	0	0	1	1	3	1	0	-1
94	4	0	0	0	0	0	0	0	0	2	1	0	0	3	1	0	0,5
95	2	2	0	0	0	0	0	0	0	2	1	0	0	3	1	0	0,5
96	1	1	1	0	0	0	0	0	0	2	0	1	0	3	1	0	1
97	3	0	1	0	0	0	0	0	0	1	1	0	1	3	1	0	-1
98	1	2	1	0	0	0	0	0	0	1	1	0	1	3	1	0	-1
99	0	1	2	0	0	0	0	0	0	1	0	1	1	3	1	0	-1
100	4	0	0	0	0	0	0	0	0	0	3	0	0	3	1	0	0,5
101	2	2	0	0	0	0	0	0	0	0	3	0	0	3	1	0	1
102	0	4	0	0	0	0	0	0	0	0	3	0	0	3	1	0	0,5
103	2	0	0	2	0	0	0	0	0	0	1	2	0	3	1	0	0,5
104	2	0	0	2	0	0	0	0	0	0	1	2	0	3	0	1	-1
105	2	0	0	0	2	0	0	0	0	0	1	2	0	3	1	0	0,5
106	2	0	0	0	2	0	0	0	0	0	1	2	0	3	0	1	-1

Marcos Pires Kassab

183

Advances on a kinematically exact rod model for thin-walled open section members: consistent warping function and nonlinear constitutive equation

Continued

107	0	2	0	2	0	0	0	0	0	0	1	2	0	3	1	0	0,5
108	0	2	0	2	0	0	0	0	0	0	1	2	0	3	0	1	-1
109	0	2	0	0	2	0	0	0	0	0	1	2	0	3	1	0	0,5
110	0	2	0	0	2	0	0	0	0	0	1	2	0	3	0	1	-1
111	2	0	2	0	0	0	0	0	0	0	1	0	2	3	1	0	0,5
112	0	2	2	0	0	0	0	0	0	0	1	0	2	3	1	0	0,5
113	1	0	1	0	0	2	0	0	1	0	0	1	0	4	1	0	-0,5
114	0	1	1	0	0	2	0	0	0	1	0	1	0	4	1	0	-1,5
115	0	1	1	0	0	1	1	0	1	0	0	1	0	4	1	0	1
116	1	0	1	0	0	1	1	0	0	1	0	1	0	4	1	0	1
117	1	1	1	0	0	1	0	0	1	0	1	1	0	4	1	0	2
118	2	0	1	0	0	1	0	0	0	1	1	1	0	4	1	0	1
119	0	2	1	0	0	1	0	0	0	1	1	1	0	4	1	0	3
120	1	0	1	0	0	0	2	0	1	0	0	1	0	4	1	0	-1,5
121	0	1	1	0	0	0	2	0	0	1	0	1	0	4	1	0	-0,5
122	2	0	1	0	0	0	1	0	1	0	1	1	0	4	1	0	-3
123	0	2	1	0	0	0	1	0	1	0	1	1	0	4	1	0	-1
124	1	1	1	0	0	0	1	0	0	1	1	1	0	4	1	0	-2
125	1	0	1	0	0	0	0	2	1	0	0	1	0	4	1	0	-0,5
126	0	1	1	0	0	0	0	2	0	1	0	1	0	4	1	0	-0,5
127	1	1	1	0	0	0	0	1	2	0	0	1	0	4	1	0	-1
128	2	0	1	0	0	0	0	1	1	1	0	1	0	4	1	0	1
129	0	2	1	0	0	0	0	1	1	1	0	1	0	4	1	0	-1
130	1	0	2	0	0	0	0	1	1	0	0	1	1	4	1	0	-1
131	1	1	1	0	0	0	0	1	0	2	0	1	0	4	1	0	1
132	0	1	2	0	0	0	0	1	0	1	0	1	1	4	1	0	-1
133	1	2	1	0	0	0	0	0	3	0	0	1	0	4	1	0	-0,5
134	2	1	1	0	0	0	0	0	2	1	0	1	0	4	1	0	1
135	0	3	1	0	0	0	0	0	2	1	0	1	0	4	1	0	-0,5
136	1	1	2	0	0	0	0	0	2	0	0	1	1	4	1	0	-1
137	3	0	1	0	0	0	0	0	1	2	0	1	0	4	1	0	-0,5
138	1	2	1	0	0	0	0	0	1	2	0	1	0	4	1	0	1
139	2	0	2	0	0	0	0	0	1	1	0	1	1	4	1	0	1
140	0	2	2	0	0	0	0	0	1	1	0	1	1	4	1	0	-1
141	3	0	1	0	0	0	0	0	1	0	2	1	0	4	1	0	-1,5
142	1	2	1	0	0	0	0	0	1	0	2	1	0	4	1	0	-1,5
143	1	0	1	2	0	0	0	0	1	0	0	3	0	4	1	0	-0,5
144	1	0	1	2	0	0	0	0	1	0	0	3	0	4	0	1	1
145	1	0	1	0	2	0	0	0	1	0	0	3	0	4	1	0	-0,5
146	1	0	1	0	2	0	0	0	1	0	0	3	0	4	0	1	1
147	1	0	3	0	0	0	0	0	1	0	0	1	2	4	1	0	-0,5
148	2	1	1	0	0	0	0	0	0	3	0	1	0	4	1	0	-0,5
149	1	1	2	0	0	0	0	0	0	2	0	1	1	4	1	0	1
150	2	1	1	0	0	0	0	0	0	1	2	1	0	4	1	0	-1,5
151	0	3	1	0	0	0	0	0	0	1	2	1	0	4	1	0	-1,5

Advances on a kinematically exact rod model for thin-walled open section members: consistent warping function and nonlinear constitutive equation

Continued

152	0	1	1	2	0	0	0	0	0	1	0	3	0	4	1	0	-0,5
153	0	1	1	2	0	0	0	0	0	1	0	3	0	4	0	1	1
154	0	1	1	0	2	0	0	0	0	1	0	3	0	4	1	0	-0,5
155	0	1	1	0	2	0	0	0	0	1	0	3	0	4	0	1	1
156	0	1	3	0	0	0	0	0	0	1	0	1	2	4	1	0	-0,5
157	0	1	2	0	0	1	0	0	2	0	0	2	0	5	1	0	-0,5
158	1	0	2	0	0	1	0	0	1	1	0	2	0	5	1	0	-1
159	0	1	2	0	0	1	0	0	0	2	0	2	0	5	1	0	-1,5
160	1	0	2	0	0	0	1	0	2	0	0	2	0	5	1	0	1,5
161	0	1	2	0	0	0	1	0	1	1	0	2	0	5	1	0	1
162	1	0	2	0	0	0	1	0	0	2	0	2	0	5	1	0	0,5
163	2	0	2	0	0	0	0	0	2	0	1	2	0	5	1	0	1,5
164	0	2	2	0	0	0	0	0	2	0	1	2	0	5	1	0	0,5
165	1	1	2	0	0	0	0	0	1	1	1	2	0	5	1	0	2
166	2	0	2	0	0	0	0	0	0	2	1	2	0	5	1	0	0,5
167	0	2	2	0	0	0	0	0	0	2	1	2	0	5	1	0	1,5
168	1	0	3	0	0	0	0	0	3	0	0	3	0	6	1	0	-0,5
169	0	1	3	0	0	0	0	0	2	1	0	3	0	6	1	0	-0,5
170	1	0	3	0	0	0	0	0	1	2	0	3	0	6	1	0	-0,5
171	0	1	3	0	0	0	0	0	0	3	0	3	0	6	1	0	-0,5

Monomials for Q																	
1	0	0	0	1	0	1	0	0	0	0	0	0	0	1	0	1	1
2	0	0	0	0	1	0	1	0	0	0	0	0	0	1	0	1	1
3	1	0	0	0	1	0	0	0	0	0	1	0	0	1	0	1	1
4	0	1	0	1	0	0	0	0	0	0	1	0	0	1	0	1	-1
5	0	0	0	2	0	0	0	0	0	0	0	1	0	1	0	1	1
6	0	0	0	0	2	0	0	0	0	0	0	1	0	1	0	1	1
7	0	0	0	1	0	1	0	1	0	0	0	0	0	2	0	1	1
8	0	1	0	1	0	1	0	0	1	0	0	0	0	2	0	1	1
9	0	0	1	0	0	1	0	0	0	1	0	0	0	2	0	1	1
10	1	0	0	1	0	1	0	0	0	1	0	0	0	2	0	1	-1
11	0	0	1	1	0	1	0	0	0	0	0	0	1	2	0	1	1
12	0	0	0	0	1	0	1	1	0	0	0	0	0	2	0	1	1
13	0	0	1	0	0	0	1	0	1	0	0	0	0	2	0	1	-1
14	0	1	0	0	1	0	1	0	1	0	0	0	0	2	0	1	1
15	1	0	0	0	1	0	1	0	0	1	0	0	0	2	0	1	-1
16	0	0	1	0	1	0	1	0	0	0	0	0	1	2	0	1	1
17	1	0	0	0	1	0	0	1	0	0	1	0	0	2	0	1	1
18	0	1	0	1	0	0	0	1	0	0	1	0	0	2	0	1	-1
19	0	0	0	2	0	0	0	1	0	0	0	1	0	2	1	0	1
20	0	0	0	0	2	0	0	1	0	0	0	1	0	2	1	0	1
21	1	0	1	0	0	0	0	0	1	0	1	0	0	2	0	1	-1
22	1	1	0	0	1	0	0	0	1	0	1	0	0	2	0	1	1
23	0	2	0	1	0	0	0	0	1	0	1	0	0	2	0	1	-1
24	0	0	1	0	1	0	0	0	1	0	0	1	0	2	0	1	-2

Marcos Pires Kassab

Advances on a kinematically exact rod model for thin-walled open section members: consistent warping function and nonlinear constitutive equation

185

Continued

25	0	1	0	2	0	0	0	0	1	0	0	1	0	2	1	0	1
26	0	1	0	0	2	0	0	0	1	0	0	1	0	2	1	0	1
27	1	1	0	1	0	0	0	0	0	1	1	0	0	2	0	1	1
28	0	1	1	0	0	0	0	0	0	1	1	0	0	2	0	1	-1
29	2	0	0	0	1	0	0	0	0	1	1	0	0	2	0	1	-1
30	0	0	1	1	0	0	0	0	0	1	0	1	0	2	0	1	2
31	1	0	0	2	0	0	0	0	0	1	0	1	0	2	1	0	-1
32	1	0	0	0	2	0	0	0	0	1	0	1	0	2	1	0	-1
33	1	0	1	0	1	0	0	0	0	0	1	0	1	2	0	1	1
34	0	1	1	1	0	0	0	0	0	0	1	0	1	2	0	1	-1
35	0	0	1	2	0	0	0	0	0	0	0	1	1	2	1	0	1
36	0	0	1	0	2	0	0	0	0	0	0	1	1	2	1	0	1
37	0	0	0	2	0	2	0	0	0	0	0	1	0	3	1	0	0,5
38	0	0	0	2	0	2	0	0	0	0	0	1	0	3	0	1	-1
39	0	0	0	0	2	2	0	0	0	0	0	1	0	3	1	0	0,5
40	0	0	0	0	2	2	0	0	0	0	0	1	0	3	0	1	-1
41	0	0	1	0	0	1	0	1	0	1	0	0	0	3	1	0	1
42	0	1	1	0	0	1	0	0	1	1	0	0	0	3	1	0	1
43	1	0	1	0	0	1	0	0	0	2	0	0	0	3	1	0	-1
44	0	0	2	0	0	1	0	0	0	1	0	0	1	3	1	0	1
45	0	1	0	2	0	1	0	0	0	0	1	1	0	3	1	0	-1
46	0	1	0	2	0	1	0	0	0	0	1	1	0	3	0	1	2
47	0	1	0	0	2	1	0	0	0	0	1	1	0	3	1	0	-1
48	0	1	0	0	2	1	0	0	0	0	1	1	0	3	0	1	2
49	0	0	0	2	0	0	2	0	0	0	0	1	0	3	1	0	0,5
50	0	0	0	2	0	0	2	0	0	0	0	1	0	3	0	1	-1
51	0	0	0	0	2	0	2	0	0	0	0	1	0	3	1	0	0,5
52	0	0	0	0	2	0	2	0	0	0	0	1	0	3	0	1	-1
53	0	0	1	0	0	0	1	1	1	0	0	0	0	3	1	0	-1
54	0	1	1	0	0	0	1	0	2	0	0	0	0	3	1	0	-1
55	1	0	1	0	0	0	1	0	1	1	0	0	0	3	1	0	1
56	0	0	2	0	0	0	1	0	1	0	0	0	1	3	1	0	-1
57	1	0	0	2	0	0	1	0	0	0	1	1	0	3	1	0	1
58	1	0	0	2	0	0	1	0	0	0	1	1	0	3	0	1	-2
59	1	0	0	0	2	0	1	0	0	0	1	1	0	3	1	0	1
60	1	0	0	0	2	0	1	0	0	0	1	1	0	3	0	1	-2
61	0	0	0	2	0	0	0	2	0	0	0	1	0	3	1	0	0,5
62	0	0	0	0	2	0	0	2	0	0	0	1	0	3	1	0	0,5
63	1	0	1	0	0	0	0	1	1	0	1	0	0	3	1	0	-1
64	0	0	1	0	1	0	0	1	1	0	0	1	0	3	0	1	-2
65	0	1	0	2	0	0	0	1	1	0	0	1	0	3	1	0	1
66	0	1	0	0	2	0	0	1	1	0	0	1	0	3	1	0	1
67	0	1	1	0	0	0	0	1	0	1	1	0	0	3	1	0	-1
68	0	0	1	1	0	0	0	1	0	1	0	1	0	3	0	1	2
69	1	0	0	2	0	0	0	1	0	1	0	1	0	3	1	0	-1

Advances on a kinematically exact rod model for thin-walled open section members: consistent warping function and nonlinear constitutive equation

Continued

70	1	0	0	0	2	0	0	1	0	1	0	1	0	3	1	0	-1
71	0	0	1	2	0	0	0	1	0	0	0	1	1	3	1	0	1
72	0	0	1	0	2	0	0	1	0	0	0	1	1	3	1	0	1
73	1	1	1	0	0	0	0	0	2	0	1	0	0	3	1	0	-1
74	0	0	2	0	0	0	0	0	2	0	0	1	0	3	0	1	1
75	0	1	1	0	1	0	0	0	2	0	0	1	0	3	0	1	-2
76	0	2	0	2	0	0	0	0	2	0	0	1	0	3	1	0	0,5
77	0	2	0	0	2	0	0	0	2	0	0	1	0	3	1	0	0,5
78	2	0	1	0	0	0	0	0	1	1	1	0	0	3	1	0	1
79	0	2	1	0	0	0	0	0	1	1	1	0	0	3	1	0	-1
80	1	0	1	0	1	0	0	0	1	1	0	1	0	3	0	1	2
81	0	1	1	1	0	0	0	0	1	1	0	1	0	3	0	1	2
82	1	1	0	2	0	0	0	0	1	1	0	1	0	3	1	0	-1
83	1	1	0	0	2	0	0	0	1	1	0	1	0	3	1	0	-1
84	1	0	2	0	0	0	0	0	1	0	1	0	1	3	1	0	-1
85	0	0	2	0	1	0	0	0	1	0	0	1	1	3	0	1	-2
86	0	1	1	2	0	0	0	0	1	0	0	1	1	3	1	0	1
87	0	1	1	0	2	0	0	0	1	0	0	1	1	3	1	0	1
88	1	1	1	0	0	0	0	0	0	2	1	0	0	3	1	0	1
89	0	0	2	0	0	0	0	0	0	2	0	1	0	3	0	1	1
90	1	0	1	1	0	0	0	0	0	2	0	1	0	3	0	1	-2
91	2	0	0	2	0	0	0	0	0	2	0	1	0	3	1	0	0,5
92	2	0	0	0	2	0	0	0	0	2	0	1	0	3	1	0	0,5
93	0	1	2	0	0	0	0	0	0	1	1	0	1	3	1	0	-1
94	0	0	2	1	0	0	0	0	0	1	0	1	1	3	0	1	2
95	1	0	1	2	0	0	0	0	0	1	0	1	1	3	1	0	-1
96	1	0	1	0	2	0	0	0	0	1	0	1	1	3	1	0	-1
97	2	0	0	2	0	0	0	0	0	0	2	1	0	3	1	0	0,5
98	2	0	0	2	0	0	0	0	0	0	2	1	0	3	0	1	-1
99	2	0	0	0	2	0	0	0	0	0	2	1	0	3	1	0	0,5
100	2	0	0	0	2	0	0	0	0	0	2	1	0	3	0	1	-1
101	0	2	0	2	0	0	0	0	0	0	2	1	0	3	1	0	0,5
102	0	2	0	2	0	0	0	0	0	0	2	1	0	3	0	1	-1
103	0	2	0	0	2	0	0	0	0	0	2	1	0	3	1	0	0,5
104	0	2	0	0	2	0	0	0	0	0	2	1	0	3	0	1	-1
105	0	0	0	4	0	0	0	0	0	0	0	3	0	3	1	0	0,5
106	0	0	0	2	2	0	0	0	0	0	0	3	0	3	1	0	1
107	0	0	0	0	4	0	0	0	0	0	0	3	0	3	1	0	0,5
108	0	0	2	2	0	0	0	0	0	0	0	1	2	3	1	0	0,5
109	0	0	2	0	2	0	0	0	0	0	0	1	2	3	1	0	0,5
110	0	0	1	0	0	3	0	0	0	1	0	0	0	4	1	0	0,5
111	0	0	1	0	0	2	1	0	1	0	0	0	0	4	1	0	-0,5
112	1	0	1	0	0	2	0	0	1	0	1	0	0	4	1	0	-0,5
113	0	1	1	0	0	2	0	0	0	1	1	0	0	4	1	0	-1,5
114	0	0	1	0	0	1	2	0	0	1	0	0	0	4	1	0	0,5

Marcos Pires Kassab

187

Advances on a kinematically exact rod model for thin-walled open section members: consistent warping function and nonlinear constitutive equation

Continued

115	0	1	1	0	0	1	1	0	1	0	1	0	0	4	1	0	1
116	1	0	1	0	0	1	1	0	0	1	1	0	0	4	1	0	1
117	0	0	1	0	0	1	0	2	0	1	0	0	0	4	1	0	0,5
118	0	1	1	0	0	1	0	1	1	1	0	0	0	4	1	0	1
119	1	0	1	0	0	1	0	1	0	2	0	0	0	4	1	0	-1
120	0	0	2	0	0	1	0	1	0	1	0	0	1	4	1	0	1
121	0	2	1	0	0	1	0	0	2	1	0	0	0	4	1	0	0,5
122	1	1	1	0	0	1	0	0	1	2	0	0	0	4	1	0	-1
123	0	1	2	0	0	1	0	0	1	1	0	0	1	4	1	0	1
124	1	1	1	0	0	1	0	0	1	0	2	0	0	4	1	0	1
125	2	0	1	0	0	1	0	0	0	3	0	0	0	4	1	0	0,5
126	1	0	2	0	0	1	0	0	0	2	0	0	1	4	1	0	-1
127	2	0	1	0	0	1	0	0	0	1	2	0	0	4	1	0	0,5
128	0	2	1	0	0	1	0	0	0	1	2	0	0	4	1	0	1,5
129	0	0	1	2	0	1	0	0	0	1	0	2	0	4	1	0	1,5
130	0	0	1	2	0	1	0	0	0	1	0	2	0	4	0	1	-3
131	0	0	1	0	2	1	0	0	0	1	0	2	0	4	1	0	1,5
132	0	0	1	0	2	1	0	0	0	1	0	2	0	4	0	1	-3
133	0	0	3	0	0	1	0	0	0	1	0	0	2	4	1	0	0,5
134	0	0	1	0	0	0	3	0	1	0	0	0	0	4	1	0	-0,5
135	1	0	1	0	0	0	2	0	1	0	1	0	0	4	1	0	-1,5
136	0	1	1	0	0	0	2	0	0	1	1	0	0	4	1	0	-0,5
137	0	0	1	0	0	0	1	2	1	0	0	0	0	4	1	0	-0,5
138	0	1	1	0	0	0	1	1	2	0	0	0	0	4	1	0	-1
139	1	0	1	0	0	0	1	1	1	1	0	0	0	4	1	0	1
140	0	0	2	0	0	0	1	1	1	0	0	0	1	4	1	0	-1
141	0	2	1	0	0	0	1	0	3	0	0	0	0	4	1	0	-0,5
142	1	1	1	0	0	0	1	0	2	1	0	0	0	4	1	0	1
143	0	1	2	0	0	0	1	0	2	0	0	0	1	4	1	0	-1
144	2	0	1	0	0	0	1	0	1	2	0	0	0	4	1	0	-0,5
145	1	0	2	0	0	0	1	0	1	1	0	0	1	4	1	0	1
146	2	0	1	0	0	0	1	0	1	0	2	0	0	4	1	0	-1,5
147	0	2	1	0	0	0	1	0	1	0	2	0	0	4	1	0	-0,5
148	0	0	1	2	0	0	1	0	1	0	0	2	0	4	1	0	-1,5
149	0	0	1	2	0	0	1	0	1	0	0	2	0	4	0	1	3
150	0	0	1	0	2	0	1	0	1	0	0	2	0	4	1	0	-1,5
151	0	0	1	0	2	0	1	0	1	0	0	2	0	4	0	1	3
152	0	0	3	0	0	0	1	0	1	0	0	0	2	4	1	0	-0,5
153	1	1	1	0	0	0	1	0	0	1	2	0	0	4	1	0	-1
154	1	0	1	0	0	0	0	2	1	0	1	0	0	4	1	0	-0,5
155	0	1	1	0	0	0	0	2	0	1	1	0	0	4	1	0	-0,5
156	1	1	1	0	0	0	0	1	2	0	1	0	0	4	1	0	-1
157	0	0	2	0	0	0	0	1	2	0	0	1	0	4	1	0	1
158	2	0	1	0	0	0	0	1	1	1	1	0	0	4	1	0	1
159	0	2	1	0	0	0	0	1	1	1	1	0	0	4	1	0	-1

Advances on a kinematically exact rod model for thin-walled open section members: consistent warping function and nonlinear constitutive equation

Continued

160	1	0	2	0	0	0	0	1	1	0	1	0	1	4	1	0	-1
161	1	1	1	0	0	0	0	1	0	2	1	0	0	4	1	0	1
162	0	0	2	0	0	0	0	1	0	2	0	1	0	4	1	0	1
163	0	1	2	0	0	0	0	1	0	1	1	0	1	4	1	0	-1
164	1	2	1	0	0	0	0	0	3	0	1	0	0	4	1	0	-0,5
165	0	1	2	0	0	0	0	0	3	0	0	1	0	4	1	0	1
166	2	1	1	0	0	0	0	0	2	1	1	0	0	4	1	0	1
167	0	3	1	0	0	0	0	0	2	1	1	0	0	4	1	0	-0,5
168	1	0	2	0	0	0	0	0	2	1	0	1	0	4	1	0	-1
169	1	1	2	0	0	0	0	0	2	0	1	0	1	4	1	0	-1
170	0	0	3	0	0	0	0	0	2	0	0	1	1	4	1	0	1
171	3	0	1	0	0	0	0	0	1	2	1	0	0	4	1	0	-0,5
172	1	2	1	0	0	0	0	0	1	2	1	0	0	4	1	0	1
173	0	1	2	0	0	0	0	0	1	2	0	1	0	4	1	0	1
174	2	0	2	0	0	0	0	0	1	1	1	0	1	4	1	0	1
175	0	2	2	0	0	0	0	0	1	1	1	0	1	4	1	0	-1
176	3	0	1	0	0	0	0	0	1	0	3	0	0	4	1	0	-0,5
177	1	2	1	0	0	0	0	0	1	0	3	0	0	4	1	0	-0,5
178	1	0	1	2	0	0	0	0	1	0	1	2	0	4	1	0	-1,5
179	1	0	1	2	0	0	0	0	1	0	1	2	0	4	0	1	3
180	1	0	1	0	2	0	0	0	1	0	1	2	0	4	1	0	-1,5
181	1	0	1	0	2	0	0	0	1	0	1	2	0	4	0	1	3
182	1	0	3	0	0	0	0	0	1	0	1	0	2	4	1	0	-0,5
183	2	1	1	0	0	0	0	0	0	3	1	0	0	4	1	0	-0,5
184	1	0	2	0	0	0	0	0	0	3	0	1	0	4	1	0	-1
185	1	1	2	0	0	0	0	0	0	2	1	0	1	4	1	0	1
186	0	0	3	0	0	0	0	0	0	2	0	1	1	4	1	0	1
187	2	1	1	0	0	0	0	0	0	1	3	0	0	4	1	0	-0,5
188	0	3	1	0	0	0	0	0	0	1	3	0	0	4	1	0	-0,5
189	0	1	1	2	0	0	0	0	0	1	1	2	0	4	1	0	-1,5
190	0	1	1	2	0	0	0	0	0	1	1	2	0	4	0	1	3
191	0	1	1	0	2	0	0	0	0	1	1	2	0	4	1	0	-1,5
192	0	1	1	0	2	0	0	0	0	1	1	2	0	4	0	1	3
193	0	1	3	0	0	0	0	0	0	1	1	0	2	4	1	0	-0,5
194	0	0	2	0	0	2	0	0	2	0	0	1	0	5	1	0	0,5
195	0	0	2	0	0	2	0	0	0	2	0	1	0	5	1	0	1,5
196	0	0	2	0	0	1	1	0	1	1	0	1	0	5	1	0	-2
197	0	1	2	0	0	1	0	0	2	0	1	1	0	5	1	0	-1
198	1	0	2	0	0	1	0	0	1	1	1	1	0	5	1	0	-2
199	0	1	2	0	0	1	0	0	0	2	1	1	0	5	1	0	-3
200	0	0	2	0	0	0	2	0	2	0	0	1	0	5	1	0	1,5
201	0	0	2	0	0	0	2	0	0	2	0	1	0	5	1	0	0,5
202	1	0	2	0	0	0	1	0	2	0	1	1	0	5	1	0	3
203	0	1	2	0	0	0	1	0	1	1	1	1	0	5	1	0	2
204	1	0	2	0	0	0	1	0	0	2	1	1	0	5	1	0	1

Marcos Pires Kassab

189

Advances on a kinematically exact rod model for thin-walled open section members: consistent warping function and nonlinear constitutive equation

Continued

205	0	0	2	0	0	0	0	2	2	0	0	1	0	5	1	0	0,5
206	0	0	2	0	0	0	0	2	0	2	0	1	0	5	1	0	0,5
207	0	1	2	0	0	0	0	1	3	0	0	1	0	5	1	0	1
208	1	0	2	0	0	0	0	1	2	1	0	1	0	5	1	0	-1
209	0	0	3	0	0	0	0	1	2	0	0	1	1	5	1	0	1
210	0	1	2	0	0	0	0	1	1	2	0	1	0	5	1	0	1
211	1	0	2	0	0	0	0	1	0	3	0	1	0	5	1	0	-1
212	0	0	3	0	0	0	0	1	0	2	0	1	1	5	1	0	1
213	0	2	2	0	0	0	0	0	4	0	0	1	0	5	1	0	0,5
214	1	1	2	0	0	0	0	0	3	1	0	1	0	5	1	0	-1
215	0	1	3	0	0	0	0	0	3	0	0	1	1	5	1	0	1
216	2	0	2	0	0	0	0	0	2	2	0	1	0	5	1	0	0,5
217	0	2	2	0	0	0	0	0	2	2	0	1	0	5	1	0	0,5
218	1	0	3	0	0	0	0	0	2	1	0	1	1	5	1	0	-1
219	2	0	2	0	0	0	0	0	2	0	2	1	0	5	1	0	1,5
220	0	2	2	0	0	0	0	0	2	0	2	1	0	5	1	0	0,5
221	0	0	2	2	0	0	0	0	2	0	0	3	0	5	1	0	1
222	0	0	2	2	0	0	0	0	2	0	0	3	0	5	0	1	-2
223	0	0	2	0	2	0	0	0	2	0	0	3	0	5	1	0	1
224	0	0	2	0	2	0	0	0	2	0	0	3	0	5	0	1	-2
225	0	0	4	0	0	0	0	0	2	0	0	1	2	5	1	0	0,5
226	1	1	2	0	0	0	0	0	1	3	0	1	0	5	1	0	-1
227	0	1	3	0	0	0	0	0	1	2	0	1	1	5	1	0	1
228	1	1	2	0	0	0	0	0	1	1	2	1	0	5	1	0	2
229	2	0	2	0	0	0	0	0	0	4	0	1	0	5	1	0	0,5
230	1	0	3	0	0	0	0	0	0	3	0	1	1	5	1	0	-1
231	2	0	2	0	0	0	0	0	0	2	2	1	0	5	1	0	0,5
232	0	2	2	0	0	0	0	0	0	2	2	1	0	5	1	0	1,5
233	0	0	2	2	0	0	0	0	0	2	0	3	0	5	1	0	1
234	0	0	2	2	0	0	0	0	0	2	0	3	0	5	0	1	-2
235	0	0	2	0	2	0	0	0	0	2	0	3	0	5	1	0	1
236	0	0	2	0	2	0	0	0	0	2	0	3	0	5	0	1	-2
237	0	0	4	0	0	0	0	0	0	2	0	1	2	5	1	0	0,5
238	0	0	3	0	0	1	0	0	2	1	0	2	0	6	1	0	1,5
239	0	0	3	0	0	1	0	0	0	3	0	2	0	6	1	0	1,5
240	0	0	3	0	0	0	1	0	3	0	0	2	0	6	1	0	-1,5
241	0	0	3	0	0	0	1	0	1	2	0	2	0	6	1	0	-1,5
242	1	0	3	0	0	0	0	0	3	0	1	2	0	6	1	0	-1,5
243	0	1	3	0	0	0	0	0	2	1	1	2	0	6	1	0	-1,5
244	1	0	3	0	0	0	0	0	1	2	1	2	0	6	1	0	-1,5
245	0	1	3	0	0	0	0	0	0	3	1	2	0	6	1	0	-1,5
246	0	0	4	0	0	0	0	0	4	0	0	3	0	7	1	0	0,5
247	0	0	4	0	0	0	0	0	2	2	0	3	0	7	1	0	1
248	0	0	4	0	0	0	0	0	0	4	0	3	0	7	1	0	0,5

Marcos Pires Kassab

Advances on a kinematically exact rod model for thin-walled open section members: consistent warping function and nonlinear constitutive equation

Continued

	Monimials for B																
1	0	0	1	0	0	0	0	1	0	0	0	0	0	1	1	0	1
2	0	1	1	0	0	0	0	0	1	0	0	0	0	1	1	0	1
3	1	0	1	0	0	0	0	0	0	1	0	0	0	1	1	0	-1
4	0	0	2	0	0	0	0	0	0	0	0	0	1	1	1	0	1
5	0	0	1	0	0	2	0	0	0	0	0	0	0	2	1	0	0,5
6	0	1	1	0	0	1	0	0	0	0	1	0	0	2	1	0	-1
7	0	0	1	1	0	1	0	0	0	0	0	1	0	2	0	1	1
8	0	0	1	0	0	0	2	0	0	0	0	0	0	2	1	0	0,5
9	1	0	1	0	0	0	1	0	0	0	1	0	0	2	1	0	1
10	0	0	1	0	1	0	1	0	0	0	0	1	0	2	0	1	1
11	0	0	1	0	0	0	0	2	0	0	0	0	0	2	1	0	1,5
12	0	1	1	0	0	0	0	1	1	0	0	0	0	2	1	0	3
13	1	0	1	0	0	0	0	1	0	1	0	0	0	2	1	0	-3
14	0	0	2	0	0	0	0	1	0	0	0	0	1	2	1	0	3
15	0	2	1	0	0	0	0	0	2	0	0	0	0	2	1	0	1,5
16	1	1	1	0	0	0	0	0	1	1	0	0	0	2	1	0	-3
17	0	1	2	0	0	0	0	0	1	0	0	0	1	2	1	0	3
18	2	0	1	0	0	0	0	0	0	2	0	0	0	2	1	0	1,5
19	1	0	2	0	0	0	0	0	0	1	0	0	1	2	1	0	-3
20	2	0	1	0	0	0	0	0	0	0	2	0	0	2	1	0	0,5
21	0	2	1	0	0	0	0	0	0	0	2	0	0	2	1	0	0,5
22	1	0	1	0	1	0	0	0	0	0	1	1	0	2	0	1	1
23	0	1	1	1	0	0	0	0	0	0	1	1	0	2	0	1	-1
24	0	0	1	0	2	0	0	0	0	0	0	2	0	2	1	0	0,5
25	0	0	1	2	0	0	0	0	0	0	0	2	0	2	1	0	0,5
26	0	0	3	0	0	0	0	0	0	0	0	0	2	2	1	0	1,5
27	0	0	1	0	0	2	0	1	0	0	0	0	0	3	1	0	0,5
28	0	1	1	0	0	2	0	0	1	0	0	0	0	3	1	0	0,5
29	1	0	1	0	0	2	0	0	0	1	0	0	0	3	1	0	-0,5
30	0	0	2	0	0	2	0	0	0	0	0	0	1	3	1	0	0,5
31	0	2	1	0	0	1	0	0	1	0	1	0	0	3	1	0	-1
32	0	1	1	0	0	1	0	1	0	0	1	0	0	3	1	0	-1
33	1	1	1	0	0	1	0	0	0	1	1	0	0	3	1	0	1
34	0	0	2	0	0	1	0	0	0	1	0	1	0	3	1	0	1
35	0	1	2	0	0	1	0	0	0	0	1	0	1	3	1	0	-1
36	0	0	1	0	0	0	2	1	0	0	0	0	0	3	1	0	0,5
37	0	1	1	0	0	0	2	0	1	0	0	0	0	3	1	0	0,5
38	1	0	1	0	0	0	2	0	0	1	0	0	0	3	1	0	-0,5
39	0	0	2	0	0	0	2	0	0	0	0	0	1	3	1	0	0,5
40	1	0	1	0	0	0	1	1	0	0	1	0	0	3	1	0	1
41	1	1	1	0	0	0	1	0	1	0	1	0	0	3	1	0	1
42	0	0	2	0	0	0	1	0	1	0	0	1	0	3	1	0	-1
43	2	0	1	0	0	0	1	0	0	1	1	0	0	3	1	0	-1
44	1	0	2	0	0	0	1	0	0	0	1	0	1	3	1	0	1

Continued

45	0	0	1	0	0	0	0	3	0	0	0	0	0	3	1	0	0,5
46	0	1	1	0	0	0	0	2	1	0	0	0	0	3	1	0	1,5
47	1	0	1	0	0	0	0	2	0	1	0	0	0	3	1	0	-1,5
48	0	0	2	0	0	0	0	2	0	0	0	0	1	3	1	0	1,5
49	0	2	1	0	0	0	0	1	2	0	0	0	0	3	1	0	1,5
50	1	1	1	0	0	0	0	1	1	1	0	0	0	3	1	0	-3
51	0	1	2	0	0	0	0	1	1	0	0	0	1	3	1	0	3
52	2	0	1	0	0	0	0	1	0	2	0	0	0	3	1	0	1,5
53	1	0	2	0	0	0	0	1	0	1	0	0	1	3	1	0	-3
54	2	0	1	0	0	0	0	1	0	0	2	0	0	3	1	0	0,5
55	0	2	1	0	0	0	0	1	0	0	2	0	0	3	1	0	0,5
56	0	0	1	0	2	0	0	1	0	0	0	2	0	3	1	0	0,5
57	0	0	1	2	0	0	0	1	0	0	0	2	0	3	1	0	0,5
58	0	0	3	0	0	0	0	1	0	0	0	0	2	3	1	0	1,5
59	0	3	1	0	0	0	0	0	3	0	0	0	0	3	1	0	0,5
60	1	2	1	0	0	0	0	0	2	1	0	0	0	3	1	0	-1,5
61	0	2	2	0	0	0	0	0	2	0	0	0	1	3	1	0	1,5
62	2	1	1	0	0	0	0	0	1	2	0	0	0	3	1	0	1,5
63	1	1	2	0	0	0	0	0	1	1	0	0	1	3	1	0	-3
64	2	1	1	0	0	0	0	0	1	0	2	0	0	3	1	0	0,5
65	0	3	1	0	0	0	0	0	1	0	2	0	0	3	1	0	0,5
66	1	0	2	0	0	0	0	0	1	0	1	1	0	3	1	0	-1
67	0	1	1	2	0	0	0	0	1	0	0	2	0	3	1	0	0,5
68	0	0	2	0	1	0	0	0	1	0	0	2	0	3	0	1	-1
69	0	1	1	0	2	0	0	0	1	0	0	2	0	3	1	0	0,5
70	0	1	3	0	0	0	0	0	1	0	0	0	2	3	1	0	1,5
71	3	0	1	0	0	0	0	0	0	3	0	0	0	3	1	0	-0,5
72	2	0	2	0	0	0	0	0	0	2	0	0	1	3	1	0	1,5
73	1	2	1	0	0	0	0	0	0	1	2	0	0	3	1	0	-0,5
74	3	0	1	0	0	0	0	0	0	1	2	0	0	3	1	0	-0,5
75	0	1	2	0	0	0	0	0	0	1	1	1	0	3	1	0	-1
76	1	0	1	2	0	0	0	0	0	1	0	2	0	3	1	0	-0,5
77	1	0	1	0	2	0	0	0	0	1	0	2	0	3	1	0	-0,5
78	0	0	2	1	0	0	0	0	0	1	0	2	0	3	0	1	1
79	1	0	3	0	0	0	0	0	0	1	0	0	2	3	1	0	-1,5
80	2	0	2	0	0	0	0	0	0	0	2	0	1	3	1	0	0,5
81	0	2	2	0	0	0	0	0	0	0	2	0	1	3	1	0	0,5
82	0	0	2	2	0	0	0	0	0	0	0	2	1	3	1	0	0,5
83	0	0	2	0	2	0	0	0	0	0	0	2	1	3	1	0	0,5
84	0	0	4	0	0	0	0	0	0	0	0	0	3	3	1	0	0,5
85	0	0	2	0	0	1	0	1	0	1	0	1	0	4	1	0	1
86	0	1	2	0	0	1	0	0	1	1	0	1	0	4	1	0	1
87	1	0	2	0	0	1	0	0	0	2	0	1	0	4	1	0	-1
88	0	0	3	0	0	1	0	0	0	1	0	1	1	4	1	0	1
89	0	0	2	0	0	0	1	1	1	0	0	1	0	4	1	0	-1

Continued

90	0	1	2	0	0	0	1	0	2	0	0	1	0	4	1	0	-1
91	1	0	2	0	0	0	1	0	1	1	0	1	0	4	1	0	1
92	0	0	3	0	0	0	1	0	1	0	0	1	1	4	1	0	-1
93	1	0	2	0	0	0	0	1	1	0	1	1	0	4	1	0	-1
94	0	1	2	0	0	0	0	1	0	1	1	1	0	4	1	0	-1
95	1	1	2	0	0	0	0	0	2	0	1	1	0	4	1	0	-1
96	0	0	3	0	0	0	0	0	2	0	0	2	0	4	1	0	0,5
97	2	0	2	0	0	0	0	0	1	1	1	1	0	4	1	0	1
98	0	2	2	0	0	0	0	0	1	1	1	1	0	4	1	0	-1
99	1	0	3	0	0	0	0	0	1	0	1	1	1	4	1	0	-1
100	1	1	2	0	0	0	0	0	0	2	1	1	0	4	1	0	1
101	0	0	3	0	0	0	0	0	0	2	0	2	0	4	1	0	0,5
102	0	1	3	0	0	0	0	0	0	1	1	1	1	4	1	0	-1
103	0	0	3	0	0	0	0	1	2	0	0	2	0	5	1	0	0,5
104	0	0	3	0	0	0	0	1	0	2	0	2	0	5	1	0	0,5
105	0	1	3	0	0	0	0	0	3	0	0	2	0	5	1	0	0,5
106	1	0	3	0	0	0	0	0	2	1	0	2	0	5	1	0	-0,5
107	0	0	4	0	0	0	0	0	2	0	0	2	1	5	1	0	0,5
108	0	1	3	0	0	0	0	0	1	2	0	2	0	5	1	0	0,5
109	1	0	3	0	0	0	0	0	0	3	0	2	0	5	1	0	-0,5
110	0	0	4	0	0	0	0	0	0	2	0	2	1	5	1	0	0,5

Marcos Pires Kassab   193

Advances on a kinematically exact rod model for thin-walled open section members: consistent warping function and nonlinear constitutive equation

APPENDIX J. RECOVERING THE 6-DOF KINEMATICALLY EXACT ROD MODEL FROM THE 7-DOF MODEL

The 6-DOF rod model can be obtained from the 7-DOF model by imposing $p = \kappa_3^r$ (thus, also $\delta p = \delta \kappa_3^r$) and by neglecting the bi-moment contribution for the virtual work (both internal and external). Hence, one gets,

$$\delta W_{int} = \int_{V^r} \boldsymbol{P} : \delta \boldsymbol{F} dV^r = \int_0^L \boldsymbol{\sigma}^r \cdot \delta \boldsymbol{\varepsilon}^r d\zeta = \int_0^L \boldsymbol{\sigma}^r \cdot \boldsymbol{\Psi} \boldsymbol{\Delta} \delta \mathbf{d}_\theta d\zeta \, , \forall \delta \boldsymbol{d}_\theta(\zeta) \in \tag{J.1}$$
$$\mathcal{H}_1^0(\Omega),$$

with

$$\boldsymbol{\sigma}^r = \begin{bmatrix} \boldsymbol{n}^r \\ \boldsymbol{m}^r + Q \boldsymbol{e}_3^r \end{bmatrix}, \delta \boldsymbol{\varepsilon}^r = \begin{bmatrix} \delta \boldsymbol{\eta}^r \\ \delta \boldsymbol{\kappa}^r \end{bmatrix}, \tag{J.2}$$

and

$$\delta W_{ext} = \int_0^L \overline{\boldsymbol{q}} \cdot \delta \boldsymbol{d}_\theta d\zeta, \quad \forall \delta \boldsymbol{d}_\theta(\zeta) \in \mathcal{H}_1^0(\Omega), \tag{J.3}$$

with

$$\overline{\boldsymbol{q}} = \begin{bmatrix} \overline{\boldsymbol{n}} \\ \overline{\boldsymbol{\mu}} \end{bmatrix}, \delta \boldsymbol{d}_\theta = \begin{bmatrix} \delta \boldsymbol{u} \\ \delta \boldsymbol{\theta} \end{bmatrix}. \tag{J.4}$$

Using linear elastic materials, one gets

$$\boldsymbol{\sigma}^r = \boldsymbol{D}_L \boldsymbol{\varepsilon}^r, \tag{J.5}$$

with

$$\boldsymbol{D}_L = \begin{bmatrix} GA & 0 & 0 & 0 & 0 & -GAs_2 \\ & GA & 0 & 0 & 0 & GAs_1 \\ & & EA & EAg_2 & -EAg_1 & 0 \\ & & & EI_1 & EI_{12} & 0 \\ & Sym. & & & EI_2 & 0 \\ & & & & & G(I_T + Ag_\alpha s_\alpha) \end{bmatrix}, \tag{J.6}$$

which is precisely what is found in [22].

Note that the sixth input of $\boldsymbol{\sigma}^r$ is $m_3^r + Q$. As discussed on section 3.2, the sign of Q used in the current development is the opposite as the one defined in the Vlasov's theory. Having that in mind, one can interpret $T_u = m_3^r + Q$ as the uniform torsion contribution from the total torsion experienced by the rod. Thus, in the equilibrium equation, the external torsional moment ($\overline{m}_3$) is only balanced by T_u explaining why the 6-DOF rod model is usually less stiff than the 7-DOF counterpart.

Marcos Pires Kassab 195

Advances on a kinematically exact rod model for thin-walled open section members: consistent warping function and nonlinear constitutive equation

APPENDIX K.   BASIC CONCEPTS FOR FINITE ELEMENTS METHOD (FEM)

Introducing the method

For a specially constructed vectorial space of approximation $(\tilde{V})$, the real solution $\boldsymbol{s}$, that is in a higher order vectorial space (V), is projected into $\tilde{V}$, obtaining the approximated solution $\tilde{\boldsymbol{s}}$. Let $\bar{\boldsymbol{s}} \in \tilde{V}$ be an arbitrary vector, herein called trial function. In the rod contexts (one-dimensional, in ζ), let the scalar product be the trivial $< \boldsymbol{a}, \boldsymbol{b} > = \int_0^L \boldsymbol{a} \cdot \boldsymbol{b} d\zeta$. Using the fact that $\tilde{\boldsymbol{s}}$ is a projection, with the aid of the residual function $\boldsymbol{r}(\zeta) = \boldsymbol{s} - \tilde{\boldsymbol{s}}$,

$$< \boldsymbol{r}, \bar{\boldsymbol{s}} > = \int_0^L \boldsymbol{r} \cdot \bar{\boldsymbol{s}} d\zeta = 0 \tag{K.1}$$

Let us compare equation (3.22) with (K.2). It becomes evident that, if the virtual displacement $\delta \boldsymbol{d_\theta}$ is interpreted as the trial function, and the stress resultants calculated based on some approximation as the residue, this form of the Virtual Work Theorem represents a projection problem for kinematically exact rods. Therefore, the residual function is minimized.

The FEM is based on the Bubnov-Galerkin's method, in which the trial function (virtual displacements) is built exactly as the approximation function. This method itself is a "Weighted Residue Method", such as the colocation method, the least squares method, and others. This denomination is due to the form of the interpolation function

$$\tilde{\boldsymbol{s}} = \sum_{i=1}^N \boldsymbol{\Phi_i} \boldsymbol{a_i}, \tag{K.2}$$

with $\boldsymbol{\Phi_i}$ representing the interpolation shape functions and $\boldsymbol{a_i}$ being the weights that minimizes the residues. In the mechanical context, these weights represent generalized displacements quantities on each node.

In the FEM, the interpolation functions are taken in a manner that only the nodes that belongs to a given elements influence on the interpolation of this sub-domain, rendering sparse matrixes for the system solution.

Interpolation functions – isoparametric rod element

In order to efficiently parametrize any rod element, a standard approach is to perform a change of variables from the reference configuration $0 \leq \zeta \leq L$ to natural coordinates $-1 \leq Z \leq 1$. A direct implication of this transformation is that a Jacobian J_ζ will be needed to perform the integrations.

Consider the definitions of $p, \delta p, d_\theta, \delta d_\theta, N$ from chapter 5 (equations (5.1) to (5.5))

With the proposed interpolation, it is also possible to map the position of the element points in the reference configuration using the isoparametric transformation

$$\zeta(Z) = N_i(Z)\zeta_i. \tag{K.3}$$

Consider the integration of a generic function $f(\zeta)$ in the domain of a given element. Then, let us use the isoparametric transformation

Advances on a kinematically exact rod model for thin-walled open section members: consistent warping function and nonlinear constitutive equation

$$I = \int_0^l f(\zeta)d\zeta = \int_{-1}^1 f(Z)J_Z dZ. \tag{K.4}$$

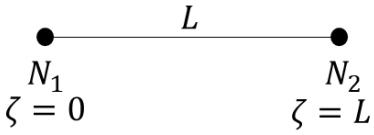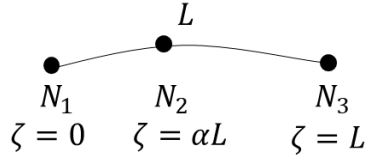The Jacobian J_ζ, for functions that are $\mathbb{R} \to \mathbb{R}$ is simply

$$J_Z = \frac{d\zeta}{dZ} = \frac{dN_i(Z)}{dZ}\zeta_i. \tag{K.5}$$

Consider now the derivatives of the shape form. In the formulation, the derivative with respect to the reference configuration (ζ) is needed, although the parametrization is on (Z). This can be circumvented with the aid of the chain rule, hence

$$\frac{\partial N_a}{\partial \zeta} = \frac{\partial N_a}{\partial Z}\frac{\partial Z}{\partial \zeta} = (J_Z)^{-1}\frac{(\partial N_a)}{\partial Z}. \tag{K.6}$$

For this work, elements with 2 and 3 nodes are of interest. They represent, respectively, linear and quadratic interpolations. See the table below (Table 13) for details about their interpolation.

Table 13– Finite element interpolation for 2 and 3 nodes rod elements

	2 nodes	3 nodes
Element description	N_1 N_2 $\zeta = 0$ $\zeta = L$	N_1 N_2 N_3 $\zeta = 0$ $\zeta = \alpha L$ $\zeta = L$
Natural coordinates	$\zeta_1 = 0; \zeta_2 = L$	$\zeta_1 = 0; \zeta_2 = \alpha L; \zeta_3 = L$ $0 < \alpha < L$
Isoparametric coordinates	$Z_1 = -1; Z_2 = 1$	$Z_1 = -1; Z_2 = 0; Z_3 = 1$
Interpolation functions	$N_1(Z) = l_1^1(Z) = \frac{1}{2}(1 - Z)$ $N_2(Z) = l_2^1(Z) = \frac{1}{2}(1 + Z)$	$N_1(Z) = l_1^2(Z) = \frac{1}{2}Z(Z - 1)$ $N_2(Z) = l_2^2(Z) = -Z^2 + 1$ $N_3(Z) = l_3^2(Z) = \frac{1}{2}Z(1 + Z).$
Natural coordinates interpolation	$\zeta_i = \frac{1}{2}(1 - Z) * 0 + \frac{1}{2}(1 + Z)$ $* L$ $= \frac{1}{2}(1 + Z) * L$	$\zeta_i = \frac{1}{2}Z(Z - 1) * 0 + (-Z^2 + 1)\alpha L +$ $\frac{1}{2}Z(1 + Z)L = \left[Z^2\left(-\alpha + \frac{1}{2}\right) + \frac{1}{2}Z + \alpha\right]L$
$\frac{(\partial N_a)}{\partial Z}$	$N_{1,Z} = -\frac{1}{2}$ $N_{2,Z} = \frac{1}{2}$	$N_{1,Z} = \frac{1}{2}(2Z - 1)$ $N_{2,Z} = -2Z$ $N_{1,Z} = \frac{1}{2}(1 + 2Z)$
Jacobian	$J_Z(Z) = \frac{1}{2} * 0 + \frac{1}{2} * L = \frac{L}{2}$	$J_Z(Z) = \frac{1}{2}(1 - 2Z) * 0 + (-2Z) * \alpha L +$ $\frac{1}{2}(1 + 2Z) * L = \left[Z(-2\alpha + 1) + \frac{1}{2}\right]L$